Design Synthesis Exercise - 28 January 2018

Final Report - Inspiration Mars

Faculty of Aerospace Engineering

TU Delft Delft University of Technology

I.M. DELFT

Challenge the future

[This page is intentionally left blank]

Delft University of Technology

Faculty of Aerospace Engineering

Final Report - Inspiration Mars

Design Synthesis Exercise

Authors:
Verschoor, T.
Hosseini, S.
Gezels, G.
Blanco Maceiras, R.
Kranendonk, L.M.
Caenen, R.
Georgiev, M.
Stevens, C.D.J.
Ahmad, S.
Fatemi Ghomi, P.

Version Number:
Version 2.0

Supervisors:
Dr.ir. E. Mooij
Ir. M.C. Naeije

Coaches:
Dr. A.M. Grande
Ir. W.C.P. van der Velden

January 28, 2014

Revision record

Version	Date	Chapters affected	Brief description of changes
1.0	January 21, 2014	all	First version of the final report.
2.0	January 28, 2014	all	Revised version of the final report

Preface

A new era of spaceflight has set upon mankind, as it gets its first chance to become a multi-planetary species. In order to prepare for the colonization of Mars and taking the first step, the idea of a manned end-to-end fly-by mission to Mars by the year 2018 was introduced by the Mars Society. In addition to the main objective, the mission must be as cheap, safe and simple as possible [1].

This groundbreaking challenge has inspired the student team of Delft University of Technology, Inspiration Mars Delft (I.M. Delft), and it has motivated the team to perform a thorough investigation on this inspirational mission. Working as a team of ten Aerospace Engineering students for ten weeks, and as part of the Aerospace Engineering curriculum, the results of this investigation and a mission proposal are presented in this final report.

Prior to the creation of this final report, I.M. Delft worked in a serie of steps as a part of a Design Synthesis Exercise (DSE). First a project plan was composed, to guide the team through the process of designing the mission. Next, a baseline concept was set up to identify all the necessary requirements and preliminary design options. Five weaks into the project a preliminary concept elimination led to four concepts, from which the final design was chosen after a thorough trade-off. Finally, in this final report, the detailed design of the mission is presented which covers the end-to-end mission.

Acknowledgements

The I.M.Delft team wants to thank the following people for their support in the realization of this report. First of all, Dr. Mooij and Ir. Naeije for their supervision, their enthusiastic input and for introducing this project in the Design Synthesis Exercise. The coaches, Dr. Grande and Ir. van der Velden, who were present every step of the way. During the system design phase the team was supported by professionals, who stimulated the mission design. Ir. Noomen, Ir. Kumar and Ir. Boon are thanked for their advice in the trajectory determination process. Special thanks go to Ir. Lemmen for his time and support in the thermal system design. Furthermore, the team wants to thank Ir. Sudmeijer and Dr. Walpot for their guidance in the re-entry procedures, Dr. Cervone and Ir. Zandbergen for their advice for the propulsion and power system design, and E.J. van den Bos for his help on the CATIA drawings. Great appreciation for the help of Ir. Sundaramoorthy on the communications system design. Last but certainly not least the contacts at ESA/ESTEC, Ir. Martinez Barrio and Ir. Trigo, are greatly thanked for their interest in the project and their support.

The I.M. Delft team was honored to work on this inspiring mission, and hopes that the reader enjoys reading this report just as much as the creation of it.

Abstract

Flying a manned spacecraft to Mars is a vision within the space industry which is developing gradually and inspiring more citizens and companies to take a step towards the Red Planet. For this reason, this mission focuses on the design of an end-to-end fly-by mission launched by the year 2018, while accommodating for a man and a woman on board of the ADRESTIA spacecraft.

The design proces was initiated by the determination of optional trajectories and preliminary sub-system designs. After this phase, the design options were analyzed and critical design choices led to the foundation for the overall mission overview of this end-to-end mission. Following this phase, the detailed design process began in which all mission specifications were thoroughly identified from launch through landing, as follows.

The first step of the mission is the launch of the SpaceX Dragon re-entry capsule and two extended trunks, which carry the crew and the living module to a Low Earth Orbit on board of a SpaceX Falcon Heavy launcher. After this phase, a second Falcon Heavy is launched, which carries extra fuel to this orbit. Next, on-orbit docking is performed and the refueling process, assisted by the crew with an Extravehicular Activity takes place. Thereafter, the system undocks and the spacecraft is ready to start its interplanetary journey. This journey is initiated by an injection into a Trans Mars trajectory due to the generation of a velocity change.

Since this mission marks the very first manned mission towards Mars, the Environmental Control and Life Support System is of great importance. It ensures the safety of the crew and sustains human life and workability. This opportunity allows for a number of scientific experiments to be brought on board, bringing to life the interplanetary mission experiments that have been performed in different projects on Earth.

Halfway the 500-day mission, the first manned Martian fly-by is performed. It will have a duration of ten hours, approaching Mars to an altitude of 180km. Using the gravity of Mars, the spacecraft obtains a velocity boost to continue its trajectory and journey back to Earth.

In the final phase of the mission, the spacecraft starts approaching Earth and the crew moves back to the Dragon capsule with an Extravehicular Activity. Following this process, the re-entry capsule is jettisoned and it performs a direct re-entry. The living module will continue on its trajectory into a heliocentric orbit where it will be used to collect deep space environment measurements. Finally, the crew is retrieved from the capsule and this inspirational and innovative mission is completed successfully.

List of Abbreviations

Abbreviation	Meaning	Abbreviation	Meaning
AGI	Analytic Graphics Inc.	MYr	Man-Year
AIAA	American Institute of Aeronautics and Astronautics	NASA	National Aeronautics and Space Administration
AMCM	Advanced mission cost model	NLP	Non Linear Programming
AutoNav	Autonomous Optical Navigation	QPSK	Quadrature Phase Shift Keying
BER	Bit Error Rate	RAM	Random Access Memory
BWG	Beam Wafe Guide	RAMS	Reliability, Availability, Maintainability, Safety
CCF	Cumulative Cost Fraction	REID	Risk of Exposure Induced Death
C&DH	Command and Data Handling	RF	Reserve Factor
CER	Cost Estimation Relationship	RP-1	Rocket Propellant 1
CPU	Central Processing Unit	PFL	Pumped Fluid Loop
DLS	Descent and Landing System	PROM	Programmable Read-Only Memory
DSE	Design Synthesis Exercise	SLOC	Source Lines of Code
DSN	Deep Space Network	SOI	Sphere of Influence
ECLSS	Environmental Control and Life Support Systems	SPE	Solar Particle Events
EIRP	Effective Isotropic Radiated Pressure	SWOT	Strenght, Weakness, Opportunities, Threats
EEPROM	Electrically Erasable Programmable Read-Only Memory	TCS	Thermal Control System
EMU	Extravehicular Mobility Unit	TMI	Trans-Mars Injection
EOL	End-of-Life	TOF	Time of Flight
EPS	Electrical Power System	TPBVP	Two-point Boundary Value Problem
ESA	European Space Agency	TPS	Thermal Protection System
EVA	Extravehicular Activity	TRL	Technology Readiness Level
FFD	Extravehicular Activity	TT&C	Telemetry, Tracking and Command
FY	Fiscal Year	TUDAT	Technical University of Delft Astrodynamic Toolbox
GCR	Galactic Cosmic Radiation	ULA	United Launch Alliance
GMAT	General Mission Analysis Tool	VAB	Vehicle Assembly Building
GNC	Guidance Navigation and Control	VDMLI	Variable Density Multi Layer Insulation
I/O	Input/Output		
IOC	Initial Operational Capability		
IR	Infrared Radiation		
iRED	interim Resistance Exercise Device		
ISA	Instruction Set Architecture		
ISS	International Space Station		
JPL	Jet Propulsion Lab		
KIPS	Thousand instructions per second		
LEO	Low Earth Orbit		
LSS	Life Support System		
LOX	Liquid Oxygen		
MAI	Manufacturing, Assembly and Integration		
MAnE	Mission Analysis Environment		
MANS	Microcosm Autonomous Navigation System		
MBps	Mega Bits per second		
MICAS	Miniature Integrated Camera and Spectrometer		
MIPS	Millions of Instructions Per Second		
MLI	Multi Layer Insulation		
MMOD	Micrometeorite and Orbital Debris		

List of Symbols

Symbol	Description	Dimension
	Latin Alphabet	
A	Cross-Section Area	mm^2
a	Acceleration	m/s^2
a	System-Specific Constant Value	-
a_{tr}	Semi-Major Axis Transfer Orbit	km
B	Earth's Magnetic Field	Tesla
C	Chapman Constant	$kW/m^{3/2}$
C_3	Characteristic Energy	km^2/s^2
C_D	Drag Coefficient	m/s^2
C_p	Heat Capacity	J/kgK
C_r	Reactant Consumption Rate	kg/Whr
c	Speed of Light in Vacuum	m/s
D	Drag	N
D	Residual Dipole	Am^2
d	Projectile Diameter	cm
d_{Earth}	Distance from Sun to Earth	km
d_{Mars}	Distance from Sun to Mars	km
E	Modulus of elasticity	MPa
E	Energy	J
e_{tr}	Eccentricity of Transfer Orbit	-
F	Visibility Factor	-
F_{tu}	Allowable Tensile Stress	MPa
F_s	Solar Radiation Force	N
F_{ty}	Allowable Yield Stress	MPa
f_1	Technical Development Status Factor	-
f_2	Technical Quality Factor	-
f_3	Team Experience Factor	-
f_{cu}	Elastic Buckling	MPa
f_t	Tensile Stress	MPa
G_y	Radiation Dose	-
G	Antenna Gain Receiver	-
G	Gravitational Constant	$m^3kg^{-1}s^{-2}$
g_0	Gravitational Constant of the Earth Surface	m/s^2
H_{eff}	Effective Heat of Ablation	-
h	Momentum	Ns
h_{park}	Height of Parking Orbit	km
h_{fly-by}	Fly-by Altitude at Mars	km
I	Moment of Inertia	mm^4
i	Angle of Incidence of the Sun	deg
J_a	Albedo Intensity	W/m^2
J_s	Solar Constant	W/m^2
k	Boltzmann Constant	J/K
L_{f_s}	Propagation Loss for a Signal	dB
L_{other}	Link Loss Other	dB
L	Distance	m
M_{max}	Maximum Bending Moment	N.mm
M	Magnetic Moment of the Earth	$Tesla*m^3$

M	Projectile Mass	g
m	Capsule Mass	kg
m_b	Bumper Areal Density	g/cm^2
m_{Mars}	Mass Mars	kg
m_s	Mass Spacecraft	kg
m_{Earth}	Mass Earth	kg
m_w	Kevlar Rear Wall Areal Density	g/cm^2
n_x	Load Factor in x-Direction	g
$n_{y,z}$	Load Factor in y,z-Direction	g
P	Power	W
P_c	Compressive Force	N
P_{sun}	Power of the Sun	W
p_b	Burst Pressure	Pa
p	Internal Pressure	MPa
Q	Heat	W
q	Reflectance Factor	-
R_{Mars}	Orbit radius Mars	km
R_n	Nose Radius	m
r	Radius of Cylinder	mm
r_{dep}	Distance from the Sun at Departure Position	km
r_{Earth}	Radius of Earth	km
r_{Mars}	Radius of Earth	km
r_{tar}	Distance from the Sun at Target Position	km
S_{ref}	Surface Area	m^2
S	Distance from Sun to Destination	km
S	Gap Distance	cm
SR	Spinning Rate	deg/s
T	Thrust	N
T	System Noise Temperature of Noise Ratio	-
T_D	Disturbance Torque	Nm
T_{tr}	Transfer Time	days
T_{total}	Period of Revolution	days
$T_{Earth,Arrival}$	Arrival Time at Earth	mm/dd/yyyy
$T_{Earth,Departure}$	Departure Time at Earth	mm/dd/yyyy
T_g	Gravity Gradient Torque	Nm
T_m	Magnetic Field Torque	Nm
T_{sp}	Solar Radiation Torque	Nm
$T_{Mars,Arrival}$	Arrival Time at Mars	mm/dd/yyyy
$T_{Mars,Departure}$	Departure Time at Mars	mm/dd/yyyy
t	Burn time	s
t_{hs}	Heat Shield Thickness	[m]
t_w	Kevlar Rear Wall Thickness	cm
V	Velocity	m/s
V_c	Local Circular Velocity	m/s
V_{c0}	Circular Velocity of Parking Orbit	km/s
V_{Earth}	Heliocentric Velocity of the Earth	km/s
V_{Mars}	Heliocentric Velocity of Mars	km/s
V	Volume	m^3
V_0	Velocity in Pericenter around Departure Planet	km/s
V_∞	Hyperbolic Escape Velocity	km/s
$V_{\infty,1}$	Excess Velocity at Earth	km/s
$V_{\infty,2}$	Excess Velocity at Mars	km/s
$V_{Mars,Arrival}$	Heliocentric Arrival Velocity at Mars	km/s
$V_{Mars,i}$	Initial Heliocentric Velocity of Mars before GA	km/s

$V_{Mars,f}$	Final Heliocentric Velocity of Mars after GA	km/s
V_n	Normal Component of Projectile Velocity	km/s
$V_{Earth,Arrival}$	Heliocentric Arrival Velocity at Mars	km/s
$V_{s,i}$	Initial Heliocentric Velocity of the Spacecraft before GA	km/s
$V_{s,f}$	Final Heliocentric Velocity of the Spacecraft after GA	km/s
ΔV	Change in Velocity	km/s
ΔV_{park}	Change in Velocity to go into Parking Orbit	km/s
ΔV_0	Change in Velocity to Enter TMI	km/s
w	Load per Unit Length	N/m
W	Weight	N
$w_c b$	Radial Velocity	[rad/s]
	Greek Alphabet	
α	Solar Absorptivity	-
β	Ballistic Coefficient	-
γ	Correlation Factor	-
ϵ	Emissivity	-
η_{fc}	Fuel Cell System Efficiency	-
θ	Plasticity Correction Factor	-
θ	Impact Angle from Target Normal	deg
θ	Maximum Deviation of the z-axis from Local Vertical	deg
$\ddot{\theta}$	Angular Acceleration	deg/s
κ	Thermal Conductivity	W/mK
λ	Carrier Wave Length	m
μ_{Earth}	Gravitational Constant of the Earth	km^3/s^2
μ_{Mars}	Gravitational Constant of Mars	km^3/s^2
μ_{Sun}	Gravitational Constant of the Sun	km^3/s^2
ϕ_{tank}	Tank Mass Factor	m
ρ	Atmospheric Density	kg/m^3
ρ_0	Atmospheric Density at Sea Level	kg/m^3
ρ_p	Projectile Density	g/cm^3
$\sigma_{p,long}$	Longitudinal Stress	MPa
$\sigma_{p,hoop}$	Hoop Stress	MPa
σ	Axial Stress	MPa
σ	Stefan-Boltzmann Constant	W/m^2K^4

Contents

Chapter 1

Introduction

Mars has been an object of fascination for humanity since the time of the ancients. Up until this day, there have been numerous notable milestones from the early telescopic observations of Galileo and Huygens to the modern era of spacecraft-based exploration. Since the Mariner 4 fly-by in 1964, there have been several dozen spacecraft sent to Mars. Now, in the 21st century, a new era of spaceflight has set upon mankind as it gets its first chance to become a multi planetary species. In order to prepare for the colonization of Mars and taking the first step, an idea of a manned spacecraft mission to Mars and back was introduced by the Mars community. Flying a manned spacecraft to Mars could give the "spark" again to the Space Industry and become a catalyst for growth, education, knowledge and global leadership around the world. The mission would not only be an inspiration to the people but also a success of the whole mankind.

The Inspiration Mars project, launched by the Mars Society, has become the innovators' beacon to contribute to this extraterrestrial adventure. The project aims to design an end-to-end fly-by mission to Mars by the year 2018. Next to this mission objective, the Mars society stated that the mission should be as cheap, safe and simple as possible [1]. This groundbreaking challenge has inspired the student team of Delft University of Technology, I.M. Delft (Inspiration Mars Delft), and it has motivated the team to perform a thorough investigation on this suggested mission. Working as a team of ten Aerospace Engineering students, and part of the Aerospace Faculty education program, knowledge from both academic and professional resources are used in a scientific, yet creative, approach.

The findings of this study are presented in this final report, aiming to guide the reader through a scientific journey in which the final design arose. This starts by presenting the Project Organization and Mission Overview in chapter 2, wherein the general project organization and a flow of the mission are described. Also an approach to sustainability, to safety and one to the verification and validation of the results is given. Next in chapter 3, the journey of the spacecraft is presented wherein the trajectory is analyzed. In chapter 4, the re-entry characteristics of the spacecraft to Earth are given. Next, in chapter 5, the Spacecraft System Characteristics are presented, covering all the sub-system designs. Chapter 6 includes the crew specifications. Then, in chapter 7, a cost and market analysis is given. In chapter 8, a risk analysis of the mission and all its sub-systems is made. Next, in chapter 9 a reliability, availability, maintainability and safety analysis is performed. In chapter 10 the operations and logistics plan of the mission is presented. Next to last, in chapter 11, the final design overview is given. Finally, in the last chapter, a conclusion and recommendations are given for future studies.

Chapter 2

Project and Mission Overview

The overview of the project and the mission is discussed in this section. In section 2.1 an introduction to the mission is given. Then, the mission development in terms of a functional flow diagram and a functional breakdown structure is explained in section 2.2. Additionally, the verification and validation approach is discussed in section 2.3. Once concluded, the sustainable development strategy is given in section 2.4. To conclude this chapter, in section 2.5 the margins and safety factors used during the design process are indicated. This chapter therefore gives a global understanding of the mission and the design process.

2.1 Mission Introduction

Humanity has lost its drive for space exploration. After the Apollo missions there has not been a manned mission to another body within the solar system. A spark needs to be made which will reignite manned space exploration to other worlds. Inspiration Mars Delft (I.M. Delft) wants to generate that spark. I.M. Delft's vision statement is to inspire humanity by taking the next step towards setting a footprint on Mars. This will be accomplished by designing the first end-to-end Mars fly-by mission for a crew of two. This mission needs to be as safe, simple and cost effective as possible. This mission will be a step towards sending a man to Mars. Since it is an end-to-end mission, all aspects from launch to Earth re-entry need to be considered. The mission's launch date is January 2018 and will approximately take 500 days to complete. The crew of two will have to endure launch, in orbit assembly, Trans Mars Injection, a Martian fly-by and Earth re-entry. While on the mission, the safety and well-being of the crew is the number one requirement. To ensure their safety, all systems must be designed with safety and reliability in mind. To reduce the cost and complexity of the mission, a simple design needs to be made. To achieve this, off-the-shelf components are preferred. The design must be made by complying to all the requirements.

2.2 Mission Development and Organization

The I.M. Delft mission is relatively simple but very extensive. Therefore, a Functional Flow Diagram (FFD) and a Functional Breakdown Structure (FBS) are made. In each of these diagrams the mission is split into multiple sections, where the function of each section is identified. The FFD is explained in section 2.2.1 and the FBS is explained in section 2.2.2

2.2.1 Functional Flow Diagram

The FFD divides the mission into ten phases. Each phase has multiple functions which are required to occur in a specific order. The FFD is shown in figure 2.1. As can be seen in the diagram, each phase is identified along with the corresponding functions. During a critical phase, the functions may lower until the third level. These functions in turn, determine the required procedures and systems required. If these functions are met from start to end, the mission will be a success.

2.2.2 Functional Breakdown Structure

The FBS indicates multiple phases within a group. In order to complete the mission, the functions within that group need to be executed correctly. The FBS is shown in figure 2.2. Different to the FFD, the breakdown illustrates functions that each system needs to accomplish in the mission. Therefore, the breakdown is not time distributed but system distributed. It can be seen what function is completed by which system.

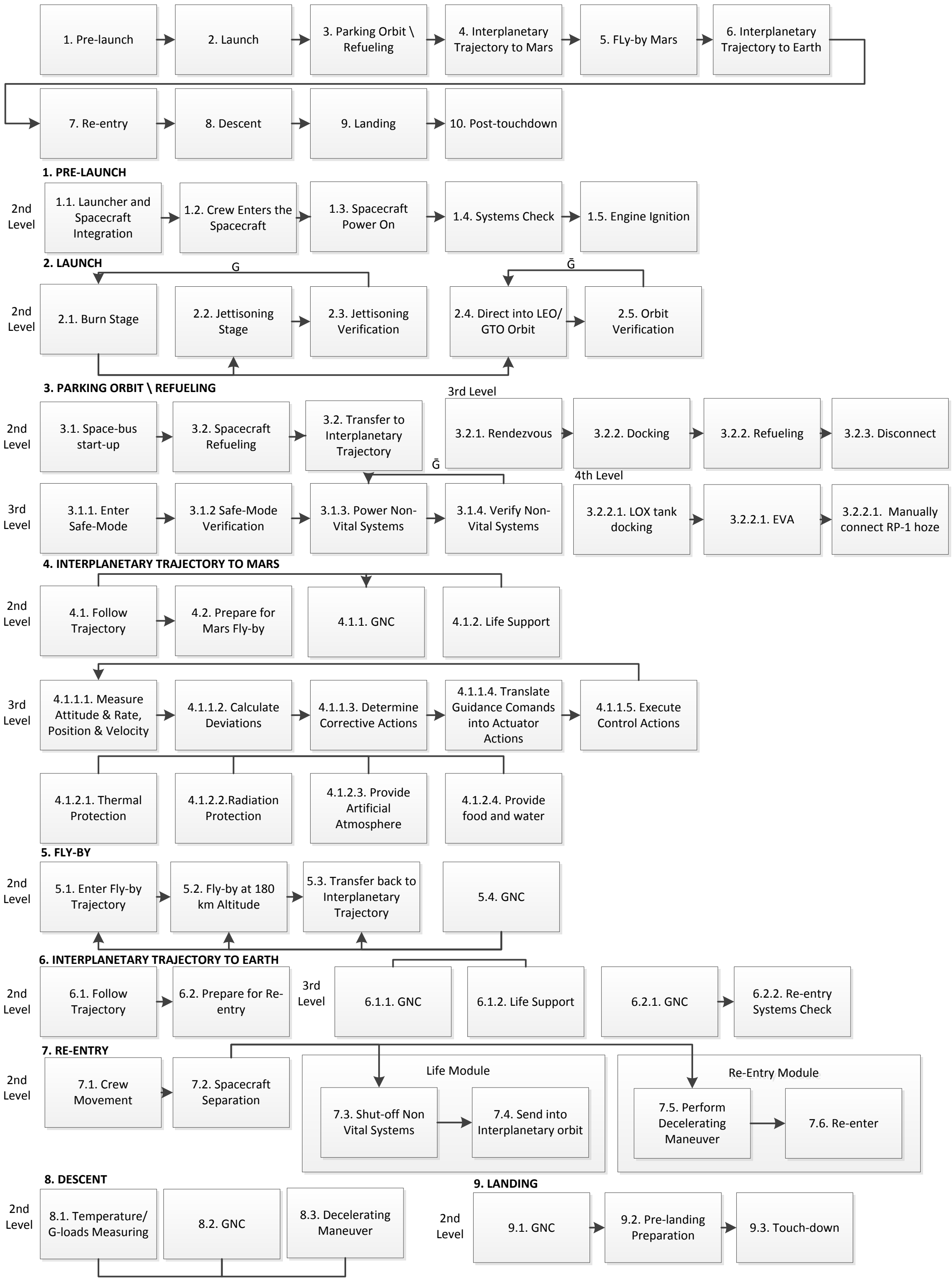

Figure 2.1: Inspiration Mars Delft Functional Flow Diagram

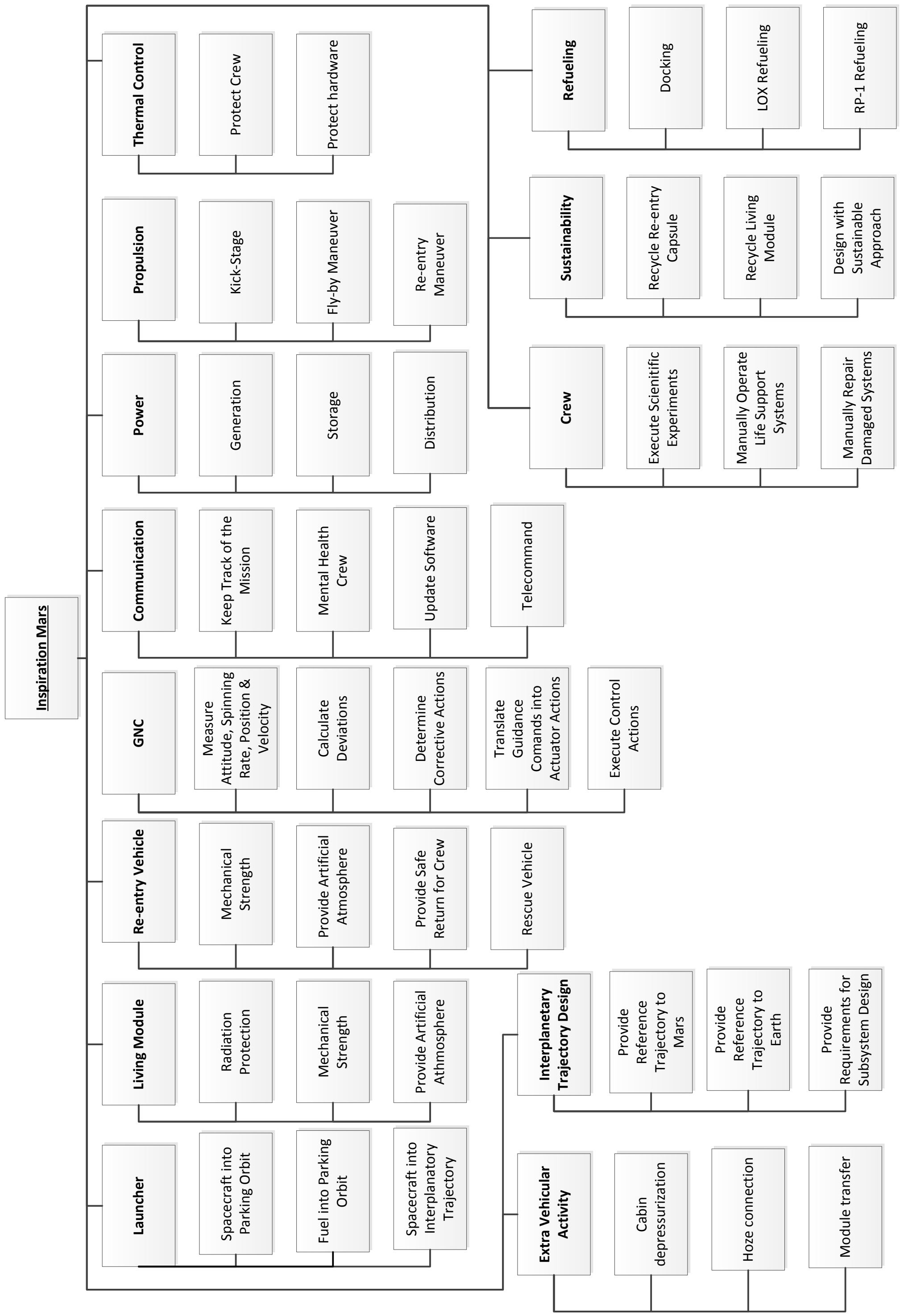

Figure 2.2: Inspiration Mars Delft Functional Breakdown Structure

2.3 Verification and Validation Approach

To ensure that a model is correct, it must be verified and validated. The general verification and validation procedure that takes place in the design is explained in this section. Verification provides compliance of a model by using equations or other independent models. During the design process, verification must be introduced before determining system characteristics with a newly generated model. The verification procedure that is used varies per sub-system. Each verification procedure used for a sub-system is discussed in the section of the sub-system. Validation provides compliance of the model to real life experiments or situations. Validation also differs per sub-system and is explained per sub-system. In general, verification and validation is an important part which shows compliance of a model with the requirements.

2.4 Sustainable Development Strategy

In order to make I.M. Delft adhere to the sustainable requirements of today, a strategy was developed. This strategy has been and will be implemented at every stage of mission. Sustainability is not a deliverable but a mindset, resulting in long- and short term strategies for a mission. These strategies are explained in section 2.4.1. Each phase of the mission has a strategy applicable to it. Sustainable strategies are developed for launch, in-orbit assembly, Trans Mars Injection (TMI), the Mars fly-by and re-entry. These strategies are shown in table 2.1 in section 2.4.2. Additionally, the manufacturing and end-of-life disposal is accounted for. This topic is discussed in section 2.4.3.

2.4.1 Long- and Short Term Strategy

The sustainability strategies are composed of two groups. These two groups are long- term and short term strategies. Long term strategies aim at completing sustainability goals which have an effect on the environment over a longer period of time[2]. These strategies are applied to I.M. Delft, so that future Mars missions can benefit from them. The long term strategies are stated below.

- Provide data that is measured, using the scientific payload for future studies.
- Developing reusable components that cause less damage to the environment.
- Minimizing environmental impact during the development phase, by using off-the-shelf components.
- Developing an approach that aims to decrease the use of fossil fuels and reduce greenhouse gas emissions.

A short term strategy is a sustainable approach which has direct effect on its environment. Listed below are the short term strategies which are used during the mission's design [2]. The short term strategies are stated below.

- Solar panels generate all the needed energy.
- The launcher's strap-on boosters will be recovered after launch and reused for future missions.
- The water is recycled during the trip.
- Waste is stored in the walls of the spacecraft to be reused as radiation protection.
- The use of toxic materials is minimized in the development- and final design.
- All jettisoned spacecraft components are either sent into a graveyard orbit or disintegrate in Earth's atmosphere to reduce space debris.
- The jettisoned spacebus at the end of the mission will be used as a deep space measuring satellite.
- The most energy efficient orbit is used.
- Requirements are analyzed to reduce the use of resources.
- Fuel cells are used to generate water, decreasing the amount of water stored on board.
- A human dynamo machine is used to generate power and provide the necessary exercise for the crew.
- Left-over components, like a re-entry capsule, are put on display in a history museum.

2.4.2 Sustainability Table

Table 2.1 indicates the strategy used during each phase of the mission. From the strategies, main design parameters are identified which take them into consideration.

Table 2.1: Sustainability strategy during each phase of the mission

Number	**Strategy**	**Resulting Design**
1. Launch		
1.a 1.b	Reduce emissions Use light weight material	Two rocket system using in-orbit refueling with compatible systems.
2. In orbit assembly		
2.a 2.b	Reduce the use of energy demanding machinery Decrease propellant used for maneuvering	EVA are performed to reduce machinery and no pressurized docking is required
3. Trans-Mars Injection		
3.a 3.b 3.c	Use renewable energy for power Use power efficiently Recyle waste generated	Solar panels generate power for simple and efficient sub-systems, one of which is recycling bodily waste
4. Mars Orbit		
4.a 4.b	Increase sustainable knowledge Reduce pollution to atmosphere	Scientific payloads are carried to analyze the Martian atmosphere without waste
5. Earth re-entry		
5.a 5.b	Decrease carbon footprint Reduce waste generated	Trajectory is determined which uses minimal ablative material

As can be seen in table 2.1, sustainable development is present in every part of the mission. Some important strategies are recycling waste, decreasing emissions and increasing efficiency. Increasing mankind's sustainable knowledge by performing experiments on Mars is also an important strategy. All in all, it can be seen that sustainability is a determining factor for the mission design.

2.4.3 Manufacturing and Disposal

The sustainable mindset must be applied before, during, and after the mission. Therefore, the strategies must be present during all phases. During manufacturing, the reduction of waste and emissions is crucial. I.M. Delft plans on reducing these factors in multiple ways.

The design focuses on using off-the-shelf components, and this results in the use of systems which have already been tested. Therefore, less tests have to be conducted, resulting in a decrease of waste and emissions. The transportation during manufacturing will also be kept to a minimum, increasing the sustainability. Furthermore, recyclable components are used as much as possible. If this strategy is used during development, this mission's manufacturing process will be as sustainable as possible.

I.M. Delft's strategy aims at decreasing the waste, generated at the end of the mission. To accomplish this, two disposal steps are introduced. The first is to use the orbiting spacecraft as a measuring system after the re-entry vehicle with the crew is detached. This vehicle is then sent into a deep space orbit causing its remaining fuel to deplete. Throughout its lifetime, it will continue to measure and send data until the power source reaches its end-of-life. This will provide a unique opportunity for the science community to take full advantage of scientific payload on board, long after the mission is completed. The second disposal step is the recycling of the re-entry vehicle. This vehicle can be sold to a museum, which will result in revenue and increase the sustainability. This procedure can also be applied to retrieved launch vehicle components during launch. This two-step disposal system will guarantee compliance with the sustainability requirements.

2.4.4 Conclusion

Sustainable development is conducted at every stage of the mission. Having a sustainable mission means that the environmental harm from all aspects of the mission are taken into account and minimized. Using the indicated strategies in sections 2.4.1 through 2.4.3, I.M. Delft aims to meet all sustainability requirements. Sustainability is not a parameter that must be taken into account, but a state of mind during every stage of the mission's lifetime.

2.5 Margins Approach

In the development phase of a mission, margins and safety factors are added to ensure that the design meets all sensitivity demands. Due to the scale of the design, not all sub-systems can be designed to their final state. Therefore, uncertainties are taken into consideration. The margins used for the I.M. Delft design are identical to the European Space Agency (ESA) margins [3]. The general design margins are discussed first, followed by a table identifying the sub-system margins.

The ESA design margins are split into three categories. These categories are:
- 5% for fully developed items
- 10% for items to be modified
- 20% for items to be developed

If a sub-system uses a combination of items varying in development level, equation 2.1 is used.

$$margin_{subsystem} = \frac{\sum_{all} X_{item} \times margin_{equipment}}{\sum_{all} X_{item}} \tag{2.1}$$

As can be seen, an average of the margins of each item is taken and this results in the final margin for that sub-system. Other specific margins are identified in table 2.2.

Table 2.2: Margins for Spacecraft systems

Number	**System**	**Margin**	**Unit**
1.0	Dry mass of spacecraft	10	[%]
2.1	Propellant mass for maneuvers	5	[%]
2.2	Propellant mass for AOCS thruster	100	[%]
3.0	Delta-V required for mission	10	[%]
4.0	Data processing mass memory	50	[%]
5.1	Data processing computing power	100	[%]
5.2	Communication link budget	3	[dB]
6.0	Equipment temperature	±10	[°C]
7.0	Required spacecraft power budget	10	[%]

The margins identified in table 2.2 can be applied to every aspect of the mission to ensure that all uncertainties are taken into consideration.

Chapter 3

Trajectory Design

The trajectory design chapter is divided into five main parts. The first part consists of section 3.1 where the trajectory design is introduced and the specific mission requirements, imposed by the Inspiration Mars design competition, are given. Next, the assumptions, the transfer type, software and reference data used will be given in order to understand how the trajectory was designed. The second part of this chapter consists of the actual design, analysis and optimization process in order to determine an optimized trajectory for Earth departure. The third main part exists of the verification and validation of the calculated trajectory and used software. In the fourth part, a sensitivity analysis of the trajectory is given. The last part describes further recommendations which can be taken for further analysis and more detailed design.

3.1 Trajectory Introduction

3.1.1 General Information

From the assignment [4], a relative large degree of freedom is given in deciding how to perform a free-return fly-by Mars mission. However, the wish is to have the shortest, minimal cost and safest mission possible that can be launched around the beginning of January 2018 [1]. Due to the planetary alignments, there are only a few trajectories possible that are viable for this mission. In order to determine these trajectories, first a solution is given to the Lambert Problem together with a launch window that meets the mission constraints. Once an initial guess for the launch date is determined, the fly-by characteristics and date are optimized for a fly-by altitude requirement of 180 km [4]. Finally the return trajectory and arrival at Earth is determined which is directly related to the fly-by characteristics and the outbound trajectory. These impose limitations for the Earth return trajectory and are taken into account from the beginning. Afterwards, the results are verified by comparing them with the trajectory obtained by the Inspiration Mars community [5]. Finally, the software is validated using the Mariner 10 mission from 1973 [6] as a benchmark.

3.1.2 Trajectory Related Requirements

The main requirements, imposed by the project guide and Inspiration Mars competition rules [4, 1], are the following:

- Launch Date: January 2018.
- Mars Fly-by Free-Return Trajectory.
- Fly-By Altitude 180 km.

From the leading requirements, the following sub-requirements also need to be considered:

- A 200 km Earth parking orbit at 28.5 deg inclination is required to provide a possibility for docking, refueling, Extra Vehicular Activity (EVA), and to provide test and checkout of the spacecraft and transfer vehicle systems.
- The Earth Arrival speed should not exceed 14.2 km/s [30].
- Use a 10% safety margin for the velocity budget to take into account trajectory perturbations and correction maneuvers [3].

3.1.3 Assumptions

In order to calculate the transfer trajectory the following assumptions are made:

- During maneuvers, velocity changes of the spacecraft due to propulsive effects, occur instantaneously.
- The initial parking orbit is circular.
- The planet positions and velocities are modeled using the Jet Propulsion Lab (JPL) DE 421 ephemeris from the National American Space Agency (NASA) [7].
- Patched conics theory is used which includes planets having a non-zero Sphere of Influence (SOI) [8].
- The mass of the spacecraft is negligible with respect to that of other bodies.
- No collisions will occur with asteroids, comets, natural or man-made satellites.
- Lift over drag ratio is assumed to be too small to use an aerogravity assist.
- Trajectory perturbations such as unsymmetrical Earth (2nd order), third body effects (2nd order), solar radiation (2nd order), atmospheric drag (2nd order) and others like relativity (3rd order) are neglected [25].

3.1.4 Trajectory Transfer Type

In the previous delivered Midterm report [9], after a preliminary option elimination, four main trajectory options were available. From these four options, a trade-off was made in order to determine the optimal transfer trajectory. Finally, a conclusion was made and the optimized Earth-departure free-return trajectory was chosen.

Optimized Earth-Departure Free-Return Trajectory

The spacecraft will leave Earth in a hyperbolic escape trajectory until the end of the Earth's SOI. Then the spacecraft will travel to Mars in an elliptical trajectory around the Sun. Next, it arrives in a hyperbolic trajectory at Mars where it performs a fly-by and leaves again in a hyperbolic escape. It leaves Mars' SOI and flies in an elliptical trajectory back to Earth where the spacecraft will re-enter the Earth's atmosphere. The trajectory will be optimized for departure. This means it requires the least change in velocity, which reduces the fuel budget, needed to perform the a Trans Mars Injection (TMI) and meet all the mission requirements within the constraints.

3.1.5 Numerical Solution Software

To be able to determine a feasible trajectory by 2018 for the Mars fly-by mission, various existing trajectory determination programs were examined, in order to prevent to have to redo work that does not necessarily has to be redone. After a selection on availability, legal issues, ease of use and available knowledge; the programs that were useful were selected and are further presented below.

TUDAT

The Technological University of Delft Astrodynamic Toolbox (TUDAT) is a set of C++ software libraries, developed and maintained by staff and students in the Astrodynamics and Space Missions research group at the Faculty of Aerospace Engineering of the Delft University of Technology. The guide for the TUDAT Course: Interplanetary Orbit Transfers is used[10]. This guide contains among other things a Mars sample return mission with a stay-over. Using the accompanying C++ code from the TUDAT library [11], the code variables can be adjusted to obtain the applicable trajectory needed for the Inspiration Mars mission.

GMAT

The General Mission Analysis Tool (GMAT) is an open-source space mission design tool developed by a team of NASA, private industry, public and private contributors [12]. The program is able to make space trajectory simulation, analysis, and optimizations. The programming code is written in C++. Externally, the software has already been used by entities as varied as the Air Force Research Lab, Iowa State University, and the European Space Agency [13].

MATLAB

MATLAB, developed by MathWorks, is a high-level programming language and interactive environment for numerical computation, visualization, and programming. The software is able to analyze data, develop algorithms, and create models and applications. A MATLAB script, made by David Eagle [14], is used to calculate the viable trajectories. The script specifies the launch, fly-by and destination planets, and the desired fly-by altitude. Therefore, the algorithm also requires initial guesses for the launch, fly-by and arrival calendar dates. The script then searches for a patched-conic gravity-assist trajectory that satisfies the flyby mission constraints (V_∞ matching a user-defined flyby altitude). It is also possible to minimize the launch, arrival or total impulsive ΔV for the mission with the program. The planet positions and velocities are modeled using the JPL DE 421 ephemeris. The trajectory optimization is performed with the SNOPT nonlinear programming (NLP) algorithm [15].

3.1.6 Astronomical and Mission Reference Data

Below, in table 3.1, all the required data is given to follow the steps taken in the trajectory determination section 3.2. Data from Venus is given as well in order to see if Venus would cross the spacecraft's trajectory and therefore influence the trajectory.

Table 3.1: Astronomical and mission reference data [16, 17, 18, 19]

Parameter	**Unit**	**Sun**	**Venus**	**Earth**	**Mars**
Standard Gravitational parameter	km^3/s^2	132712400018.9	324858.599	398600.436	42828.314
Mass	10^{24} kg	1988500	4.8676	5.9726	0.64174
Equatorial Radius	km	696000	6051.9	6378.14	3397.0
Mean Distance to Sun	AU	-	0.72	1.00	1.52
Escape Velocity	km/s	617.6	10.36	11.19	5.03
Sphere-of-influence radius	10^5 km	$\simeq$ 149597871	6.1628	9.246	5.772
Semi-major Axis	10^6 km	-	108.21	149.60	227.92
Period	days	-	224.701	365.256	686.98
Perihelion	10^6 km	-	107.48	147.09	206.62
Aphelion	10^6 km	-	180.94	152.10	249.23
Average Orbital Velocity	km/s	-	35.02	29.78	24.13
Orbit Inclination	deg	-	3.39	0.00	1.850
Fly-by altitude	km	-	-	-	180
Parking Orbit Altitude	km	-	-	200	-

3.2 Trajectory Determination

To be able to design a interplanetary trajectory, transfer orbits between planets need to be determined. This can be done using so-called Lambert targeting which is explained in section 3.2.1. Afterwards the solution obtained through a MATLAB script is explained and analyzed. Finally a TMI launch window is made wherein the spacecraft could start its journey to Mars.

3.2.1 Lambert Targeting

The Lambert problem is actually a way of defining the problem of determining a trajectory that passes between two positions within a specified time of flight (TOF). This is a classic astrodynamic problem which is also known as the orbital Two-Point Boundary Value Problem (TPBVP) [20, 21]. The Lambert theorem states that the time to traverse a trajectory depends only upon the length of the semi-major axis of the transfer trajectory, the sum of the distances of the initial and final positions relative to a central body, and the length c of the chord joining these two positions. Specified for the the Mars fly-by mission, if the position of Earth and Mars is known on some given day, and the maximum time it should take to go to Mars, the departure conditions needed at Earth can be determined.

Solution to Lambert Problem - Porkchop Plot (TUDAT)

In the Midterm Report [9], a Lambert targeting using TUDAT was used for the outbound trajectory to Mars and for the total mission. However, the software was primarily used for an energy-efficient (Hohmann) transfer to Mars and having a stay-over before coming back. Using a gravity assist was not incorporated in the software. The software was modified for having a stay-over of zero days, then coming back to Earth. However, the dates are used in the MATLAB program as initial guesses wherein the program searches within a boundary large enough to provide reliable results.

The results of the solution for the Lambert problem can be represented in a "pork-chop" plot. These are computer-generated, contour plots that display the launch date and arrival date characteristics of an interplanetary flight path for a given launch opportunity to Mars or any other planet. For this mission, the results from TUDAT for the complete transfer are given in figure 3.1 and table 3.2. As one can see in the plot, the lowest change in velocities happens at the given mark within the area where the TOF is within the constraints. The closest date to the target with the lowest ΔV and TOF, is on the 26th of February 2018.

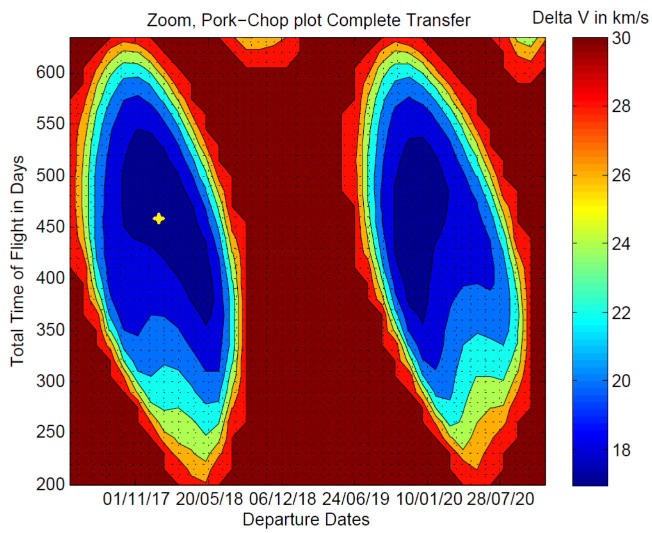

Figure 3.1: Pork-Chop plot for the total transfer, zoomed in (generated with TUDAT).

Table 3.2: Possibilities complete mission

Departure Date	Transfer Time [days]	Minimum Δ V [km/s]
25/07/18	800	13.81
26/02/18	455	16.96

3.2.2 Trajectory Solution - Departure Optimized (MATLAB)

The program used to determine the final trajectory, which includes a fly-by segment, uses a couple of steps in order to give an estimation of the departure, fly-by and arrival date. First an initial guess is given to the departure date. Using the JPL DE 421 ephemeris data, it determines the position and velocity of the Earth at that date. Also a boundary of 200 days (based on the TUDAT launch window) is given wherein the program will search later on to optimize the trajectory for departure and the required fly-by altitude. The same is done for the fly-by and arrival dates. The next step of the program is calculating the optimum Lambert solution and the initial velocity vector for the outbound trajectory. It also calculates the launch ΔV vector from the launch planet's velocity vector and the initial velocity vector of the first leg of the trajectory. The following step, repeats the same process for the second leg and determines the initial and final velocity vectors. Finally, in the last step, the program couples these legs together with a fly-by segment and the required fly-by altitude. It matches the incoming and outgoing V_∞ of the spacecraft with many iterations and checks if the required turn angle can be achieved. An overview of the main inputs and outputs for an Earth optimized departure is given in tables 3.3 and 3.4. Afterwards, a more detailed analysis of the departure, fly-by and Earth arrival segment is given.

Table 3.3: MATLAB inputs

Input	Value
Departure Date Guess	26/02/2018
Fly-by Date Guess	1/10/2018
Arrival Date Guess	1/6/2019
Days Boundary Search	200 days
Mars Fly-by Altitude	180 km
Parking altitude	200 km
Inclination	28.5 deg

Table 3.4: Result Earth departure optimized

Output	Value
Departure Calender Date	6/1/2018
Mars Fly-by Date	20/8/2018
Earth Arrival Date	22/5/2019
Mars Fly-by Altitude	180 km
Total TOF	500.83 days

3.2.2.1 Launch into Low Earth Parking Orbit

Prior of launching the spacecraft into a TMI. a parking orbit is required to be able to perform a rendez-vous with the refueling tank. This parking orbit was set at 200 km at an inclination of 28.5 deg due to the available performance provided by the Falcon Heavy from SpaceX [22]. The circular velocity of the spacecraft required can then be calculated with equation 3.1.

$$V_{circ,LEO} = \sqrt{\frac{\mu_{Earth}}{r_1}} = \sqrt{\frac{\mu_E}{h_{park} + r_{Earth}}} = 7.7843 \text{ km/s} \tag{3.1}$$

Where μ_{Earth} is the gravitational parameter of Earth $V_{circ,LEO}$ the circular velocity at LEO and r_1 the radius of the Earth (r_{Earth}) plus the height of the parking orbit (h_{park}).

3.2.2.2 Earth Departure

The Earth departure will require a change in velocity which will occur at the perigee of the new TMI orbit. From the program, the excess velocity required to perform the injection at the 6th of January 2018, is calculated to be 6.205 km/s. With this value known, the required change in velocity can be calculated to reach this excess velocity with equations 3.2 and 3.3.

$$V_{peri,dep} = V_1 = \sqrt{\frac{2\mu_{Earth}}{r_1} + V_{\infty,dep}^2} = 12.639 \text{ km/s} \tag{3.2}$$

$$\Delta V_{TMI} = V_{peri,dep} - V_{circ,LEO} = 4.855 \text{ km/s} \tag{3.3}$$

Where $V_{peri,dep}$ is the velocity at perigee w.r.t. the Earth,$V_{\infty,dep}$ the departure excess velocity and ΔV_{TMI} the change in velocity required for TMI.

3.2.2.3 Mars Fly-By - Gravity Assist

In order to let the spacecraft return to Earth without having to do a propulsive maneuver, it can use a gravity assist from Mars to change its trajectory and velocity. The spacecraft is in a heliocentric orbit until it crosses the boundary of Mars' SOI. After crossing this boundary, the effect of the Sun is neglected and it goes into a hyperbolic orbit around Mars with an excess velocity V_∞ which is equal to the difference in their heliocentric speeds. The spacecraft will leave Mars' SOI with the same excess velocity but at a different angle. This angle is called the turn angle δ. The gravity assist is further explained on the next page.

Gravity Assist Principle

During an interaction between a planet and a spacecraft the momentum is conserved:

$$m_s\ V_2 + m_{Mars}\ V_{Mars}^{-} = m_s\ V_3 + m_{Mars}\ V_{Mars}^{+} \tag{3.4}$$

Where m_s is the mass of the spacecraft, m_{Mars} the mass of Mars, V_2 and V_3 the spacecraft's heliocentric velocity before and after the gravity assist respectively. V_{Mars} is the heliocentric velocity of Mars, both with respect to the heliocentric reference frame. Superscripts $-$ and $+$ represent the initial and final SOI arrival and departure respectively. Rewriting equation 3.4, it is found that:

$$V_{Mars}^{+} - V_{Mars}^{-} = \frac{m_s}{m_{Mars}}(V_2 - V_3) \tag{3.5}$$

Since the mass of the spacecraft (+-15000 kg) is really small compared to the mass of Mars, the indicated mass fraction is approximately zero. Hence, the assumption is made that the speed of the planet remains the same after the fly-by. However for the spacecraft the speed will change. Taken at a sufficiently large distance the spacecraft's velocity with respect to the planet is equal to the hyperbolic excess velocity. Applying energy conservation in the planet reference frame results in the notion that, although the direction is different, the magnitudes of V_∞^- and V_∞^+ are the same. Figure 3.2 shows that if the satellite passes behind the planet, a modest gravitational deflection aligns V_∞ more with V_{Mars} and thus $|V_3| > |V_2|$; the spacecraft accelerates. Passing in front of the planet, the opposite takes place, so the spacecraft slows down.

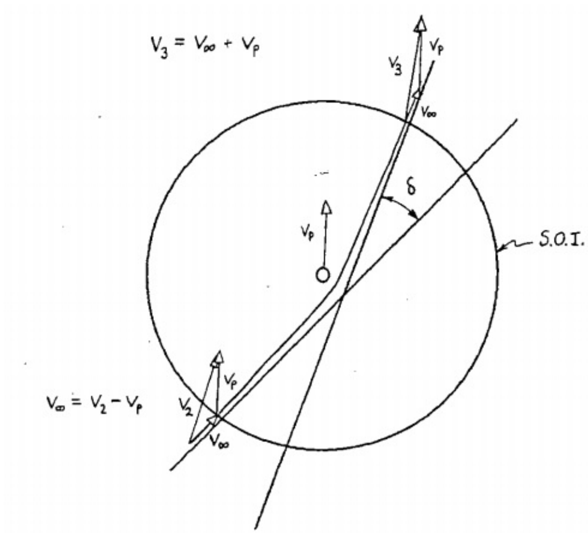

Figure 3.2: Fly-by illustration

Increase in Heliocentric Velocity

The vector relationships between the incoming v-infinity vector V_∞^- , the outgoing v-infinity vector V_∞^+ and the two legs of the heliocentric transfer orbit are as follows:

$$V_\infty^- = V_{Mars} - V_2 \tag{3.6}$$

$$V_\infty^+ = V_3 - V_{Mars} \tag{3.7}$$

Where

V_{Mars} = heliocentric velocity vector of the flyby planet at the flyby date
V_2 = heliocentric velocity vector of the first transfer orbit at the flyby date
V_3 = heliocentric velocity vector of the second transfer orbit at the flyby date

With the excess velocity determined by the program to be 5.432 km/s, the spacecrafts velocities were calculated from where the total change in velocity was determined with the following equation:

$$\Delta V_{flyby} = V_2 - V_3 = 3.136 \text{ km/s} \tag{3.8}$$

Fly-by Velocity at Mars

The moment the spacecraft reaches its closest distance to Mars (180 km), it is the pericenter of a new hyperbolic trajectory around Mars. The velocity at this point can be calculated with the following equation:

$$V_{peri,Mars} = \sqrt{\frac{2\mu_{Mars}}{r_2} + V_\infty^2} = \sqrt{\frac{2\mu_{Mars}}{h_{flyby} + r_{Mars}} + V_\infty^2} = 7.30 \text{ km/s} \tag{3.9}$$

Where r_2 is equal to the sum of the radius of Mars (r_{Mars}) and the fly-by altitude at Mars (h_{flyby}). μ_{Mars} is the gravitational constant of Mars and V_∞ the excess velocity at 180 km from the surface of Mars ($V_\infty =$ 5.42 km/s).

Turn Angle

Mars can only provide a maximum turning angle which is dictated by its radius, mass and indirect its atmosphere, as hitting the planets' atmosphere can cause the spacecraft to decelerate and enter an orbit around the planet or even crash on the planet's surface. However, due to the requirement of a 180 km fly-by, the influence of the Martian atmosphere is neglected as its density is very small [16]. Mars also has a minimum fly-by altitude which can be assumed, for now, to be equal to the radius of Mars. Now the maximum and actual turn angle can be calculated, given the excess velocity at the closest approach ($V_\infty =$ 5.43 km/s), with the following equation:

$$\delta_{max} = 2\ sin^{-1}\left(\frac{1}{1 + \frac{r_{Mars}V_\infty^2}{\mu_{Mars}}}\right) = 34.84^\circ \tag{3.10}$$

$$\delta_{actual} = 2\ sin^{-1}\left(\frac{1}{1 + \frac{(r_{Mars}+h_{flyby})V_\infty^2}{\mu_{Mars}}}\right) = 33.55^\circ \tag{3.11}$$

Where δ_{max} is the maximum turn angle, δ_{actual} the actual turn angle , V_∞ is the magnitude of the incoming (or outgoing) excess velocity. One can clearly see that the actual turn angle is lower than the maximum turn angle which means the gravity assist is possible.

3.2.2.4 Earth Arrival

The spacecraft will arrive at Earth with an excess velocity of 8.93 km/s. With this velocity known, the velocity of the spacecraft, at perigee of 56.5 km from the Earth's surface, can be calculated. This altitude is required to prevent skipping back into space which will be explained further in chapter 4 on re-entry.

$$V_{peri,arrive} = \sqrt{\frac{2\mu_{Earth}}{r_2} + V_{\infty,arrive}^2} = \sqrt{\frac{2\mu_{Earth}}{r_{Earth} + h_{arrival}} + V_{\infty,arrive}^2} = 14.27 \text{ km/s} \tag{3.12}$$

Where $V_{peri,arrive}$ is the velocity at perigee w.r.t. the Earth, $V_{\infty,arrive}$ the arrival excess velocity and r_2 the sum of the Earth's radius and the arrival height $h_{arrival}$. As we can see from the result, the re-entry speed is higher then the allowed 14.2 km/s. This means further optimization was required to define a trajectory that is within this constraint. This process is further explained in section 3.2.3.

3.2.3 TMI Launch Window

There is a fixed time and finite window of time in which the TMI can be achieved. Due to the Thermal Protection System (TPS) and g-force limitations, the maximum re-entry speed should not be higher than 14.2 km/s (determined in chapter 4). Secondly, due to the technological limitations that are available today, the maximum change in velocity that can be achieved from a 200 km parking orbit is 5 km/s which is determined in section 5.3. Using the numerical solutions, several other trajectory options were analyzed ranging from launching the 1st of December 2017 to mid January 2018. First, a fixed departure date was given together with initial guesses for the fly-by and Earth arrival dates. After applying a boundary search for the fly-by and arrival dates of 90 days, the fly-by altitude was set at 180 km. Then the program started looking for the most optimized Earth departure solution for each different launch date. Then, the results were used to determine the change in velocity required from a 200 km parking orbit with 28.5 deg inclination. The results of this analysis are plotted in figure 3.3.

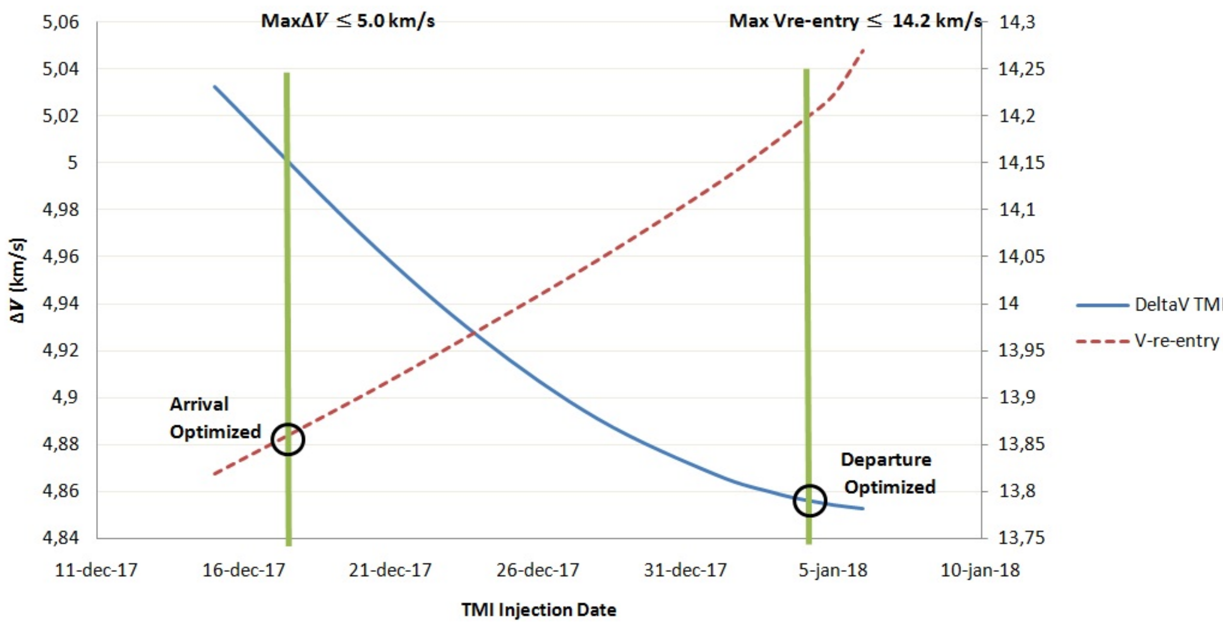

Figure 3.3: TMI launch window

One can clearly see that the TMI launch window opens at the moment the required ΔV drops below 5 km/s which is at the 18th of December 2017. The window closes again at the fifth of January as the re-entry speed would higher than 14.2 km/s. One can clearly see there is a trade-off between the required change in velocity and the re-entry speed. The optimized Earth arrival trajectory would take place at the 18th of December 2017. The most optimized Earth departure solution would be a departure on the 4th of January 2018.

3.2.4 End-of-Mission Maneuvers

3.2.4.1 Re-entry

Nearly at the end of the mission, the spacecraft will be approaching Earth at a velocity of nearly 14.2 km/s. Three days before the crew has to re-enter the Earth's atmosphere, they will have been transferred from the living module to the re-entry capsule. Afterwards, the re-entry vehicle will be jettisoned and the crew will begin their communications with the ground station immediately after entering the re-entry capsule. This will enable the crew to be guided through the re-entry procedure and performing small re-entry trajectory correction maneuvers to ensure the precise targeting required. Further specification on the re-entry procedure and trajectory is given in chapter 4.

3.2.4.2 Re-use of Living module

After the re-entry vehicle is jettisoned, there are two options for the living module. One option is to destroy the living module by letting it burn up in the Earth's atmosphere. A second option is re-using the living module in a way that it still would be useful. An idea is used of swinging the re-entry vehicle back into space by using a gravity assist from Earth. With the measurement equipment and the scientific payload already installed, the data it could generate by being longer in space, can be send back to Earth with the communication and data handling system that is already installed.

The three days before re-entering the Earth's atmosphere, provide enough time for the re-entry vehicle to target the right re-entry corridor with a low amount of propellant to change its incoming height. The living module was targeted, before the jettisoning, to not cross the orbital height of the ISS (400 km) and many satellites in a LEO orbit. An analysis was done to determine the risk of the living module coming back (uncontrolled) to Earth and causing more space debris. A velocity at perigee of 14.2 km/s was used at a height of 800 km to see which trajectory the spacecraft would follow in the future.

3.2.5 Final Transfer Trajectory

After optimizing the trajectory for Earth departure, it was clearly seen that this optimized trajectory exceeded the re-entry speed. An analysis was done to determine the window wherein the re-entry speed would be lower than 14.2 km/s and the ΔV for TMI injection would not be higher than 5.0 km/s. In section 3.2.3 is was determined that the most optimized trajectory, within the mission constraints meeting the requirements, would be on the 4th of January 2018. The results of this trajectory are given below in tables 3.5 and 3.6. An illustration can be found in figure 3.4. C3 is the characteristic energy required, equal to the square of the excess velocity (C3=V_∞^2).

Table 3.5: Earth-Mars free-return solution values from MATLAB

		Departure			**Arrival**	
Leg	**V∞ [km/s]**	**V_{peri} [km/s]**	**C3 [km^2/s^2]**	**V∞ [km/s]**	**V_{peri} [km/s]**	**C3 [km^2/s^2]**
1	6.2133	12.637	38.605	5.344	7.26	28.89
2	5.344	7.24	28.56	8.812	14.20	77.65

Table 3.6: Final trajectory details

Output	**Value**
Departure Calender Date	4/1/2018
Launch Energy (C3)	38.605 km^2/s^2
TMI ΔV	4.857 km/s
Departure Time	14:49:58
Mars Fly-by Date	20/8/2018
Fly-by Altitude	180 km
Earth Arrival Date	20/5/2019
Earth Re-entry Speed	14.2 km/s
Total TOF	501 days

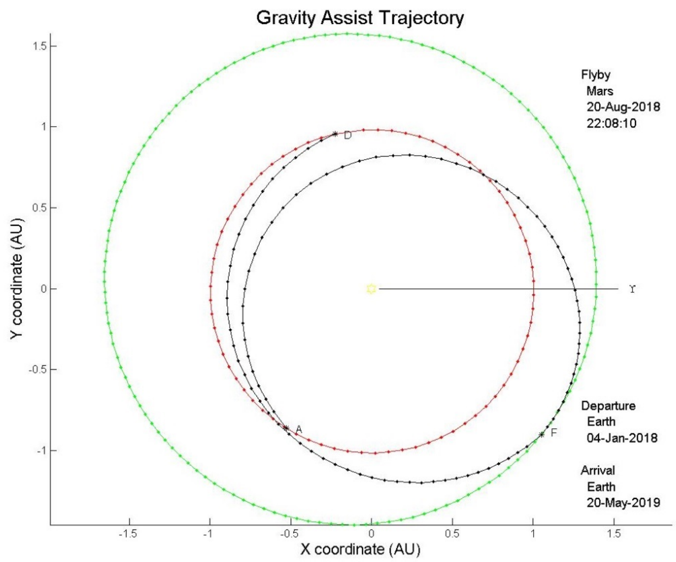

Figure 3.4: Final trajectory solution - departure optimized

3.3 Verification and Validation

In this section the verification and validation of the used models is described. First the verification of the trajectory is described. The results are compared with values from other scientific research. The validation of the software is done by comparing the results with the Mariner Mission.

3.3.1 Verification of Trajectory

The software that is used to determine the final trajectory can be verified with the results obtained from other scientific research. The Inspiration Mars community determined their own trajectory by using STK/Astrogator software, made by Analytic Graphics Inc.(AGI) [5]. As an initial guess for the first launch date (5 January 2018), they used a date based on a technical paper by Patel et al. [23] that calculated various fly-by options to Mars and back. In their own verification procedure, they recreated the trajectory using the Mission Analysis Environment (MAnE) software [24] from Space Flight Solutions. The same dates were used for departure and the trajectory that resulted from both software programs matched very well. The trajectory determined in this report, using the MATLAB script, gave very similar results with the ones calculated by the authors of the feasibility analysis [5]. Below, in tables 3.7 and 3.8, the most important data are presented next to each other. One can conclude that the software used is verified.

Table 3.7: Earth-Mars free-return solution values from MATLAB

		Departure			**Arrival**	
Leg	**V∞ [km/s]**	**V_{peri} [km/s]**	**C3 [km^2/s^2]**	**V∞ [km/s]**	**V_{peri} [km/s]**	**C3 [km^2/s^2]**
1	6.21	12.64	38.55	5.375	7.26	28.89
2	5.375	7.26	28.89	8.854	14.22	78.39

Table 3.8: Earth-Mars free-return solution values from Astrogator [5]

		Departure			**Arrival**	
Leg	**V∞ [km/s]**	**V_{peri} [km/s]**	**C3 [km^2/s^2]**	**V∞ [km/s]**	**V_{peri} [km/s]**	**C3 [km^2/s^2]**
1	6.232	12.578	38.835	5.417	7.272	29.344
2	5.417	7.272	29.344	8.837	14.18	78.094

3.3.2 Validation of Trajectory Software

In order to validate the software used to determine the trajectory, the Mariner mission 10 was used. In this mission, the spacecraft was launched on the first day of the scheduled launch period, November 3, 1973 from Cape Canaveral, Florida. The spacecraft received a gravity assist (altitude of 6378 km) from Venus on February 5, 1974 and encountered Mercury on March 29, 1974, 146 days after launch. Afterwards it used another second and third fly-by of Mercury but these are not used for the validation of the software. The dates were filled into the MATLAB script as an initial guess for the launch, fly-by and arrival dates. Then, a boundary search of 60 days was applied for every date guess. Finally telling the program to target a fly-by altitude of 6378 km at Venus and to optimize the trajectory for total ΔV, very similar values came out. The results can be compared below in tables 3.9 and 3.10.

Table 3.9: Mariner 10 mission dates

Segment	**Date**
Earth launch	November 3, 1973
Venus fly-by	February 5, 1974
Mercury arrival	March 29, 1974

Table 3.10: Mariner 10 mission dates (MATLAB)

Segment	**Date**
Earth launch	November 7, 1973
Venus fly-by	February 6, 1974
Mercury arrival	March 30, 1974

The dates coming from the MATLAB script are very close to the dates actually used for the trajectory. A reason for the slight difference in dates could be that the trajectory is not entirely optimized. Another reason could be if they launched with a slightly different trajectory because of requirements of the multiple fly-by of Mercury and Venus. However, one can conclude that the software program is validated for preliminary design of a trajectory.

3.4 Sensitivity Analysis

In this section a sensitivity analysis is made. The results are listed in table 3.11. Two parameter changes are analysed, a change in launch date and a change in fly-by altitude. A change in launch date, later than the 5th of January, would simply mean that the mission can not be launched in 2018. However, if re-entry technology would better than expected by 2018 and a higher re-entry velocity can be reached, the launch date can be extended by two or three days. A lower fly-by altitude could make the trajectory to require less fuel and have a lower re-entry speed. The final trajectory determined in this chapter was analyzed for different fly-by altitudes ranging between 100 km and 220 km. The results are given in table 3.11. One can see that at 100 km, there is a decrease of 0.23% for the departure ΔV and 0.21% for the arrival velocity respectively.

Table 3.11: Sensitivity fly-by altitude

Fly-by Altitude	**100 km**	**140 km**	**180 km**	**220 km**
ΔV_{TMI}	4.846 km/s	4.850 km/s	4.857 km/s	4.859 km/s
$V_{re-entry}$	14.17 km/s	14.19 km/s	14.20 km/s	14.23 km/s

3.5 Further Recommendations

The trajectory given can be further optimized by doing further analysis on the trajectory perturbations and not making all the assumptions made for determining this trajectory. This could lower the margins needed and possible the total amount of extra fuel needed on the spacecraft.

3.5.1 Lunar Gravity Assist

The principle of using a gravity assist to change the spacecrafts velocity was already explained in section 3.2.2.3. In the first case, the Earth's moon could be used to increase its velocity. However, due to limitations of the current available technology and equipment, no available upper stages are able to perform deep space burns. Their upper stages are designed for quick use in LEO and are only able to perform within a few hours of initial launch [5] .Note, if a future launch date would be used, and modifications to an available upper stage can made, this would be viable option. The second option would slow down the spacecraft by flying on the other side of the Earth's moon. For this, no big modifications have to be made to any available equipment and it provides the possibility to slow down the spacecraft enough to ensure a safe re-entry. This can also increase the launch window and reduce the total amount of fuel needed for the initial burn as a lower departure velocity could be used.

3.5.2 Space Debris Prediction

Space debris, also known as orbital debris, space junk, and space waste, is the collection of defunct objects in orbit around Earth. This includes everything from spent rocket stages, old satellites, fragments from disintegration, erosion, and collisions. Since our trajectory will pass through all Earth orbit altitudes and deep space, the chance of colliding with other man made or natural objects should be analyzed. Then, when a collision course is determined, how a change in direction can prevent the spacecraft from colliding and possibly create even more space debris.

3.5.3 Influence of Phobos and Deimos

Mars has two moons, Phobos and Deimos, each in the equatorial plane. Phobos is located on average at 5982 km from the surface while Deimos is further away at 20,063 km [16]. The location of these natural satellites could be crucial for the Mars incoming or outgoing trajectory of the spacecraft when they are in the way (or very close) of the spacecraft, they could collide. However, with initial analysis or correction maneuvers, this event can "easily" be avoided.

3.5.4 Venus Gravity Assist by 2021

When the launch date can not be met, there is another trajectory which could be used in 2021. This trajectory would use a gravity assist from Venus to Mars and then come back to Earth. This mission would require less fuel and have a lower re-entry speed. The only disadvantage would be the TOF which is around 90 days longer than the current trajectory [25].

3.5.5 Influence Martian Atmosphere

The influence of the Martian atmosphere on the spacecraft can be studied more as it will have an influence on the spacecraft, and especially on the sensitive solar panels. However, by flying at 180 km, this effect was assumed to be negligible. That being said, if the spacecraft would fly lower to Mars' surface, the effects should be studied more in detail.

Chapter 4
Re-entry Design

The final phase of this end-to-end mission is re-entry in the Earth atmosphere. The trajectory will be a direct re-entry from a return Mars orbit. The re-entry capsule that will be used is a modified Dragon capsule. In order to modify the capsule to withstand the re-entry conditions a model is created. Using this model the optimum trajectory (section 4.2) with respect to the peak g-load, heat flux and flight path angle is determined. From these values the required Thermal Protection System (TPS) (section 4.3) and Descent and Landing System (DLS)(4.4) required for the mission will be designed. A sensitivity analysis (section 4.5) will be done in order to determine the quality of the final design. Lastly, the models will be verified and validated (section 4.6) to determined their accuracy to real-life situations.

4.1 Re-entry Vehicle Properties

For the re-entry procedure the Dragon capsule has been selected for a number of reasons. The first reason is to keep the design integration as simple as possible. Since the whole design is based on components made by SpaceX, the integration will not be too complicated. The launcher that is used (the Falcon Heavy) is also designed to carry the Dragon capsule. Another reason to choose the Dragon capsule over other capsules is the availability. The Dragon capsule will be rated for human flight in 2018. Furthermore, the Dragon capsule is equipped with a state-of-the-art Thermal Protection System (TPS).

4.1.1 Aerodynamic Properties

Since the Dragon capsule is a modern spacecraft that is currently under development little aerodynamic data is available. Therefore data of comparable re-entry vehicles need to be used. The most extensive data available is the data collected from the Apollo missions. In the hypersonic regime the lift and drag coefficients are comparable to those of the dragon [26]. The specific C_L and C_D values were retrieved from an Apollo database [27].

4.1.2 Geometric Properties

In figure 4.1 a schematic of the Dragon capsule is found. In table 4.1 the most important properties are summarized. These geometric parameters are used to determine the aerodynamic and aerothermodynamic properties of the vehicle during re-entry.

Table 4.1: Properties of the Dragon capsule

Name;	**Value**
Nose Radius (R_N)	4.8 [m]
Diameter	3.7 [m]
Surface Area	10.75 [m^2]
Mass	4200 [kg]
Side wall angle	15 [deg]

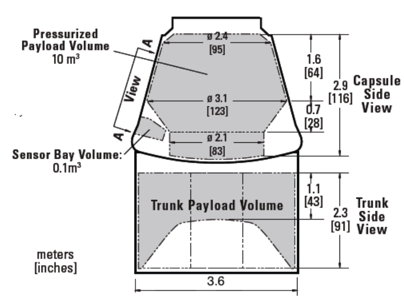

Figure 4.1: Schematic of Dragon capsule

4.2 Re-entry Trajectory

To design the re-entry procedure a model is generated. This model determines the required manuevers that need to be taken in order to meet the requirements. The requirements for re-entry trajectory are stated in table 4.2.

Table 4.2: Re-entry requirements

Requirement	Value	Unit
Peak g load sustained by the crew	8	[g]
Average g load sustained by the crew	6	[g]
Minimum corridor width	0.04	[deg]

4.2.1 Equations and Assumptions

To model the vehicle's behaviour during re-entry the equations of motion need to be determined. The re-entry vehicle is assumed to be a lift-generating point mass. Figure 4.2 is used to aid with the derivations of these equations. In the figure all relevant forces, angles and distances are shown.

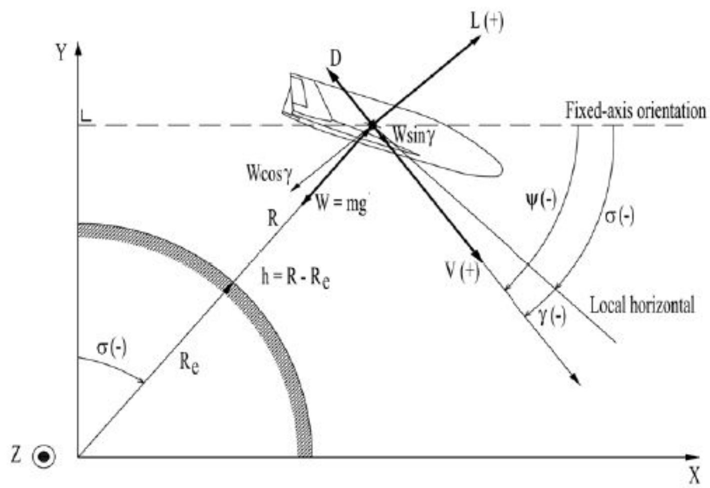

Figure 4.2: Schematic drawing of planar motion [28]

Pointing to the center of the Earth is the position vector R, which consists of the radius of the earth R_e and the altitude h. Three angles can be defined. The angle between the fixed axis orientation and the local horizontal is σ. By definition σ is defined negative. The second angle is the flight path angle γ, which is the angle between the local horizontal and the velocity vector. The final angle is the auxiliary angle ψ which gives the angle between the velocity vector and the fixed axis orientation (e.g. $-\psi = -\sigma - \gamma$). There are three forces which act on the point mass. The drag force D acts in the opposite direction of the velocity vector. The lift force L acts perpendicular to the velocity vector. The gravitational force W is pointed towards the center of the Earth and has a component parallel and perpendicular to the velocity vector. Using Newton's second law in the direction of V yields the derivation shown in equation 4.1.

$$m\frac{dV}{dt} = -D - mg\sin\gamma \tag{4.1}$$

The acceleration in the normal direction is given by $V\frac{d\psi}{dt}$. Applying Newton's second law in the normal directions results in equation 4.2.

$$mV\frac{d\psi}{dt} = L - mg\cos\gamma \tag{4.2}$$

However an expression for $\frac{d\gamma}{dt}$ is required. Remembering that $-\psi = -\sigma - \gamma$ an expression for $\frac{d\gamma}{dt}$ can be derived, shown in equation 4.3.

$$\frac{d\psi}{dt} = \frac{d\sigma}{dt} + \frac{d\gamma}{dt} \tag{4.3}$$

The position vector R describes an instantaneous circular motion which can be expressed as $R\frac{d\sigma}{dt}$. This motion is equal to the projection of V on the local horizontal, $V cos\gamma$. Rewriting these two equations yields equation 4.4.

$$\frac{d\sigma}{dt} = \frac{V\cos\gamma}{R} \tag{4.4}$$

Substitution of equation 4.3 and equation 4.4 into equation 4.2 yields the result shown in relation 4.5.V_c is the local circular velocity calculated using $\sqrt{(}gR)$.

$$V\frac{d\gamma}{dt} = \frac{L}{m} - g\cos\gamma\left(1 - \frac{V^2}{gR}\right) = \frac{L}{m} - g\cos\gamma\left(1 - \frac{V^2}{V_c^2}\right) \tag{4.5}$$

The equations of motion that are derived are valid for a point mass moving in two dimensions. However, it is is preferred to incorporate 3D-effects in the equations of motion. The bank angle σ (not to be confused with the σ in figure 4.2) determines the direction at which the lift vector L is pointed. This can be accounted for by multiplying the lift vector by $\cos\gamma$. Furthermore, the Coriolis effect and the centripetal acceleration can be calculated using the following equations:

$$2\omega_{cb}V\cos\delta\sin\chi \tag{4.6}$$

For the Coriolis effect, and for the centripetal accelerations:

$$\omega_{cb}^2 R\cos\delta\,(\cos\delta\cos\gamma + \sin\gamma\sin\delta\cos\chi) \tag{4.7}$$

For simplification a flight along the equator is assumed, meaning that the latitude $\delta = 0°$ and heading $\chi = 90°$. This reduces equations 4.6 and 4.7 to:

$$2\omega_{cb}V \tag{4.8}$$

And:

$$\omega_{cb}^2 R\cos\gamma \tag{4.9}$$

Adding equation 4.8 and equation 4.9 to equation 4.5 and taking the bank angle into account the final equation for the flight path angle is determined:

$$V\frac{d\gamma}{dt} = \frac{L}{m}\cos\sigma - g\cos\gamma(1 - \frac{V^2}{V_c^2}) + 2\omega_{cb}V + \omega_{cb}^2 R\cos\gamma \tag{4.10}$$

Finally, an expression for the rate of change of altitude is required. This is equal to the downward velocity component of the velocity shown in Equation 4.11.

$$\frac{dR}{dt} = V\sin\gamma \tag{4.11}$$

These equations are now used to determine the change in position at each time increment. The results of the model are shown in section 4.2.1.1 and the verification and validation procedures is shown in section 4.6.1.

4.2.1.1 Results

The equations presented in section 4.2.1 can be used to model the accelerations and velocities during re-entry. Table 4.3 indicates the final design parameters for the trajectory determination. The results of these design parameters are shown in figure 4.3 through 4.8. The perigee altitude determined in section 3 is 56.5 km. The model for re-entry runs from an altitude of 220 km, this additional margin will result in the start of the re-entry procedure before the perigee is reached. This safety margin includes a higher perigee due to unforeseen events resulting in a different altitude.

Table 4.3: Input values for the re-entry model

	Parameter	Description	Value	Unit
Earth	C	Chapman constant [29]	1.06584×10^5	$[\mathrm{kW/m}]^{3/2}$
	V_c	Local circular velocity	7874	[m/s]
	R_e	Radius Earth	6356.7	[km]
	$\omega_c b$	Angular velocity of Earth [28]	7.29211×10^{-5}	[rad/s]
	ρ	Atmospheric density	Varies	$[\mathrm{kg/m^3}]$
	ρ_0	Atmospheric density at sea level	1.225	$[\mathrm{kg/m^3}]$
	h_0	Starting altitude	220	[km]
Spacecraft	A	Vehicle surface area	10.75	$[\mathrm{m^2}]$
	V	Re-entry velocity	14.2	[m/s]
	m	Capsule mass	5000	[kg]
	R_n	Nose radius	4.8	[m]

In order to meet the requirements some variables have to be optimized. The first variable that has to be determined is the flight path angle γ. To determine the flight path angle the bank angle σ is fixed on 180 deg so the lift force is pointed down. This will help the spacecraft get caught and remain in the atmosphere by generating a negative lift. As can be seen in figures 4.3 and 4.4 the spacecraft will enter the atmosphere for an initial flight-path angles between -11 and -10.8 deg. However, when the initial flight-path angle is -10.6 degrees, the spacecraft will first descent to about 60 kilometers. At this altitude the atmosphere becomes more dense, causing the spacecraft to skip off into outer space. To incorporate a safety margin the flight path angle is chosen to be 11 deg.

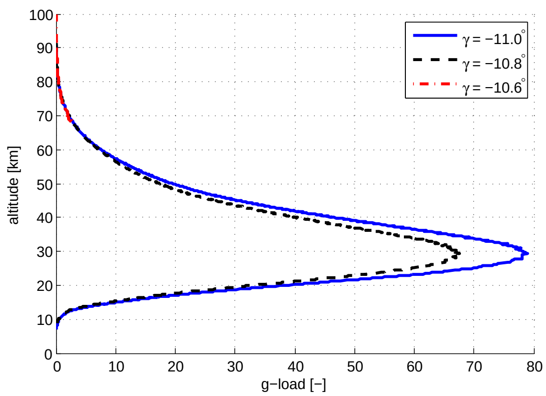

Figure 4.3: Altitude vs. g-load

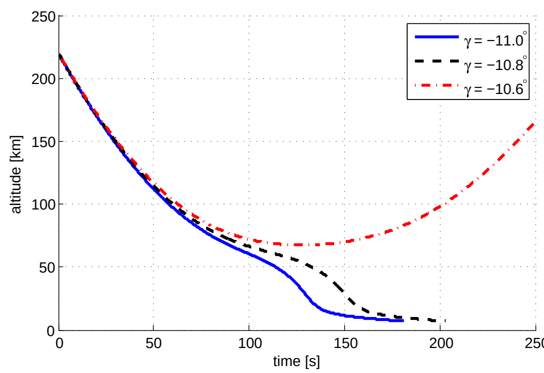

Figure 4.4: Altitude vs. Time

From previous studies it was concluded that a minimum pointing accuracy of 0.04° can be achieved [30]. For an unmanned re-entry vehicles, (Stardust and Genesis) the corridor width is ±0.08° [30], since a manned re-entry capsule will be used an additional safety margin of 100 % is taken. At 14.2 km/s a $\Delta\gamma$ of 0.04° requires a vertical velocity accuracy ($V \sin\gamma$) of 9.91 m/s. Therefore a corridor width of 0.04° is selected for which the maximum g-load are calculated. As can be seen in figure 4.3, the g-load vary from 65 to 77 g which are too high for the crew. Therefore the bank angle σ has to be optimized in order to reduce the peak g-load. The bank angle can be varied over time, the possibilities for this configuration are infinite. During the design process it was a trial-and-error process which after many iterations led to the optimized bank angle variation over time. These bank angles lead to the lowest peak g-load, as well as the lowest peak heat flux and total heat seen can be seen in section 4.3.1.1. The calculations have been made for flight path angles of -10.99, -11.01 and -11.03°. As can be seen in figure 4.5 the g-load remain just under 8 g which meets the requirements. Similarities between the different flight path angles are that there are two peaks in the g-load. The first peak is smaller than the second peak. This can be explained by looking at the altitude versus time in figure 4.6. The spacecraft descents to about 60 km where the atmosphere becomes denser. This causes the first deceleration peak. After approximately 150 seconds it has lost enough velocity to descent lower into the atmosphere where the second, more extreme peak in deceleration occurs this is due to the increasing density as the altitude decreases. All the graphs stop at an altitude of 7.2 kilometers. This is the point where the parachutes are deployed, which will be discussed in section 4.4. The change in bank angle as a function of time can be seen in figure 4.7. As can be seen the re-entry procedure is commenced with a lift vector pointing up. This is done to achieve a more shallow flight-path angle in the first phase. When the vehicle enters the lower layers of the atmosphere, the lift vector is pointed downwards in order to prevent the vehicle from skipping into space. Each trajectory had its own bank angle configuration to keep the g-load and heat load as low as possible. Therefore figure 4.7 indicates the commands that the Guidance, Navigation and Control (GNC) system must follow in order to have a safe re-entry procedure.

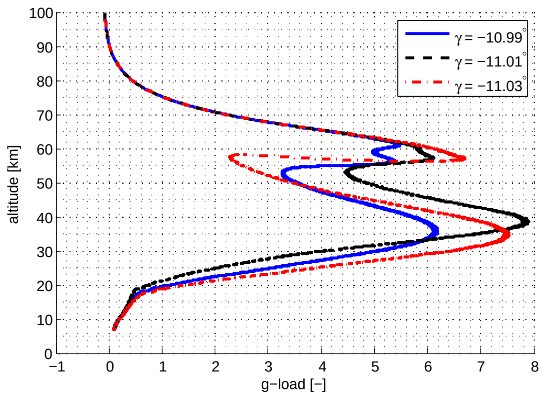

Figure 4.5: Altitude vs. g-load

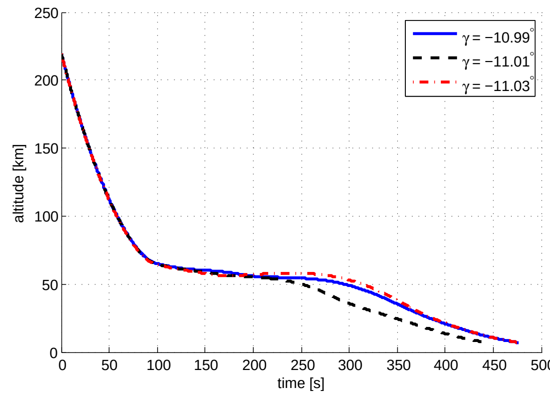

Figure 4.6: Altitude vs. Time

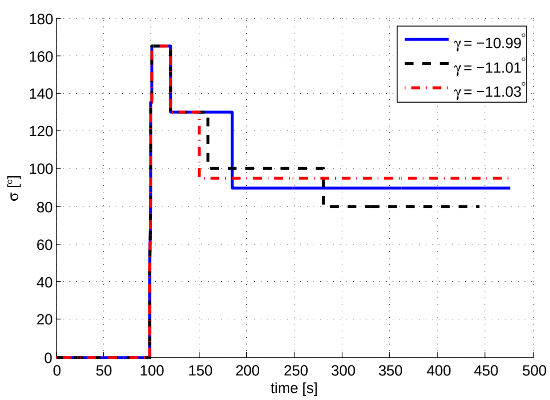

Figure 4.7: Bank angle vs. Time

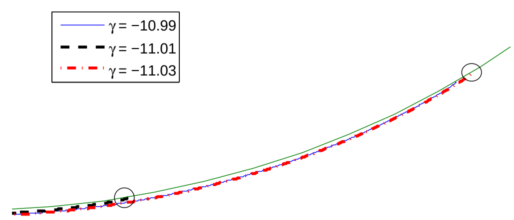

Figure 4.8: Landing positions on Earth

4.3 Thermal Protection System

A critical subsystem during re-entry is the thermal protection system (TPS). This system is responsible for shielding the crew during the high heat change while re-entering in the Earth atmosphere. The requirements for this system are shown in table 4.4.

Table 4.4: Re-entry requirements

Requirement	Value	Unit
Peak heat flux sustained	20,000	kW/m^2
Temperature inside cabin below	40	°C

4.3.1 Equations and Assumptions

To calculate the heat flux in the stagnation point the Chapman equation is used [31].

$$\dot{q}_w = \frac{C}{\sqrt{R_N}}\sqrt{\frac{\rho}{\rho_0}}\left(\frac{V}{V_c}\right)^3 \tag{4.12}$$

In Equation 4.12 the C represents the Chapman constant, which is taken to be 1.06584×10^5 [29]. R_N represents the nose radius of the re-entry vehicle which is indicated in section 4.1. Once the heat flux is known it is possible to determine the heat shield deterioration. Equation 4.13 [32] relates the effective heat of ablation to the recession rate.

$$\dot{s} = \frac{\dot{q}_{cw}}{H_{eff}\rho_v} \tag{4.13}$$

To calculate the temperature on the inside of the re-entry module the general equation of thermal energy flow equilibrium is used:

$$mC_p\frac{dT}{dt} = P_i + \sum_j \epsilon A_i B_{ij}\sigma\left(T_j^4 - T_i^4\right) + \sum_j C_{ij}\left(T_j - T_i\right) \tag{4.14}$$

The heat shield is modeled as several layers which all conduct heat to each other. In this way an accurate value for the inside temperature can be computed. In equation 4.14 C_p stands for the specific heat, $\frac{dT}{dt}$ is the rate of change of temperature, P_i is the received heat flux, ϵ_i is the emissivity, A_i is the area, B_{ij} is the Gebhart factor, σ is the Boltzmann constant and C_{ij} is the thermal conductivity. The Gebhart factor is calculated by the equation shown in relation 4.15.

$$B_{12} = \frac{\epsilon_2}{\epsilon_1 + \epsilon_2 - \epsilon_1\epsilon_2} \tag{4.15}$$

4.3.1.1 Results

The equations presented in section 4.3.1 can be used to model the heat flux and cabin temperature during re-entry. Table 4.5 indicates the final design parameters for the TPS. The results of these design parameters are shown in figures 4.9 and 4.10.

Table 4.5: Input values for the thermal protection model

	Parameter	Description	Value	Unit
TPS	ρ_{hs}	Heat shield density[32]	255	[kg/m^3]
	H_{eff}	Effective heat of ablation[32]	4.388×10^7	[-]
	C_p	Heat capacity[32]	651.28	[J/kgK]
	ϵ	emissivity[32]	0.8	[-]
	κ	Thermal conductivity[32]	0.16	[W/mK]
	t_{hs}	Heat shield thickness	0.08	[m]

In figure 4.9 the heat flux is given as a function of time. The peak heat flux is 3200 kW/m^2, this is below the 20,000 kW/m^2 requirement. Since the heat flux over time is known it is possible to calculate the heat shield deterioration using equation 4.13. The input variables of this equation are given in table 4.5. The nominal flight path angle of -11.01° leads to a heat shield deterioration of 3.2 cm. The heat shield is designed with a thickness of 8 cm to increase the safety margin to 100 %.

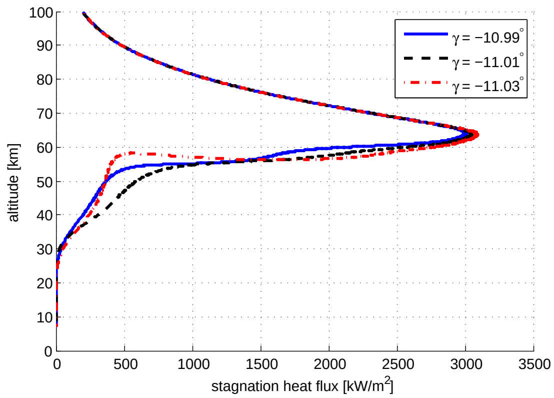

Figure 4.9: Altitude vs. Flight path angle

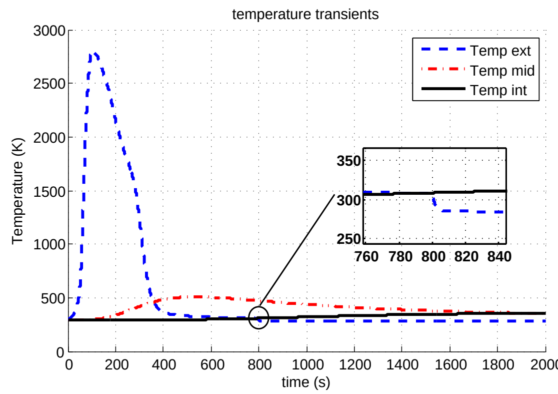

Figure 4.10: Bank angle vs. Time

Figure 4.10 depicts the temperature development of the heat shield as a function of time. From figure 4.6 it can be seen that for the nominal flight path angle the time of flight until parachute deployment is about 440 s. As can be read in section 4.4 the time of flight with deployed parachutes is 360 s. The cooling of the heat shield due to the water is incorporated, this explains the sudden drop of the external temperature at 800 s, depicted in detail in figure 4.10. As can be seen from the graph in figure 4.10 , the re-entry module will continue to heat up even after splashdown. 1000 s after splashdown the temperature is already at 90 °C. Therefore the choice is made to jettison the heat shield after 600 seconds. This is when all the parachutes are deployed. The interior temperature is 29.5 °C at that point. After the heat shield is jettisoned, this temperature will decrease gradually. It has to be mentioned that the cooling effects of the air at subsonic speeds are not accounted for, but since this will only lead to a lower interior temperature the impact will not harm the mission. Having the heat shields jettisoned will also lower the cost of the retrieval operation. The spacecraft has a landing zone with a radius of 250 km, as shown in figure 4.8, this will require an intensive recovery process. When the heat shield is not jettisoned the spacecraft has to be recovered within a certain amount of time or the module will heat up, this would be a serious situation for the crew because the internal temperature could raise to values above 40 °C. Without the heat shield, the time of retrieval is less critical so less ships have to be deployed.

4.4 Descent and Landing System

To ensure safe delivery to the earth surface a Descent and Landing System (DLS) is required. An analysis of the required parachute systems needed in the descent and landing phase is made. The relations and model used are explained in section 4.4.1 and the results leading towards final design are explained in section 4.4.2. The requirements that need to be met during the descent landing phase are stated in table 4.6.

Table 4.6: Descent and landing system requirements

Requirement	**Value**	**Unit**
Load during parachute deployment [33]	6	g
The maximum impact velocity [34]	10	m/s
The Re-entry footprint	500	km

4.4.1 Equations and Assumptions

Due to the high re-entry velocity a robust and reliable parachute system needs to be developed. The first step is the analysis of the initial conditions for parachute deployment. It is determined that the drogue parachute opening window is between an altitude of 17.3 and 7.3 km [33]. The main chutes open between an altitude of 8 and 1.7 km [33]. The minimal values for the altitudes were used in the designing process, the thought process is, if the descent and landing systems could withstand those conditions they could withstand all conditions. From the model in section 4.2.1.1 it can be deduced that at an altitude of 7.3 km the Mach number is 0.4. To ensure maximum reliability during the descent phase a safety margin of 50% was used on the Mach number. The mass of the re-entry vehicle is assumed to be 5 tons. The same value was used as in section 4.2. However, during the descent the heat shield is jettisoned reducing its mass. This model will therefore take heat shield jettison failure into consideration. All initial values used in the model are shown in table 4.7.

Table 4.7: Parachute initial values

	Parameter	**Description**	**Value**	**Unit**
DSL	h_1	Drogue shoot deployment altitude[33]	7.3	[km]
	M_1	Drogue shoot deployment Mach number[33]	0.6	[-]
	m	Capsule mass	5000	[kg]
	C_d	Parachute drag coefficient[34]	1.3	[-]

To mitigate risks involved in this process, redundancies need to be included. The main redundancy that is used is a back-up parachute. This means that the system needs to be designed so that 1 drogue and 2 main parachutes can be used for landing. An extra redundant parachute will be added at each phase in case of failure. The relations used to determine the DLS model are shown in equations 4.16 and 4.17.

$$F = ma \tag{4.16}$$

$$D = \frac{1}{2}\rho V^2 S C_d \tag{4.17}$$

The model calculates the drag force at every time increment starting from the initial conditions and generates an acceleration. This acceleration is then used to determine the velocity of the following time step. Illustrations of the situations taken into consideration by the models are shown in figure 4.11 and 4.12.

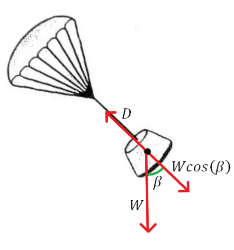

Figure 4.11: Forces acting on drogue parachute

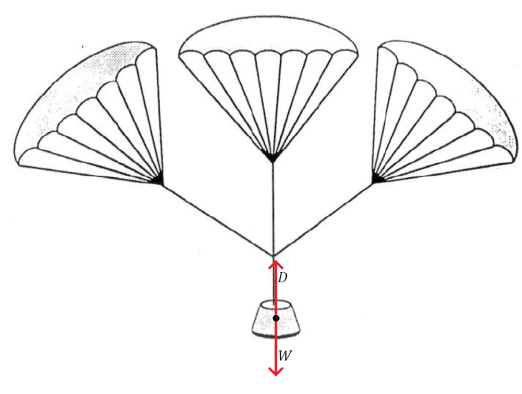

Figure 4.12: Forces acting on main parachute

Looking at figure 4.11 the weight of the vehicle acts in a different direction then the velocity. The model in section 4.2 indicates that the β in figure 4.11 is 5° during drogue deployment. It is assumed once the main parachutes are deployed the vehicle's velocity direction correlates with the force direction shown in figure 4.12.

4.4.2 Results

The results for the descent system are explained in section 4.4.2.1 and in section 4.4.2.2 for the landing system.

4.4.2.1 Descent

The surface area of each parachute stage along with its deployment time and altitude can now be determined. Two models are generated, one model used one drogue chute and two pilot and main chutes, the other used two drogue chutes and three pilot and main chutes. The results for the DLS procedure which best satisfies all the requirements are shown in figures 4.13 and 4.14.

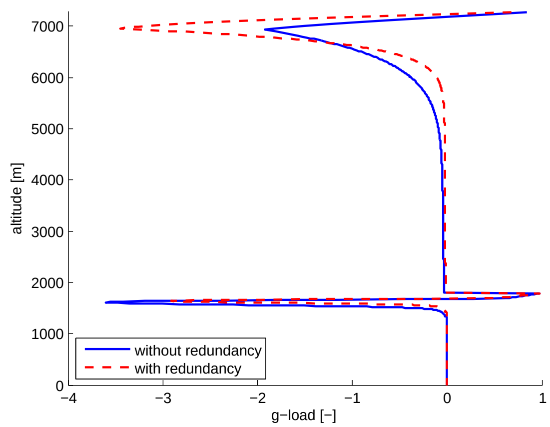

Figure 4.13: Altitude vs. acceleration

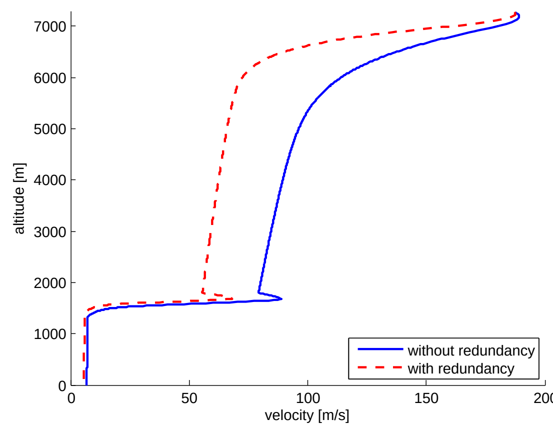

Figure 4.14: Altitude vs. velocity

The figures 4.13 and 4.14 indicate some key design points. The first point of interest is the g-load, looking at figure 4.13 two g-load peaks can be identified the first is located at an altitude of 7 km. This g-load peak signifies the deployment of the drogue parachute. The second peak at 1.7 km signifies the deployment of the main parachute. When there is a redundancy the second peak is lower than the first. When there is no redundancy the first peak is lower than the second. This is due to the fact that having no redundancy results is less surface area provided to generate drag. This lower surface area results in less deceleration, hence the velocity at which the main parachute is deployed is higher. This results in a greater deceleration once the main parachutes are deployed. The difference in velocities can be seen in figure 4.14. Modifying the parachutes to decrease the peak load generated when no redundancy is present increase the peak load when redundancy is present. Both peaks are therefore situated at 3.7 g to reduce discrepancies between both situations. The resulting design parameters are indicated in table 4.8 and a schematic of the mission is given in figure 4.15.

Table 4.8: Descent system parameters

Parameter	Description	Value	Unit
d_d	Diameter per drogue chute	4	[m]
d_p	Diameter per pilot chute	2	[m]
d_m	Diameter per main chute	30	[m]
n_d	Number of drogue chutes	2	[-]
n_p	Number of pilot chutes	3	[-]
n_m	Number of main chutes	3	[-]
V_{tdr}	Splashdown velocity with redundancy	5.4	[m/s]
V_{tdnr}	Splashdown velocity without redundancy	6.6	[m/s]

To provide compliance with all requirements the final touchdown velocity needs to be multiplied by a margin determined in the validation procedure. This margin of 40% is explained in section 4.6.3.2. Adding a 40%

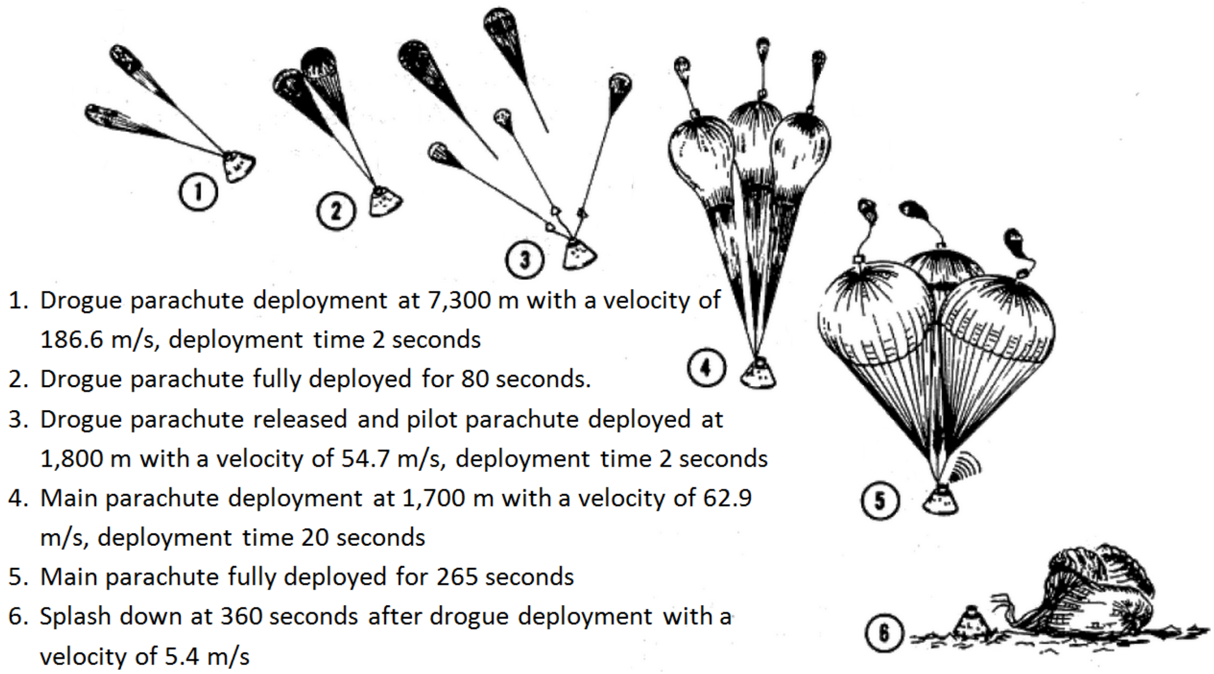

Figure 4.15: Schematic of the descent (modified from [34])

margin to the splashdown velocity without redundancy results in a final maximum splashdown velocity of 9.3 m/s. This ensures that all design parameters meet the requirements.

4.4.2.2 Landing

Providing safety for the crew is the main concern in the landing and recovery system. This system is responsible for what occurs when the re-entry vehicle touches down either on land or water. There are two parts to this system the first is to provide a stable landing and the second is to increase the ease of recovery. There are two landing methods applicable for this mission. The first is a landing on land the second is on sea. Depending on where the vehicle lands different systems need to be used. Because the mission has a high re-entry velocity, therefore resulting in a high heat transfer to the crew compartment. This high heat could be dissipated at quicker pace by landing in water, as shown in figure 4.10. Additionally, the impact velocity with the water can be higher due to it's absorbing nature. Flotation devices already installed on the dragon are sufficient enough to support the crew. However there are some drawbacks when having a splashdown. The first is the landing position of the vehicle once it has splashed down. The two stable conditions are shown in figure 4.16.

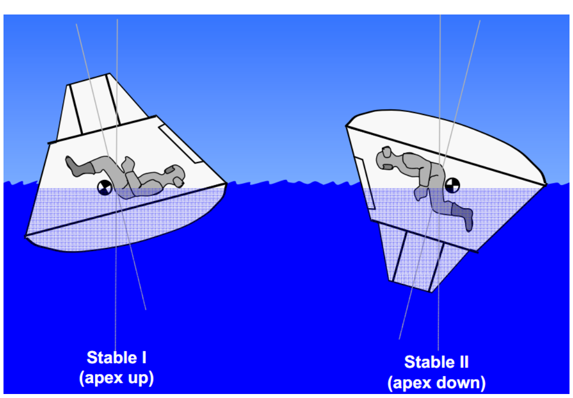

Figure 4.16: Splashdown stable positions [35]

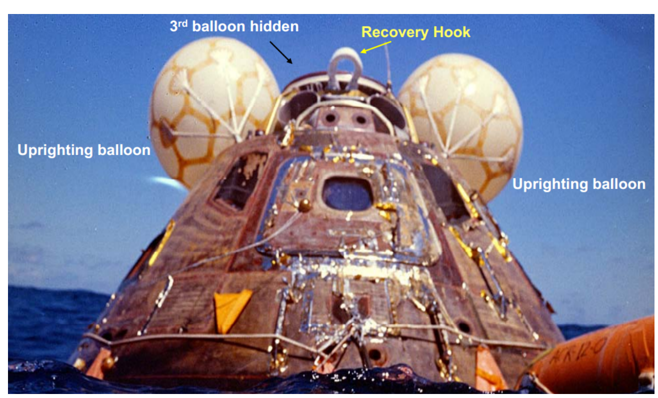

Figure 4.17: Up-righting balloon with hook [35]

Condition I is preferred due to the accessibility of the crew door. If the capsule lands in position II measures need to be taken in order for it to rotate to position I. Figure 4.17 indicates the use of uplifting balloons placed on top of the capsule to ensure that the correct stable position is achieved. A hook can also be used by a ship or helicopter the orientate the capsule correctly. If these measures are taken, this landing system would be able to support the crew.
Recovery is the final phase in the mission. The adequate amount of ships need to be determined in order to have a fast recovery. All the systems required to find the command module also need to be stated. Using the model in section 4.2 the difference in landing position with respect to the edges of the corridor width is taken into consideration. The model indicated that there is a 520 km difference in landing area. That value was taken as the diameter of a circle and the landing zone can be determined. The recovery procedure will make use of 10 ships able to carry the re-entry vehicle and 3 helicopters used for spotting. This will result in a maximum recovery time of one hour. During the procedure RADAR, flashing light, beacons and radio communication will be used to spot the vehicle. Once spotted the crew will be safely removed via helicopter and the one of the nearest vessels will pick-up the re-entry vehicle.

4.5 Sensitivity Analysis

A number of assumptions and estimations have been made to calculate the previously presented results. Some of these estimations might be inaccurate. To asses the consequence of these inaccuracies a sensitivity analysis is made. The first estimations that is going to be assessed is the density. Many mathematical models exist to calculate the properties Earth's atmosphere. Each method differs slightly from the each other. Furthermore, the density is calculated for an average day, with a certain ground temperature, and a certain density at sea level. In real life these values will often differ from the calculated values. Therefore the consequences of a change in density are assessed. At sea level the temperature is assumed to vary between 20 and -5°C. This will cause the density to vary about 10%. Therefore a 5% increase and a 5% decrease in density is assessed. The next parameter that will be assessed, is the flight path angle accuracy which is γ =0.04°. For the sensitivity analysis the consequences of a flight-path angle accuracy of 0.06° will be assessed. The final parameter that could change in the design process is the total weight of the re-entry vehicle. Multiple factors could contribute to an increase in total weight of the re-entry vehicle. The heat shield mass could change, the scientific payload can change or the GNC-systems can weigh more than expected. To account for all these possibilities a weight change of 300 kg is assessed. The results for the sensitivity analysis are shown in table 4.9.

Table 4.9: Sensitivity analysis

Changed input parameter	**G-load (Δ%) [-]**	**Peak heat flux (Δ%)[kW/m^2]**	**Total heat load (Δ%)[kW]**	**Splashdown velocity (Δ%)[m/s]**
Nominal conditions	7.9	3,089	3.7413×10^{5}	5.39
+5% density	9.176(+16%)	3,122 (+1%)	3.496×10^{5} (-7%)	5.26 (-2%)
-5% density	6.35 (-20%)	3,064 (-1%)	3.9153×10^{5} (+4%)	5.53 (+3%)
0.06 degrees flight-path angle accuracy	7.9 (0%)	3,108 (+1%)	3.5630×10^{5} (-5%)	5.39 (0%)
extra weight +300 kg	7.9 (0%)	3,089 (0%)	4.17×10^{5} (+11%)	5.55 (+3%)

Table 4.9 indicates that certain sensitivity parameters have a higher impact than others. The change in density contributes the most to a change in g-load by an increase in 16% when the density is increased by 5%. This would result in a maximum g-load higher than stated in the requirements. Fortunately, the flight path and bank angle can be altered to a lower starting value indicated in figure 4.4, decreasing the g-load to 6.2 g resulting in a sensitivity value of 7.2 g. The mass has the most impact on the total heat load with a maximum increase of 11%. No major concern is needed because with this increase the value is still within the requirements. The change in peak heat flux and splashdown velocity is minimal resulting in low sensitivity in those areas. Overall, the critical factor is the increase density and its effect on the peak g-load, but with an initial flight path correction this value can remain within the requirements.

4.6 Verification and Validation of Re-entry

In order to determine if the models used are correct a verification and validation procedure must be conducted. In order to model the re-entry two models where generated. These two models are the trajectory model (section 4.6.1) and the descend and landing system (DLS) model (section 4.6.3).

4.6.1 Trajectory Model

The trajectory model explained in section 4.2 determines the re-entry trajectory that will be conducted during the mission. In order to prove that the model is correct it was verified and validated. The verification for this model is shown in section 4.6.1.1 and the validation is shown in section 4.6.1.2.

4.6.1.1 Verification

In order the verify the model the Apollo missions were used. They are chosen due to the high amount of available data which was measured during their re-entry. The model shown in section 4.2.1.1 was then verified with an independent model presented in [28]. The initial values of the trajectory model were modified in order to mimic the procedure conducted in the paper. The initial values are indicated in table 4.10.

Table 4.10: Initial Conditions for Apollo Re-Entry

Parameter	Description	Value	Unit
γ	Flight path angle	-9.393 to -9.563	[deg]
d	Capsule diameter	3.9	[m]
m	Capsule mass	4976	[kg]
R_n	Nose radius	4.69	[m]
V	Entry velocity	11.0×10^3	[m/s]
h	Entry height	220×10^3	[m]
σ	Bank angle	110	[deg]

All the initial conditions are shown in table 4.10. An important note is that the flight path is modeled for five flight path angles between -9.393 and -9.563 °. Additionally, during the simulation the bank angle remains constant at 110 °. This does not model the real life conditions since the bank angle was altered to decrease the g-load. However for a verification procedure this assumption can be made. The results from literature for the altitude against g-load are shown in figure 4.18 and for the altitude against stagnation heat flux in figure 4.20. These models are then compared with the trajectory model calculated in section 4.2.1.1. The results are shown in figure 4.19 and 4.21.

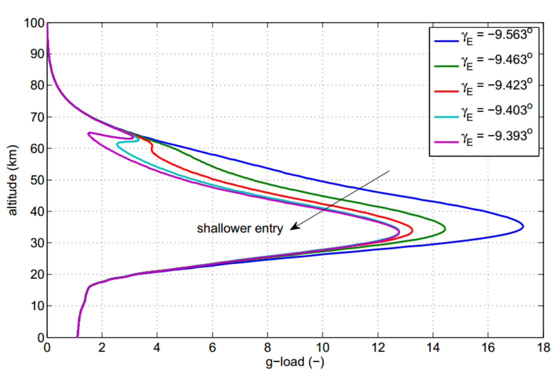

Figure 4.18: Altitude vs. g-load [28]

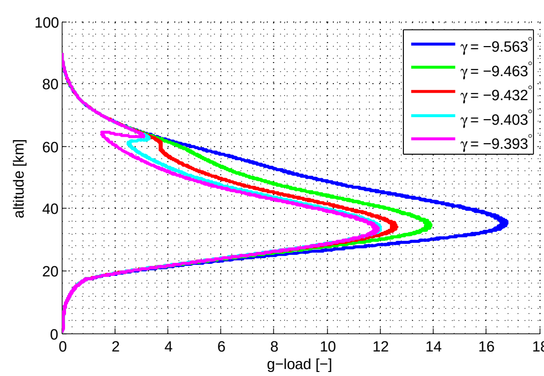

Figure 4.19: Altitude vs. g-load

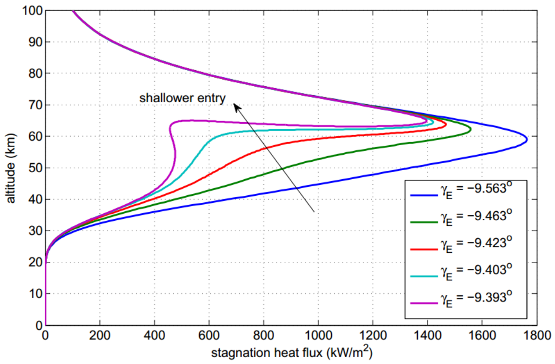

Figure 4.20: Altitude vs. stagnation heat flux [28]

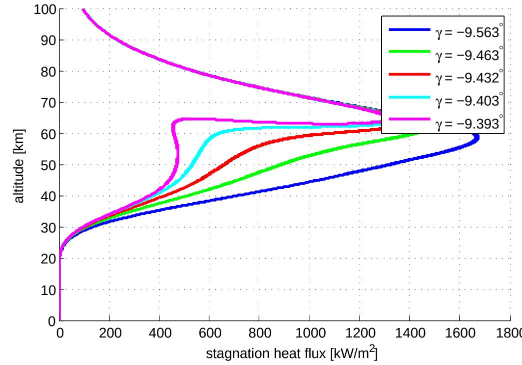

Figure 4.21: Altitude vs. stagnation heat flux

Looking at figures 4.18 through 4.21 the model generated to compute the trajectory can be verified. Some points of interests when looking at figure 4.18 and 4.19 can be identified. At an altitude of 65 km both graphs show a disturbance in the g-load. This disturbance increases as the flight path angle decreases due to the re-entry vehicle bouncing off the atmosphere. Both plots also indicated a peak load higher than 16 g for the steepest flight path angle. The g-load decreases as the flight path angle decreases. However there are small differences between these two plots. The first, is that the maximum g-load on figure 4.18 is 17 g at an altitude of 35 km for a γ of -9.563 ° while on figure 4.19 this is 16.3 g. This results in a correlation of 96%. The steeper the angle becomes the less the difference between the values found in literature and in the model become. Another difference in the two plots is the disturbance in g-load found at 65 km altitude. Figure 4.18 indicates a g-load of 1.8 while figure 4.19 indicates a g-load of 2. This shows a correlation of 90%, the correlation increases as the angle γ increases.

The stagnation heat flux as a function of altitude is also shown between the two models. Both models calculate the heat flux with the Chapman relation indicated in equation 4.12. The shape of the two plots shown in figures 4.20 and 4.21 correlate with on another. Both models indicate a low starting heat flux and a heat flux of zero at low atmospheres. There is a peak heat flux ranging from 1500 to 1700 Kw/m^2 for all values of γ between 58 and 65 km altitude. The same discrepancies indicated in the g-load correlation can be applied to the stagnation heat flux. The outer boundaries of γ have a correlation of 98%. Once the flight path angle converges to the nominal value the correlation increases.

From the verification procedure it can be concluded that there is a correlation between the results found in both models. A minimum correlation of 90% is an acceptable value. The discrepancies could arise due to a slight difference in atmospheric density and earth rotational velocity used for both models. Therefore the trajectory model generated is verified and must be validated to ensure its accuracy.

4.6.1.2 Validation

The validation of the trajectory model needs to be conducted. Due to the high g-load received during a fixed bank angle re-entry as shown in figures 4.18 and 4.19 the bank angle needs to be adjusted throughout the procedure. An illustration of the bank angle is shown in figure 4.22 as can be seen the angle of attack varies depending on the bank angle. This change in angle of attack alters the lift generated by the capsule. By varying the lift the acceleration of the capsule can be reduced so that the crew can withstand the procedure. The adjustment of bank angle for the mission is explained further in section 4.2.1.1. The bank angle during the Apollo mission is shown in figure 4.23. Due to the complexity of the bank angle generated over time during the Apollo mission, the validation procedure is not possible with the re-entry model. However, the plots shown in figure 4.18 and 4.20 are from a reviewed and revised report. Therefore, it can can be concluded that the model is of sufficient quality to make the required calculations.

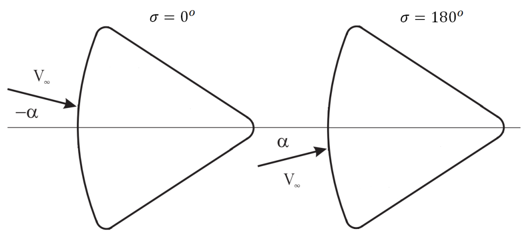

Figure 4.22: Bank angle illustration

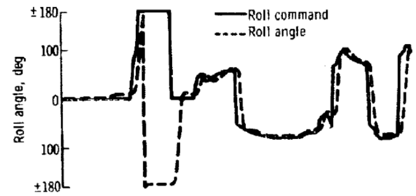

Figure 4.23: Roll angle over time for the Apollo

4.6.2 Thermal Protection System Model

The thermal calculations are necessesary to determine the heat shield thickness. The model is verified in section 4.6.2.1.

4.6.2.1 Verification

To verify the temperature calculations the external temperature is calculated by hand. This can be done using equation 4.18. The peak heat flux is 3089 kW/m^2, σ is the Boltzmann-constant, and ϵ the emissivity of the heat shield given in table 4.3.

$$T_{ext} = \left(\frac{q_{ext}}{\epsilon\sigma}\right)^{\frac{1}{4}} \tag{4.18}$$

This gives a peak external temperature of 2872 K. The peak external temperature calculated by the model is 2795 K. Comparing these temperatures gives a difference of 2,7%, which is acceptable. An explanation for the lower temperature in the model is that the peak heat flux lasts for a very short time after which it decreases rapidly. Therefore the material does not have enough time to heat up to the final calculated temperature.

4.6.3 Descent and Landing System Model

The landing and descent phase is the final phase of the mission. A model was generated to determine the surface area and the amount of parachutes needed to have a successful descent and landing. The verification of this model is shown in section 4.6.3.1 and the validation is shown in section 4.6.3.2.

4.6.3.1 Verification

In order to confirm the compliance of the DLS model shown in section 4.4 verification has to be done. Figure 4.24 indicates the velocity of the re-entry vehicle as a function of height from when the parachute is deployed.

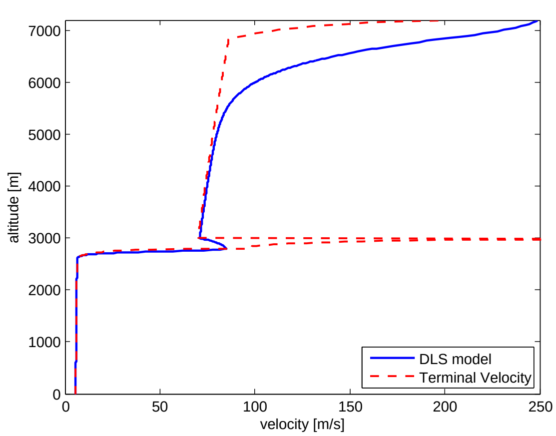

Figure 4.24: Comparing DLS model velocity with terminal velocity

$$D = \frac{1}{2}\rho V^2 S C_d \tag{4.19}$$

$$W = mg \tag{4.20}$$

$$mg = \frac{1}{2}\rho V_{terminal}^2 S C_d \tag{4.21}$$

$$V_{terminal} = \sqrt{\frac{2mg}{\rho S C_d}} \tag{4.22}$$

The plot in figure 4.24 shows the relation between the modelled velocity and the terminal velocity at each section. The terminal velocity was calculated using equation 4.22 at every time increment. It can be seen that there is a correlation between the model and the terminal velocity. When looking at a single parachute procedure the modelled velocity moves towards the terminal velocity. The terminal velocity indicates the asymptote where the modelled velocity cannot cross. It can be seen that at the end of each parachute phase the modelled value is nearly identical to the terminal velocity, with a correlation of 99%. The main difference occurs at the beginning of each parachute phase. This occurs at an altitude of 7, 4 and 3 km. At these altitudes the DLS detaches a parachute and deploys the following parachute. During this period the terminal velocity increases greatly due to the decrease in surface area. The model indicates a cumulative velocity change therefore it does not have a peak as severe. When the following parachute is fully deployed the modelled velocity progresses towards the terminal velocity once more. Overall this analysis verifies the model used for the DLS.

4.6.3.2 Validation

To validate the DLS model the descent procedure of the Apollo program was used. Table 4.11 indicates all the important variables.

Table 4.11: Apollo descent and landing system data [33]

Phase	Height [km]	Velocity [m/s]	Diameter [m]	Amount
Drogue chute	7.2	247.80	4	2
Pilot chute	3.0	72.43	2	3
Main chute	2.8	72.22	25	3
Splash down	0	8.88	25	3

These values were inserted in the DLS model generated for the Inspiration Mars mission. The results for the data are shown in figure 4.25 and figure 4.26.

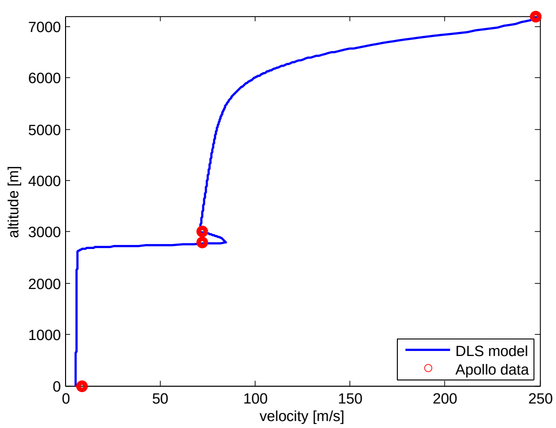

Figure 4.25: DLS velocity against height

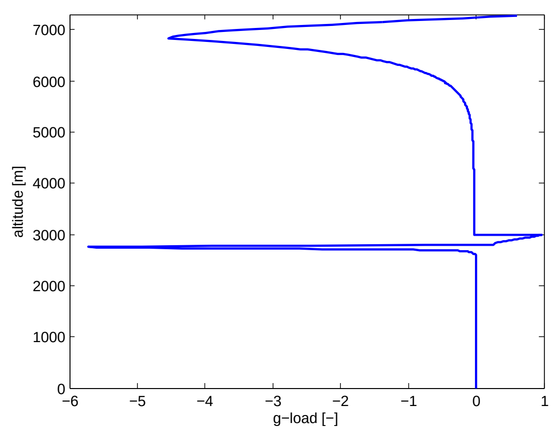

Figure 4.26: DLS acceleration against height

In the validation process some correlations and discrepancies can be identified. The first correlation is that the Apollo data follows the general trend of the model. All points lie close to the velocity lines generated by the model. Additionally, the g-load received remain below 6 g which is a feasible value. The main discrepancies occur when looking at the main chute deployment and the touch down velocity. The main chute deployment phase differs from the flight data due to the connection system of the parachute. During the Apollo mission the pilot chute deployed the main chute continuously while the model first releases the pilot chute and then deploys the main chute. This explains the rise in velocity due to the decrease in surface area. During landing the touchdown velocity for the Apollo mission is 8.8 m/s while the model indicates a touchdown velocity of 6.8 m/s. This difference in touchdown velocity can be explained by the fact that the model assumes a perfect single surface area parachute. In reality this is not the case, due to wind discrepancies and the interaction between the three separate parachutes. These disturbance result in a less efficient system. That is the reason why an additional safety margin of 40% was taken into consideration in section 4.4. To conclude the model can be validated if an additional safety margin is taken.

4.7 Cost Estimation

There are two aspects to this mission that require an investment. The first, is the cost if the re-entry capsule, the relation to determine the total man hours is shown in equation 4.23[36]. The second is the recovery cost, this is shown in equation 4.25[36].

$$H_{vc} = 275M^{0.48} f_1 f_2 f_3 \tag{4.23}$$

$$f_2 = (NT_m)^{0.15} \tag{4.24}$$

$$C_{Rec} = 1.5/L(7L^{0.7} + M^{0.83}) \tag{4.25}$$

As can be seen equation 4.23 has four unknowns. The first is the mass of the vehicle which is 2800 kg. The factor f_1 is dependent on the technology used. Since the dragon capsule is a modification of an existing project the factor is 0.4 [36]. The factor f_2 indicated in equation 4.24[36] is dependent on the number of passengers and the mission time. To determine f_3 the experience of the development team needs to be considered. The team responsible for the modifications have already preformed developments on similar projects therefore the factor is 0.6 [36]. The costs for recovery now needs to to be determined. The undetermined variable is L, this indicates the launch rate, since only one mission is being launched the for L is one. The final costs are shown in table 4.12.

Table 4.12: Cost for the re-entry vehicle and retrieval

Description	**Value**	**Unit**
Re-entry vehicle man years	3476	MYr
Re-entry vehicle cost	862M	Eur
Retrieval man years	13	MYr
Retrieval cost	4.02M	Eur

Looking at table 4.12 the total cost of the re-entry vehicle is 862 million. This is calculated from the amount of total man years. The exact value for man years is given in section 7.2. The cost of the re-entry vehicle includes buying, modifying and testing. The complete cost of the mission is indicated in section 7.2.

4.8 Conclusion and Recommendations

4.8.1 Conclusion

It can be concluded that it is possible to re-enter the earth atmosphere using the dragon capsule with modifications. The peak load during the procedure is 8 g with an average load below 4 g. The critical sub-system would be the GNC it would have to have a pointing accuracy of 0.04 degrees. Additionally, the maneuvers to change the bank angle would have to be timed correctly to reduce the load. The temperature inside the crew cabin is kept below 30 degrees Celsius during this procedure. Below 7.5 kilometers altitude the Descent and Landing System (DLS) activates. The first step is to jettison the heat shield, eliminating heat transfer from the heat shield to the crew cabin. Then the parachute system is activated. The system comprises of two drogue chutes, three pilot chutes and three main chutes. To reduce risk a redundant parachute is used, this means that the capsule would be able to land with one drogue chute and two main parachutes. The vehicle is design to land in water to absorb the shock and reduce the temperature of the cabin further. The footprint of the vehicle will be high due to high re-entry velocity, therefore a small fleet ships scattered across the Ocean will need to be used to pick-up the vehicle. This will give the crew a maximum waiting time of one hour before recovery. This procedure can be accomplished with current technologies if these steps are followed.

4.8.2 Recommendations

Recommendations for the future is to further optimize the flight path trajectory and determining the exact corridor width. This will help in minimizing the footprint reducing recovery time. A full 3D model of the capsule to simulate the movement though Earth could be made. This could be used to analyze the lift and drag ratios with greater accuracy. To improve the LDS model the interaction of separate parachutes should be analyzed. Finally, a further investigation needs to be made into radiated and absorbed heat as well ablative properties of the heat shield.

Chapter 5

Spacecraft Subsystem Design

5.1 Environmental Control and Life Support System

The Environmental Control and Life Support System (ELCSS) is needed to sustain human life and workability. Since Inspiration Mars is a manned mission, an ELCSS needs to be selected to ensure the safety of the mission and to provide for the basic needs of the crew. Below, the list of general requirements for the ECLSS is presented.

5.1.1 ECLSS Requirements

- The ECLSS shall carry a crew of two people.
- The ECLSS shall provide a safe living space for the crew.
- The ECLSS shall carry the equipment and consumables to support the crew for a period of 501 days.

5.1.2 Selecting an ELCSS

To select the appropiate ECLSS for Inspiration Mars, different options are considered. The first question is whether or not the mission requires a regenerative or a non-regenerative system, and thus whether an open or a closed loop is required. For this mission, a non-regenerative system is required since there will not be any form of re-supplying and therefore a closed loop system is used. Within the closed loop systems two options are available, the Bio-regenerative and the Physico-chemical system. The Bio-regernative system uses living organisms to produce and break down molecules in the ECLSS, and the Physico-chemical system uses physical, chemical and mechanical devices [38]. A trade-off study between these two systems is presented in table 5.1.

Table 5.1: Trade-off between bio-regenerative systems and physico-chemical systems

System type	**Advantages**	**Disadvantages**
Bio-regenerative	Able to produce O_2 Able to remove CO_2 High sustainability	Requires higher volume Requires higher power Requires more crew input time
Physico-checmical	Simple maintenance High reliability	Low sustainability Limited system duration

From the trade-off study presented in table 5.1, the conclusion is drawn that the Physico-chemical life-support system is the best option for Inspiration Mars and this conclusion is mainly based on the criteria for volume and power. The next step is to find the mass, volume and power values for the ECLSS elements and this is done using [37, table 3.1.10] and is presented in table 5.2. In the next section further information is provided on the composition of the values in this table.

5.1.3 Advanced technology

In the preliminary design phase, mass and volume was estimated using baseline technologies from [25, table 18-3]. For the detailed design though, advanced technologies are considered. This is defined by technologies which are lighter, less power intensive, and require less volume [37]. This model uses a Physico-chemical life-support system, and in order to scale it for the Inspiration Mars mission duration and crew size a number of assumptions are made. First of all a distinction is made between the mass and the Equivalent System Mass[2] (ESM). Both these masses and volumes are scaled down linearly for the mission duration and crew size to match the Inspiration Mars profile. This choice, in contrary to make a distinction between fixed and variable percentages of the sub-system values, was made since also the system sizes will change with the crew size. E.g. less crew members require a lower amount of potable water, and will thus result in a decrease in the water tank size. The assumption is made that the fixed components do not represent a significant percentage of the total, so neglecting them will not lead to severe underestimations [39]. The results of these calculations are presented in table 5.2.In 5.1 the diagram of this advanced ECLSS system is presented.

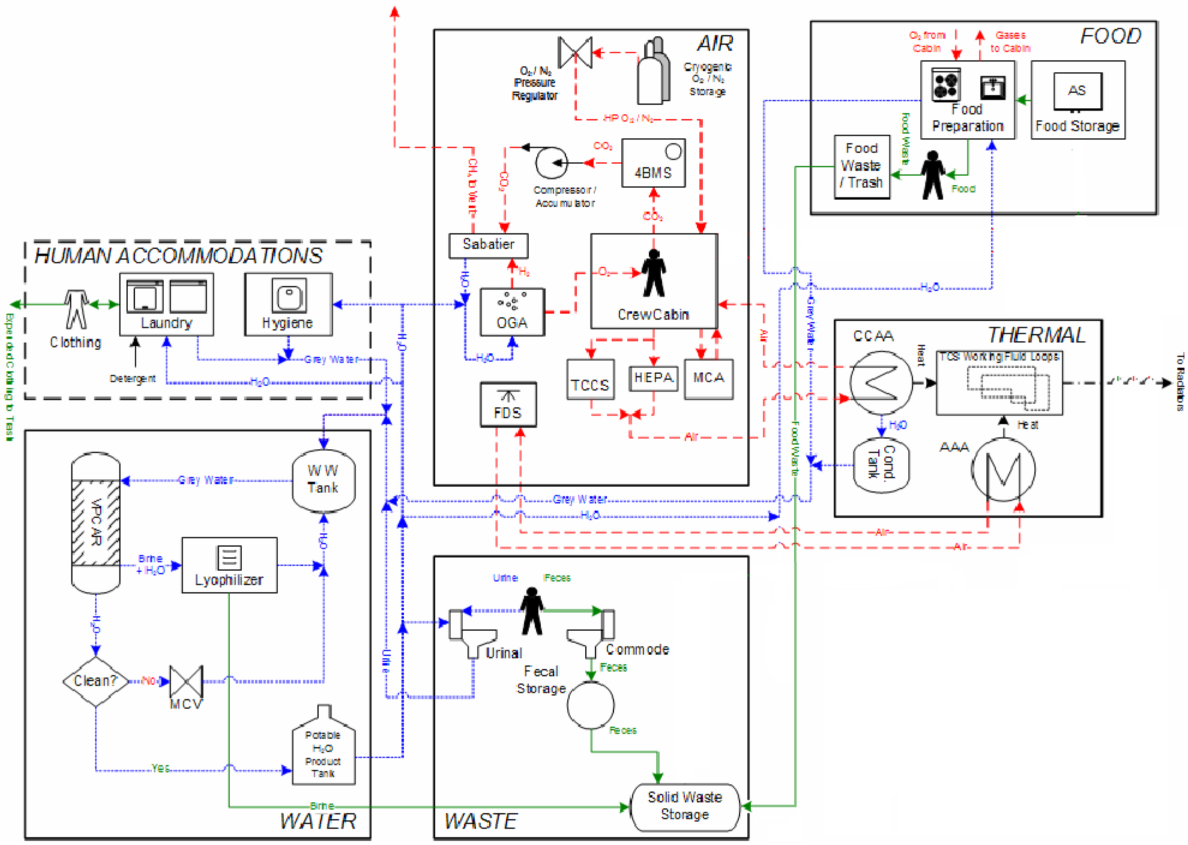

Figure 5.1: ECLSS using advanced technologies (modified from [37])

5.1.3.1 Specifications on ECLSS values

To specify on the ECLSS values, the composition of the different elements of the ECLSS sub-system is presented here. First of all, the air system consists of an atmospheric control system, to control pressure, and revitalization system, to generate oxygen and remove carbon dioxide. Furthermore, this system takes care of the gas storage and fire detection and suppression. Next, the food system accounts for the food processing, packaging and storage. To safe on mass and volume food is not individually packed but multiple items per package is aimed for[40]. Note that the food is pre-packed and not hydrated, again to save mass and volume. The thermal system contains the cabin air assembly system, atmosphere circulation and microbial control within the module. The waste system consists of a solid waste collection system and a solid waste processing system. Next, the water system takes into account the urine and waste collection system, a water recovery system and a water storage system. In fact, the largest contribution to advanced technology gain is from water recycling systems [40], and this technology is very beneficial for long missions since less potable water is required to launch and more can be recycled. Items as clothing, laundry equipment and wipes are accounted for in the human accomodations section [37, table 6.10].

Table 5.2: ECLSS values using advanced technology

Sub – system[1,3]	**Mass [kg]**	**Volume [m^3]**	**Power [kW]**	**ESM**[2] **[kg]**
Air	696	1.50	2.21	1,283
Food	1,146	5.11	0.47	1,317
Thermal	172	0.52	0.46	301
Waste	130	3.16	0.01	161
Water[6]	315	1.49	1.56	694
EVA[4]	435	3.00	-	435
Human Accomodations	440	0.69	0.32	531
Space Free *Component*[5]	-	10.20	-	-
Totals	3,334	25.66	5.03	4,722

[1] Sub-system values based on Hanford, 2005 [37]
[2] Equivalent System Mass (ESM) is the sum of the masses of life support equipment and supplied commodities, plus the mass penalties for infrastructure support
[3] Values for the sub-systems include a 10% contingency
[4] Accounts for the Extravehicular Activity (EVA), [25, table 22-2]
[5] Accounts for the space free volume for the crew
[6] More details on this value are given in section 5.1.3.3

5.1.3.2 Peak power determination

For the determination of the peak power, two assumptions are made. The first assumption [41] [42] counts for the group of food, water and waste, which is approximated and assumed as an activity. This activiy contains the act of eating and using the water and waste system for metabolic reasons. This is calculated for four times 1h, per crew member per day. This gives a total of 8h for the peak power. The calculation which follows is taking the sum of average power, given in table 5.2, of these three sub-systems over 24 hours and comparing that to the peak power over 8h. The peak power for this activity, and thus sub-system group, follows from this and gives a value of 6.12 kW. The second assumption [41] [42] is for the air and thermal sub-system, for which a day and night cycle is accounted. The average power is multiplied by the factors [40] used for the day and night cycle, and this gives a peak power of 3.09kW and 1.38kW for the air sub-system and the thermal sub-system respectively. This results in a total peak power of 10.59kW.

5.1.3.3 Water management

After calculating the mass, volume and power of the water system, the mass is reduced by 300 kg. This is due to the use of fuel cells in the Low Earth Orbit (LEO). In LEO, the power source of the spacecraft are the fuel cells, and aside from generating power these cells also produce water . This amount of water, 300 kg, is taken off the original potable water value of 615 kg and therefore the total potable water mass is reduced to 315 kg. This lower value is beneficial for the system, and the power generation by fuel cells also adds to the sustainability of the ECLSS. Note that the values for power and volume of the water do not change due to this change in mass, since the water tanks will have to manage the total of the 315 kg plus the 300 kg, and also the same power is needed to manage this.

5.1.3.4 Dietary radiation protection

In addition to the general radiation protection 5.2.4, dietary radiation protection is used to protect the crew during the flight. The first option is the use of antioxidants. Antioxidants as vitamins A and C soak up the free radicals which are produced due to radiation, before they have the chance to harm the body. Omega-3 fish oil can be used during and after the journey, to act as a countermeasure from the long-term exposure. Another countermeasure is the use of Radiogardase, which is a drug which increases the rate at which radioactive substances are eliminated from the body [45]. In addition to that, another type of drug that can be used are radioprotectants [44] which cause faster recovery after radiation damage. Radiation protection is realized by stimulating the growth of surviving stem cells and progenitor cells. This drug also increases the duration of the cell cycle segment which checks for damaged genes and repairs them.

5.1.4 Extravehicular Activity

In order for the crew to perform an Extravehicular Activity (EVA) the Extravehicular Mobility Unit (EMU) needs to be studied. The EMU functions as a critical protection system and allows the crew to perform the EVA, which is an event that takes place two times in this mission design. In this regard, the two EMUs used on the ISS are traded off in this section, namely the U.S. enhanced Extravehicular Mobility Unit (EMU) and the Russian Orlan-MK. In table 5.3 the trade-off study between the two options is presented.

Table 5.3: Trade-off study between the U.S. enhanced EMU and the Russian Orlan-MK

EMU type[7]	**Advantages**	**Disadvantages**
Russian Orlan -MK	High operation pressure (40 kPa) Minimal pre-breathe time Shorter don/doff time due to rear entry Disposable consumables Allows don/doff without assistance One-size design results in lower costs	Difficult manipulation due to high pressure Higher stowage volume One-size dsign Less comfort Political issues
U.S. EMU	Lower operating pressure (29.6 kPa) Allows relatively better manipulation Less demanding phsysical activity Custom fit suit design Modular design includes replacement parts	Increased pre-breathe time due to lower pressure Higher don/doff time Higher costs More back-up suits required Regenerative consumables demand crew input time

[7] Based on a study on deep space habitation modules, for the AIAA [43]

Though the costs and crew input time are relatively higher for the U.S. EMU design, the low operating pressure, the comfort and the mobility of the U.S. EMU design, lead to the decision of choosing the U.S. EMU design for the mission. In table 5.4, the specifications for the U.S. EMU are presented.

Table 5.4: U.S. EMU specifications

Parameter[8]	**Value**
Mass[4]	145 kg
Volume[4]	1.0 m^3
Portable Life Support duration	8 h
Operating pressure	29.6 kPa
Don/doff entrance	Waist
Biomedical monitoring	ECG3, skin electrodes
CO2 removal	Metox canisters
Battery	21.8 VDS, 1.5-1.6 A
Umbicial length	1 fluid/electrical, 3.53 m
Suit life-time	25 EVAs

[4] Based on EVA, [25, table 22-2]
[8] Based on [43, table 9-2]

5.1.5 Sensitivity Analysis

In this sensitivity analysis of the ECLSS the change in a number of parameters is presented, to account for changes in mission duration. Two situations are analyzed, one being a mission duration of 10% more than planned and one of 10% less than planned. This 10% range is chosen in case of an emergency which forces a longer duration in LEO, or a change in trajectory which takes a longer time. An improvement in the trajectory though, would result in a shorter mission duration. In table 5.5 the combined values of mass, volume and power are given for food and water, in case of a change in mission duration. From this table the conclusion is drawn that the ECLSS design is sensitive, since the change in mass, volume and power is within the range of 10% and this within the requirements of the maximum launch mass.

Table 5.5: Sensitivity ECLSS

Changed input parameter	**ESM [kg] (Δ%)**	**Volume** $[m^3]$ **(Δ%)**	**Power [kW] (Δ%)**
Nominal conditions	2011 (0)	6.6 (0)	2.03 (0)
+10% Mission duration	2212 (+10)	7.26 (+10)	2.23 (+10)
-10% Mission duration	1810 (-10)	5.94 (-10)	1.83 (-10)

5.1.6 Verification and Validation of the ECLSS

In order to check whether the designed ECLSS meets the mission requirements and needs, the system needs to be verified and validated. The verification method is described below, comparing the results with specified calculations. Yet, there are no comparable operating ECLSS in service for a deep space mission, and the technology used is a step beyond the state-of the-art technology. For these two reasons, validation of the ECLSS is not applicable.

5.1.6.1 Verification

Since this is the very first manned mission to Mars, it is not possible to compare results of the system to reference missions. Though there are no executed missions to refer to, there are a number of concepts in which manned deep space missions are studied. To verify the obtained ECLSS, it is compared to these concepts. What makes these concepts reliable are the years of research by qualified scientists in the space industry, in both European studies [107] and American studies [38] [37].
Regarding the requirement to use off-the-shelf components, this is met by studying the ECLSS results of a Mars Transfer Vehicle which was published in The Mars Journal [37]. This model for a manned mission to Mars has strong resemblance to the Inspiration Mars mission, and is therefore used as a fundamental source for the determination of the ECLSS. The specifications of the Extravehicular Activity though, are based on [25] and compared to results of a study on Deep Space Habitation Modules [43].
After the determination of all values for this system, the complete system is compared to the only Mars study with identical mission requirements, namely the study of the Inspiration Mars Foundation [40]. The conclusion of this verification process is that the ECLSS design is definitely comparable with these studies, but differs on a number of aspects due to the use of advanced technology. This technology is mainly noted in the mass results of the water system, which is relatively low [40]. This difference though is aimed for and thus expected, since advanced technology used in the design result in higher efficiency of the water cycle and requires less potable water to be brought on board. The average power, on the other hand, is expected to be relatively higher to ensure this recycling efficiency, and this is indeed the case when compared [40].

5.2 Spacecraft Structural Design

The structure is the base for all sub-systems and defines the shape of the spacecraft. Its integrity is of primary importance for the mission success. In this chapter, the design of the structure to shield against Micrometeorite and Orbital Debris (MMOD) and deep space radiation will be discussed. Furthermore, the structure will be checked for the critical loads that will occur during the mission.

5.2.1 Micrometeorite and Orbital Debris Protection

In space, spacecraft are under the constant risk of MMOD impact damage which have the potential to decrease its performance or result in catastrophic loss of the vehicle. Micrometeorites are particles in deep space as well as in Earth orbit that weight up to one gram and can travel at hypervelocity up to 72 km/s with respect to the spacecraft. Orbital debris consists of high density materials on Earth orbit that travel at hypervelocity up to 15 km/s [55]. It is thus seen that the MMOD risk is higher in Earth orbit, where only a small percentage of the mission duration will take place, due to the orbital debris presence.

MMOD Protection Design

The typical MMOD design process used by NASA is shown through the flow diagram in figure 5.2.
For the scope of this report, the hypervelocity test & analysis and MMOD probability analysis code results

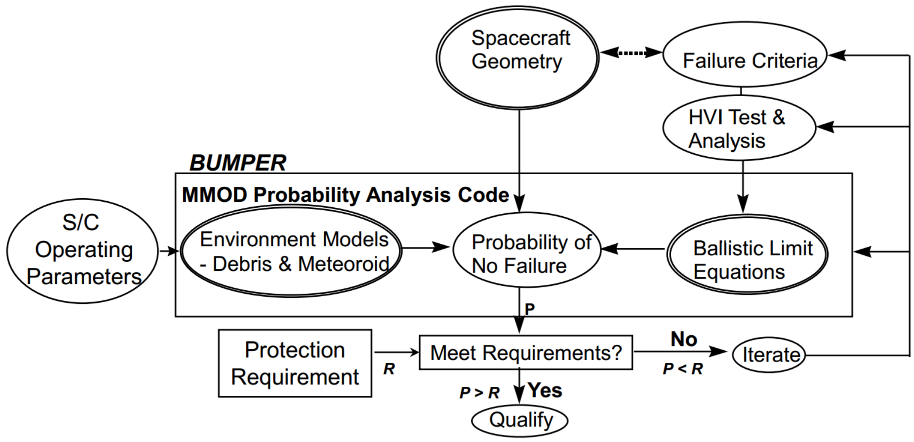

Figure 5.2: MMOD protection design and evaluation process [55]

will be used from existing shield configurations. Then taking into account the spacecraft geometry, operating parameters and requirements for the mission, the most optimal solution is designed. The following main requirements were identified:

- Protect the crew from MMOD impact.
- Protect the critical spacecraft hardware from MMOD impact.
- Minimize damage to all spacecraft elements from MMOD impact.
- Reliability of the MMOD protection of 99%

To meet this requirements while keeping in mind the general objective of minimizing mass and cost, the design is optimized to have increased protection on the higher impact risk areas of the spacecraft. The objective is then to make MMOD risk equal per unit area across the spacecraft during the whole mission. For this, the mission is then divided in two phases: Earth orbit phase and Interplanetary Trajectory phase. The first phase, will account for 2% of the mission duration and the forward face of the spacecraft (which has the higher risk of MMOD impact) will be the back part of the Dragon reentry capsule. The Dragon spacecraft is already designed to resist MMOD impacts for a mission duration of up to 2 years in Low Earth Orbit (LEO) [68]. Therefore for this phase of the mission, the protection available by default is assumed to be sufficient to meet the requirements.

The second phase will account for the remaining 98% of the mission duration thus it is the main concern for the design of MMOD protection. During this phase, protection must be provided against micrometeorites as bigger particles can be detected with a radar or telescope system and avoided by maneuvering the spacecraft.
The MMOD shielding capability is mainly influenced by both configuration (more standoff distance and number of layers is better, see figure 5.4) and material selection. This can be seen on figure 5.3 as the shields with more bumper layers require less mass for the same protection level.

A trade off was performed between the available MMOD shielding designs that have been tested. The following three were considered and compared with different projectile impact tests: Whipple shield, Multi-Shock Shield and Mesh Double-Bumper Shield. The way these work is that a single or several outer bumpers break up, melt or vaporize the particles that impact the spacecraft reducing its kinetic energy before they

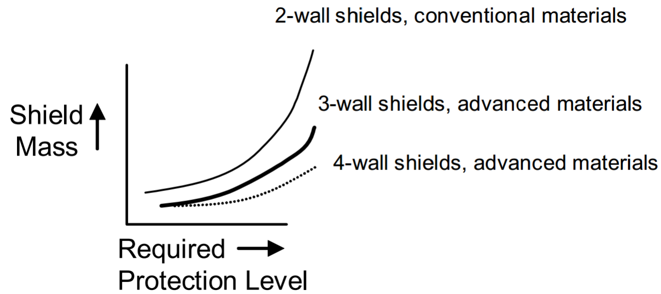

Figure 5.3: Different shield types needed mass to meet the protection level required [55]

reach the rear wall. The results of the impact tests in terms of the shield mass per unit area that resulted in no perforation or crack of the rear wall are shown on table 5.6.

Table 5.6: MMOD shields impact test results at 6-7 km/s in terms of areal density needed for no shield failure [55]

Overall Shield Spacing [cm]	**Impact Angle [deg]**	**Whipple Shield**	**Multi-Shock Shield**	**Mesh Double-Bumper Shield**
		Shield Areal Density [g/cm^2]		
0.32 cm (0.045 g) aluminum projectile				
10	0	0.6	0.29	0.25
10	45	1.50	0.31	0.36
0.64 cm (0.37 g) aluminum projectile				
10	0	2.07	1.10	0.94
20	0	0.96	0.63	0.64
0.95 cm (1.3 g) aluminum projectile				
30	0	1.35	1.02	1.08

From the test results it is observed that the Multi-Shock Shield performs the best as the shield spacing becomes higher. Since minimizing mass is more important for the design of the spacecraft than volume, this shield is the the most optimal. It can support an impact of a 1.3 grams projectile with a shield areal density of 1.02 g/cm^2. This shield composed of four ceramic fabric bumpers followed by an Aluminum or Kevlar rear wall as can be seen on figure 5.4.

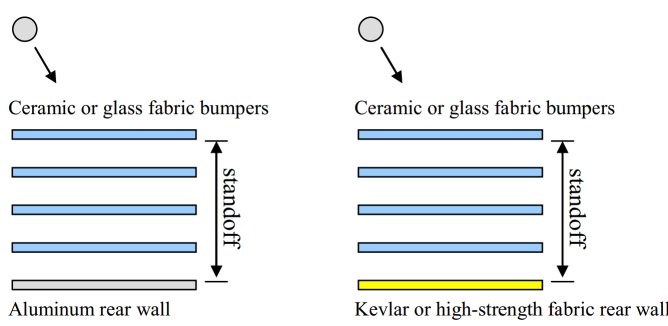

Figure 5.4: Multi-Shock shield configurations [55]

The reason why multiple bumper configurations are more effective for MMOD protection is that they provide a greater breakup of hypervelocity projectiles for same weight of single bumpers. Also the ceramic fabric bumpers produce no extra debris once hit by a particle as opposite to aluminum bumpers. The size and exact configuration of the Multi-Shock shield can now be calculated for the specific requirements of the mission. With equation 5.1 the areal density of all four bumpers is calculated and equations 5.2 and 5.3 give the thickness of the aluminum rear wall and areal density for the Kevlar rear wall [55]. All this equations are used together with equation 5.4 (critical projectile diameter at shield failure threshold) to build a Excel sheet that provides the areal density of the Multi-Shock shield needed for different projectile mass, velocity and standoff distances.

$$m_b = 0.185 d\rho \tag{5.1}$$

$$t_w = kMV_n {\rho_w}^{-1} S^{-2} {\sigma'}^{-0.5} \tag{5.2}$$

$$m_w = KMV_n S^{-2} \tag{5.3}$$

$$d_c = K_{H-MS} {m_w}^{1/3} {\rho_p}^{-1/3} V^{-1/3} (\cos(\theta))^{-1/3} S^{2/3} \tag{5.4}$$

After several iterations for different impact scenarios it is found that the Kevlar configuration of the Multi-Shock shield requires less areal density for the same MMOD resistance. The final values used for the chosen configuration to meet the requirements are shown on table 5.7. In the next sections it will be calculated

Table 5.7: Multi-Shock MMOD shield sizing parameters

Symbol	Parameter	Value	Unit
m_b	bumper areal density	0.53	g/cm^2
t_w	Kevlar rear wall thickness	0.34	cm
m_w	Kevlar rear wall areal density	1.01	g/cm^2
M	projectile mass	1.5	g
d	projectile diameter	1.02	cm
ρ_p	projectile density	2.8	g/cm^3
S	gap distance	30	cm
θ	impact angle from target normal	0	deg
V	projectile velocity	10	km/s
V_n	normal component of projectile velocity	10	km/s
k	coefficient	41.6	s/km
K	coefficient	29	s/km

whether this structure can withstand the required loads for the mission and it will be explained how it can be combined with radiation protection.

5.2.2 Design for Structural Loads

The process for sizing the module structure is presented in this section. The thickness of the module for different materials is driven by either strength or stiffness requirements. The process will start by sizing the thickness for different potential materials and checking the resulting natural frequency. To simplify the process, some assumptions are made:

- The module is assumed to be a cylindrical shell.
- The shell is a solid-skin monocoque.
- The cylinder has uniform thickness and, by definition, no ring or longitudinal stiffeners.
- The rear wall of MMOD shield will be the load carrying structure.

Structural Load Requirements

Load paths are considered as a tree. Load path for any leaf in the tree through a twig could be traced, into a climb, and down the trunk to the ground. As with a tree, the structural members in a spacecraft should be strongest where the load are highest, at the launch vehicle interface. Additional design must be designed to carry the launch loads, applied in any direction. The following requirements are identified:

- The structure must be able to support the maximum load factors.
- The payload should withstand a lateral vibration greater than 10 Hz, and a axial vibration greater than 25 Hz.[22]
- The structure must be able to support ultimate loads without failure.

Sizing for Internal Pressure

For a manned mission it is necessary to pressurize the crews living module to an acceptable internal pressure. In Space, the maximum internal pressure for the crew-module design is 0.0337 MPa [56].
The internal pressure creates a longitudinal and a hoop stress in the walls of the cylindrical tube. These stresses are expressed as stated in equation 5.5. [25].

$$\sigma_{p,long} = \frac{pr}{2t}; \sigma_{p,hoop} = \frac{pr}{t} \tag{5.5}$$

Where p is internal pressure [MPa], t is thickness [mm] , and r is the radius of cylinder [mm]. The properties of the materials considered in section in 5.2.1 and other commonly used for space operations are shown in table 5.8.

Table 5.8: Material properties [25],[60]

Material	Al 2219-T851	Kevlar 49	Al 6061-T6	Steel 17-4PH
Ultimate Tensile Strength [MPa]	420	3757	290	860
Yield Tensile Strength [MPa]	320	3620	240	690
Youngs Modulus [MPa]	72,000	112,400	68,000	196,000
Density [kg/m^3]	2850	1440	2710	7860
Cost [USD/kg]	5.5	15	7.55	9.2
Ratio (Ultimate/Yield)	1.3125	1.04	1.21	1.25

The design factors of safety during launch are 2 for ultimate stregth and 1.5 for yield strength [25]. The ratio of these factors is 1.33. For the materials which the ratio exceeds the ratio of allowable ultimate and yield strengths, only the ultimate hoop stress will be calculated by equation 5.6. For the materials which the ratio is less than the ratio of allowable ultimate and yield strengths, both equations 5.6 and 5.7 are required.

$$t_{u,h} = k\frac{pr}{F_{tu}}; t_{y,h} = k\frac{pr}{F_{ty}} \tag{5.6}$$

$$t_{u,l} = k\frac{pr}{2F_{tu}}; t_{y,l} = k\frac{pr}{2F_{ty}} \tag{5.7}$$

Where p is the internal pressure, F_{tu} is the allowable tensile stress, F_{ty} is the allowable yield stress and k is the corresponding safety factor, t is the required skin thickness, where u stands for ultimate tensile strength, y for yield tensile strength, h for hoop stress and l for longitudinal stress. Table 5.9 summarizes the required thickness that has been calculated for each material.

Table 5.9: Required wall thickness for internal pressure

Material	Al 2219-T851	Kevlar 49	Al 6061-T6	Steel 17-4PH
Thickness t_1 [mm]	0.289	0.0322	0.418	0.141

Applied and Equivalent Axial Loads

Since the Falcon Heavy is still in experimental stage, the Falcon 9 is chosen as the most comparable launcher. Falcon 9 design load factors are used from the plot envelope of this launcher. The two highest design load factors are chosen for further calculations [22]. For initial sizing some assumptions are made:

- The structure is assumed to be simply supported.
- The axial compression is caused only by axial force and bending moment.
- Any torsional and shear stresses are ignored.
- The cylinder is a simple beam, with the module mass uniformly distributed between trunnion supports.

By multiplying the spacecraft weight by the load factors, the maximum expected forces acting on the structure are calculated. The compressive force P_c and the bending moment M_{max} are calculated with equation 5.8 and equation 5.9.

$$P_c = W n_x \tag{5.8}$$

$$M_{\max} = \frac{wL^2}{8} = \frac{WLn_{y,z}}{8} \tag{5.9}$$

Where w is the load per unit length, W is the total weight of the crew module, L is length, n_x and $n_{y,z}$ are the load factors in x direction and y and z direction. Table 5.10 shows the results of launch loads.

Table 5.10: Applied loads on cylinder

Event	**Limited Load Factors**		**Expected Loads**	
	$\mathbf{n}_x$	$\mathbf{n}_{yz}$	$\mathbf{P}_c$ **[N]**	$\mathbf{M}_{max}$ **[10^3 Nmm]**
Case 1	6	0.5	689,839.2	61,798.1
Case 2	3.5	2	402,406.2	247,192.4

Sizing for Tensile Strength

The equation for axial stress, σ , is $\sigma = \frac{P_c}{A}$ [8]. To size the thickness of the cylinder for tensile strength, the compressive force P_c from the case one, and the material allowable stress σ which is equal to ultimate tensile strength are used to solve for the required thickness. The required thicknesses for each material are given in table 5.11.

Table 5.11: Required wall thickness for tensile strength

Material	**Al 2219-T851**	**Kevlar 49**	**Al 6061-T6**	**Steel 17-4PH**
Thickness t_2 [mm]	0.145	0.016	0.210	0.071

Sizing for Stability

The buckling stress for an unpressurized, isotropic and monocoque cylinder is:

$$f_{cu} = \frac{Et}{r} 0.6\eta\gamma \tag{5.10}$$

Where E is the modulus of elasticity, t is shell thickness, r is the cylinder radius, η is a plasticity correction factor equal to 1.0, and γ is a correlation factor which is equal to 0.5.[25]

The maximum normal stress imposed on the structure during the launch, is originated from the axial stress and bending stress, which are both normal to the cross section. It can be expressed as:

$$\sigma_{\max} = \frac{P_c}{A} + \frac{Mr}{I} \tag{5.11}$$

Where P_c is the normal force in [N], A is the structures cross-sectional area, M is the maximum bending moment due to the lateral load factors, r is the radius, and I is the structures cross-sectional area moment of inertia.

Now, the cylinder isf sized for stability. The maximum normal stress (equation 5.11) in addition to the longitudinal pressure stress (equation 5.5) which is equal to equation 5.12, must not exceed the critical buckling stress equation 5.10.[25] (See equation 5.12).

$$f_t = 1.4\left(\frac{p_c}{2\pi rt} + \frac{M_{\max}r}{\pi r^3 t}\right) - 1.5\frac{pr}{2t} \leq \frac{Et}{r}0.6\eta\gamma \tag{5.12}$$

Where p is the maximum pressure difference expected during launch (which is assumed to be equal to the internal pressure specified in section 5.2.2), t is thickness, E is modulus of elasticity, and 1.5 and 1.4 are the design safety factors specified for inertia loads and compressive pressure stress.[25]
The ultimate compressive stress needs to be kept less than or equal to the elastic stress buckling stress. Therefore, the required thickness for equation 5.12 will be calculated with equation 5.13. The determined thickness will be the base of the elastic buckling equation 5.10 [25]. The buckling stress should be less than ultimate tensile strength, for the structure to not fail.

$$t = \sqrt{\frac{r}{0.3E}\left[1.4\left(\frac{P_c}{2\pi r} + \frac{M_{\max}}{\pi r^2}\right) - 1.5\frac{pr}{2}\right]} \tag{5.13}$$

Table 5.12: Required wall thickness for tensile strength

Material	Al 2219-T851	Kevlar 49	Al 6061-T6	Steel 17-4PH
Thickness t_3 [mm]	1.825	1.46	1.88	1.106
Buckling Stress f_{cu} [MPa]	21.89	27.36	21.28	36.13

Check the Result by Natural Frequency

The checking process starts with meeting the natural frequency requirements. The applied vibration has lateral frequency of 10 Hz and a axial frequency of 25 Hz as mentioned in section 5.10. The most critical thickness t_3 from the stability can be used to calculate the frequency of the module. This should be higher than or equal to the applied vibration by the Falcon Heavy. Note that the calculation for frequency depends on the assumption of equally distributed mass [8].
The natural frequency of a lateral beam can be calculated by equation 5.14 and the natural frequency for a axial beam is shown in equation 5.15. The calculated natural frequencies are presented in table 5.13.

$$f_{nat} = 0.560\sqrt{\frac{EI}{mL^3}} \tag{5.14}$$

$$f_{nat} = 0.250\sqrt{\frac{AE}{mL}} \tag{5.15}$$

Table 5.13: Natural frequency

Material	Al 2219-T851	Kevlar 49	Al 6061-T6	Steel 17-4PH
f_n for Lateral Beam [Hz]	10.06	11.2	9.92	12.93
f_n for Axial Beam [Hz]	30.4	33.9	29.9	38.9

All materials meet the requirements except for Al 6061-T6, because it has a lower lateral frequency than required.

5.2.3 Module Door Design

The opening or cut-out for the door, produces discontinuities in the cylinder structure; therefore, the loads are in the vicinity of the cut-out and affecting loads in the skin of the living module. Large openings in living module, such as the door and window, needs to be calculated. There are several ways to design a door and the associated cut-out in the living module. To show that the living model (cylinder) with a cut-out for

door carries the loads, the next method is used. First it is assumed that there is no cut-out for the door, therefore the maximum shear flows in the skin can be determined. Then, the door surrounding structure takes all the loads and the door itself will then be treated as a cut-out.[57]
The door design in terms of geometry (and material), is a result of the applied loads. Consider the living module situation shown in Fig. 5.5.

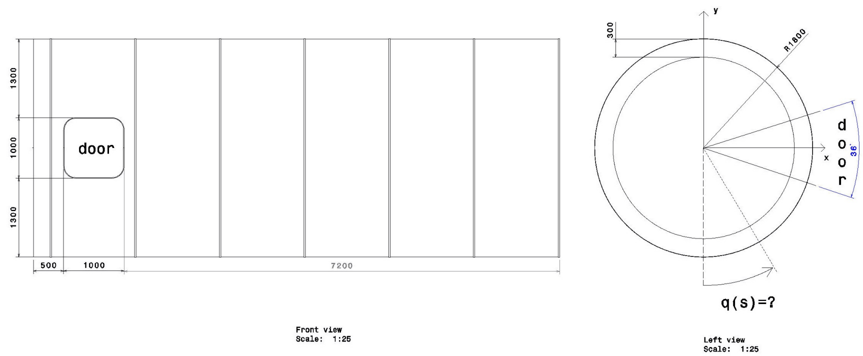

Figure 5.5: Module section with Door

Shear Flow

To determine the maximum shear flows in the skin portion corresponding to the door, it is assumed that there is no cut-out for the door. Figure 5.5 shows the cross-section of the living module and the position of the door. The next steps are done to calculate the shear flow.
The loading on the model is a weight force (with a load factor of 6 g, see table reftab:Applied Loads on Cylinder)at a horizontal location c from the center of the living model. Therefore it could be replaced by a combination of the same shear load acting through the shear center and a torque. This means that knowing the location of the shear center of the circular cross-section, can be crucial for the further calculation. Since the circular cross-section has two axis of symmetry, the shear center must, of course, lie on intersection point of these axes.
The torque caused by the weight force is equal to the moment by shear flow as shown in equation 5.16

$$6Wc = 2A_{encl}q_0 \Longrightarrow q_0 = \frac{6Wc}{2\pi r^2} \tag{5.16}$$

Recall that the basic shear flow distribution due to shear forces is given by:[58]

$$q_b\left(s\right) = -\frac{S_z I_{zz} - S_y I_{zy}}{I_{zz} I_{yy} - I_{xy}^2} \int_0^s tzds - \frac{S_y I_{yy} - S_z I_{zy}}{I_{zz} I_{yy} - I_{xy}^2} \int_0^s tyds \tag{5.17}$$

The expression for the basic shear flow distribution $q_b(s)$ in terms of W, r and θ using formula 5.17 is:

$$q_b = \frac{6W}{\pi r} \cos\theta \tag{5.18}$$

The principle of superposition will be used to determine the shear flow distribution in the cylinder:

$$q(s) = q_b\left(s\right) + q_0 = \frac{6W}{\pi r} \cos\theta + \frac{6Wc}{2\pi r^2} \tag{5.19}$$

Where c is equal to 0.1 m, W is 143.5 [kN], r is 1.8 m, θ is 36 degree. The shear flow distribution is 129.8 [kN/m].

Cut-Out

A single isolated cut-out in the middle of a skin is a non-periodic case. To solve this problem from this point, it is assumed that the door takes no loads, so all the loads that would be at the door must be (appropriately) distributed on the structure surrounding the door such as the cylinder skin. Figure 5.6 shows a module panel provided by a cut-out for the door. The panel is subjected to an shear flow q which would be the value of the shear flow distribution in the panel without cut-out[57]. Now, an opposite shear flow (-q) can be applied to the door panel.

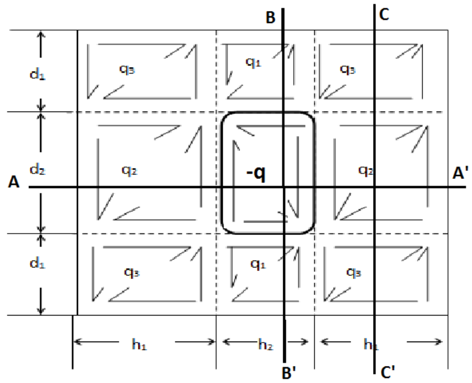

Figure 5.6: Force along A-A', B-B' and C-C'

Horizontal and vertical equilibrium along any line A-A', B-B' and line C-C' (Fig: 5.6), crossing the three middle panels; force summations in x and y direction give:

$$2q_2h_1 = qh_2 \Rightarrow q_2 = \frac{h_2}{2h_1}q \tag{5.20}$$

$$2q_1d_1 = qd_2 \Rightarrow q_1 = \frac{d_2}{2d_1}q \tag{5.21}$$

$$2q_3h_1 = q_1h_2 \Rightarrow q_3 = \frac{h_2}{2h_1}\frac{d_2}{2d_1}q \tag{5.22}$$

Consider the cylinder as a panel. The complete panel has a width of 11.3 m and a height of 8.6 m. To make it simpler, a cut-out with a width of 11.3 m and a height of 2 meter from the complete panel is considered. The dimensions in [m] and the shear flow in [kN/m] are shown below:

$$d_1 = 0.5; d_2 = 1; h_1 = 5.085; h_2 = 1.13 \tag{5.23}$$

$$q_1 = 261.3; q_2 = 145.2; q_3 = 116.1 \tag{5.24}$$

Using the shear strength τ of the material which is almost 60% of its yield tensile strength, [60] and a safety factor 'j' of 1.5, the minimum thicknesses in [mm] of the individual skin panel around the door cut-out, from equation 5.25 are: t_1=0.18; t_2=0.10; t_3=0.08 .

$$t = \frac{q}{\tau}j \tag{5.25}$$

The thickness of rear wall from MMOD is higher, thus the living model can carry the loads with a cut-out for the door.

5.2.4 Radiation Protection

Earth provides protection from deep space radiation environment through solar winds, the atmosphere and its magnetic field. For this first manned interplanetary mission, radiation protection is a critical aspect. The crew will be subjected to three types of radiation, classified by their source:

- Van Allen Radiation Belts: bands of increased radiation trapped close to Earth. Due to the small amount of time that the crew will be under their influence, they are not considered a dangerous source of radiation.
- Galactic Cosmic Radiation (GCR): it is composed of high energy particles with an isotropic flux in all directions. Due to its high energy, it is the most difficult kind of radiation to shield against. GCR is affected by the Sun's natural 11 year cycle in such a way that when there is a solar minimum, GCR is at its maximum and vice versa as seen on figure 5.7.
- Solar Cosmic Radiation: it is composed of two different kinds of radiation, low energy constant radiation which is considered not to be dangerous and highly energetic solar particle events (SPE) which occur in only small regions of space but can be critical for the crew if not shielded for. Their activity level can be observed in figure 5.7.

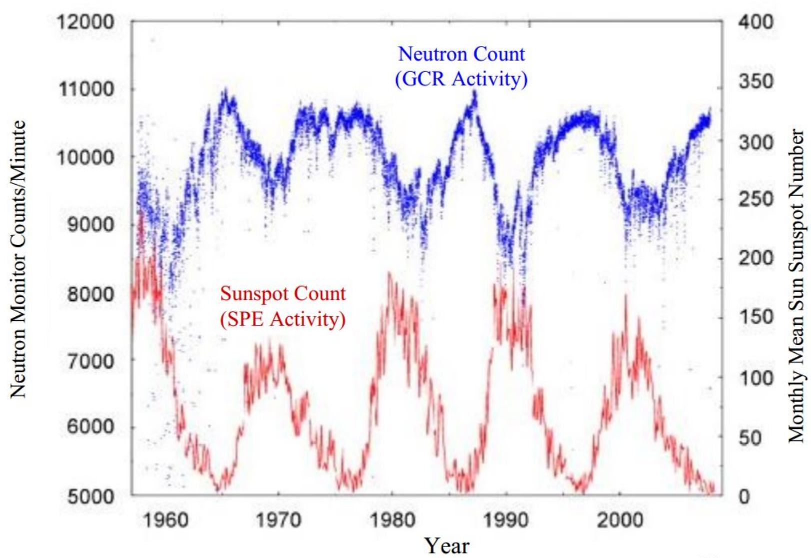

Figure 5.7: GCR and SPE activity through the solar cycles [67]

Radiation Protection Design

The design of the radiation protection for this mission starts from the basic requirements as specified by NASA for manned space missions [62]. Assuming a crew age of 40 years old at the time of exposure, the radiation dose should not exceed 0.8 Sv for a duration of 1 year for less than a 3% Risk of Exposure Induced Death (REID) sometime in life. For this particular mission, with a duration of 501 days the maximum radiation dose for a 3% REID is estimated to be 0.16 cSv/day Also the limit for a single acute dose of radiation (from SPE) is set to 0.5 Sv [63].
With the available technology for the launch date of the Imspiration Mars Delft mission, only passive bulk shielding is practical to protect the crew against radiation. Different tests in Space and on Earth have showed that light materials with a high hydrogen content are best for this task. Water and polyethylene are two of the most efficient radiation shielding materials with water having also the advantage that it can be used during the mission.
The expected dose from GCR if no radiation protection is provided will be: 0.17 cSv/day during solar minimum and much lower doses during solar maximum. It is expected that around the date of the mission a solar minimum will occur so the worst case scenario is considered for GCR protection design. This means that the GCR radiation dose must be reduced by at least 6%. The reduction of dose provided by the MMOD protection shield is estimated: it is compossed of nextel and Kevlar which both perform similar to polyethylene as shown in different tests [64] and it is tested that 1g/cm^2 of Polyethylene reduces the radiation dose by 4%. There is an extra 2% dose reduction that can be assumed from the subsystems that will surround the free space of the crew in the living module since a 2.2% reduction of GCR dose is obtained

from just 1g/cm^2 of aluminum [65].
The maximum expected dose for SPE is 3.38 Sv as it was the strongest SPE recorded (August 1972) till date [65]. This is considered a extreme SPE on the NOAA clasification and it would only occur a maximum of one time during the mission, much less severe SPE could occur up to 9 times during the duration of the mission. This acute doses of radiation are life threatening for the crew if higher than 0.5 Sv, thus a dose reduction of at least 85% is required to ensure crew health. For this, water, food and, as the mission develops, waste products will be mainly used as SPE radiation protection. Taking advantage of the directional nature of SPE and the fact that the spacecraft will have its back part oriented towards the sun during the whole interplanetary trajectory, an optimal mass efficient protection can be designed. The water tank will be placed on the back wall of the spacecraft and it will contain 515 liters of water. The water tank will be made of polyethylene and its walls will have an areal density of 7 g/cm^2 which will provide 24.5% dose reduction per wall for a total of 49% [64]. The water inside the tank will then have an areal density of 9.6 g/cm^2 which will provide a 37% radiation dose reduction as estimated from [5]. Then the total reduction of the water tank system is thus 86%. The dosage estimation and its reduction through radiation protection is summarized on table 5.14:

Table 5.14: Dosage estimation after radiation protection for mission duration

Type of Radiation	**Flux (cSv/day)**	**Reduction of Dose (%)**	**Dosage to Crew in 501 days (cSv)**
GCR	0.17	6.4	79.7
SPE	3.38	86	0.47

Additionally to the radiation shielding explained above, the food for the whole mission duration will be evenly distributed through the back of the spacecraft and will be replaced for waste bags as they are consumed. This, together with the extra protection from the MMOD shield for SPE, it will make up for for the loss of water through filtering efficiencies during the mission, to keep required level of protection from radiation. Other measures to reduce the space radiation effects on the crew through specific diet or drugs are discussed in section 5.1.3.4.

5.2.5 Sensitivity Analysis

In this part the effect of variations on the requirements or input parameters for the design of the structure will be discussed.
Starting by the MMOD shield, the main parameters that define the characteristics of the shield configuration are projectile mass, density, velocity and impact angle as well as the gap distance of the shield. On table 5.15 the effect of a change on these parameters for the areal densities and total mass of the MMOD shield are shown.

Table 5.15: MMOD shield sensitivity analysis

Changed Input Parameter	**Bumper Areal Density [g/cm^2]**	**Kevlar Rear Wall Areal Density [g/cm^2**	**MMOD Shield Total Mass [kg]**
Nominal	0.53	0.48	1085
Projectile mass increased by 10%	0.55 (+3.6%)	0.53 (+9.4%)	1158 (+6.3%)
Projectile density increased by 10%	0.56 (+5.36%)	0.48	1126 (+3.64%)
Projectile velocity increased by 10%	0.53	0.53 (+9.4%)	1141 (+4.91%)
Gap distance reduced by 10%	0.53	0.58 (+17.2%)	1198 (+9.43%)
Impact angle from 0 to 45 deg	0.53	0.34 (-41.17%)	937 (-15.8%)

It is observed on table 5.15 that the MMOD shield is most sensitive for an increase in projectile mass and velocity or a decrease in the gap distance between the first layer and rear wall. Nevertheless, it must be noted that the changes were calculated for no damage at all on the rear wall and that the probability that the input parameters increase is very low.

Next, it is important to investigate how a change in dimensions of the design requirements influence the structural thickness and total mass. The results are summarized in table 5.16.

Table 5.16: Structure loads sensitivity analysis

Increase Input Parameter by 10%	**Thickness [mm]**	**Lateral Vibration [Hz]**	**Axial Vibration [Hz]**	**Total Mass [kg]**
Nominal	1.46	11.25	33.93	204.54
Load Factors	1.61	11.81	35.61	225.34
Internal Pressure	1.37	10.91	32.92	192.55

The Falcon 9 is chosen as the most similar launcher to Falcon Heavy. So, the natural frequencies and load factors of Falcon 9 are used. Increasing the load factors by 10%, thickness will increase by 10.2%. This means a higher permissible thickness which is still less than required thickness. Thus, the total mass is not sensitive to this thickness.
The system is designed for the maximum internal pressure of 0.0337 MPa. For an increment of 10% in the internal pressure, still the thickness for stability is the driven thickness and will decrease by 6.2%. The lateral and axial vibrations will decease. However, they still meet the requirements. This thickness is less than permissible thickness of 3 mm, the total mass is not sensitive.
Finally, the radiation protection is considered. For the design of the the radiation protection the worst case scenarios are considered for radiation flux of GCR and SPE and thus it is deemed very unlikely that this values will increase. The only variable parameter that makes a significant difference is the amount of water on the water tank for SPE shielding. This variation is accounted for with the extra radiation shielding provided by the food and waste.

5.2.6 Verification and Validation

To ensure reliability of the spacecraft and crew safety, the preliminary detail design method needs to be verified and validated. This is essential to develop a reliable design and helps to avoid downstream problems. Firstly, each calculation method needs to be verified so that it meets the requirements. Secondly the results need to be validated to make sure the modeled design performs the same in a real environment.

MMOD protection

Verification The relations and equations used to compose the numerical model used to design the MMOD structure are assumed to be accurate as they taken from NASA Handbook for Designing MMOD protection [55]. The numerical model made in excel with this relations is verified by making the same calculations analytically and obtaining the same results.

Validation The numerical model is validated using the data from MMOD tests where all parameters used by the model are specified [55]. The results show that the model provides a 1 to 4 % higher total areal density than the required areal density during the tests. This small difference means that the model is validated for real environment performance yielding a slight over designed result. It must be noted that tests of the full structure configuration should be made when it is manufactured to complete the validation of the structure as a whole.

Structural Loads

Verification:
The approach for designing the structural components follows well established analytical methods for a structural sizing, and no numerical methods were used for the analysis. The conventional meanings of verification, where numerical results are verified with analytical results, are therefore not applicable. Therefore, for method verification it is only possible to verify with the method used in the book. In the book [25], an example is given where a lunar crew modules structure is sized for pressure and buckling stability. Since the methods are identical to each other, the method is verified.

Validation

The results obtained for the structural dimensions of the module can be validated with values found in the book [25]. In the book an exercise was given where a lunar crew modules structure which is made of Al 6061-T6, is sized for pressure and buckling stability. The results of Al 6061-T6 will be validated with the results from the book. Since the same method is used for each material, it comes to the conclusion that once results from one material are valid, the results from other materials will be valid too.

To support pressurization a thickness of 1.61 mm is calculated in the book, which is not similar to the value obtained for the Inspiration Mars in table 5.8. However, taking in calculation a 1.186 times higher radius and a 3.26 times higher pressure will give the same results. Therefore, result is valid.

In the exercise the structure is designed as a monocoque cylinder made of Al 6061-T6 as material, so a skin thickness of 2.57 mm is calculated to withstand a compressive launch load of -3.2 g. Since the maximum launch load of the Falcon 9 is approximately twice in magnitude in x direction and , the skin thickness obtained for Al6061 as shown in table 5.11 also seems reasonable. The results obtained for the module skin thickness is therefore shown to be validated.

Radiation Protection

Radiation protection design is still not a very advanced field in terms of modeling the radiation behavior. Most data available comes from material radiation tests. Thus, the design is done using reference data and graphs for material performance against each kind of radiation. The required thickness levels for the desired radiation reduction for different materials is identified and optimal design combining these is elaborated. Since no numerical models and only very simple analytical calculations are performed the verification of the method is straight forward just by checking no mistakes are made. Validation of the design is performed by comparing it with the results of different radiation tests for each material used. A complete test of the whole radiation protection lay-out will need to be performed to validate the design performance as a whole system.

5.2.7 Conclusion

The spacecraft is composed of the dragon re-entry capsule and the living module. The re-entry capsule structure is left unchanged, and the living module structure is designed inspired on the dimensions and connecting mechanisms of two Dragon spacecraft extended trunks. The living module structure consists of a multi-shock micrometeorite and orbital debris protection shield with Kevlar as rear wall. This Kevlar rear wall is used as the main load carrying structure for the launch and pressurizing loads as well as for radiation protection. For the loading checks, the required thickness from the stability test is the highest, thus the shell is critical for stability and the minimum thickness of the module is calculated. Also with this thickness, the structure will not buckle. Furthermore, the mentioned shell thickness t_3 meets the natural frequency requirements.
For space radiation protection, the MMOD shield, together with the subsystems placed around the habitable space provide enough dose reduction for Galactic Cosmic Rays. For Solar Particle Events, the water tank made of polyethylene as well as the hydrogen and oxygen tanks of the spacecraft are placed at the rear of the spacecraft which will be pointed towards the sun through the whole trajectory.

5.3 Propulsion

In this section the propulsion system of the spacecraft is designed. First, the requirements of this subsystem are listed. Next, the launch vehicle is described and its performance is calculated, including the propellant masses needed to deliver the required ΔV. Since there is currently no launcher available that can carry these amounts of fuel into space, the second stage will be refueled by a fuel depot, launched with a second launcher. Once the second stage holds enough fuel, the second stage is reignited and the spacecraft is send on its way to Mars. Second, the in-space propulsion system is described, that will be used to provide small orbit corrections and evasive maneuvers. This will be done by chemical thrusters. Lastly, a sensitivity analysis will be given and the verification and validation is described.

5.3.1 Propulsion Requirements

- The launcher internal payload fairing shall have an internal diameter with a minimum of 3.6 m. This is the diameter of the Dragon capsule and the extended trunks [68].
- The launcher shall be able to provide a ΔV of 8.4 km/s to get the payload from the Earth to a circular LEO parking orbit at 200 km. This number is calculated using equation 3.1. From this equation a value of 7.8 km/s is found, and for redundancy 600 m/s is added. From [9], a value of 7.67 km/s was found, but since this value is lower than the one calculated with equation 3.1, that value will be used for safety.
- The propulsion system shall be able to provide a ΔV of 4.9 + 10% = 5.39 km/s to bring the payload into the required trajectory from the parking orbit, including some small trajectory changes during the mission. This value is taken from the feasibility analysis by the Inspiration Mars Foundation, and it is validated in section 3 [5].
- The thrusters shall have a minimum thrust of 100 N to be able to avoid space debris in time.
- The in-space propulsion system shall have enough redundant thrusters to acount for failure.

5.3.2 Launcher

The selected launcher for this mission is the Falcon Heavy. This launcher is under development at this moment, but it uses a lot of already proven technologies (like the Merlin 1D engine, which has been flight qualified in 2013 [70] and is based on the Falcon 9, which has been launched succesfully multiple times. Therefore, it is assumed that in 2018 this launcher will be available for this mission.
Since the launcher is still under development and SpaceX is a private company, very little information is known about the Falcon Heavy (and Falcon 9). Therefore, its performance has to be calculated using values that is made available by SpaceX. This data can be found in table 5.17.

Table 5.17: Falcon 9 and Falcon Heavy data [71, 22]

	Falcon 9 v1.1	**Falcon Heavy**
Height [m]	68.4	68.4
Diameter [m]	3.7	11.6 (max. width)
Mass [kg]	505,846	1,462,836
Oxidizer/Fuel	Liquid Oxygen / RP-1	Liquid Oxygen / RP-1
Stage 1		
Number of engines	9	27
Burn time [s]	180	180
Thrust at sea level [kN]	5,885	17,615
Thrust in vacuum [kN]	6,672	20,017
Stage 2		
Burn time [s]	375	375
Thrust [kN]	801	801

The engines used on the Falcon rockets are Merlin 1D engines. For the first stage, Merlin 1D is used, which has a specific impulse of 282 s at sea level and 311 s in vacuum. For the second stage, the Merlin 1D vacuum is used, which has a specific impulse of 340 s [71].
Using these values, the mass flow can be determined using equation 5.26 (for the first stage, the average of the vacuum and sea level thrust and impulse is used). When multiplied by the burn time, the propellant mass for both launchers and stages is found. The results are listed in table 5.18.

$$I_{sp} = \frac{F}{\dot{m} \cdot g_0} \tag{5.26}$$

Since the oxidizer-to-fuel ratio of the engine is not known, it is assumed that this is 2.25. For this ratio, the engine has the highest specific impulse [72, Appendix B]. The total liquid oxygen (LOX) and kerosine (RP-1) masses can then be calculated for both stages, and with the density (1142 kg/m^3 for LOX, 810 kg/m^3 for RP-1, [72]) the volumes can be calculated. The Falcon 9 has a diameter of 3.7, therefore it is assumed the fuel tanks have a diameter of 3.6 m. Using this, the length of the fuel tanks can be calculated. The tank mass is estimated using equation 5.27, [72]. This method is used, since it is an empirical approach and therefore takes into account factors that will not be taken into account when the tank mass is calculated by determining the required tank thickness and area. All results are listed in table 5.18.

$$\phi_{tank} = \frac{p_b \cdot V_{tot}}{g_0 \cdot m_{tank}} \tag{5.27}$$

Where ϕ_{tank} is the tank mass factor (2500 for metallic tanks), p_b is the burst pressure ($2 \cdot 0.6MPa$, [72]) and V the propellant volume.

Table 5.18: Falcon launchers calculation results

	Falcon 9 v1.1	**Falcon Heavy**
Stage 1		
Mass flow [kg/s]	2157.1	6464.2
Propellant mass [kg]	388,276.8	1,163,558.6
Engine dry mass [kg]	503.8	503.8
Tank mass LOX	11,862.51	11,849.79
Tank mass RP-1	7,433.4	7,425.08
Dry mass	23,830.11	71,427.21
Stage 2		
Mass flow [kg/s]	240.2	240.2
Propellant mass [kg]	90,056.7	90,056.7
Engine dry mass [kg]	544.3	544.3
Tank mass LOX	2,857.99	2,857.99
Tank mass RP-1	1,574.07	1,574.07
Dry mass	4,976.36	4,976.36

Propellant

The Merlin 1D rocket engine is a bipropellant engine using liquid oxygen and RP-1. Bripropellants have the best specific impulse of existing chemical rockets, and therefore a lower propellant mass [72]. A disadvantage of the liquid oxygen is that it is a cryogenic propellant, and therefore storage is harder than for space storables, that can be stored at higher temperatures. For launch vehicles cryogenic storage is usually not a problem, but if they have to be stored for a longer time this may be a problem.

Δ V and Propellant Mass

Using the values calculated for the launcher as listed in table 5.18, it is calculated using equation that for a payload of 53,000 kg (which is the maximum payload to LEO according to SpaceX [22]) the ΔV that can be deliverd is 8.48 km/s. This is higher than the requirement set, which is 8.4 km/s.
For this mission, the payload is 15,580.8 kg (spacecraft mass including dry mass, with 10% margin taken over the dry mass). The first stage is able to provide a ΔV to this payload of 5.8 km/s, using equation 5.28. This means, the second stage needs to give a velocity change of 8.4 - 5.8 = 2.6 km/s. Using (5.28), it can be found that there is 30,453.8 kg of fuel left in the second stage when the spacecraft is in parking orbit.

$$\Delta V = I_{sp} \cdot g_0 \cdot ln \frac{m_{initial}}{m_{final}} \tag{5.28}$$

5.3.3 Refueling

The second stage of the Falcon Heavy will be used to provide the ΔV needed to bring the spacecraft from the parking orbit to the required trajectory. Using 5.28, it is found that with a payload mass of 15,580.8 kg, the amount of fuel required in the second stage is 71,488.1. This means 41,034.3 kg needs to be refueled. Using equation 5.27, the tank mass is estimated. Including the masses of the cryocooler and insulation, a total launch mass of 45,594.1 kg is found.

Payload Fairing

The Falcon launcher uses a standard payload fairing, which can be seen in figure 5.9. The layout of the Dragon with its extended trunks can be seen in figure 5.8.

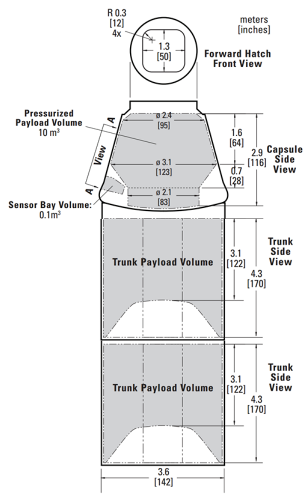

Figure 5.8: Dimensions of the Dragon capsule with two extended trunks [68]

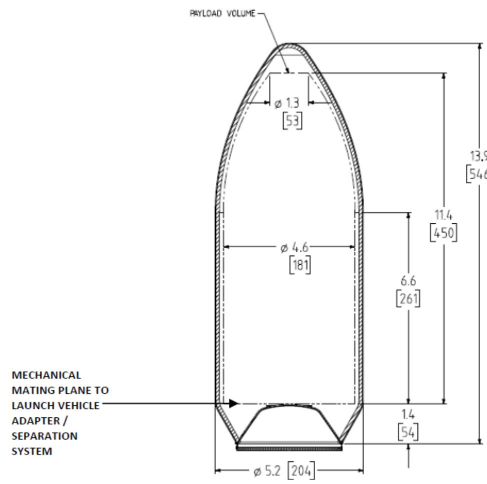

Figure 5.9: Payload fairing of the Falcon Launch Vehicle, in meters [inches] [73]

5.3.4 In-space Propsulsion System

Following from the requirements, the spacecraft has to be able to perform a ΔV of 300 m/s during the trajectory for evasive maneuvers, orienting the spacecraft and some unexpected maneuvers. The Dragon capsule standard has 18 Draco thrusters and a fuel tank capacity of 1,230 kg [74]. Since there is hardly any data available on the Draco thrusters, for this mission the Draco thrusters will be replaced with a flight-qualified thruster of which more information is known. To be able to control the spacecraft, twelve thrusters will be added at the lower end of the living module. Therefore a total of 30 thrusters will be installed in the spacecraft.
From [8, table 17-13], a thruster with a high specific impulse and high total impulse is chosen. The thruster produced by Marquardt is chosen, its details can be found in table 5.19. This thruster is chosen because it is capable of short pulses and longer burn times. From the thrusters that are capable of this, the Marquardt thruster has the highest specific and total impulse, while it also has a high nominal thrust.
From the requirements it is found that the thrusters need to be able to perform a ΔV of 400 m/s, as well as the thrust needed for the guidance, navigation and control (GNC) system. From the propulsion requirement, using Tsiolkovski's rocket equation, a propellant mass is found of 2,400 kg. It is assumed that the fuel that is already available in the Dragon capsule (1,230 kg)a is needed for the re-entry. Therefore a total of 3630 kg kg of propellant is needed.
Using equation 5.29 [8, p. 712], the total propellant mass that can be brought is calculated using the values from table 5.19 and is found to be 400.5 kg per thruster. For 30 thrusters (see section 5.4), the total amount of propellant that can be carried is 12,015 kg of fuel, which is more than is needed. Therefore, this type and amount of thrusters is sufficient for the mission.

$$m_p = \frac{I_t}{g \cdot I_{sp}} \tag{5.29}$$

5.3.5 Sensitivity Analysis

The sensitivity of the propsulsion system is analysed by investigating what happens when some of the parameters change. For the launch phase, the spacecraft mass is changed with 10%. In table 5.20 it can be seen that if the spacecraft mass increases with 10 %, the fuel depot cannot be launched since its mass is

Table 5.19: Marquardt flight-qualified thruster

Specifications	Values
Nominal thrust [N]	111
Propellant	N_2O_4/MMH
Total Impulse [10^3 Ns]	1,100
Specific Impulse (Steady State) [s]	300
Specific Impulse (Pulse) [s]	220
Weight [kg]	1.4

higher than the maximum payload mass the Falcon Heavy can carry. The thruster sensitivity is analysed by changing the spacecraft mass by 10 % and by changing the specific impulse. The results are listed in table 5.21.

Table 5.20: Sensitivity analysis launcher

Changed input parameter	Mass needed for refueling [kg]	Fuel depot launch mass [kg]
Nominal conditions	44,488.4	49,381.4
+10% spacecraft mass	47,623.3 (+16.1 %)	52,818.9 (+15.8%)
-10% spacecraft mass	34,449.3 (-16.0%)	38,373.6 (-15.8 %)

Table 5.21: Sensitivity analysis in-Space propulsion

Changed input parameter	Fuel mass (when ΔV remains constant	ΔV possible (when fuel mass remains constant)with 10% contingency	ΔV possible (when fuel mass remains constant) without 10% contingency
Nominal conditions	2400	400	434.7
+ 10% spacecraft mass	2640 (+10%)	361.1 (-9.7 %)	392.2 (-9.8 %)
- 10% spacecraft mass	2160 (-10%)	448.3 (+12 %)	487.5 (+12.1 %)
- 5% specific impulse	2516.8 (+4.9%)	380 (-5%)	412.9 (-5%)

5.3.6 Verification and Validation

For the calculations in this section, no program was made. Therefore only the used assumptions will be listed and the results will be compared with existing launchers.
The assumptions are the assumptions used for Tsioloksky's equation and the ideal rocket theory and are listed below [75]:

- No gravity force
- No atmospheric drag
- No other external forces acting on the rocket
- Propellant is expelled with relative velocity v_e, constant throughout time
- Propellant is expelled in a direction opposite to flight direction
- Steady, isentropic and 1-dimensional flow
- Propellant is a perfect, calorically ideal gas with homogeneous and constant chemical composition.
- Propellant in the chamber has negligible velocity

The Centaur upper stage of the Atlas V 551 is used to compare the calculations with [76]. For a thrust of 99.5 kN, a specific impulse of 451 and the maximum burn time of the RL-10 rocket (720 s) a fuel mass is found of almost 19 tonnes (including errors, [72]). This is lower than the amount of fuel that the upper

stage can hold (20,830 kg), but this difference (of 8.7 %) can be explained by the ideal rocket theory. This theory assumes a perfect gas and steady, isentropic and 1-dimensional flow. In real-life this is not the case, therefore the needed propellant mass for this amount of thrust is higher.
To calculate the tank mass, equation 5.27 is used. With the same tank pressure and safety factor (0.6 MPa, safety factor is 2) a tank mass is found of 3000 kg. Using a slightly lower safety factor of 1.5, a tank mass of 2250 kg is found. The tank mass of the Centaur is 2247 kg, so the first safety factor gives an error of 33 %. The safety factor of 1.5 is a much better estimation.

5.4 Guidance, Navigation and Control

This section will present the design of Guidance, Navigation and Control (GNC) system. It start with an overview of the necessary control modes during each mission phase in section 5.4.1 which lead to the system requirements in section 5.4.2. Section 5.4.3 continues with a general discussion on guidance and navigation systems. The choice on the guidance and navigation system is made in section 5.4.4, this section also includes performance characteristics of the system. Section 5.4.5 presents the entire GNC system design with the determination of the hardware components of the attitude determination and control system. This is followed by the sensitivity analysis in section 5.4.6 and the verification and validation in section 5.4.7. The GNC system is concluded in section 5.4.8.

5.4.1 Control Modes

In the Funtional Flow Diagram (FFD) presented in 2.2.1 several phases are identified in which the GNC systems needs to be active. This starts during Parking Orbit / Refueling phase. In this phase the GNC system ensures safe rendezvous and docking procedures. At the end of this phase the GNC provides an accurate trajectory insertion. During the cruise phase, which consists of the interplanetary trajectories and the fly-by, the GNC is a continues process of trajectory keeping and pointing the spacecraft towards the Sun. During these phases the GNC has to perform evasive maneuvers. The last phases in which GNC is necessary are the re-entry, descent and landing phases. Because the design includes a Dragon Capsule, which already has its own GNC-system, there is no need to design for these last phases. The GNC during these phases will be performed by the already designed GNC system in the Dragon Capsule.

5.4.2 Requirements

The requirements for the GNC system follow from mission requirements and other subsystems. The fly-by altitude is an important mission requirement, therefore meeting this requirement accurately is an important requirement of the GNC system. Meeting this requirement is also beneficial for the requirements of the spacecraft. If the spacecrafts fly-by altitude is too low the Martian atmosphere will cause drag and thermal loads on the spacecraft.
For the re-entry procedure accurate attitude determination and control is required. Also knowing the spacecrafts velocity is needed for to maintain the required corridor width (section 4.2), for the re-entry velocities. The pointing stability is required for the communications system for the efficiency of the communication system (section 5.6). The slew rate is determined by the MMOD protection system (section 5.2.1). The spacecrafts orientation with respect to the Sun shall be known at all times during the mission, this is due to thermal system requirements (section 5.10). These requirements are listed below.

- Fly-by altitude accuracy <1 km.
- Attitude determination accuracy <0.004 °.
- Attitude control accuracy 0.012 °.
- Knowing spacecraft velocity within 9 m/s accuracy.
- Pointing stability 0.1 °.
- Slew rate 0.5 °/s.
- Knowing spacecraft orientation with respect to the Sun at all times.

5.4.3 Guidance and Navigation system

For the vast majority of previous deep space missions the GNC is performed on ground using radiometric tracking and, when required, on-board optical data [77]. The Deep Space Network (DSN) provides the navigation capability for numerous missions beyond the Earth-Moon system. As more missions are planned and DSN availability becomes more constrained and other navigation methods become attractive [78]. Another drawback of the ground-based navigation is the time delay between the acquiring navigation data and performing corrective maneuvers. Therefore the need for autonomous navigation systems grows. Autonomous navigation systems have the advantage of a smaller time between acquiring data and performing corrective maneuvers. This results in smaller ΔV maneuvers, thus using less fuel, and more accurate GNC systems [79]. It also decreases the necessary capability of the communication system. On the downside, autonomous navigation systems are heavier because of the necessary on-board hardware to analyze the obtained data and to determine corrective maneuvers. These heavier hardware components also increase the power requirements of the spacecraft. At this point an initial trade-off is made and the autonomous navigation system is chosen over the ground-based navigation system. The fly-by altitude is a driving mission requirement, thus meeting this requirement within acceptable margins is an important mission aspect. The choice for autonomous navigation is thus driven by the better fly-by altitude accuracy.

5.4.4 Autonomous Navigation Systems

This section presents two proposed autonomous navigation systems. It is followed by a trade-off and a more detailed performance.

Microcosm Autonomous Navigation System

The Microcosm Autonomous Navigation System (MANS) was the first fully autonomous navigation system demonstrated on the TAOS mission in 1994. MANS uses the Sun, Moon and Earth reference sets for orbit determination. With the modern technology it is possible to extend the autonomous navigation to use stars and a central planet [79], this makes it suitable for planetary missions. So far, MANS is only used on Low Earth Orbits (LEO).

AutoNav

The Deep Space 1 mission introduced the first fully Autonomous Optical Navigation system (AutoNav) to be used in deep space [80]. The theoretical basis of AutoNav is taking images of asteroids or planets against distant stars. The images of the asteroids or planets provide line-of-sight vectors, while the distant stars provide a reference frame [77]. A succession of these images provide multiple line-of-sight vectors which passes through a filter to determine the spacecrafts position and velocity.

Trade-off

At this point a trade-off between MANS and AutoNav is made. Although MANS is a navigation system which can easily be modified for deep space flight, AutoNav is chosen. This is because AutoNav has already successfully been used in deep space flight. AutoNav was designed in 1998, so if this system is upgraded with the latest hardware it is able to fulfil the GNC requirements [81] stated in section 5.4.2.

AutoNav performance

The imager used on the Deep Space 1 mission is a Miniature Integrated Camera and Spectrometer (MICAS). MICAS consists of one ultraviolet spectrometer (UV Imaging spectrometer), two high-resolution imagers (APS and VISCCD imagers) and one infrared spectrometer (SWIR Image spectrometer) [82]. During the cruise phase of the mission, the images are taken by the UV Imaging spectrometer, SWIR Image spectrometer and the VISCCD imager. This provides an 250 km and 0.25 m/s accuracy of the spacecraft's position and velocity [80]. Orbit determination can be performed in 30 min [83]. Hours before the fly-by maneuver the high resolution camera is switched to the APS imager. This camera uses landmarks on the surface of Mars to determine its position and velocity. In 1999, this system was capable of achieving a position accuracy of 1.5 km and a velocity accuracy of 0.18 m/s [80]. With the current technology it is possible to achieve position accuracies below 1 km and a velocity accuracies of 0.1 m/s [80]. Orbit determination during the fly-by can be performed in 15 sec [83].

Parking Orbit Navigation

AutoNav requires for the rendezvous, docking and orbit insertion maneuvers additional information concerning the relative motion of the spacecraft with the refueling tanks and the motion of the spacecraft with respect to the Earth. Earth-based radiometric tracking combined with on-board sensing will provide this additional information for AutoNav.

5.4.5 Attitude Determination and Control

For the attitude determination and control two important aspects need to be considered. First of them being the disturbance torques. The second aspect is the constant pointing of the circular area towards the Sun due to thermal control requirements as explained in section 5.10.

Disturbances

During the mission the spacecraft will encounter several disturbance torques. The external disturbances the spacecraft will encounter are a gravity gradient until 35,000 km, a magnetic field until 35,000 km and solar radiation above 700 km [47, Table 9.1]. It follows that in parking orbit the spacecraft experiences two disturbances, the gravity gradient and the magnetic field. Equations for the gravity gradient torque and magnetic field torque are respectively given in equations 5.30 and 5.31 [8, Table 11-9A].

$$T_g = \frac{3\mu}{2R^3}|I_z - I_y|\sin(2\theta) \tag{5.30}$$

$$T_m = DB \tag{5.31}$$

The Earth's magnetic field B can be approximated by equation 5.32 [8, Table 11-9A]:

$$B = \frac{2M}{R^3} \tag{5.32}$$

The mass moment of inertia is estimated by modelling the spacecraft's subsystem and the dragon capsule as a point mass. The placement of the mass points corresponds with the internal layout presented in 11.3. The extended trunks are modelled as a hollow cylinder. To determine the gravity gradient torque the worst case scenario is taken, therefore the maximum deviation angle from the z-axis with the local vertical θ will be equal to $\frac{\pi}{4}$. The magnetic dipole D of the spacecraft can be estimated by the type of spacecraft. Because this mission requires a Class III spacecraft the magnetic dipole D will be equal to 149.23 [84]. An overview of all the variables can be found in table 5.22.

Table 5.22: Variables for the gravity gradient and magnetic field torques

Symbol	Description	Value	Unit
μ_{Earth}	Earth's gravity constant	$3.986 \cdot 10^{14}$	[m^3/s^2]
μ_{Mars}	Mars's gravity constant	42,828	[m^3/s^2]
R_{Earth}	Orbit radius Earth	$6{,}578 \cdot 10^3$	[m]
R_{Mars}	Orbit radius Mars	$3{,}576 \cdot 10^3$	[m]
I_z	Mass moment of inertia about z-axis	133,274.4	[kgm^2]
I_y	Mass moment of inertia about y-axis	17,511.7	[kgm^2]
θ	Maximum deviation of the z-axis from local vertical	$\frac{\pi}{4}$	[rad]
D	Residual Dipole	149.23	[Am^2]
M	Magnetic moment of the Earth	$7.96 \cdot 10^{15}$	[Tesla m^3]

During the cruise phase of the mission only one disturbance acts on the spacecraft, the solar radiation. The solar radiation torque can be determined with equation 5.33 [8, Table 11-9A].

$$T_{sp} = \frac{F_s}{c} A_s (1+q)\cos(i)(c_{ps} - cg) \tag{5.33}$$

The solar radiation force F_s can be modelled with equation 5.34:

$$F_s = \frac{P_{sun}}{4\pi R^2} \tag{5.34}$$

In these equations the surface area A_s is determined by the side of the spacecraft that will be pointing towards the Sun. Due to thermal requirements the spacecraft will always be pointing with its small circular side, with a surface area of 10.18 m^2, towards the Sun. The center of solar pressure will be in the middle of this circular area, therefore at coordinates (0,0). As for the mass moment of inertias, the center of gravity is calculated by modelling the subsystems as point masses within the spacecraft. This resulted in a center of gravity location at (0.00,0.10). The reflectance factor is determined by the material on the outside of the spacecraft, the factor used is 0.6 [8]. To determine the worst case scenario the angle of incidence is equal to 0. The power of the Sun is found to be $3.6{\cdot}10^{26}$ Watts [85]. The distance between the Sun and the spacecraft changes during the mission.

Table 5.23: Variables for the solar radiation torque

Symbol	**Description**	**Value**	**Unit**
c	Speed of light	$3{\cdot}10^8$	[m/s]
A_s	Surface area	10.18	[m^2]
q	Reflectance factor	0.6	[-]
i	Angle of incidence of the Sun	0	[rad]
c_{ps}	Center of solar pressure	(0,0)	[m]
cg	Center of gravity	(0.00,0.10)	[m]
P_{sun}	Power of the Sun	$3.6{\cdot}10^{26}$	[W]
R	Distance between Sun and spacecraft	-	[m]

Filling in the variables, given in tables 5.22 and 5.23, in equations 5.30 - 5.34 results in table 5.24. This table shows the maximum disturbance torques experienced during the mission.

Table 5.24: Maximum disturbance torques

Torque	**Earth**	**Mars**	**Cruise**
T_g [Nm]	0.24	$1.61{\cdot}10^{-10}$	-
T_m [Nm]	$8.35{\cdot}10^{-3}$	$5.20{\cdot}10^{-6}$	-
T_{sp} [Nm]	-	-	$1.25{\cdot}10^{-5}$

Hardware Selection and Sizing

To meet the accurate attitude determination and control requirements, reaction wheels in combination with thrusters mostly used [8, Tables 11-6, 11-7, 11-8]. To size the reaction wheels, the momentum storage due to the maximum disturbance torque is determined for the parking orbit and the cruise phase of the mission. When in parking orbit, the maximum disturbance torque is the gravity gradient at Earth, which is equal to 0.24 Nm. To determine the momentum storage needed equation 5.35 [8, Table 11-12].

$$h = T_D \frac{OrbitalPeriod}{4} 0.707 \tag{5.35}$$

Where the Orbital Period in seconds can be calculated with:

$$OrbitalPeriod = 2\pi \sqrt{\frac{(R_{Earth} + h_{Orbit})^3}{\mu}} \tag{5.36}$$

The momentum storage needed during the cruise phase is calculated by integrating the solar radiation torque over time. The solar radiation torque is given in figure 5.10, the resulting momentum storage needed is given in figure 5.11.

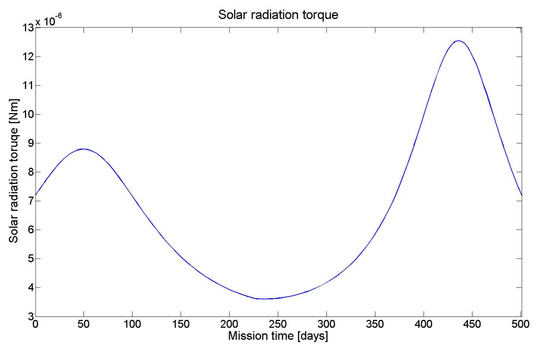

Figure 5.10: Solar radiation torque

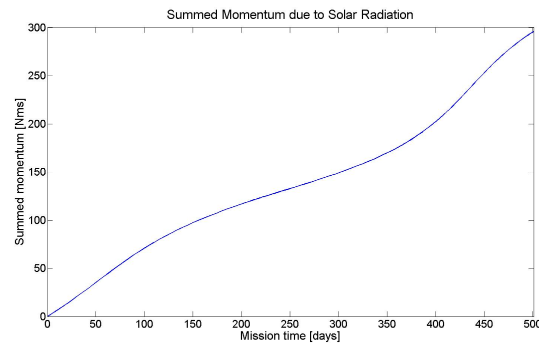

Figure 5.11: Solar radiation momentum storage

The momentum storage needed in parking orbit is 227.04 Nms and 298.91 Nms during the cruise phase. The reaction wheels are sized for the largest momentum storage. Due to the limited space in the spacecraft, the radius of the momentum wheel is fixed to a maximum of 0.25 m. The Spinning Rate (SR) of the momentum wheel is equal to 2000 rpm [8, Table 11-11]. Using equation 5.37 the mass of the momentum wheels can be calculated to be 4.78 kg.

$$I = \frac{h_{max}}{SR} = \frac{1}{2}mr^2 \tag{5.37}$$

The thrusters need to perform several functions. They need to be able to dump the momentum build up in the reaction wheels and provide the correction maneuvers to stay on trajectory. The momentum build up in the reaction wheels due to the gravity gradient will be dumped after the orbit insertion. During the mission the momentum build up due to solar radiation will be dumped once a day, thus yielding 501 dumps per axis. The force necessary for momentum dump is given by equation 5.38 [8, Table 11-13].

$$F = \frac{h}{Lt} \tag{5.38}$$

Where h is the build up momentum, L the distance between the thrusters and the center of gravity and t the burn time of the thruster. In this equation L will be 2.50 m and t is equal to 1 sec. This yields a dumping force of 91.25 N for the gravity gradient and 119.67 N for the solar radiation. For an accurate trajectory control a correction maneuver is needed every 5 days. A maneuver includes 2 pulses and is performed on all 3 axis. This maneuver provides also the constant turning of the spacecraft. A slew rate of 0.5 deg/s is required, the burn time for correction maneuvers is 3 s. This yields an angular acceleration of 0.17 deg/s^2. Using equation 5.39 [8, Table 11-13] the force is calculated to be 25.69 N.

$$F = \frac{I_z \ddot{\theta}}{L} \tag{5.39}$$

To calculate the total impulse of the thrusters the force is multiplied by the amount of impulses, thus 1503 impulses for the dumping maneuvers during the trajectory, 3 impulses for dumping the gravity gradient torque and 606 impulses for the correction maneuvers, and the burn time of each impulse:

$$Impulse = 3 * 1 * 91.25 + 1503 * 1 * 119.67 + 606 * 3 * 25.69 \tag{5.40}$$

The propellant mass can be calculated by equation 5.41 [8, Table 11-13]. In this equation the specific impulse is equal to 220 s and the gravitational acceleration of 9.81 m/s^2 which leads to a propellant mass of 104.0 kg.

$$M_p = \frac{Impulse}{I_{sp} g} \tag{5.41}$$

Now that the initial sizing of the actuators is done, a risk analysis (chapter 8) is made. Due to the mitigation of the risk back up actuators and sensors are included in the final GNC design. Also, in case a thruster keeps thrusting this will be counteracted by thrusting the opposite thruster. This will be done until the tanks are empty, therefore the other thrusters need to have enough propellant to continue the mission. There will be an additional 12 thrusters on the spacecraft, 4 clusters of 3 thrusters each. In case of continues thrusting, two cluster tanks will be empty. As contingency, the propellent in each tank is doubled. The propellant mass will therefore be 208.0 kg. To control all three axis at least three reaction wheels are needed. There will be an additional one for back up. The reaction wheels are sized for the solar radiation torque, which will be dumped during the trajectory. Therefore, sizing for the solar radiation is oversizing the reaction wheels. The main sensor for the guidance and navigation is the MICAS camera. Between images the GNC will use information provided by the IMU, star tracker and sun sensors to determine its position. Table 5.25 provides an overview of the entire GNC system.

Table 5.25: Overview of the GNC system components

Component	**Details**	**Number**	**Total [8] Weight [kg]**	**Total Power consumption [W]**
Thrusters	Propellant mass 208.0 kg	12	224.8	-
Reaction Wheel	Radius 0.25 m Spinning Rate 2,000 rpm	3 + 1 Backup	19.2	45
Camera	MICAS	1 + 1 Backup	20	10
IMU		1 + 1 Backup	0.3	3
Star Tracker	Accuracy 0.001 °	1 + 1 Backup	7.4	9.9
Sun Sensor	Accuracy 0.005 °	2 + 1 Backup	0.3	1
Total			**272.0**	**68.9**

Control Algorithm

The control algorithm, given in figure 5.12, of the GNC system starts with the sensor dynamics. Here the IMU, sun sensors, star tracker and MICAS camera measure all the relevant parameters. Together with noise, this information is provided to the flight computer. The flight computer analyzes the information, determines the position and attitude and calculates the correction maneuvers and attitude corrections. If the spacecraft is close to Mars the flight computer automatically switches to the other high resolution camera of the MICAS. The outputs of the flight computer are momentum dumping thruster burns, necessary control torques on the spacecraft and orbit correction maneuvers. These, combined with external disturbances, form the vehicle dynamics. The vehicle dynamics are then measured by the sensors which completes the loop.

5.4.6 Sensitivity Analysis

The main input parameters for the GNC design are the spacecraft mass and mass moment of inertia. In this sensitivity analysis a analysis is made of a spacecraft mass and mass moment of inertia increase or decrease of 10%.

Table 5.26: Sensitivity analysis

Changed Input parameter	**I_z [kgm^2]**	**h_{GG} [Nms]**	**h_{SR} [Nms]**	**M_{RW} [kg]**	**M_p [kg]**
Nominal conditions	133,274.4	229.8	298.9	4.78	208.0
Spacecraft Mass +10%	141,512.9 (+6.2%)	244.0 (+6.2%)	298.9 (0%)	4.78 (0%)	210.6 (1.3%)
Spacecraft Mass -10%	125,033.5 (-6.2%)	215.6 (-6.2%)	269.0 (-10.0%)	4.30 (-10.0%)	188.8 (-9.2%)
I_z +10%	146,605.5 (+10%)	256.2 (+11.5%)	298.9 (0%)	4.78 (0%)	212.4 (+2.1%)
I_z -10%	119949.9 (-10%)	203.4 (-11.5%)	298.9 (0%)	4.78 (0%)	203.6 (-2.1%)

As can be seen in table 5.26, increasing of the spacecraft mass increases the mass moment of inertia and thus the gravity gradient momentum. This increased momentum needs to be dumped, which results in an

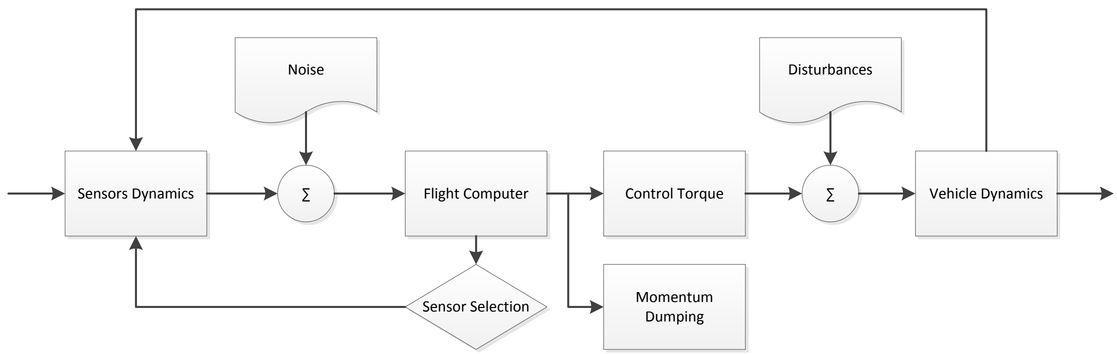

Figure 5.12: Control algorithm

increase of the propellant mass. There is no noticeable change in center of gravity, so the solar radiation momentum remains the same. The reaction wheels are sized for this solar radiation, and thus remain the same. If the spacecraft mass is decreased, the center of gravity shifts by 1cm, yielding a change in solar radiation momentum and thus a decrease in the propellant mass.
Increasing the moment of inertia, yields an increase of the gravity gradient momentum. This results in a small increase in propellant mass. Decreasing the moment of inertia, yields the same percentage decrease.
It can be concluded that the GNC system is not sensitive to changes in the moment of inertia. An 10% increase or decrease leads to a 2.1% change in the propellant mass. The GNC system is more sensitive to changes in the spacecraft mass, or more specific, to changes in the center of gravity. If the center of gravity remains the same, changing the spacecraft mass results in low (1.3%) propellant mass changes. If the the center of gravity is shifted, the reaction wheels and propellant mass are changed drastically (-10% and -9.2% respectively).

5.4.7 Verification and Validation

The model used in the GNC design process is a simulation of the solar intensity versus the distance from the Sun given by equation 5.34. This model is used in the calculations for solar radiation disturbances during the cruise phase of the mission. The model is verified by manually calculating three different points. The validation of the model is done by comparing the calculated solar intensities at Earth and Mars against the solar constants at Earth and Mars, this is shown in table 5.27.

Table 5.27: Verification of the solar intensity model

Planet	**Solar Constant [W/m^2] [87]**	**Averaged Distance [km] [86]**	**Date**	**Solar Intensity [W/m^2]**	**Distance [km]**
Earth	1,366.1	$1.496\cdot10^8$	04-01-2018	1,323.8	$1.464\cdot10^8$
Mars	588.6	$2.279\cdot10^8$	20-08-2018	664.2	$2.070\cdot10^8$
Earth	1,366.1	$1.496\cdot10^8$	20-05-2019	1,258.1	$1.502\cdot10^8$

There is a difference between the solar constants and the calculated solar intensities. This is partly due the fact that the solar constants use an average distance between the Sun and the planets. If the solar intensity with the average distance is calculated, a 6% error remains. This error is caused by different values for the Sun's power. Literature suggest different methods for deriving the Sun's power, resulting in a power range of $3.6 \cdot 10^{26}$ - $4.1 \cdot 10^{26}$ W [88]. Because the literature has a range, instead of an absolute value, there will always be an error with respect to the literature. Therefore, this error is acceptable and the model is valid to use.

5.4.8 Conclusion and Recommendations

Table 5.25 shows the details of hardware components of the GNC system. This designed system can meet the requirements given in section 5.4.2. The sensitivity analysis showed that the sizing of the actuators is not sensitive to changes in the spacecraft mass.
The recommendations for finalizing the GNC system are:

- Detailed rendezvous and docking maneuvers. For a complete GNC system the rendezvous and docking maneuvers and their impact on the GNC system need to be specified further.
- Testing of the autonomous GNC system. Although AutoNav has already proven its capability on the Deep Space 1 mission, it still needs to be tested further to ensure its safety and reliability for human space flight.
- The noise levels of the system are in this design approach neglected. To improve the GNC system design, these noises need to be modelled and taken into account in a more detailed design.

5.5 Refueling

In this section an overview of the refueling operation is given. The requirements are listed, after which a general overview of the operation and the used technologies is given. The propellant and tank masses are calculated, and the cryogenic cooling system is explained. The section finishes with a sensitivity analysis.

5.5.1 Requirements

- The fuel depot shall be able to store the fuel and oxidizer at the required temperatures. The oxidizer, liquid oxygen (LOX), shall be stored at temperatures lower than 90 K. The fuel, Rocket Propellant 1 (RP-1), shall be stored between 291 and 445 K [72].
- The fuel depot shall hold enough fuel to refuel the second stage attached to the spacecraft. This means it has to carry 12,626 kg of RP-1 and 28,408 kg of LOX, see section 5.3.2.

5.5.2 Concept

The refueling is based on a concept developed by the United Launch Alliance (ULA), a disposable single-use pre-depot [89]. The concept described in this paper consists of a delivery tanker cryogenic supply tank modified with thermal insulation. This tank will be a derivative of the Centaur upper stage, with enhanced thermal isolation [93]. Tests and projections show that boil-off rates can be reduced to 1% per day, making three-day missions feasible for 2018 [93]. Because such a tank can only carry one single fluid, two tanks are designed for this mission, based on the amount of propellant needed for the refueling.
The LOX tank will have a coupling system similar to the one proposed in [90]. This system will be redesigned so that it has the right diameter to get the required mass flow. Because the system has swivels that are internal to the coupling system, it can compensate for axial and angular misalignment of the two parts. The coupling can handle at least 1 degree of angular misalignment, 0.0625 inch (0.159 cm) of lateral offset and 0.05 inch (0.127 cm) of axial misalignment. This is illustrated in figure 5.13. The system is tested with water and was able to transfer 0.34 pound/s, which is equivalent to 540 kg/hour.
Since almost 45 tonnes of fuel will have to be transferred (see section 5.5.4), the standard diameter of 5.4 cm will be resized. With the density of water and a mass flow rate of 540 kg/hour, the flow velocity can be calculated using equation 5.42.

$$\dot{m} = \rho * A * V \tag{5.42}$$

Assuming the flow velocity stays the same when the coupling system is resized, and using that the density of LOX is 1142 kg/m3 and the density of RP-1 is 810 kg/m^3 [72], the diameters are calculated to be respectively 17.1 cm and 13.6 cm (including a 10% margin) to achieve refueling within 6 hours.

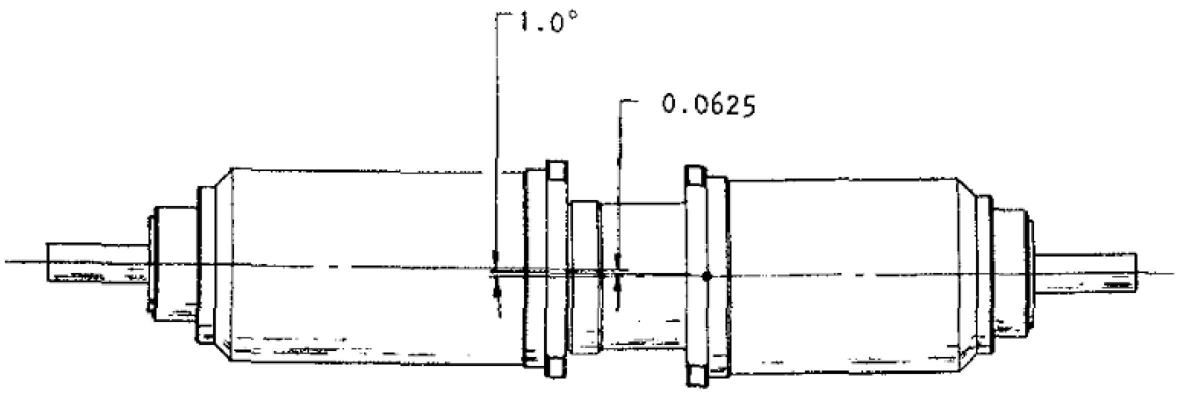

Figure 5.13: Accuracy of the coupling system [90]

5.5.3 Rendezvous and Docking

First the fuel depots will be launched. Since a cryocooler will be used to control the temperature of the fuel depots (see section 5.5.6), the fuel depots can stay in parking orbit for a few days, untill the spacecraft with the crew is launched.
When the spacecraft and the tanks are in the same orbit only a few kilometers appart, the rendezvous maneuver starts. The maneuver consists of one passive spacecraft, the fuel tank, and one active spacecraft, the spacecraft with the attached second stage. Measurements, taken on-board of the spacecraft and on the ground, will provide the necessary information concerning the relative motion of the spacecraft with the tanks and the motion of the spacecraft with respect to the Earth. The spacecraft needs to be maneuvered in a way that it has at all times the same angle with respect to the tanks [96]. This would mean that the spacecraft would only have to move along a straight line. To implement the rendezvous the spacecraft would only need an accelerating pulse, a cruise phase and a braking pulse immediately before the spacecraft and tanks touch.
When the spacecraft and tanks touch, the coupling system of the LOX tank dock. The connection of the RP-1 tank will be performed manually. The RP-1 propellant has lower thermal requirements and therefore a hose can be used to connect the RP-1 tank with the second stage. This connection is made during the Extra Vehicular Activity (EVA) when the astronauts move from the Dragon capsule to the living module. When both tanks are connected, the refueling starts. When the tanks are filled, the coupling system is disconnected automatically. To mitigate the risks associated with the docking, an extra coupling system is included in both propellant tanks. Also, a second hose is attached to the RP-1 tank, in case the first one fails.

5.5.4 Refueling propellant mass

It is found that the maximum percentage of tank refueling has been 95% [91]. In section 5.3.3, the refueling masses are calculated. A total amount of 44488 kg needs to be transferred, and with a oxidizer-to-fuel ratio of 2.25 it can be found that 12,626 kg of RP-1 and 28,408 kg of LOX needs to be transferred.

5.5.5 Tank Sizing

The necessary volume of each tank can be found by dividing the required propellant mass by its density and including a 5% ullage factor [95]. The density of LOX is 1142 kg/m^3 and for RP-1 the density is equal

to 810 kg/m^3 [72]. This yields a minimum tank volume of the LOX and RP-1 tanks is 25 m^3 and 16 m^3 respectively.
For the minimum heat transfer, the surface area of the tank should be as low as possible. This is achieved by increasing the diameter of the tank within the payload fairing constraints of the Falcon Heavy. The resulting tank dimensions are presented in table 5.28.

Table 5.28: Tank dimensions

	LOX	**RP-1**
Diameter [m]	4.25	4.25
Height [m]	1.90	1.20

For cylindrical pressure vessels the critical stress is given by the hoop stress. The hoop stress is given by equation 5.43. In this equation σ_h is the hoop stress in N/mm^2, p the tank pressure, r the tank radius and t is the tank thickness.

$$\sigma_h = \frac{pr}{t} \tag{5.43}$$

For pump feed tanks the pressure should be 0.6 MPa [72], the radius of each tank is 2.13 m. The material used to create the tank is Al 7075 T6, which has an ultimate stress of 530 N/mm^2. By rearranging equation 5.43 the tank thickness is calculated to be 0.25 cm. With the tank dimensions and material known, the tank masses are found to be 1,320 kg for the LOX tank and 827 kg for the RP-1 tank.

5.5.6 Cryogenic Cooling

The insulation protection is based on the Centaur upper stage, enhanced with Variable Density Multi-Layer Insulation (VDMLI)[93]. Multi-Layer Insulation (MLI) is already a commonly used insulation system. VDMLI, as can be seen in figure 5.14, has a variable gap thickness between the shielding layers. Ideally the density would vary along the cross-section, but in theory there will be three layers, one with a high density for the outermost region, a medium density for the middle region and a low density for the innermost region. During tests in 1993 (where the system thus had a technology readiness level (TRL) of 4) it was found that the heat transfer can be reduced by 58%. Therefore the total boil-off of the entire system can be reduced to 1% up to 0.7% for LOX. Furthermore, the weight increase for a 20-25 layer (which is used for these tests) is 100 lbs for these tanks of 22,000 kg. For the Inspiration Mars mission, we need two tanks of approximately this size, therefore the weight increase is assumed to be 200 lbs, or 100 kg[93].
Passive storage is only feasible for three days [93]. This is because there will still be some heat transfer into the tank, causing some of the fuel to boil-off. After a while, this will cause the tank pressure to become too high and the tank will rupture [89].
To mitigate the boil-off risks in case the fuel depot needs to stay in parking orbit longer than three days, an active storage system is added to the system. A cryocooler pumps haet out of the propellant. This method has a TRL of 4 [92], but there is a lot of research going on due to the promising zero boil-off performance [89].

5.5.7 Sensitivity

The sensitivity of the refueling will be tested at two points, the maximum refueling rate and an increase in needed fuel depot mass. An overview of the the sensitivity is presented in table 5.29.
The total tank mass of the second stage is found to be 90,057 kg 5.3.2. Under nominal conditions it needs to be filled up to 71,488.1, which means it has to be refueled to 80%.
If the second stage is refueled to its maximum refuel rate of 95% the fuel depot has a mass of 64,240 kg. This results in a total propellant mass of 85,464 kg which can bring 19,600 kg of payload into the Mars trajectory. The limiting factor however, is the maximum fuel depot mass to fit the refueling tanks into one Falcon Heavy launcher. This means that the maximum fuel depot mass will be equal to 53,000 kg, which means the second stage can be refueled to 77,049 kg, a 85.5% refuel rate. The maximum payload mass that can be brought into deep space is 17,180 kg.

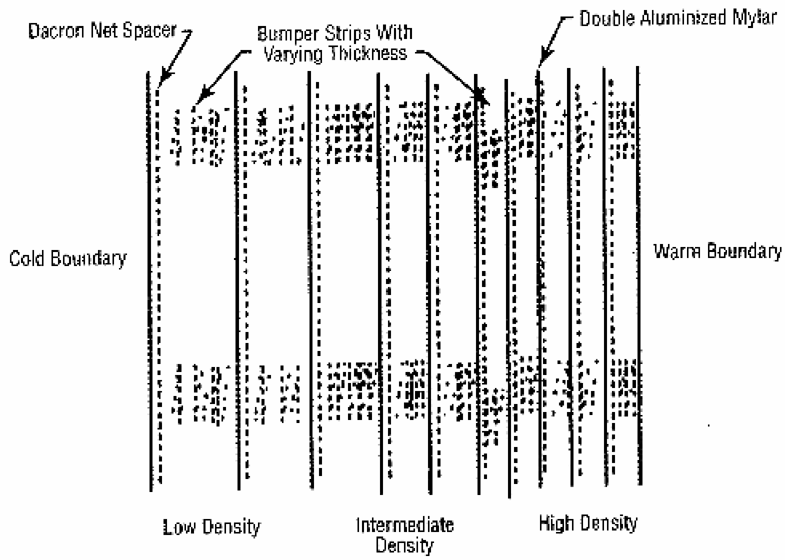

Figure 5.14: Representative cross-section of VDMLI [93]

Table 5.29: Sensitivity analysis

Changed Input parameter	Refuel rate	Fuel Depot Mass [kg]	Propellant Mass [kg]	Payload Mass [kg]
Nominal conditions	80%	45,594	71,488	15,581
Maximum refuel rate	95%	64,240	85,465	19,600
Maximum fuel depot mass	85.5%	53,000	77,049	17,180

The refueling system is not sensitive when it comes to the maximum refuel rate. There is room left for an additional 13,977 kg of propellant. This would mean that the maximum payload mass can increase to 19,600 kg. However, to fit the entire mission into two Falcon Heavy launchers and thus the refueling into one Falcon Heavy launcher, the maximum fuel depot mass is equal to 53,000 kg. This would mean that the spacecraft mass can increase by a maximum of 1599 kg. The refueling system is thus sensitive when it comes to fitting the system info one launcher.

5.6 Telemetry, Tracking and Communications (TT&C)

The used Dragon capsule contains complete TT&C and C&DH sub-systems that are tested and can be used for LEO purposes, the properties are shown in table 5.30 [68]. The required range is significantly larger than the incorporated TT&C and C&DH sub-systems can cope. Therefore the TT&C and C&DH sub-systems need to be redesigned. The C&DH subsystem is discussed in section 5.7. In this chapter the communication architecture is discussed, this is followed by the link budget calculation and finally the required hardware is elaborated upon.

5.6.1 Communication Architecture

For the communication architecture an overview with the required level of communications and their specifications is required. The overview is shown in table 5.31. During the fly-by the complete duration that the spacecraft is eclipsed by Mars is 15 minutes. This is negligible compared to the complete mission. Therefore the use of NASA's relay satellites [98] are not required. Therefore the data dissemination architecture is Point-to-Point and is realized in the Deep Space Network (DSN), which consists of three groundstations. The Ka-band frequency is used, therefore on each of these ground stations the 34 [m] Beam Wafe Guide

Table 5.30: The standard properties of the Dragon capsule with respect to the telemetry, command, and communcations

Telemetry & Command	Communications
Payload RS-422 serial I/O, 1553, and Ethernet interfaces (all locations).	Fault tolerant S-band telemetry & video transmitters.
IP addressable payload standard service.	Onboard compression and command encryption/ decryption.
Command uplink: 300 kbps.	Links via TDRSS and groud stations.
Telemetry/data downlink: 300 Mbps (higher rates available).	

(BWG) antenna's are used. Additionally one extra control station is used to process all the data, which is sent from the station and which needs to be sent.

Table 5.31: Complete communications overview per mission phase

Phase	Levels of communication	Level per phase	Activities
Launch	High	100%	System start up, communication with ground station, fuel level measurements, guidance and navigation control.
	Medium	0%	
	Low	0%	
LEO	High	5%	EVA, video conversations and schedualing.
	Medium	95%	Refueling and systems start-up.
	Low	0%	
TMI	High	10%	Video conversations and schedualing.
	Medium	60%	Scientific Payload data sharing, accounting for SOS messaging and maneuvres.
	Low	30%	Crew sleeping only Telemetry, Tracking and Command
Re-entry	High	90%	Communication with ground station. EVA transfer to the re-entry vehicle. Re-entry positioning: positioning. Atmospheric entry: Angle measurements, G-loads, heatflux, cabin temperature. Descent and landing: angle measurements, G-loads, heatflux, cabin temperature. Retreval: location measurements.
	Medium	10%	Time step between EVA and Re-entry. Safety check: Communication with ground station.
	Low	0%	

The data rates for the up- and downlink are related to the levels in table 5.32. In case of the high communication level, the values for maximum data rate are based on reference values for manned missions [25]. The low communication data rates are based on simple communication satellites in LEO [8]. Finally, the medium communication data rate values are estimated considering the data rate of the activities and the high and low communication levels.

Table 5.32: Distribution of the communication level over the entire mission

	Percentage of mission duration	Downlink in kbps	Uplink in kbps
High	10%	1000	300
Medium	65%	300	100
Low	25%	20	1

The type of components required for this communications architecture are shown in figure 5.15, the TT&C flow diagram. It is a two-way stream, with telemetry in the downlink and the commands in the uplink. Every component in the communications architecture is duplicated to prevent contingency errors. The filters reduce second- and higher-order harmonics to decrease frequency spurs and intermodulation products from the spacecraft's receiver. The diplexer allows the transmitter and receiver to have the same antenna. It also isolates the transmitter form receiver port at the receiver's center frequency, so the transmitter does not lock, jam or damage the receiver. The transponders modulate, demodulate and route the digital command bit stream.

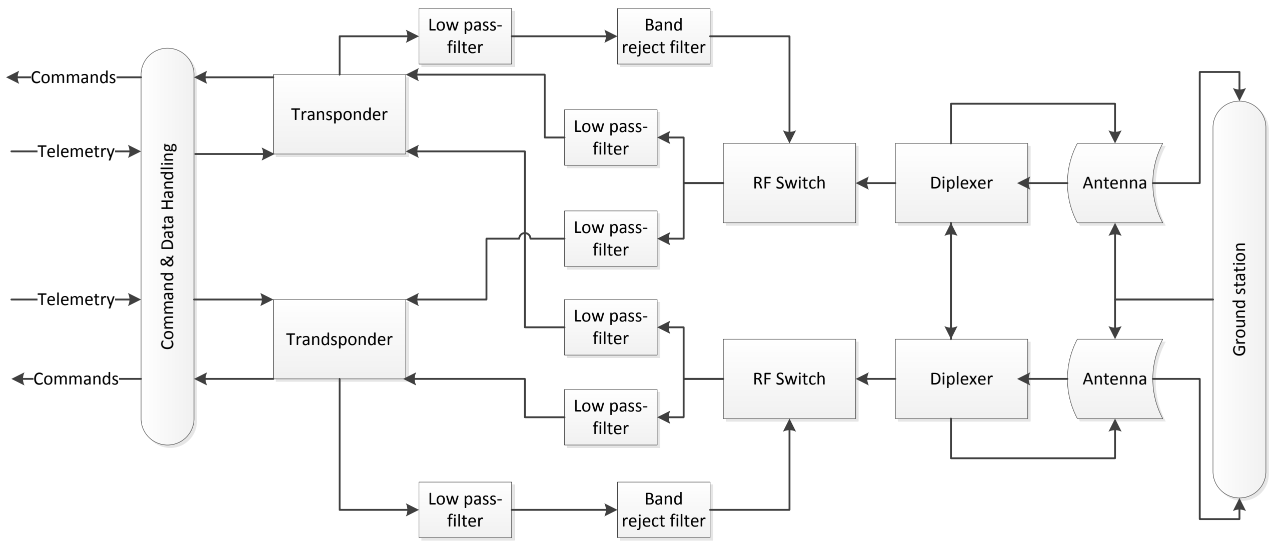

Figure 5.15: TT&C flow diagram

5.6.2 Link Budget

The process for developing the communications architecture and determining the link requirements are based on the link budget. Recall that this analysis is based on the worst case scenario thus the communications must overcome the furthest distance, shown in figure 5.16. The furthest distance is estimated to be $1.45{\cdot}10^8$ km. The free-space loss in dB results from the distance and the carrier fequency shown in equation 5.44 [8].

$$L_s = constant + 20log(f) + 20log(s) \tag{5.44}$$

Equation 5.45, the link equation, is for convenience expressed in terms of dB. It relates all parameters needed to analyze and design the link design. The effective isotropic radiated power is required to enable the calculation of the transmitter power with equation 5.47. The bit error rate can not exceed 10^{-5} [8]. To enable the achievement of this requirement the QPSK Plus R-1/2 Viteribi decoding modulation technique is used. This follows in an $\frac{E_b}{N_0}$ value of 4.4. All other obtained values are listed in table 5.33.

$$EIRP = \frac{E_b}{N_0} - L_{pr} - L_s - G_r + 228.6 - 10logT_s - 10logR \tag{5.45}$$

Subsequently, the transmitter antenna gain G_t is determined. This is done with equation 5.46 [8]. The antenna efficiency (η) is stated to be 0.55 [8]. This efficiency is stated to be only for the antenna and not the processing afterwards. Therefore, a 20% margin need to be added to the transmitter power [102]. The diameter of the transmitter antenna is chosen to be 0.25 m [100]. Furthermore the obtained G_t value is listed in table 5.33. After these values are known the transmitter power is determined using equation 5.47.

$$G_t = 20.4 + 10log(\eta) + 20log(f) + 20log(D) \tag{5.46}$$

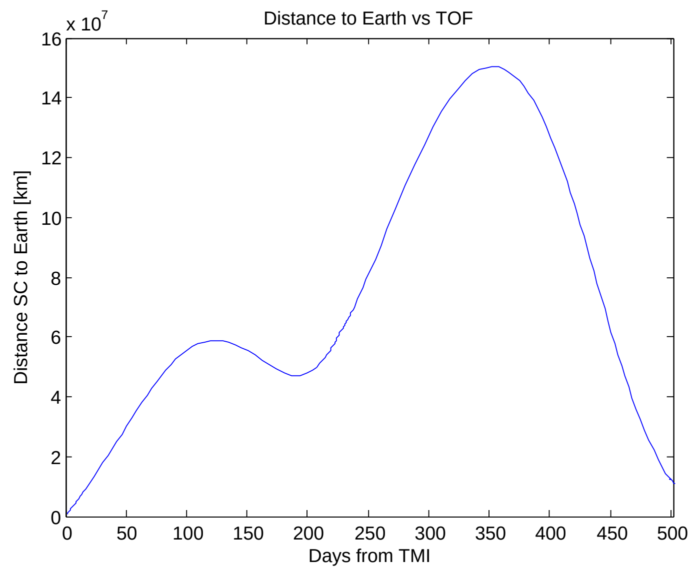

Figure 5.16: Distance of spacecraft from Earth generated by GMAT.

$$P_t = EIRP - L_l - G_t \tag{5.47}$$

As mentioned before, an extra margin of 20% is added to account for the complete antenna sub-system. Applying this the total transmitted power is found and listed in table 5.33. Repeating the same procedure, the medium and low communication level, shown in table 5.32, obtained respectively a 47 W and 4 W total transmit power requirement.

Table 5.33: Communications link budget

Item	**Symbol**	**Unit**	**Value**	**Source**
Maximum distance earth to spacecraft	s	km	$1.45{*}10^8$	graph 5.16
Downlink frequency	f	GHz	32.3	[99]
Space loss	L_s	dB	-285.9	5.44
Effective isotropic radiated power	$EIRP$	W	58.9	5.45
Receiver antenna pointing loss	L_{pr}	dB	-3	[8]
Receiver antenna gain	G_r	dBi	62	[101]
System noise temperature	T_s	K	424	[8]
Line loss	L_l	dB	-0.5	[25]
Transmitter Power	P_t	dBW	21.2	5.47
Transmitter antenna gain	G_t	dBi	38.3	5.46
Ratio Energy per bit to Noise density	$\frac{E_b}{N_0}$	dB	4.4	[8]
Bit Error Rate	BER	-	10^{-5}	[8]
Transmitter Antenna efficiency	G_t	-	0.55	[8]
Total transmit power	P_t	W	157 W	5.6.2

5.6.3 Hardware

As stated in section 5.6.2 the antenna diameter is 0.25 m. It is found that the diameter and the mass per satellite type is proportional [8]. The mass of the antenna is estimated by comparing the mass and diameter of the SUPERBIRD antenna. The mass is 47.1 kg and the diameter is 1.7 m. Calculating the relation and applying a 20% margin 2.5 follows in a 8.3 kg antenna. The antenna is steerable, in order to point into the right direction. To have communication in a two-way traffic, the antenna needs a diplexer. Finally, Ka-band transponders are required to modulate the data. For each of the phases discussed in table 5.32, a power rate of 82.3 W needs to be added for the transponders and diplexers. The total mass of the communication system is 32 kg, this is attained by including a contingency margin of 20% 2.5. The specifications of these items are listed in table 5.34. The volume of the communications sub-system, excluding the volume of the antenna's, is 0.035 [m^3] [8]. The quantity of each item is doubled to prevent single point faillure.

Table 5.34: Mass and power estimation

Item	**Quantity**	**unit mass**	**unit power**	**Source**
Filters/ Switch/Diplexer	2	1 kg	24.3W	[8]
Antenna	2	8.3 kg	5.6.2	[8]
Ka band transponder	2	4 kg	10 W	[8]
Total		**32 kg**	**82.3 W**	

5.6.4 Sensitivity Analysis

The assumptions made to create the link budget need to be analyzed in order to find out if a deviation would be of great impact on the spacecraft. The main output value, that in case of change will have impact on the entire spacecraft, is the power. In part 5.6.1 of this chapter, the distribution is made between the levels of data rate. The sensitivity analysis is applied on each of these phases. For the nominal conditions, the worst case scenario is used for the distance. This is $1.45{\cdot}10^8$ km according to figgure 5.16. The average distance according to this figure is $0.8{\cdot}10^8$ km. The effect on the required power for each level of communications, when using the avarage distance, is listed in table 5.35. Comparing the percentages with respect to the nominal conditions for each level show that the sensitivity is higher in case of low data rates. Furthermore, the sensitivity is analysed in case the antenna efficiency is reduced due to damage or errors. The nominal efficiency is 0.55 the reduced efficiency is assumed to be 0.4. The results and the percentages with respect to the nominal conditions for each level are shown in table 5.35. Again, the result states that the change in required power is less in case of low data rates.

Table 5.35: Sensitivity analysis TT&C.

Changed input parameter	**High data rate total transmitted power**	**Medium data rate total transmitted power**	**Low data rate total transmitted power**
Nominal conditions 100%	157 W	47 W	4 W
Average distance	48 W	15 W	1 W
percentage w.r.t nominal	31 %	32 %	25 %
Antenna efficiency reduced	162 W	49 W	4 W
percentage w.r.t nominal	104 %	105%	100 %

5.6.5 Verification and validation

In order to make sure the calculated values are plausible, the used method needs to be verified and the results need to be validated.The used methods are obtained from [8] and [47]. No program was made for the calculations in this section. The methods are presentented in two independent books, it can therefore be assumed that the method are verified. Comparable weight estimations [[47], table 12.5] and the power-estimation [[47], table 12.4] are used to verify the made estimations for sizing. The exact data rate over the maximum Earth-Mars distance can not be validated, because such a system does not exsist. The link budget required for a manned Mars mission[25], is used. Therefore it can be concluded that the roughly equivalent values are correct for the current design stage.

5.7 Command and Data Handling (C&DH)

As shown in table 5.30, the Dragon capsule is already equipped with a C&DH sub-system. However, this built-in part is only tested for LEO missions. Because the Inspirations Mars mission contains a fly-by around Mars, the level of complexity is higher than the complexity of the built-in part. Therefore this section will discuss the C&DH required for the entire mission. Firstly the requirements will be mentioned and the sub-systems architecture will be explained.

5.7.1 Command and Data Handeling Architecture

The requirements are to have a computer throughput of 2.5 millions of instructions per second (MIPS) and a processor speed of 10709 Source lines of code (SLOC). The C&DH sub-system is responsible to receive, validate, decode, and distribute commands to other spacecraft systems. Furthermore it has to gather, process, and format the spacecraft housekeeping and mission data for downlink or use by the on-board computer. In Figure 5.17 the C&DH flow diagram is shown. It gives an overview of the downlink and uplink. The downlink contains telemetry, it is a collection of all payload data and housekeeping data for monitoring. The uplink excists of the telecommands. These are required to control and operate the satellite, to upload user data and to upload new software. Data enccryption and decryption techniques are applied for the security of the data. It contains communications security (COMSEC) and transmission security (TRANSSEC) [25]. COMSEC involves disguising the actual transmitted data and typically includes data encryption. TRANSEC involves disguising the transmitted signal and normally involves generating security keys and variables that support spread-spectrum techniques. Finally some additional functions performed by the C&DH sub-system are mission timekeeping and providing computer health monitoring. Storage of the data is required since the data rates listed in section 5.6 can exceed the rate of 200 [kbps] [8].

5.7.2 Hardware

As already listed in table 5.30 the Dragon capsule already contains a C&DH sub-system which is tested for LEO usage. The computer in the Dragon capsule has a RS-422 serial I/O, 1553, and Ethernet interfaces (all locations)connectivity [68]. According to [8] this is typically comparable to a SC-1750A computer with a 1750A Instruction Set Architecture (ISA). This machine code uses a word length of 16 bits, it contains a Random Acces Memory (RAM) and an Electrically Erasable Programmable Read-Only Memory (EEPROM) of 512 KB. Furthermore it has a performance of 1 million instructions per second (MIPS) and a radiation hardness of 10 [KRad]. In order to determine whether or not the C&DH sub-system on board of the Dragon capsule is suitable, the size and throughput of on-board software needs to be estimated. This is required to determine how much computing power is needed, to make sure the hardware capacity will not be exceeded and to be able to estimate the size and cost. In table 5.36 a rough size and throughput estimation is made based on values for 32 bits common on-board applications. The code is calculated to be 2342.6 Kbits and the computer throughput of 672,2 KIPS. The computer language C assemblies the maximum instructions per SLOC, one SLOC equals 224 bits on a 32-bits computer. Therefore this language is chosen for the spacecraft, this results in a 10709 SLOC. The applied rule of thumb sets the amount of computer memory and throughput, at the System Requirements Review, at four times the estimate of what is needed for software size and throughput [8]. Ths results in a throughput capacity of 2.5 MIPS. When comparing these values to the SC-1750A capacities it shows that the throughput will not satisfy the requirements. Therefore

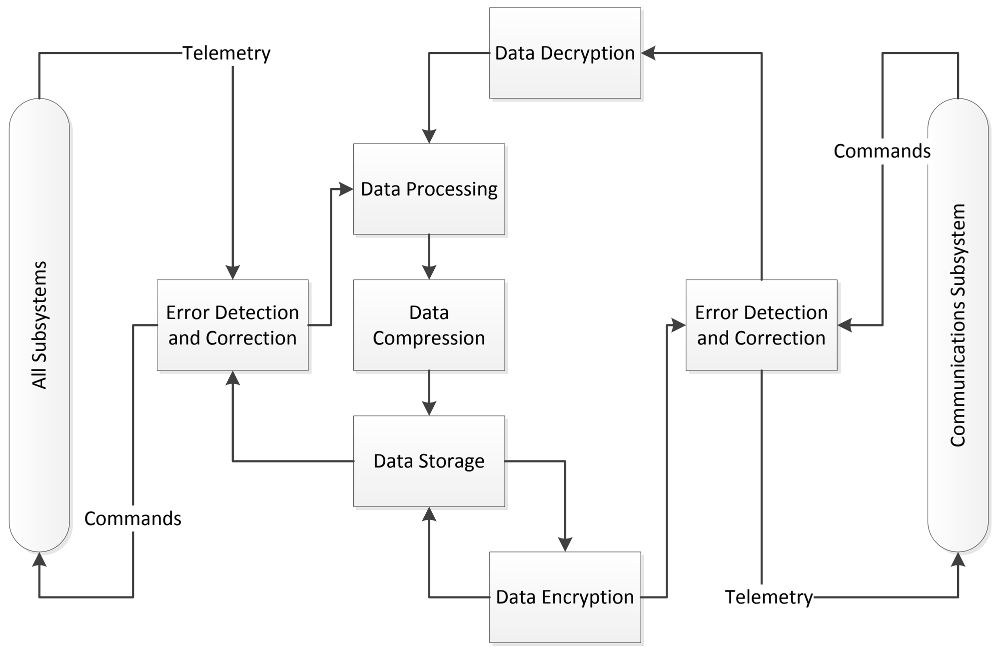

Figure 5.17: C&DH flow diagram

another on-board computer will be required. The MOPS R6000 is chosen because it shows a sufficient performance of 25 [MIPS] and the memory contains 128 [RAM + EEPROM].
The C&DH sub-system for the Inspiration Mars mission is qualified as a complex system because it is a manned mission. According to reference [8], this would require the highest values for the complex range of C&DH sub-systems [8]. Furthermore the system is completely duplicated to prevent single point failure. This results in a complete mass of 21 kg and a volume of 0.07 m^3. The nominal required power is stated to be 25 W and the peak power is estimated on 5 times the nominal power, thus 125 W.

5.7.3 Sensitivity Analysis

The C&DH is designed to be able to handle 4 times the amount of required throughput [25]. Therefore it can be stated that the amount of data which needs to be processed will not affect the sensitivity of the entire mission. According to Moore's law, the number of transistors incorporated in a chip will approximately double every 24 months. Thus, even when in the next design phase it is found that the processors should be able to handle more channels, the size can be assumed constant.

5.7.4 Verification and Validation

In order to make sure the used method is plausible it needs to be verified. No program was made for the calculations in this section. The method which is used comes from reference [8]. The on-board computer is based on the the Gravity Probe B and International Space Station Alpha mission, [[8], table 16-17]. The required throughput for these missions exceeds the calculacted required throughput, therefore the methods are validated.

5.8 Scientific Experiments

Numerous studies on Earth have aimed to obtain the effect of manned, interplanetary spaceflights. Though projects [107] have extensively studied the effect of space habiation and isolation, no mission has ever conducted a test of such an extent in which a crew faces microgravity during the experiment. Therefore, Inspiration Mars is the first mission to obtain results from scientific experiments performed in space. Both physiological and the psychological effects on the crew are tested and this brings to life the endless list

Table 5.36: Size and throughput estimates on-board applications [8]

Function	Code [Kbits]	Data [Kbits]	Throughput [KIPS]	Execution Frequency [Hz]
Telecommunications				
Command processing	32.0	128.0	7.0	10.010.0
Telemetry processing	32.0	80.0	3.0	5.0
Monitors	128.0	32.0	15.0	5.0
Fault correction	64.0	320.0	5.0	
Guidance Navigation & Control				
Rate gyro	25.6	16.0	9.01.0	10.0
Sun sensors	32.0	6.4	2.0	1.0
Star tracker	64.0	480.0	15.0	0.01
Kinematic integration	64.0	6.4	12.0	10.0
Error determination	32.0	3.2	1.2	10.0
Thruster control	19.2	12.8	5.0	2.0
Reaction wheel control	32.0	9.6	4.0	2.0
Complex ephemeris	112.0	80.0	20.0	0.5
Orbit propagation	416.0	128.0		1.0
Complex autonomy	480.0	320.0	20.0	10.0
Power management	38.4	16.0	5.0	1.0
Thermal control	25.6	48.0	3.0	0.1
Kalman filter	253.0	32.0	80.0	0.01
On-board Operating System Software				
Executive	112.0	64.0	270	-
Run-time kernel	256.0	128.0	-	-
I/O device handlers	64.0	22.4	-	-
Built-in test and diagnostics	22.4	12.8	150	0.1
Math utilities	38.4	6.4	-	-
Total	**2342.6**	**1952**	**627.2**	

of uncertainties and questions about interplanetary spaceflights. Results from pre-, and post-mission are later compared to previously perfomed on-ground experiments. These previous experiments [107] [106] have inspired this mission for its scientific experiments and the main experiments are presented in this section.

5.8.1 Identical twin study

An option which can be considered for the mission, is to select at least one member which is one of identical twins. The DNA of an identical twin is not identical, but it is the most similar DNA possible. An ageing study can be done, in which the physiological and psychological conditions of two people can be compared through time, from which one has lived in deep space for a long duration and the other has not. From this long-term study, possible effects of deep space on the human body can be determined. Since it will only account for one single person the results of this test can not be verified, but we will have a certain level of comparison data. This will require a long-life, regular medical examination for both siblings, in order to obtain data on them in time.

5.8.2 Psychology and cardiac functioning

During the mission, emotional stress is simply evitable and this can lead to altered cardiovascular functions and effect the wellbeing of the crew. Tests on this topic will aim to find the relation between mood changes and the cardiac regulations. For this serie of tests, portable Holter devices are used for short- and long durations of electrocardiographic data. Furthermore, a kit is needed to measure blood pressure and a spectrometer to monitor sleep alterations, heart rate and respiration. For more cardiac functions data, tele-echocardiography is used to study the heart mechanics and hemodynamics [103].

5.8.3 Bones and muscles

The crew will live in a state of microgravity during the spaceflight and due to this, the bones in the lower body part bear lower load than on Earth's surface. The effect of this is the breakdown of the bones and the release of calcium. The muscles will also decrease in mass and volume due to weightlessness. Tests can be performed, using screenings before and after the mission. The ISS U.S. National Lab [106] performs experiments on this topic and ISS crew members are screened for their fitness level, strenth and bone density, also as a test to support future interplantetary missions [105]. Inspiration Mars has the first opportunity to screen the human body within these situations for this amount of time. The tests and their results can be a step towards reducing the amount of degradation of muscles and bones and, if succesful, this can help future Mars missions. For continuous support of the bones and muscles daily exercise is crucial, and this is presented in section 5.8.4.

5.8.4 Exercise equipment

For the support of bones and muscles, exercise equipment are needed in the living module. Two devices used for this mission are the interim Resistice Exercise Device(iRED) and the Human Dynamo [104]. iRED makes use of a spring system for resistance training and the Human Dynamo is a power generating full-body workout device. The Human Dynamo can generate a peak power of 75W per hour of exercise, and is a sustainable element in this design. A minimum daily exercise duration of three hours is required and the exercise schedule is lined out in a typical day schedule in table 6.1.

5.8.5 Stress and Immunity

The relation between stress and immunity has been the subject of multiple studies [103], since the knowledge of this relation can lead to improving the immunity of astronauts during weightlessness and confinement. For this investigation, blood-, saliva- and urine samples are taken from the crew and analyzed and therefore medical kit needed for these samples needs to be included in the medical supplies.

5.8.6 Effect of blue-enhanced light

One of the factors that influence the performance of the crew is the level of lighting in the spacecraft. Insufficient lighting can lead to mental and physical effects, in the form of a reduction in alertness, disturbances in sleep and also the metabolism can be affected. In order to measure this effect for studies which focus on the crew's performance as a function of module lighting, small sensors are worn by the crew that analyse the light. A visual sensory system is used which detects light irrandiance and its sensitivity peaks in the blue range of the light spectrum. Using this system, the effect on the crew's characteristics is measured and an increase in alertness and sleep quality is expected [103].

5.8.7 Cognitive and emotional adaptation

Perhaps the most common known effect of confinement is the loneliness. Although there is a crew of two on board, both crew members will be away from their family, house, city etc. for nearly one and a half years. This has serious effects on a human being and requires both cognitive and emotional adaption. This study is performed using questionnaires and keeping a journal [103]. Using this data, a timeline of emotion as a function of time and event can be constructed and this is useful for future missions. If a pattern can be found using this data, this can be used as predictions for further missions and time dependant emotional support can be given to the crew.

5.8.8 Effect of dietary supplements

To determine the effect of exercise and diet during long duration manned missions, the use of supplements is introduced in combination with training. Studies have shown [103] that a combination of these two factors improve the mood and performance of the crew. Though this has been tested on ground, Inspiration Mars can perform this to test it in combination with weightlessness unlike Mars500 [107]. Results of this test are obtained using questionnaires. Fatty acids like omega-3 are of great imporance in this test and the use of this supplement has a beneficial effect on the activity of the nervous system. It also helps improving the cognitive development of the crew, so it is an important element within the diet. The mass of the supplements is accounted for in the food segment.

5.8.9 List of scientific payload elements

In this section the aforementioned scientific payload elements, the exercise equipments and other essentials, are collected and lined out.

- Human *Dynamo*[1]	- HMS Defibrillator
- *iRED*[1]	- Sphygmomanometer
- Emergency medical kit	- Spectometer
- Diagnostic pack	- Respiratory support system
- Holter device	- Portable Transthoracic Echocardiogram

[1] Further detail given in section 5.8.4

Adding the scientific payload, along with the exercise equipment, a total mass of 290kg is accounted for, using visual estimation, system lay-outs [104] and ISS exercise specifications [113].

5.9 Electrical Power Sub-system

Electrical power is necessary for life support and most of the subsystems of the spacecraft. For such a crewed mission safety and reliability of these subsystem is critical for the mission success, but also the mass and volume limitations must be taken into account to achieve an optimal design. First the electrical power subsystem(EPS) functions and requirements are explained, followed by the selection and sizing of the power sources and energy storage. At last the power management will be discussed focusing on power distribution, regulation and control.

5.9.1 Functions and Power Budget Requirements

The main functions of the electrical power system are to generate, regulate and distribute the electrical power throughout the vehicle. The first step is to identify the power budget for the whole mission. For this, the mission is divided in different phases which have different power or logistics requirements: Launch, Low Earth Orbit (LEO), Interplanetary Trajectory, Re-entry Preparation and Re-entry phase. The average power and peak power at each phase are shown on table 5.37 for the critical phases. During Launch and Re-entry phase the power requirements will be fullfilled by the default configuration of batteries in the Dragon re-entry capsule and the fly-by maneuver will be treated inside the Interplanetary Trajectory phase.

Table 5.37: Power budget during the different phases of the mission

Subsystem	**Low Earth Orbit**		**Interplanetary Trajectory**		**Re-entry Preparation**	
	$P_{avg}[W]$	P_{peak} [W]	$P_{avg}[W]$	P_{peak} [W]	$P_{avg}[W]$	P_{peak} [W]
EVA preparation	0	4500	0	0	0	4500
ECLSS	5030	10914	5030	10914	5030	10914
Comunications	10	10	116	226	116	226
C&DH	25	125	25	125	25	125
GNC	59	59	69	69	69	69
Thermal Control	982	1537	982	1537	982	1537
10% Margin	609	1254	622	1287	622	1266
Maximums	6706	13788	6844	14158	6844	13927

For the maximum peak power during LEO and Re-entry Preparation phases it is assumed that the the Extravehicular Activity (EVA) preparation (pressurization and depressurization of modules) will not coincide with the ECLSS system power peaks. For the Interplanetary Trajectory phase, the maximum peak its estimated for the worst case that all peak powers would occur at the same time.
For an interplanetary mission, it is also very important to take into account the solar intensity variations to achieve the most optimal design. Figure 5.18 shows the solar intensity through the whole mission duration.

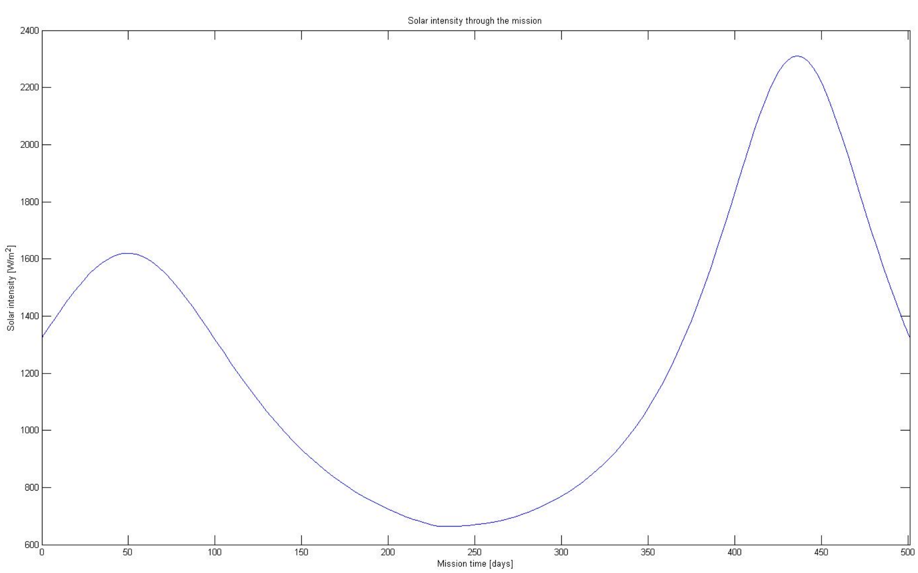

Figure 5.18: Solar intensity [W/m^2] variation through the duration of the mission [days]

Through the power budget and the solar intensity variations the following requirements were identified to design the EPS:

- The EPS must provide an average power of 6844 Watts.
- The EPS must be able to provide 14158 Watts of power during eight half an hour intervals per day.
- The EPS must conserve the required performance for at least 550 days.
- The EPS must be able to adjust the power produced with varying solar intensities (including fly-by).

5.9.2 Selection and Sizing of Power Source

The starting point is the off the shelf power generating subsystem that is installed in the Dragon Spacecraft. A single trunk contains 2 sets of solar arrays which produce up to 2000 Watts average power and up to 4000 Watts peak power on Low Earth Orbit (LEO) [68]. The total area of both solar arrays was estimated to be 23.4 m^2 using technical drawings. Knowing this and assuming a solar intensity on LEO of 1400 W/m^2 and efficiency of the path solar array-load of 90% the efficiency of the solar array cells is calculated. It yields that the installed solar arrays have a solar cell efficiency of 14 %, which is on the lower side of the range for GaAs solar cells efficiency values for space. This fact allows for increasing the total power output by using more efficient solar cells without modifying the default structure of the solar arrays. As a total power output without any modification the solar arrays from two trunks of the Dragon spacecraft produce 4000 Watts average power and 8000 Watts peak power on LEO.

Additionally, fuel cells and primary batteries are also considered as main power source. Batteries have similar characteristics to fuel cells but with a lower specific power. On top of that, after primary batteries are used, they cannot be reused for any other purpose, while fuel cells produce in addition to electrical energy, potable water that can be used as consumable and radiation protection during the mission. Table 5.38 compares solar arrays and fuel cells through important design parameters for the mission.

Table 5.38: Solar photovoltaic versus fuel cell as power source [8]

Design Parameter	Solar Photovoltaic	Fuel Cell
Power range [kW]	0.2 - 300	0.2 - 50
Power density [W/kg]	25 - 200	275
Maneuverability	Low	High
Drag (LEO)	High	Low
Degradation	Medium	Low
Obstruction of SC viewing	High	None
Fuel availability	Unlimited	Medium
Safety analysis	Minimal	Routine

From the facts on table 5.38, it appears that fuel cells are superior than solar arrays. But after some preliminary calculations fuel mass required for fuel cells for periods longer than a month becomes unfeasible. A combination of both power sources is studied to design the most optimal electric power subsystem taking into account the different logistics and operations for each phase of the mission.

For the LEO phase, taking into account the EVA, docking and refueling maneuvers and orbital debris impact risk it would be advantageous not to deploy the solar arrays. This phase has a duration of maximum of four days, so fuel cells can provide the required power with a minimum added mass, if we take into account that the reactants will be converted into usable water for the mission. The fuel cells dry mass (M_{plant}) and reactants mass ($M_{reactants}$) are calculated with equations 5.48, 5.49 and 5.50 for the average and peak powers for the LEO phase assuming an specific power of the fuel cells of 275 W/kg (as in the Space Shuttle) and reactant consumption rate of 0.45 kg/kWh [109].

$$M_{reactants} = E \times C_r \tag{5.48}$$

$$C_r = \eta_{fc} \times E_{sp,reactant} \tag{5.49}$$

$$M_{plant} = \frac{P}{P_{sp}} \tag{5.50}$$

For the four days period in LEO, a total energy (E) of 764288 Wh is required with an average power of 6706 W. This yields two fuel cells (for redundancy) of 12.2 kg each, and 343.9 kg of reactants and storage tank with a reactant consumption rate (C_r) of 0.45kg/kWh. From this 343.3 kg of hydrogen and oxygen it is assumed that 300 kg will become water as result from the fuel cell reaction and it will be used as part of the water required for ECLSS. The fact that the fuel cells are sized for 4 days use leave an extra 382144 Wh for redundancy of the EPS during the rest of the mission as the LEO phase should only require 2 days if everything goes as planned.

For the Interplanetary Trajectory and Re-entry preparation phase, the power source will be solar energy through the use of solar arrays and secondary batteries. The solar arrays will be sized for the average power during this phase (P_{avg}=6844 W) and the minimum solar intensity (S=591 W/m^2) using equation 5.51 assuming a solar array to load efficiency of 0.9 [109].

$$P_{EOL} = AS\eta_{cell} I_d L_d cos(\theta) \tag{5.51}$$

Starting from the default configuration of the solar arrays, and trading off solar array size and solar cell efficiency, a total solar array area of 57.2 m^2 for a solar cell efficiency of 30%. The solar cells with this efficiency will be Single Junction GaAs cells.Each solar array will have a size of 6.5 x 2.2 m (increase of 0.37 m in width). They will be mounted as by default on the Dragon spacecraft and will only be deployed only after the trans mars injection burn.

5.9.3 Selection and sizing of energy storage

The spacecraft requires a system to store energy for the peak power periods as well as for the fly-by. For this regenerative fuel cells and secondary batteries where considered. Due to not enough test data of regenerative fuel cells and their reactant production rate being too low, secondary batteries are chosen for energy storage of the EPS. The type of batteries selected is Nickel-Hydrogen with single pressure vessel design, as they have the highest specific energy density of the space-qualified batteries [8]. For the sizing of batteries, the mission length with a 10% margin (550 days), the trajectory characteristics (20 minutes of eclipse during fly-by), the peak power loads (14158-6844=7314 W) and the depth of discharge of the batteries (DOD= 60%) are used.

$$C_r = \frac{P_e T_e}{(DOD)Nn} \tag{5.52}$$

With equation 5.52, using a five batteries configuration (N=5) (maximum number of batteries without requiring complex components for recharging) and assuming transmission efficiency of n=90%, the required battery capacity (C_r) is calculated to be 1354.44 Wh for each of the five batteries.

5.9.4 Power Management

The power management of the EPS consist of power distribution, regulation and control. The power distribution system is composed of cabling, fault protection and switches to turn power on or off for the spacecraft loads. Power regulation and control takes care of controlling the solar array solar power input by varying the angle of incidence, regulating the bus voltage and charging the secondary batteries. Figure 5.19 shows the power management of the EPS and the connection between all of its systems.

5.9.5 Sensitivity Analysis

The effects of a change in the requirements is studied on this section. A good design should be flexible and have a low sensitivity. To achieve that, contingency measures might be needed. Table 5.39 shows the possible variations of the requirements of the mission and the effect that they have on the different parts of the EPS.
As can be seen, minor changes to the EPS design occur when the requirements are increased by 10%. The average power is found to be the paramenter for which the EPS is more sensible. Even so, there is room to increase the solar arrays, keeping in mind they should be folded and contracted using the same method as in the Dragon Spacecraft.

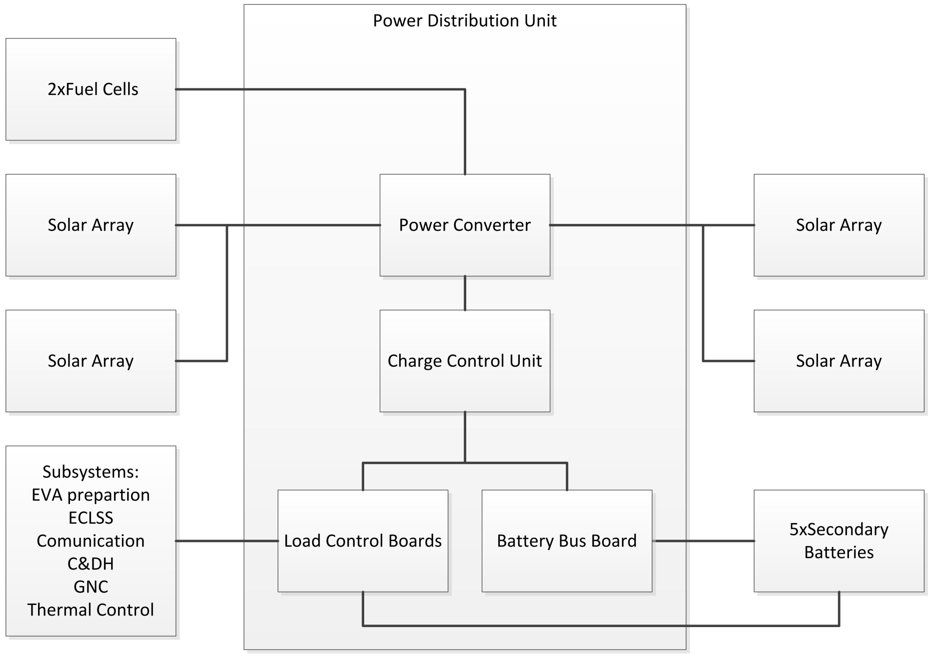

Figure 5.19: Electrical block diagram

Table 5.39: Sensitivity analysis of the EPS

Changed Input Paramenter	**Solar Array Size** [m^2]	**Batteries Capacity [Wh]**	**EPS Total Mass [kg]**
Nominal Conditions	57.2	6772	1280
Average Power 10% increase	61.89 (+8.6%)	6772	1311 (+2.4 %)
Peak Power 10% increase	57.2	7449 (+9.1 %)	1295 (+1.16 %)
Mission duration 10% increase	57.2	6772	1280

5.9.6 Verification and Validation

For the design and sizing of the EPS, all equations and calculation techniques used are derived from [109] and [8]. These equations are then assumed to be correct and verified. The equations are introduced into an Excel sheet which is verified for the different components using specific example problems from [109]. With this it is checked that the designed components of the EPS will meet the requirements (inputs of the equations) if the system performs in the real life scenario as modeled by the equations.
To make sure that the EPS will perform in the real environment as modeled, the design must be validated. For this, the main components are compared to real examples. The Fuel Cells are validated with the fuel cells used on the Space Shuttle. Each of the 3 fuel cells used on the Space Shuttle was able to provide 12 kW peak power and 7 kW average power at 27.5 volts (which is the assumed voltage for all the loads) [110]. The power provided by one of this power plants is comparable to the total power of both fuel cells in Adrestia (Peak power: 12 kW/13.8 kW ; Average power: 7kW/6.7kW). The mass of a whole fuel cell power plant is around 48 kg which is double of the mass of the 2 fuel cells from Adrestia. This first value includes all the power converters and regulators required for the fuel cells while for Adrestia the weight of those components is calculated as one system for the whole EPS (308 kg) and therefore the difference in masses. The solar panels and batteries, are validated by comparing the results with the FireSat example in [8] and the current design of the Dragon Spacecraft [68]. The power requirements are quite different to the mission but the ratios between the required power and required solar array area and battery capacity are similar (less than 10% difference in both cases which can be explained by the differece in solar array to load efficiency) when using the solar intensity at LEO and the same solar cell efficiencies. It must be noted that the solar cells selected have not yet been used in space, but enough data exists to estimate a decrease in performance of about 2 to 3 % from tests on Earth to the Space environment [8] which is already taken

into account. The secondary batteries used have been tested in space extensively and their performance is assumed to be modeled accurately with the relations used. The sizing of the EPS is therefore assumed to be validated.

5.9.7 Conclusion

The EPS consists of two fuel cells, four solar arrays and five secondary batteries as well as power management systems. The fuel cells will be the primary power source during the Low Earth Orbit (LEO) phase. Thereafter, for the Interplanetary Trajectory phase, the solar arrays are deployed and used together with secondary batteries to produce the required power for all subsystems. The power generated by the solar arrays will be kept constant by changing their inclination with respect to the sun as the solar intensity varies through the trajectory. Furthermore, the fuel cells will have reactants left to act as a redundancy measure during the Interplanetary Trajectory, while the batteries and solar arrays could be used in the same manner during the LEO phase.
The mass and volume of the components of the EPS is summarized on table 5.40.

Table 5.40: EPS components mass and volume budget

System	**Mass [kg]**	**Volume [m^3]**
Fuel cells (2)	24.4	1.15
Fuel cell reactants and storage	344	0.71
Solar arrays (4)	304	1.14
Secondary batteries (5)	150	0.04
Power distribution	150	0.02
Power converter	171	0.06
Power control unit	137	0.05
Total	1281	1.15

5.10 Thermal Control Sub-system

The Thermal Control System's (TCS) function is to ensure that all spacecraft components are in their specific operating temperature ranges during the mission, while using the minimum spacecraft resources. Besides keeping temperatures within ranges, the aim of the thermal control system is to minimize temperature gradients according to specified limits.

5.10.1 Thermal Requirements

The thermal control system design process mainly consists of two tasks. On the one hand, the appropriate thermal hardware for the spacecraft is selected. On the other hand, the temperatures of the different parts of the spacecraft are calculated for different load cases, verifying that the thermal requirements are met. The thermal requirements of common spacecraft equipment, in operational conditions, are shown in table 5.41.

Table 5.41: Thermal requirements for spacecraft components, [25, p.113], [8, p.428], [47, p.384]

	Component	**Operational Temperature Range (°C)**
Crew related	Crew compartment	+18.3 to +26.7
	Surface touch temperature	+4 to +40
	Food storage	-20 to +4
Electrical Power	Solar panels	-105 to +110
	Batteries (NiH_2)	-5 to +20
	Power control unit	-20 to +55
Attitude Control	Reaction wheels	-10 to +40
	Gyroscopes	0 to +50
	Star trackers	0 to +30
Propulsion	Propellant tank, filter, valves, lines	+7 to +55
	Thrusters	+7 to +65
	Nitrogen tetroxide	-11 to +21
	Monomethylhydrazine	-52 to +87
Thermal control	Multilayer Insulation (MLI)	-160 to +250
	Radiators	-95 to +60
	Heaters, thermostats, heat pipes	-35 to +60
Structures	Nonalignment critical	-45 to +65
	Alignment critical	+18 to +22
Antennas	Antennas	-100 to +100
Harness	Spacecraft internal	-15 to +55
	Spacecraft external	-100 to +100
Mechanisms	Deployment hinge	-45 to +65
	Electric motors	-45 to +80
	Solar array drive assembly	-35 to +60
Other	Onboard computer	-10 to +50
	Telemetry & Command units	-10 to +50

5.10.2 Thermal Environment

One of the major factors driving the thermal control system is the spacecraft environment, which drives the external loads. The spacecraft is subjected to highly variable environmental conditions. The thermal control system has to fulfil thermal requirements over all mission phases. In order to size the thermal control scenarios, the worst case scenarios are identified. These so-called hot and cold cases are defined by appropriate combinations of external fluxes (solar, albedo and planetary infrared (IR) radiation), material properties and unit dissipation profiles. The spacecraft shall depart from Low Earth Orbit (LEO), perform a fly-by on the dark side of Mars and head back to Earth. On its trajectory back to Earth the spacecraft passes through Venus's orbit, which is the closest the spacecraft will be to Sun. The solar constant at Venus can therefore be taken as the maximum solar constant. The external fluxes due to solar radiation, albedo and planetary infrared radiation are calculated next.

Solar Radiation

Within 2AU of the Sun, the Sun is the main source of heating and power [46, p.23]. Close to the Earth (at 1 AU), the nominal value of the direct solar incident energy on a surface normal to a line from the Sun is the so-called solar constant (J_s). The values of the solar constant depend on the distance from the Sun, it has higher value closer to the Sun and a lower value further away. The mission will go through three different solar constant values. The equation with which the solar radiation intensity can be calculated using equation 5.53 [47, p.358].

$$J_s = \frac{P_s}{4 \cdot \pi \cdot d^2} \tag{5.53}$$

In which P_s is the total power output from the Sun, 3.8×10^{26} W and d is the distance from the sun. The most critical values for the mission are provided in table 5.42.

Table 5.42: Relevant data for the solar constants, [47, Table 11.2]

Planet	J_s **[W/m²]**
Earth	1371
Mars	590
Venus	2618

Albedo Radiation

The next significant thermal environment contributor is the albedo radiation. Albedo radiation is the part of the solar radiation incident upon the planet which is reflected by the planet surface and atmosphere. The albedo coefficient, a, is defined as the fraction of incident solar radiation which is reflected from the planet. The albedo coefficients of Earth and Mars can be found in table 5.43, the albedo coefficient of Venus is not necessary because the spacecraft is not performing a fly-by at Venus.

Table 5.43: Albedo coefficients, [46, p.28]

Planet	**Albedo Coefficient [-]**
Earth	0.34
Mars	0.15

When in LEO, and also during some part of the fly-by at Mars, some of the sunlight will be reflected on the spacecraft. The albedo intensity, J_a that is incident on the spacecraft can be calculated by equation 5.54. [47, p.340]

$$J_a = J_s \cdot a \cdot F \tag{5.54}$$

Where a is the planetary albedo coefficient and F is the visibility factor, which depends on the altitude of the spacecraft from the planet. The visibility factor is calculated with equation 5.55 [47].

$$F = \frac{1}{2} \cdot (1 - \frac{\sqrt{H^2 + 2H}}{1 + H}) \tag{5.55}$$

In this equation H=h/R, with h being the altitude of the spacecraft above the given planet and R is the planet's radius. For Earth, h is 200 km and R is 6371 km, for Mars h is 180 km and R is 3400 km. Thus the visibility factors for Earth and Mars are 0.38 for Earth and 0.34 for Mars. The albedo radiation that the spacecraft will experience in 200 km LEO orbit is given by equation 5.56 and for Mars with a 180 km fly-by altitude by equation 5.57.

$$J_{a_{Earth}} = 1371 \cdot 0.34 \cdot 0.38 = 176\ [W/m^2] \tag{5.56}$$

$$J_{a_{Mars}} = 590 \cdot 0.15 \cdot 0.34 = 30.4\ [W/m^2] \tag{5.57}$$

Planetary Radiation

Planetary radiation is the thermal radiation emitted by a planet. It is a combination of the emitted radiation by the planet's surface and by the atmospheric gases. All incident sunlight not reflected as albedo is absorbed by Earth and eventually re-emitted as IR energy [8, p.433]. The average values for the planetary radiation of Mars and Earth are summarized in table 5.44 [8, p.434].
The intensity of the planetary radiation J_p decreases with altitude according to an inverse-square law [47], given by equation 5.58.

Table 5.44: Planetary radiation [8, p.434]

Planet	Planetary radiation [W/m^2]
Earth	237
Mars	145

$$J_p = p \cdot (\frac{R_{rad}}{R_{altitude}})^2 \quad (5.58)$$

In which p is the planetary IR radiation emission, R_{rad} is the radius of the planet's effective radiating surface (assumed to be the same as the radius of the planet) and $R_{altitude}$ is the altitude of the spacecraft from the given planet's center. Therefore, the received IR radiation in LEO and Mars fly-by are given by equations 5.59 and 5.60.

$$J_{p_{Earth}} = 237 \cdot (\frac{6371}{6371 + 200})^2 = 222.8 \, [W/m^2] \quad (5.59)$$

$$J_{p_{Mars}} = 145 \cdot (\frac{3400}{3400 + 180})^2 = 130 \, [W/m^2] \quad (5.60)$$

Spacecraft Heat Emission

The spacecraft itself radiates heat into space as a black body having a value of emissivity depending on the material. For practical purposes, space can be considered as a black body at 0 K. It should be noted that the heat transfer takes place from the total surface area of the vehicle.

Internal Heat Dissipation

Internal heat dissipation is caused by the electric components inside the spacecraft. Moreover, since Inspiration Mars is a human mission, there will be additional human heat production. The current standards for handling metabolic heat production with normal activity is 100 W per person [25, p.121] when the astronauts are at rest, and about 200 W per person when they are performing activities. Therefore for a crew of two, the total human heat production is assumed to be 0.4 kW. The peak heat due to the power system generated inside the spacecraft is estimated to be 13 kW 5.9. Therefore, adding the crew heat production results in the peak internal heat dissipation value of 13.4 kW. However, it should be noted that this occurs only a couple of times per day. During all other moments, the average power of 6 kW is considered as the heat contributor that has to be ejected from the spacecraft.

5.10.3 Thermal Equations

A successful thermal design must include adequate radiator area to accommodate the maximum operational power during the hottest operational environment without exceeding allowable temperatures. A generalized heat balance equation is given by equations 5.61 and 5.62 [8, p.453].

$$Q_{in} = Q_{out} \quad (5.61)$$

$$Q_{external} + Q_{internal} = Q_{radiator} + Q_{MLI} \quad (5.62)$$

In which $Q_{external}$ is the absorbed environmental heat, $Q_{internal}$ the power dissipation, $Q_{radiator}$ is the heat rejected from the spacecraft primary radiator surfaces, and Q_{MLI} is the heat lost from Multilayer Insulation (MLI) blankets and elsewhere on the spacecraft.
The contribution due to the Sun is formulated in equation 5.63 [47]. In this equation α_{eff} is the effective absorptivity of a surface to solar radiation and A is the surface area that is receiving the solar radiation.

$$Q_{solar} = J_s \cdot \alpha_{eff} \cdot A \quad (5.63)$$

The Stefan-Boltzmann equation, given in equation 5.64, relates the radiated energy from the surface with the temperature [47].

$$Q_{radiated} = \epsilon \cdot \sigma \cdot A \cdot T^4 \tag{5.64}$$

Where ϵ is the emissivity of a surface radiating in the IR region, σ is the Stefan-Boltzmann constant $5.67 \cdot 10^{-8} W/m^2K^4$, A is the surface area and T is the absolute temperature of the radiating surface.
Equation 5.62 is rewritten to formulate a relation between the surface temperature $T_{surface}$ and the radiator area A_{rad}. This is done by the fact that $Q_{external}$ is equal to Q_{solar}. Also, $Q_{radiator}$ and Q_{MLI} are radiating surfaces and can thus each by determined by equation 5.64. This is then rearranged in equation 5.65 to give the surface temperature as function of radiator area.

$$T_{surface} = ((\frac{\alpha_{EOL_{eff}} \cdot A_s \cdot J_s + Q_{in}}{\sigma} - \epsilon_{rad} \cdot A_{rad} \cdot T_{rad}^4) \cdot \frac{1}{\epsilon_{MLI_{effective}} \cdot A_{surface}})^{\frac{1}{4}} \tag{5.65}$$

5.10.4 Passive Thermal Control

Thermal conditions can be satisfied by a passive system if the spacecraft orientations and equipment power dissipation are known. Since a lot of internal heat is generated in the spacecraft, most of which needs to be dissipated, it is crucial to have as low as possible induced heat from the external environment. Therefore the sun-facing part of the spacecraft will have a small area and a highly reflective surface. Figure 5.20 shows the orientation of the spacecraft with respect to the Sun.

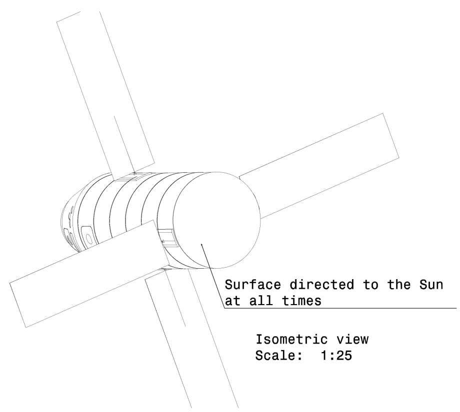

Figure 5.20: Sun facing surface of the spacecraft

The outer layer of this area is $3M^{TM}$ $Nextel^{TM}$, mainly for its MMOD protection capabilities, but also its reflective properties. It has a solar absorptivity α of 0.14 and emissivity ϵ of 0.87 [51]. However, because of ultraviolet radiation, the surface shall degradate and will have an end-of-life (EOL) solar absorptivity value of 0.35 [52].

Multilayer Insulation

It is common practice to insulate the spacecraft from outer space using MLI. The spacecraft is protected by toughened MLI, which also acts as an additional MMOD protection [55, p.101]. The MLI consists of several layers of closely spaced, highly reflecting shields, which are placed perpendicular to the heat flow direction, as shown in figure 5.21.

For the mission, 50 layers of 1/4 mil Aluminized Mylar is used. Beyond 50 layers, the advantages are negligible [47]. It is chosen because it has a very low emittance factor ϵ of 0.34 [8, Table 11-46]. However, Mylar can not be exposed to sunlight and is therefore placed behind the MMOD protection. The effective emittance of the MLI, is calculated by dividing the emittance by the number of MLI layers. In this case, the effective absorbance and emissivity are calculated by equation 5.66 and 5.67.

$$\alpha_{MLI_{effective}} = \frac{\alpha_{MLI}}{\#_{MLI-layers}} = \frac{0.35}{50} = 0.007 \tag{5.66}$$

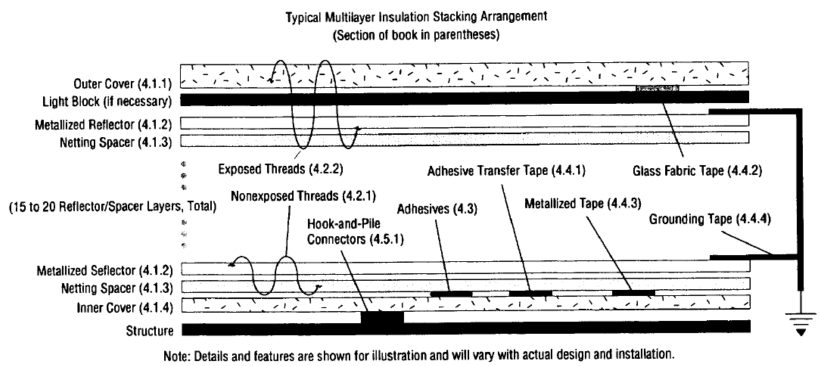

Figure 1. Schematic cross section depicts the key elements of an MLI blanket.

Figure 5.21: Composition of a typical MLI blanket, [50]

$$\epsilon_{MLI_{effective}} = \frac{\epsilon_{MLI}}{\#_{MLI-layers}} = \frac{0.3}{50} = 0.0068 \tag{5.67}$$

5.10.5 Worst Hot Case Scenario

The hot case corresponds to the maximum external loads and maximum internal dissipation. A common philosophy in spacecraft thermal control is to design the thermal subsystem for the hot operational case [46, p.337]. This implies that the radiators are sized to reject the maximum power dissipated by the equipment under maximum external loading intro space. The worst case in the mission is when the distance between the Sun and the spacecraft is minimized, thus when the spacecraft passes through Venus's orbit. At this point the solar radiation is maximum, which is the dominant contributor as compared with albedo and planetary radiation. The following assumptions will be made for the radiator sizing of the worst hot case.

1. The inside temperature should be around 20 °C, see table 5.41.
2. The radiator temperature can be increased by 50 °C more than the room temperature by the heat pump.
3. The radiator is on the sides of the spacecraft, and therefore only exposed to deep space and not to the Sun.
4. The initially assumed black paint for the radiators with surface properties α=0.92 and ϵ_{IR}=0.89 [8, p.436].
5. The radiated power is the total internal heat dissipation, Q_{in} of 13.4 kW.

In order to keep the temperature within the required crew compartment temperature range, the radiator surface area is calculated for the worst hot scenario using equation 5.65. For this, $\alpha_{EOL_{eff}}$=0.35 (equation 5.66) which is the solar absorptivity at EOL, A_s=10 m^2 which is the surface area that absorbs the solar radiation, J_s=2618 W/m^2 which is the solar constant at Venus, σ=5.67·10^{-8} which is the Boltzmann's constant, ϵ_{rad}=0.95, A_{rad} being the radiator area, T_{rad}=343.5 K is the radiator temperature and $\epsilon_{MLI_{effective}}$=0.0068 which is the effective emittance of the MLI, calculated by equation 5.67.

.

In order to get a surface temperature for the required conditions, a radiator area of 20 m^2 is calculated. Then, the surface temperature is 290 K, which equals to 16.85 °C. To allow the rejection of the internally dissipated power into space, the radiators are located on the outer surface of the spacecraft subjected to lower environmental loads (facing deep space as much as possible). The initial area of 20 m^2 means that they can be arranged on the side of the living module. The airlock is put away from the radiators, so the astronauts would not be exposed to the radiated heat from the radiators when they have to perform the EVA. Using body mounted radiators, which are almost never exposed to the Sun due to the orientation of the spacecraft, is a lightweight solution as no additional structural mass is needed, which is the case when deployable radiators are used. Also, body mounted radiators have no movable parts, which decreases the risk of failure.

5.10.6 Worst Cold Case Sscenario

The worst cold case for the spacecraft is experienced during the Mars fly-by. Using equation 5.65, while keeping the spacecraft temperature around 20 °C with the values for the worst cold case, J_s=590 W/m^2, for average and power values of 6.4 and 13.4 kW, the needed radiator area is 19.8 m^2 and 9.25 m^2. In the case that no direct sunlight reaches the spacecraft (behind Mars), for J_s=0 W/m^2, then only 9.15 m^2 radiators area needs to be used. Making fully use of the radiator size selected for the hot case during the cold conditions, can lead to extremely low temperatures because the entire radiator is ejecting the heat out of the spacecraft. The regulation is performed by active thermal control. At Mars conditions the radiator can be used to partly absorb solar radiation, so the heat pump does not need to be used. Therefore, at each part of the orbit, the radiator can absorb enough solar radiation to keep the spacecraft at room temperature. Even when the heat dissipation internally is minimal (e.g. due to an electrical failure), the spacecraft can be rotated so the radiator can absorb enough solar radiation (only attitude control has to remain functional) [53]. The calculations for these adjustments for the GNC subsystem shall be done in the later stage of the design.

5.10.7 Active Thermal Control

Due to the narrow temperature range stated in the requirements, the spacecraft cannot be controlled by the passive thermal control only. To regulate the thermal control, active thermal control is necessary. Therefore, fluids which transfer the excess thermal energy to a thermal sink (the radiators) are used.

Fluid Loops

Dual loop configurations consisting of two circulating coolant loops coupled by an inter-loop heat exchanger are in common use. These offer more precise temperature control then a single-loop and are flexible in accommodating spacecraft thermal loads, coolant inlet temperatures and changes in heat dissipating elements [47]. Moreover, the dual loop is a mechanically pumped single-phase fluid loop, which is a system that circulates a working fluid via routed tubing to all parts of the spacecraft structure. Pumped single-phase fluid loops is chosen because it is simple, robust and has a number of other advantages [46, p.240], compared to other thermal control technologies, such as:

- Flexibility in locating heat dissipating equipment inside the spacecraft.
- Ability to accept and reject heat at multiple locations.
- Ability to incorporate late design changes in the spacecraft.
- Ease of scalability to meet changes in power dissipation requirements.
- Ability to match working fluid to the required thermal environment.

Although mechanically Pumped Fluid Loop (PFL) systems have limitations, mainly due to power consumption (20% extra power), they have been used successfully [46, p.241] on manned space missions in the Space Transportation System (STS) Shuttle and the International Space Station (ISS), and on both the Mars Pathfinder [48] and two Mars Exploration Rover missions [49]. Since the pumps are mechanical, they are more prone to failure than electronic systems. A simplified schematic of the PFL is depicted in figure 5.22. At the eclipse at Mars the internal temperature can be maintained by not using the heat pump, except in cases of peak power usage, and reducing the fluid-loop velocity [53]. In order to have no single-point failure, every pump shall have a back up on-board. The list of fluids applicable for single-phase pumped fluid loops is very restrictive, and only a few have been used already. An important consideration in selecting coolant for the internal system is the crew's safety. If coolant leaks into the living area the safety of the crew shall not be compromised. For efficiency, high specific heat and low viscosity are desirable because they reduce the required pump power to circulate the fluid. Most U.S. missions selected water, which has one of the highest values of specific heat and is not toxic [25, p.531]. However, to keep the water from freezing, electrical heaters are used. The fluid loop is especially useful for the heat regulation during the different phases of the mission. With the help of a thermostat, the heat dissipation of the radiator can be controlled by controlling the fluid-loop velocity and switching off the heat pump.

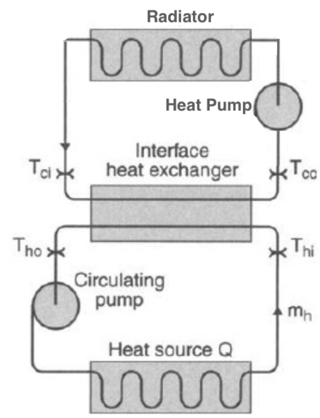

Figure 5.22: Schematic of a simplified PFL, [46, Fig.14-1]

Heaters

Keeping the spacecraft and its components within the operational temperature ranges, as shown in table 5.41, implies the warming of the item under consideration by using appropriate heaters. E.g., the water is kept above 0 °C. The most commonly used electrical heater is of the film type, which can be installed on both flat and curved surfaces, due to its flexibility. The heating power density of the film heaters is 0.7 W/m^2. The heaters are installed on the surface of the particular equipment, such as the tubes of the liquid loops, to prevent water from freezing, and on the propellant tanks, that needs to be heated using a pressure sensitive adhesive [46, p 227].

5.10.8 Thermal Control System Specification

In chapter 8, the mitigation of risks for the thermal control system is discussed. To avoid single point failure of the thermal system, contingency measures are added to the system design. With these contingency measures, the thermal control system can be sized using the relations for component's mass and power [25, Table 16.7]. The specifications of the thermal control system are presented in table 5.45.

Table 5.45: Thermal control system components characteristics

TCS Component	**Mass [kg]**	**Power Avg [W]**	**Power Peak [W]**
Heat exchanger	20.36	negligible	negligible
Water Pump (2x)	129	143.5	293.5
Heat pump (2x)	215	699.4	1416.7
Fluids	7.47	0	0
Plumbing and valves	22.41	0	0
Instruments and controls	7.47	negligible	negligible
Heaters	9.41	-	-
Radiator (78 m^2)	106	0	0
Total	**517**	**842.9**	**1710**

5.10.9 Sensitivity Analysis

A number of assumptions and estimations are made to calculate the previously presented results. Some of these estimations might be inaccurate. To asses the consequence of these inaccuracies a sensitivity analysis is made, the results are shown in table 5.46.

The thermal calculations assumed the spacecraft to be perfectly insulated with the MLI. In reality this is not the case. The connection with the re-entry capsule, the solar arrays, as well as the living module door, will all conduct part of the heat to the external environment. Therefore, the isolation efficiency was decreased.

A change of 10 % in isolation efficiency results in a change of 0.2% in radiator area and no significant change in system mass. This indicates that the system is not sensitive to changes in the isolation efficiency.

If the trajectory keeping is inaccurate, the spacecraft can get closer to the Sun. Therefore the sensitivity of the system to a 20% increase in solar intensity is assessed. This yields an increase of 10% in radiator area and a 6% increase in system mass. It can thus be concluded that the system is sensitive to changes in the solar intensity.

Another scenario is that the one of solar panels cannot rotate enough when close to the Sun, which will result in greater heat generated by the power subsystem. However, due to the power regulator the extra peak power generation does not rise above 10%. This results in an area increase of 4.5% and a system mass increase of 6.7%. It is concluded that the TCS is sensitive an increase in peak power generation.

Table 5.46: Thermal control system sensitivity analysis

Changed input parameter	**Radiator Area [m^2]**	**System mass [kg]**
Nominal conditions	20	517
Isolation efficiency $\epsilon_{MLI_{eff}}$ -10%	19.6 (-0.2%)	517 (0%)
Solar intensity +20%	22 (+10%)	548 (+6%)
Solar absorbance area +15%	21.5 (+7.5%)	538 (+4.1%)
Peak power +10%	20.9 (+4.5%)	5 (+6.7%)

5.10.10 Verification and Validation

A simplified model consisting of analytical calculations is used for the thermal analysis. It is verified with the examples from the books [8], [47], in which the equations are presented. Because the equations used are presented in two independent books, it is verified that the equations used are correct.
For validation, the example design of a TCS for a manned Mars mission in [25] is considered for comparison. It also includes an active system that works with an ECLSS to keep the crew comfortable and the vehicle's electronic equipment within its thermal operating range. Moreover, it also includes single-phase, pumped fluid radiators. However, the example is designed for cruise-phase power of 25 kW. The Inspiration Mars mission is based on 13 kW peak power, which is 52% less then the example from [25, Table 31-6]. Correspondingly, the mass estimation for the TCS (active and radiators) is 2088 kg and 810 kg respectively for the example and the Inspiration Mars missions. The mass ratio is 39 %. If all components in the TCS are identical, the mass and power ratios are expected to be equivalent. However, the example mission makes use of deployable radiators, which are 62% heavier then the fixed ones used by in this design. Therefore, if the deployable radiators on the Mars Design example are substituted with fixed ones, the TCS mass will be equivalent to 1585 kg. In that case, the mass ratio is 51 %, which is almost identical to the 52 % power ratio. Therefore, the sizing of the thermal control system is validated.

5.10.11 Testing

The development, qualification and acceptance tests which are needed are part of the verification process of the spacecraft thermal control system. The objective of qualification testing is the formal demonstration that the design implementations and manufacturing methods have resulted in hardware and software design which meet the requirements, with a sufficient margin, when subjected to the intended environment. In the case of thermal testing, this testing philosophy is implemented by three different types of tests: thermal cycling, thermal balance, and thermal vacuum. [46, p.351]

Chapter 6

Crew Safety and Health

6.1 Crew selection

Designing a manned mission brings along a challenging factor, namely the state of the crew during the mission. A thorough crew selection precedure is needed to make sure that the people who board the spacecraft for the 500-day period, have the required capability and skills. Different elements need to be considered in this selection, which are explained below.

6.1.1 General requirements

The crew will consist of two member, namely a man and a women. This is to represent both genders in this inspirational interplanetary mission. To speicify on an age range, a combination is made from the ideal astronaut age for the European Space Agency, ESA, and the requirements for long term interplanetary missions. ESA's [112] ideal range is 27 to 37 and for a due to radiation risks it is best to have an older crew since they are less likely to die from radiation compared to a younger crew [40]. Another requirement is that the crew is past its reproducability age, since effects of long term interplanetary space flights, mainly radiation, can be of high risk for any future pregnancies. Combining these requirements this mission aims for a crew within the age range of 35 and 45.

6.1.2 Possible crew options

In order to live in a relatively small environment for a period of nearly one anf a half year, it is important for the two crew members to socially connect. Therefore, the main suggestion for a crew composition is to select a married couple. Though a married couple is not a requirement, it is in fact a requirement that the crew members know eachother. Selecting two crew members that meet for the first time is definitely not adviced for phsyological reasons [111]. Another option that is interesting, also with regard to the scientific experiments 5.8, is to select at least one member which is one of identical twins. This will further be explained in experimental specifications 5.8.1.

6.1.3 Qualifications and Skills

To start with, a masters or preferably a doctorate level university degree is required for the crew. Scientific disciplines, outstanding skills in their own field and operational skills are of great importance. The fields include engineering, mathematics, medicine and natural sciences which include physics, chemistry, biology and Earth science.

A near-native English language skill is required to ensure the communication flow withing the crew and with the ground team during both training and the mission. The crew members must be able to clarify themselfs in this language, which is of great importance for cooperation within the team.

6.1.4 Health and Physical condition

The crew's health and their phsyical condition is also a major part of the selection, since becoming a crew member in this mission is a long-term commitment which demands a lot from the human body and mind. Below, the list of requirements is presented as proposed by ESA [112] for ISS crew members.

- An applicant should be able to pass a JAR-FCL 3, Class 2 medical examination (developed by the Joint Aviation Authority) or equivalent, conducted by an Aviation Medical Examiner certified by his/her national Aviation Medical Authority.
- The applicant must be free from any disease.

- The applicant must be free from any dependency on drugs, alcohol or tobacco.
- The applicant must have the normal range of motion and functionality in all joints.
- The applicant must have visual acuity in both eyes of 100 % (20/20) either uncorrected or corrected with lenses or contact lenses.
- The applicant must be free from any psychiatric disorders.
- The applicant must demonstrate cognitive, mental and personality capabilities to enable him/her to work efficiently in an intellectually and socially highly demanding environment

An important requirement which is specific for this mission, and perhaps differs from the ISS requirements, is the fact that the applicant must be comfortable in small spaces and not have any form of claustrophobic symptoms. This is of great importance since the space-free volume in te spacecraft is limited and, unlike the in the ISS, the crew cannot move from one area into the other. People with a great need of personal space or people who are preferably alone are unlikely to be comfortable in their limited space which they share with another crew member, and therefore are not the right applicants in this selection process.

6.1.5 General Characteristics and Personality

Not only phsycial and mental health is screened, but also the general character and personality of the applicants. The ability to work together in the crew and keeping a good atmosphere is highly required in order to make this mission as comfortable as possible for them. Requirements, proposed by ESA [112], aiming for this are listed below.

- Good reasoning capability
- The ability to work under stress
- Memory and concentration skills
- Attitude for spatial orientation
- Psychomotor coordination and manual dexterity
- High motivation
- Flexibility
- Gregariousness
- Empathy with colleague
- Low level of aggression
- Emotional stability

6.2 Crew activities

In this 500-day mission, the crew needs to be occupied sufficiently keep them motivated [111] and to avoid depression. One of the most important activities of the crew is the daily exercise sessions, to suport their muscles and bones. Next to that, not only medical conferences but also social web-conferences are provided for the crew. This includes conferencing with family and also school web-conferences to inspire the young generation and to emphasise the importance of the crew's contribution to the mission. This helps the crew to stay motivated and to maintain mental health [111]. In table 6.1 the flight plan timeline of a typical day for the crew is presented.

6.3 Post-landing procedures

After a 500-day journey, the two crew members require extensive care and medical support. After the crew has been helped out of their re-entry capsule, the first phase consists of taking care of managing heat stress, dehydration and motion sickness. This is done by the flight surgeon and the medical staff that monitored the crew throughout the mission [115]. They are taken to a medical facility where hours and days of de-briefing and recovery follow. The primary examinations must identify potential medical issues, after which more extensive tests follow. Regarding the scientific experiments, it is important that the crew is screened before the recovery phase initiates. This is to compare post-landing test results with pre-launch test results as accurate as possible.

Table 6.1: Typical Crew day schedule

Time	**Crew Member (CM)**	**Activity[1,2]**
06:00-06:20	CM1,2	Morning Inspection
06:20-06:25	CM1,2	Reaction Self Test
06:25-06:35	CM2	Reboot Laptop
06:35-06:50	CM1,2	Post-sleep
06:50-07:20	CM1,2	Breakfast
07:20-08:30	CM1	Work Prep
09:00-10:00	CM2	Physical Exercise (Human Dynamo, legs)
10:30-12:00	CM1, CM2 assisting	Scientific Experiment
12:00-12:30	CM1	Post Experiment Questionnaire
12:30-13:30	CM1,2	Lunch
13:30-13:40	CM2	Living Module inspection
14:00-15:00	CM1	Physical Exercise (Human Dynamo, arms)
15:15-15:30	CM2	Medical Conference
15:30-16:00	CM1,2	Snack
16:00-16:15	CM1	Family Conference
16:30-16:40	CM2	Urine Sample Collection
16:15-17:15	CM1	Physical Exercise (iRED)
16:45-17:45	CM2	Physical Exercise (iRED)
18:30-19:30	CM1,2	Dinner
20:00-21:00	CM1	Physical Exercise (Human Dynamo, legs)
20:00-21:00	CM2	Physical Exercise (Human Dynamo, arms)
21:00-21:30	CM1,2	Pre-sleep
21:30-06:00	CM1,2	Sleep

[1] Based on ISS timelines [114]
[2] Note that the activities are not identical on a daily basis, but represent a typical day

Chapter 7

Market and Cost Analysis

Having a good cost and market analysis for the Inspiration Mars mission is crucial to have a feasible mission. A low cost is one of the driving requirements of the whole mission. However, human interplanetary travel has never been done before which means there is no historical cost data available to compare with or base an estimation on. Nonetheless, a first-estimate for the cost is made with available cost estimation methods and data. First, in this chapter, section 7.1 describes a market analysis which includes a prediction for future markets, the establishing of new markets, all the stakeholders and a plan to fund the mission. In section 7.2, a cost estimation, using two different estimating methods, is given.

7.1 Market Analysis

As the current market for missions to Mars is almost non-existent, this will definitely change in future if humanity wants to become a multi-planetary species and prevent the human race from being extinct. Up to now, the only parties who have launched manned space missions are governments and governmental organizations. But times are changing and this century marks the beginning of the new chapter in the space market - the privatization of space. A mission to Mars is one of the next steps in the private trend and is currently under evaluation, not only the Inspiration Mars foundation, but by SpaceX and NASA as well. This section on market analysis addresses a market SWOT analysis, the possible funding, Mars initiatives, followers and a prediction of future markets.

7.1.1 SWOT Analysis

Strengths

The current market for manned interplanetary mission as enormous growth potential and is definitely the future to look forward to. Also, there are not many competitors on the market currently which leaves space for other companies to enter as well.

Weaknesses

The market has growth potential but the downside is that it has only just been developed. This means a lot of investments need to be made to be able to provide the services and products required for interplanetary missions. Also there is a lot of risk involved as failure will probably mean a bankruptcy of the company and/or lose most of its credibility.

Opportunities

There are a lot of opportunities to prove a company's worth to the customer. A lot of private services can be provided that are not possible yet. For example, orbit the Earth for a day, flying around the moon, visit Mars, etc.

Threats

The main threat to the market, to this day, is the difficulty, cost and risk to guarantee a safe mission for humans. The death of a customer due to flawed service or product is devastating to a company's image. Due to the (currently) high risk involved in interplanetary flight, this would be the main threat.

7.1.2 Future Market

The focus of this section is to give a prediction of the markets, from which Inspiration Mars can profit in the future. There are two major groups who would be interested in the Inspiration Mars mission. The first group includes the companies, which are already exploring possibilities to establish a human settlement on Mars. The second group is the one who might be interested in Inspiration Mars if the mission achieves success.

Mars initiatives

- **Mars One** is a non-profit foundation that develops a strategic plan for taking a crew to the surface of Mars in 2022, four years after the Inspiration Mars launch. Since Mars One is already on the path to move humanity closer to stepping on Mars, our findings, specifically about the human factors, could assist them in their endeavor. [116].
- **Asian** countries like India and China have been in a space-race to be the first in Asia with a successful mission to Mars. India recently launched (5 Nov 2013 [118]) its first unmanned Mars mission and will hopefully be looking for enhancing its international cooperation with other companies in order to stay ahead of China. The Chinese, however, prove to be dedicated on space leadership with their fast-growing and ambitious plans like Chinese space station [120]. That can be a great opportunity for Inspiration Mars for selling them the gained manned-interplanetary expertise.
- **NASA** has a target, promised by the president of the United States of America, of sending a manned spacecraft to Mars in the mid 30's [119]. As the technology is already available, pushing this date to 2018 could save the government a lot of time and money. This extra budget available could be used later for developing future missions or other causes.

Mars followers

- **Space tourism**. Travel and tourism is one of the world's largest businesses. According to the first professional space tourism market studies, which was conducted in several countries in the past few years, tens of millions of the people on earth would like to take a trip to space if and only if the trip would be more safe, comfortable, reliable, and at a payable stage for common people [117].
- **Spin-offs.** In the case of mission success, more people will face the fact that in many aspects the research and discovery from space programs lead to spin-offs, which are contributing to the solution of our earthly problems. The long-duration human support system and study of how people behave in confined spaces may turn to be helpful for issues we face on earth. Inspiration Mars' services can be sold to various parties.
- **Space-race.** Sending people to Mars surface is an ambitious plan. But if Inspiration Mars succeeds, interplanetary manned space flight will be a reality. Consequently, the result will be increased support for space financing which will re-inspire space agencies' boldness for human space exploration and eventually lead to a new space race. Our mission can capitalize on that by selling the unique technical and human factors data from Inspiration Mars' mission.

7.1.3 Mission Funding Plan

Next to the technical challenge, another aspect of the mars fly-by mission is gathering the needed funds. What makes this project different than other ambitious proposals is that it is funded for the first two years, until end of 2014, by Dennis Tito himself [123]. Certainly, most funds will be required after that, during the development and launching mission phases. Therefore, the Market Analysis looks into potential sources such as sponsors, supporters and advertisement.

Government Sponsorship

Governmental organizations such as NASA, ESA, Roscosmos and upcoming space agencies such as the Chinese and Indian can be approached for specific funding. For example, they can cover the launch with their existing technology and thus boost their country prestige for space exploration. Although, NASA released an official statement that 'the agency is willing to share technical and programmatic expertise with Inspiration Mars, but is unable to commit to sharing expenses with them.' [121], it is still possible that they will reconsider if the public shows interest.

Industry Sponsorship

Companies who like to be related with the daring and bold mission could be the main sponsors. Companies like GoPro and Redbull have often been related to risk and discovering boundaries of the human capabilities [122]. On the other hand, companies like SpaceX and Virgin Galactic benefit from the further creation of a private space market and space tourism.

Individual Sponsorship

Individual sponsors like millionaires Dennis Tito or Elon Musk (founder SpaceX) could also take their role in funding parts of the mission. Dennis Tito has already guaranteed to fund the initial two-years of the mission. Moreover, he goes a step further and promises to run a fund-raising campaign [123].

Selling Scientific Experiment Data

The valuable data acquired by the scientific experiments can be sold to private companies or governments who can use them for future designs or experiments.

Crowdfunding

Crowdfunding has been gaining an ever-increasing popularity in the last years and many projects have turned from an idea into a reality thanks to the small contributions of many parties. The currently most famous platform, *Kickstarter* has proven that people are willing to support projects which matter with initiatives gathering up to $10m. [124].

Other

Opportunities such like a contract with entertainment providers for live mission broadcast, selling the media rights, deals to license the Inspiration Mars name or logo (for toys, memorabilia, logo on spacecraft), celebrity events with mission participants, etc.

7.1.4 Return on Investment

Investors usually allocate capital with an expectation of a financial return on their investment. A purely philanthropic mission, which aims to inspire future scientists and engineers, promises little if any profit. However, the gain in expertise, status and prestige; will make the investors the first-to-go-to for future manned missions. These investors, that should be approached, will probably already have investments or interests in the space industry.

Knowledge and Experience gained

The scientific results, experience and knowledge gained will be significant for future manned mission. This knowledge can be sold to other companies and/or organizations.

Prestige and Honor

If this mission is funded by a select few, there is a certain prestige for the people who made the first step to manned space exploration. Also winning from China and Russia in the Space Race would be success for whole humanity, with America as a leader.

Inspiration

Our children are the foundation of the future. If it is desired to let youth to be inspired and pursue a career in the scientific field, this mission could provide the spark needed for achieving this.

7.2 Mission Cost Analysis

Costs of different parts and stages of the design of a space system are hard to be estimated with precision. However, as some aspects of the mission use off-the-shelve components, pricing is readily available for some of the components. To determine the total costs, several cost estimation methods are available. A selection was made based on availability and applicability to the I.M. Mission, and the Advanced Mission Cost Model (AMCM) is used which is further explained below. A second estimation method, TRANSCOST, is used afterwards. Finally, a comparison is made, including the actual costs of other missions.

7.2.1 Advanced Mission Cost Model (AMCM)

he Johnson Space Center developed the Advanced Mission Cost Model (AMCM) [25, p. 946] as an alternative to models solely based on mass. This model gives a way to asses rather quickly variations in the mission from the top down. It uses a database of more than 260 programs, including top-level cost, system mass, program schedule dates, developing organizations, and technical data. The model relates six different variables to the total system cost in millions $ of fiscal year 1999 (FY1999$) using equation 7.1. The constants are given in table 7.3.

$$SystemCost = \alpha Q^{\beta} M^{\Xi} \delta^{S} \epsilon^{1/(IOC-1900)} B^{\phi} \gamma^{D} \tag{7.1}$$

These six different variables in this equation are:

1. Quantity (Q): This variable includes the amount of identical spacecrafts that will be made. For the Inspiration Mars mission only one spacecraft will be made.
2. Dry Mass (M): This variable is the dry mass of the spacecraft which was determined to be 9826.54 kg.
3. Specification (S): This value represents the mission that will be flown. For a human re-entry mission the value is 2.39 [25].
4. Initial Operational Capability (IOC): This variable is the first year that the systems needs to be operative. Because the Inspiration Mars mission intends to launch in 2018, the IOC will be 2018.
5. Block (B): This variable represents the level modification that is needed for each conceptual design. An entire new design will have a block value of 1 whereas frequently used modules which only need little modifications will have a value of 5. As the I.M. mission requires some modifications to existing subsystems, a value of 3 is assumed.
6. Difficulty (D): This variable represents a relative technical difficulty to the mission. This difficulty value is in the range of -2.5 (extremely easy) to 2.5 (extremely difficult). The IM mission is assumed to be 0 as most of the systems are already available and only need to be modified.

Table 7.1: Cost Estimation constants

Constants	Value
α	5.65 $*10^{-4}$
β	0.5941
Ξ	0.6604
δ	80.599
ϵ	3.8085$*10^{-55}$
ϕ	-0.3553
γ	1.5691

Table 7.2: Cost Estimation Variables

Variable	Value
Quantity	1
Dry Mass [kg]	9826.54
Specification	2.39
IOC	2018
Block	3
Difficulty	0

Cost-Adjustment Wrap Factors

Wrap factors account for additional costs at the program level, usually calculated as a percentage of the cost in phase C/D to design, develop, test, evaluate, and produce the hardware for the mission. The wrap factors categories are the most common in estimating costs for human programs which means they are applicable to the IM mission. The wrap factors are included for the advanced development, Phase A, Phase B, program support, operations capability development, launch and landing, program management and integration and at last the contractor's fee. The total cost wrapping factor is the sum of the wrap factor for each of the categories described above. From using the generic values for human missions [25, p. 948], the total wrap-factor is determined at 56.5 %.

Reserve Factor (RF)

The reserve factor takes into account unplanned adverse events and the cost of management. A reserve estimation is useful in case a contractor overruns, a system test was not successful, or a technology development does not meet the required delivery date. The reserve of the I.M. mission is based on the NASA Headquarters Reserve Model [25], where a risk factor can be applied on a scale from 0 to 16 (no risk to very high). The inputs for the I.M. mission are the given Risk Factors in the table.

Table 7.3: NASA Headquarters Reserve Model: Risk Factor × Weight = Product [25, p. 950]

Risk Factor Item	Risk Factor	Weight	Product
Investment in planning definition:%	8	0.3	2.4
Uniqueness of design	8	0.2	1.6
Complexity of hardware and software	14	0.1	1.4
Difficulties in systems engineering or integration and testing	10	0.2	2.0
Complications in structural organization	8	0.1	0.8
Requirements for concurrent development	12	0.05	0.6
Experience base	7	0.05	0.35
Total Risk Score			**9.15**

From the guide to Reserve Factors [25, p. 950], a score of 9.15 corresponds to a Reserve Factor of 45% which is used in the total cost estimation.

Cost-Schedule Relationship Using the Beta Curve

The cost models estimates the total cost only through Phase C/D completion in constant dollars. However, the budget perspective requires us to spread the estimate over the life of the program, applying inflation factors to get the real-year costs. To determine the spread, a beta curve is used which relates incurred cost to the time elapsed. The beta curve is a fifth-order polynomial in F, where F is the time fraction. The Cumulative Cost Fraction (CCF) can be formulated as such:

$$CCF = A(10F^2 - 20F^3 + 10F^4) + B(10F^3 - 20F^4 + 10F^5) + 5F^4 - 4F^5 \tag{7.2}$$

Based on data from previous projects [25, p. 946], crewed programs use a 60% profile with A=0.32 and B=0.68 which will be used for the I.M. mission.

Total Mission Cost (1999 $)

Using the AMCM, an estimation for the total system, wrapping and reserve costs is determined. These results are given for the FY1999 in $ in table 7.4. Using the cost-schedule relationship, a cost spread was chosen for the years 2013 to 2020 to cover the whole mission design and follow-up. The results of this cost spread are given in table 7.5.

Table 7.4: Total Mission Cost (FY1999$)

Item	Cost (Million $)
System Cost	2060.90
Wrapping Cost (56.5 %)	1164.41
Reserve Cost (45 %)	927.40
Total Cost	**4152.71**

Table 7.5: Total Mission Cost Spread (FY1999$)

Year	Time Fraction	Cumulative Cost Fraction	Annual Cost (M$)	Cumulative Cost (M$)
2013	0.125	0.0495	205.56	205.56
2014	0.250	0.188	575.15	780.71
2015	0.375	0.385	818.08	1598.79
2016	0.500	0.600	892.84	2491.63
2017	0.625	0.791	793.16	3284.79
2018	0.750	0.925	556.7	3841.26
2019	0.875	0.989	265.77	4107.03
2020	1.000	1.000	45.68	4152.71

Total Mission Cost (2013 EUR)

The total and mission spread cost determined in section 7.2.1 are applicable for FY1999. However, these are not correct for the year 2013 as it does not yet take inflation into account. To be able to determine an actual cost, an inflation index is applied in order make the cost estimation realistic for the years 2013-2020. Comparing the fiscal year in 1999 to 2013 (FY2013), there was an inflation of 39.8 % [125]. Applying this to the total cost estimation for the FY1999$, together with a dollar to Euro conversion (30 January 2013, 1$ =0.737 EUR), the total actual cost spread becomes:

Table 7.6: Total Mission Cost Spread (FY1999 $, FY2013 $ and FY2013 EUR)

Year	FY1999(M$)	FY2013(M$)	FY2013(M EUR)
2013	205.56	287.37	211.79
2014	575.15	804.06	592.59
2015	818.08	1143.68	842.89
2016	892.84	1248.19	919.92
2017	793.16	1108.84	817.22
2018	556.7	778.27	573.59
2019	265.77	371.55	273.83
2020	45.68	63.86	47.06
Total	**4125.71**	**5767.74**	**4250.83**

7.2.2 Combined Method Cost Estimation

The total cost estimation is made of a combination of the TRANSCOST model [36], Cost Estimation Relationships (CERs) from Space Mission Analysis and Design (SMAD) [8] and readily available known costs for e.g. the launch. First, the (most used) TRANSCOST method is explained and a definition of the Man-Year (MYr) value is given. Secondly, a brief description is given of the CERs used from SMAD. Lastly, an overview is given of the total cost estimation for each mission segment and in table 7.7.

7.2.2.1 TRANSCOST Cost Estimation Method

The TRANSCOST cost estimation method is a statistical and analytical model for cost estimation of launch and space transportation vehicles. The model is based on a comprehensive database gathered over a period of more than 40 years (1960-2000) from US, European and Japanese space vehicles and engine projects. It includes actual cost including unforeseen technical problems and delays. The method primarily serves as a tool for the conceptual design of modern cost-optimized expandable and/or reusable space transportation systems.

The procedure of the cost estimation is done in four steps. The first step uses a basic CER. The second step estimates the element's development cost (vehicles, engines and boosters). The third step is to estimate the complete vehicle development cost. Finally, the fourth and last step, estimates the total development program costs. An example of a basic CER that is used to determine an estimation for the mission segments is given in the following equation:

$$C = a\ M^x\ f_1\ f_2\ f_3 \tag{7.3}$$

With:

- a = System-specific Constant Value
- M = Mass [kg]
- f_1 = Technical Development Status Factor
- f_2 = Technical Quality Factor
- f_3 = Team Experience Factor

Man-Year (MYr) Cost Definition

The TRANSCOST model applies Man-Year as a costing value. It takes into account all the different inflation rates, currencies, countries and conversion rates to dollar and Euro at different years. All the CERs of the TRANSCOST cost estimating method express the costs in terms of MYr. In order to convert these into current Euro currency, these MYr units need to be converted. From the relationships going from 1960 to 2000, a value of 1 My in 2013 is extrapolated to be equal to 24786.56 EUR. This value is used to determine the final estimation costs originating from the TRANSCOST model.

7.2.2.2 SMAD Cost Estimation Relationships

The CERs used from SMAD [8] are derived from historical data, including satellites, statistical frameworks, and error models. These CERs include the research, development, testing and evaluation for each subsystem. These CERs are based on the same principle as the TRANSCOST method but give the cost estimation in dollars for the FY2000$.

7.2.2.3 Cost Estimation Overview

In table 7.7, a cost overview is given of each mission segment. Together with each estimation, a reference and page number is given to show which method is used to estimate the mission segment costs and more specific, the estimated costs of the living module's subsystems. Afterwards, in figure 7.1, a pie chart is given of the percentage of each mission segment of the total estimated cost.

Table 7.7: Cost Estimation of Mission Concept FY2013 EUR

Mission Segment	Cost [Million EUR]	Reference
Refueling Module	**417.28**	[36, p. 38]
Living and Support Module	**765.71**	
ECLSS	99.07	[127, 128]
Structure and Materials	70.65	[8, p. 795]
Scientific Payload	0.00	[8, p. 795]
GNC	57.23	[8, p. 795]
Telecommunications	8.00	[8, p. 795]
Power	245.77	[8, p. 795]
Command and Data Handling	9.77	[8, p. 795]
Propulsion	3.71	
Thermal Control	25.74	[8, p. 795]
Re-entry Capsule	**862.00**	[36, p. 62]
Launch (Including Propellant + Service + Fees)	**270.00**	
Launch 1: Falcon Heavy (Refueling Module)	135.00	[22]
Launch 2: Falcon Heavy (Living, Service and Re-entry Module)	135.00	[22]
Mission Operations and Logistics	**44.85**	
Assembly, Integration and Transport	40.32	[36, p. 124]
Communication - Deep Space Network	0.505	[126]
Recovery	4.02	[36, p. 141]
Fees and Insurance	**241.98**	
Launch Site User Fee	6.00	[36, p. 142]
Public Damage Insurance (0.1 % of Total Cost)	235.98	[36, p. 142]
Total Estimated Cost	**2601.82**	
Total Estimated Cost + 45 % Reserve Factor	**3772.64**	

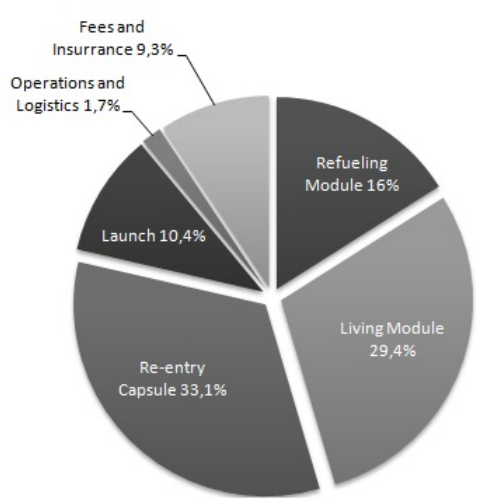

Figure 7.1: Pie Chart Cost Estimation Mission Segments in Percentages

7.2.3 Reference Mars mission cost estimates

To compare the Inspiation Mars mission cost estimates with reference missions, first of all a number of Mars missions, are identified. The selected missions are the Mars Curiosity Landing, Mars Direct and a simplified scenario for manned Mars missions. These missions are elaborated on briefly and compared to the Inspiration Mars mission.

7.2.3.1 Mars Curiosity Landing

This is a mission to Mars is a one-way journey and thus does not contain a return trajectory to Earth. Furthermore, it is an unmanned mission and thus no ECLSS is required on board and therefore it is not an element within the cost estimates. The mission relies on new technological innovations, especially for the landing, and this adds to the overall cost, unlike Inspiration Mars which uses off-the-shelf components. This mission had a total cost of 2.5 billion $ [129].

7.2.3.2 Mars Direct

The Mars Direct mission is a sustained humans-to-Mars plan which aims to use existing launch technology to generate rocket fuel using the Martian atmosphere and extract water from the planet's soil. It is comparable to Inspiration Mars, since both missions aim for a manned spaceflight to Mars and return back to Earth after a period of time. Another comparison between the two missions is the fact that off-the-shelf components are used, which keeps the cost limited compared to missions which use innovative technology. The estimated costs are significantly higher though, since Mars Direct involves a Mars landing which adds to the cost and the activities on Mars which also result in a relatively higher cost. This mission had cost of 30 billion $ [130].

7.2.3.3 Simplified Scenario for Manned Mars Missions

This Mars mission scenario aims to deliver a simplified and efficient proposal for a manned mission to the red planet. To assure security, the scenario accounts for two space vehicles. Another important characteristic of the mission is that is uses in situ resource utilization systems. Comparing this to the Inspiration Mars mission, it is similar since both contain a crew of two and aim for a simple and cost efficient approach. A significant difference is the fact that this scenario includes a Mars landing, in contrary to Inspiration Mars. The total cost of this mission is estimated at around 40 billion $ [131].

7.2.4 Cost Estimation Comparison

The combined method cost estimations uses a combination of the top-down TRANSCOST and bottom-up SERs approach. TRANSCOST was used to determine the costs of the re-entry vehicle and the refueling tank. These two components have their own sub-systems therefore an additional costs estimate needs to be made. A detailed bottom-up method was used to determine the costs of the spacebus. Each sub-system is calculated separately and the sum of all subsystems with additional margins are used to determine the cost of the spacecraft.

Comparing the AMCM approach with the combined method cost estimations it can be seen that there is a correlation of 89%. However the combined method cost estimations resulted in a value which is lower than the AMCM approach. The main reason is due to the fact that a combined method cost estimations is more precise. It is more precise because the cost of each sub-system is determined and summed with each other. This decreases the high margins used during the AMCM approach. Throughout the design process that cost of the complete mission will become more accurate. It could decreases due to removing unnecessary margins or increase if an unforeseen element of the mission needs to be taken into consideration.

Compared to the other mission this estimation should be realistic. The Curiosity mission is unmanned, so the cost estimation is lower. Compared to the other manned missions the estimated cost is low but the Inspiration Mars mission performs only a fly-by and does not land on Mars like the reference manned missions.

Chapter 8

Risk Analysis

In this chapter the risks of the different systems are analyzed. When the risks are identified, design choices are applied to decrease the impact and/or probability of these risks. The probability of every risk is assesed using the following terms: Unlikely, Possible, Even Chance, Likely and Certain. The impact of risks is assesed using the following terms: Very Light, Light, Moderate, Severe and Catastrophic. First, the risks of the Trajectory are assesed in section 8.1, then the risks of the re-entry procedure are analysed in section 8.2. Finally, the risks of the spacecraft sub-systems are analyzed in section 8.3 and at the end of the chapter a graphical display of the risks is found in section 8.4.

8.1 Trajectory Risks

To reduce most risks associated with the trajectory, some mitigation measures are incorporated. First of all, the spacecraft's trajectory is mainly determined by the launch date. The launch date determines the launch velocity required to reach Mars, within the constraints of current available technology and human capabilities. Another aspect that needs to be taken into consideration is the fact that there is a limit on the amount of time a human can be in deep space, due to the effects of radiation on the human body. Secondly, there is a limit on the amount of extra energy that current launchers can provide. Lastly, the maximum re-entry velocity for a re-entry vehicle can not be increased due to current Thermal Protection System (TPS) limitations and maximum g-loads which the human body can take. In case the required launch date is not met, and thus the launch date is postponed, the re-entry velocity will be higher than 14.2 km/s which is above the upper limit for re-entry. This means the mission cannot be launched in 2018 anymore. For a next same trajectory, one has to wait 15 years due to the synodic periods of Earth and Mars. A way to reduce this risk is accurate and realistic planning. The second risk is fuel shortage for Correction Maneuvers (CM), which is possible if more fuel is used than allowed on the way to Mars or in case of a leakage. Small changes in velocity can create huge changes in distance over a long period of time. A way to reduce this risk would be using an extra margin on fuel for correction maneuvers. Third, an engine failure during the Trans Mars Injection (TMI) is unlikely to happen. If the spacecraft reaches the escape velocity of Earth, it will enter a heliocentric orbit, unlikelt to return to Earth if it does not reach the velocity required for a Mars gravity assist. An effort is then required to restart the engines or use the fuel for a correction maneuver to decelerate and enter back in an Earth's orbit. If the engine failure occurs before it reaches the escape velocity, the vehicle can safely re-enter the Earth's atmosphere. Fourth and fifth risk, deviation of the TMI and having a different fly-by altitude, are both be reduced by applying correction maneuvers. The last risk too, is avoided by applying a correction maneuver.

Table 8.1: Trajectory Risks

		Risk before mitigation		Risk after mitigation	
Code	**Risk**	**Probability**	**Impact**	**Probability**	**Impact**
T1	Schedule Slip	Likely	Severe	Possible	Severe
T2	Fuel shortage for CM	Possible	Severe	Possible	Severe
T3	Engine failure during TMI	Unlikely	Severe	Unlikely	Moderate
T4	Deviation in TMI	Likely	Moderate	Possible	Light
T5	Fly-by at different altitude	Possible	Moderate	Possible	Light
T6	In-space collision	Unlikely	Catastrophic	Unlikely	Catastrophic

8.2 Re-entry Risks

The risks associated with the re-entry phase are given in table 8.2. A very critical point during this mission phase is the flight path angle when the maneuver starts. This will have a great impact on the rest of the phase. When the angle is too shallow, the spacecraft will skip off the upper layer of the atmosphere and fly off into space. When the angle is too steep, the deceleration might be too great and the g-forces and heat flux are too large. This risk can be mitigated by adding ΔV-budget to perform a correctional maneuver. When the deviation is detected in an early stage, it is possible to adjust the course of the spacecraft with a relatively small ΔV.

Table 8.2: Re-entry Risks

		Risk before mitigation		**Risk after mitigation**	
Code	**Risk**	**Probability**	**Impact**	**Probability**	**Impact**
R1	Initial flight path angle is too shallow	Likely	Catastrophic	Even chance	Light
R2	Initial flight path angle is too steep	Likely	Catastrophic	Even chance	Light
R3	The automatic pilot fails	Unlikely	Severe	Unlikely	Moderate
R4	A parachute does not deploy	Even chance	Catastrophic	Even chance	Moderate

There is also a chance that the automatic pilot fails. In that case there must be a possibility to control the module manually. One crew member must be trained to perform the re-entry maneuver by hand. If the system is designed in such a way that it needs all its parachutes to land safely, then the consequences of one parachute failing is dramatic. Therefore one parachute is added to account for the possible failure of one of the parachutes.

8.3 Spacecraft Subsystem Risks

In this section the risks of the different subsystems of the spacecraft are assesed. Each subsystem presents its individual risks and mitigations, which all together result in the overall risk analysis of the spacebus.

8.3.1 ECLSS

To ensure that the Environmental Control and Life Suport System (ECLSS) can provide for the crew at all times, a margin of 10% is added for this system. This allows the mission duration to increase by 10% in case of a change in trajectory. Another aspect to account for is to bring along spare parts for repairing food, waste, water and thermal systems in case these are damaged. Furthermore, an extra Extravehicular Activity (EVA) suit is needed in case one suit is severely damaged. This is needed to ensure that the crew can perform the EVAs safely, without the risk of injury and/or death due to damaged EVA suits.

Table 8.3: ECLSS Risk Table

		Risk before mitigation		**Risk after mitigation**	
Code	**Risk**	**Probability**	**Impact**	**Probability**	**Impact**
E1	Air system fails	Possible	Severe	Possible	Moderate
E2	Food system fails	Possible	Severe	Possible	Moderate
E3	Lack of food	Unlikely	Catastrophic	Unlikely	Catastrophic
E4	Waste system fails	Possible	Moderate	Possible	Light
E5	Water system fails	Possible	Catastrophic	Possible	Severe
E6	Thermal system fails	Possible	Catastrophic	Possible	Severe
E7	Fire in the living module	Even chance	Severe	Even chance	Severe
E8	An EVA suit is severely damaged	Possible	Catastrophic	Possible	Moderate

8.3.2 Crew Safety

It is of great importance that the crew is reminded of their contribution to the mission. Phychologically, having a goal in a mission is satisfying [111] and in case the crew feels their contribution is redundant there is an even chance that mental illness occurs. For this reason, an activity like educational web-conferencing with schools are implemented in the crew schedule to emphasise their contribution in this mission. An even more complicated situation is in case of a deceased crew member. If one crew member dies, the impact is severe, but the manned fly-by mission is still a fact. If both crew members die though, the manned end-to-end fly-by mission fails and the mission conclusion is that the mission started out manned and ended unmanned.

Table 8.4: Crew Safety Risk Table

		Risk before mitigation		Risk after mitigation	
Code	**Risk**	**Probability**	**Impact**	**Probability**	**Impact**
CR1	A crew member gets sick	Even chance	Moderate	Even chance	Moderate
CR2	One crew member deceases	Possible	Severe	Possible	Severe
CR3	Two crew members decease	Unlikely	Catastrophic	Unlikely	Catastrophic
CR4	Metal illness of crew	Even chance	Severe	Possible	Severe

8.3.3 Thermal Control

The thermal control system makes use of mechanically pumped loops, since these are arguably unchallenged for high heat loads (above 10 kW) [46, p.238]. However, the drawback is the involvement of moving parts, which are likely to fail. If the pump fails, then the temperature in the spacecraft might become too high and the crew and equipment might suffer. Therefore, the impact is catastrophic. Moreover, the fluid loop is possible to leak. The loop liquid is water, which is not toxic for the crew. However, leakage can cause a malfunction in the Thermal Control System (TCS), or interfere with electronic equipment. Another risk is recognized in the spacecraft, experiencing higher than expected external temperatures due to one of the following scenarios. Firstly, a closer than expected pass by the Sun can increase the heat load. Second, a higher then expected material degradation of the fun-facing surface, leading to higher solar absorbance. Third, more area exposed to the Sun due to an attitude control malfunction. In these cases more heat will be generated inside the spacecraft, which can make it uncomfortable and even fatal for the crew. Thus, the impact is catastrophic. Furthermore, to reduce the severity of a thermal pump failure, an additional pump is added to the spacecraft. The leakage risk is decreased by including additional insulation layer to the plumbing. Providing the crew with tools to repair the leak also decreases the risk impact. For the higher thermal loads, a contingency measure is included in the design.

Table 8.5: Thermal Control Risk

		Risk before mitigation		Risk after mitigation	
Code	**Risk**	**Probability**	**Impact**	**Probability**	**Impact**
TC1	Mechanical pump failure	Likely	Catastrophic	Possible	Moderate
TC2	Fluid loop leakage	Possible	Severe	Unlikely	Light
TC3	Higher heat loads	Even chance	Catastrophic	Possible	Moderate

The contingency shall be considered for a worst case scenario, which is unlikely to happen. In other words, if the spacecraft gets closer to the Sun with 10% , the solar absortivity increases with 10% and the exposed area increases by 20%. The contingency margin is chosen highly, and all these three scenarios are considered for the thermal analysis as if they happen simultaneously. Then by using the thermal equilibrium equations from section 5.10, the required radiator area is increased from 18 m^2 to 20 m^2. The increased radiator area is accommodated on the spacecraft and it will also not make the internal environment too cold, because the thermal control is actively controlled and will self-regulate.

8.3.4 Structures

The structure is the main skeleton that supports every sub-system of the spacecraft and allows for an habitable module. It is then a critical part of the spacecraft, which cannot fail. Its design is driven by requirements related to reliability and risk, thus for a well designed structure all risks with an important impact are minimized. Furthermore, safety factors are taken for all loads that the structure is designed for and extra margins of safety are also used.

Table 8.6: Structures Risk

		Risk before mitigation		Risk after mitigation	
Code	**Risk**	**Probability**	**Impact**	**Probability**	**Impact**
S1	Increase in launch loads	Possible	Light	Possible	Light
S2	Material degradation	Even chance	Moderate	Possible	Moderate
S3	Crack on main structure	Possible	Moderate	Possible	Light
S4	Impact of MMOD in critical regime	Possible	Severe	Unlikely	Severe
S5	MMOD impact damage not detected	Possible	Moderate	Unlikely	Moderate
S6	Incorrect orientation spacecraft SPE	Possible	Severe	Possible	Severe
S7	Not enough water to shield for SPE	Unlikely	Severe	Unllikely	Severe
S8	SPE during EVA	Unlikely	Catastrophic	Unlikely	Catastrophic

The Micrometeorite and Orbital Debris (MMOD) protection is designed to shield against particles that cannot be detected and avoided through a maneuver of the spacecraft. There is a critical regime of particles that are too small to be detected and heavier than the protection can shield. The design is optimized so that the chance that one of these particles will impact the spacecraft is under 1%. Furthermore, a damage detection layer is installed in front of the rear wall to detect any damage that needs to be repaired.

For radiation protection, the main concern is for Solar Particle Events (SPE) to occur. The likelihood of a SPE during the mission is very low, and the chance that the guidance, navigation and control is not working or that a water leakage occurs at that same time is even lower. Furthermore, the chance that more than one deep space Extravehicular Activities (EVA) is required in the trajectory is very low.

8.3.5 Propulsion

The Falcon launchers are designed to launch astronauts into space. Therefore, they are designed with robust design margins, 1.4 instead of 1.25 for unmanned spaceflight [71]. Additional mitigation measures are therefore not taken into account. To mitigate the consequence of a thruster failure, extra thrusters are added for contingency. In this case, if one or several thrusters fail, the other thrusters are still able to cover all directions.

Table 8.7: Propulsion Risk Table

		Risk before mitigation		Risk after mitigation	
Code	**Risk**	**Probability**	**Impact**	**Probability**	**Impact**
PR1	Fuel launch fails (engine failure)	Possible	Moderate	Possible	Moderate
PR2	Fuel launch fails (disintegration)	Unlikely	Moderate	Unlikely	Moderate
PR3	Crew launch fails (engine failure)	Possible	Moderate	Possible	Moderate
PR4	Crew launch fails (disintegration)	Unlikely	Catastrophic	Unlikely	Catastrophic
PR5	Launch to TMI fails	Possible	Severe	Possible	Severe
PR6	Thruster failure	Possissible	Severe	Possible	Light
PR7	Thruster degradation (lower I_{sp})	Likely	Moderate	Likely	Moderate

8.3.6 Guidance, Navigation and Control

To reduce the risk of a software problem, extensive testing is performed. This testing reduces the likelihood of a wrong position, velocity and attitude determination. Testing would also reduce the likelihood of the software to calculate a wrong correction maneuver. The risk of failure of hardware components of GNC system, the actuators and sensors, is reduced by implementing back-up components of each actuator and sensor. This reduces the impact of failure of a single actuator or sensor because the backup component is activated.

Table 8.8: GNC Risk

		Risk before mitigation		**Risk after mitigation**	
Code	**Risk**	**Probability**	**Impact**	**Probability**	**Impact**
G1	Incorrect trajectory software	Unlikely	Catastrophic	Unlikely	Catastrophic
G2	Incorrect position/velocity/attitude determination	Even chance	Moderate	Possible	Moderate
G3	Incorrect correction maneuver	Likely	Moderate	Even chance	Moderate
G4	Actuator failure	Even chance	Severe	Even chance	Light
G5	Sensor failure	Even chance	Severe	Even chance	Light

8.3.7 Refueling

To reduce the majority of risks associated with refueling, a number of mitigation measures are incorporated. First of all, more testing is needed to increase the technology readiness levels (TRL)of all components. This way, more data is specified about the fluid transfer and this decreases the risk of transferring insufficient fuel. The rendezvous and docking procedures are quite common and already tested and performed in space, so this is assumed to be reliable and further risk reduction is not required. The possibility of failure of the docking connection however can be reduced. The docking is done by the coupling system described in section 5.5. In case the docking fails, a second coupling system is attached to the liquid oxygen (LOX) tanks, as well as a second hose to the RP-1 tank. This way, the possibility of a connection failure is reduced.

Table 8.9: Refueling Risk

		Risk before mitigation		**Risk after mitigation**	
Code	**Risk**	**Probability**	**Impact**	**Probability**	**Impact**
F1	Rendezvous failure	Unlikely	Severe	Unlikely	Severe
F2	Docking crash	Possible	Catastrophic	Possible	Catastrophic
F3	Docking connection failure	Even chance	Severe	Possible	Severe
F4	Maximum fill not reached	Even chance	Severe	Possible	Severe
F5	Leakage during refueling	Possible	Severe	Possible	Moderate
F6	LOX boil-off	Likely	Catastrophic	Unlikely	Moderate
F7	Duration LEO longer than 3 days	Likely	Catastrophic	Likely	Light

Another measure that is taken, is increasing the sizes of the fuel depots and bringing extra fuel. The consequence of leakage and boil-off is reduced by this measure. The last risk can be reduced using an active storage system instead of a passive storage. Therefore, a zero boil-off cryocooler is added to the fuel depot. This way, the consequences are significantly lower in case the duration in parking orbit turns out to be longer than three days.

8.3.8 Command and Data handling

The risks for the Command and Data handling are shown in table 8.10. In case of hardware failure, the C&DH sub-system is not able to monitor the housekeeping data of all sub-systems. The C&DH sub-system will also not be able to send commands to all sub-systems. These consequences would be cathastrophic because the subsystems would not be able to communicate amongst each other. Due to this, the reliability of the C&DH sub-system must be high, therefore a complete redundant C&DH sub-system is added as back-up. In case of data error occuring, incorrect signals are processed. This results in undesireable situations which can lead to cathastrophic results. Therefore the C&DH system is created as watchdog and the bit-error rate is designed to be as low as possible.

Table 8.10: Command and Data Handling Risk

		Risk before mitigation		**Risk after mitigation**	
Code	**Risk**	**Probability**	**Impact**	**Probability**	**Impact**
C1	Hardware failure	Even chance	Cathastrophic	Possible	Light
C2	Data error	Even chance	Cathastrophic	Unlikely	Light

8.3.9 Tracking, Telemetry and Control

The risks of Tracking, Telemetry and Control are shown in table 8.11. In case of antenna failure or damage, the communication link between the ground station and the spacecraft will result in malfunction. This impact is critical, because it requires the spacecraft to work as a complete autonomous system, without any help for scheduling of procedures and data links. To decrease the probability and the impact, an extra identical antennna is placed on the spacecraft. In case of failure or damage, the redundant antenna is used. If the transponder fails, the data exchanged will reach the spacecraft but will not be properly transferred. Without this, the data is still not of any use and the same consequences in case of antenna failure will follow. Therefore an extra transponder is included in the spacecraft. In case of data processing failure, the message which is sent and received is expected to be either incorrect or untranslatable. This has critical consequences for the complete system. Therefore, the modulation method is designed such that the bit error rate is 10^{-5}.

Table 8.11: Telemetry, Tracking and Communications Risk

		Risk before mitigation		**Risk after mitigation**	
Code	**Risk**	**Probability**	**Impact**	**Probability**	**Impact**
TTC1	Antenna failure or damage	Possible	Severe	Unlikely	Light
TTC2	Transponder failure	Possible	Severe	Possible	Very Light
TTC3	Data processing error	Possible	Severe	Possible	Very Light

8.3.10 Power

In case the fuel cells fail to start operating during the LEO phase, secondary batteries and solar panels are deployed to provide the required power. If one or more of the four solar panels fail to deploy, the fuel cells and secondary batteries are still able to provide the required energy. Even in the most unlikely case that all four solar panels fail to deploy, the fuel cells are able to provide enough for the time it would take the crew to repair it through an EVA. The chance of solar array damage during the mission is greatly reduced by not deploying them during the LEO phase and by the orientation of the spacecraft during the rest of the mission. In case of damage, and thus a decrease in performance, would only be a problem for the short period of the mission when the solar intensity is the lowest. Decrease in power consumption through reduced used of certain subsystems for this period of time is sufficient. The power management system is built with full redundancy on all components, thus a complete failure its very unlikely. If parts fail, the crew is able to replace them before the entire system fails. Furthermore, five batteries are used for higher system reliability.

Table 8.12: Electronic Power System Risk

		Risk before mitigation		**Risk after mitigation**	
P1	Fuel cell failure	Unlikely	Severe	Unlikely	Moderate
P2	Solar panel deployment failure	Possible	Catastrophic	Possible	Moderate
P3	Solar panel damage	Even chance	Light	Possible	Light
P4	Power management failure	Possible	Severe	Unlikely	Severe
P5	Battery overcharge	Unlikely	Catastrophic	Unlikely	Severe

8.4 Risk Maps

8.4.1 Risk map before mitigation

	Very Light	Light	Moderate	Severe	Catastrophic
Certain					
Likely			T4, PR7, G3	T1	R1, R2, F6,F7,TC1
Even Chance		P3	CR1, G2, S2	E7, CR4, F3, F4, G4, G5	TC3,R4, C1, C2
Possible		S1	T5, E4, S3, S5, PR1, PR3	T2, E1, E2, CR2, F5, S4, S6, TTC1, TC2, TTC3, P4	E5, E6, E8, F2, P2
Unlikely			PR2	T3, R3, F1, P1, S7	E3, CR3, P5, S8, PR4, G1, T6

Impact

Figure 8.1: Risk map before mitigation

8.4.2 Risk map after mitigation

	Very Light	Light	Moderate	Severe	Catastrophic
Certain					
Likely		F7	T4, PR7		
Even Chance		R1, R2, G4, G5	R4, CR1, G3	E7	
Possible	TTC2, TTC3	T4, E4, PR6, C1, PR, S1, S3	E1, E2, E8, F5,TC1, TC3, PR1, PR3, G2, P2, S2, T5	T1, T2, E5, E6, CR2, CR4, F3, F4, PR5, S6,	F2
Unlikely		C2, TC2, TTC1	T3, R3, F6, PR2, P1, S5	F1, P4, P5,S4,S7	E3, CR3, PR4,G1, S8, T6

Impact

Figure 8.2: Risk map after mitigation

Chapter 9
RAMS Analysis

In the design of complex engineering systems, the engineering integrity needs to be determined. Engineering integrity includes reliability, availability, maintainability and safety of inherent systems functions and their related equipment [132].

9.1 Reliability

Reliability of a spacecraft is defined as the probability with which it will successfully complete the specified mission performance for the required mission time.[132] The reliability of a design is dependent on the amount of testing and previous space mission success rates. For all subsystems, mostly extant technologies or existing technologies which only needs to be qualified for manned mission are used.

Launcher

The Falcon Heavy Launcher is currently under development and by the time this mission is launched, the Falcon Heavy will have some launches [22] . Depending on the success rate of those launches, the reliability can be determined. Since Falcon Heavy has no launches, its success rate is unknown. Therefor for now, the assumption that the Falcon Heavy is an unreliable system has to be made. However, the Falcon 9, which is the base for the Falcon Heavy, has had six launches until now which were all successful.

Refueling

Refueling in orbit had been done before (maximal 800 kg), only not with these amounts of fuel (44 tons) and not with cryogenic fluids. Therefore, this process is critical and needs to be developed and tested. However, the loss of crew reliability is not affected because the refueling occurs before the crew is launched to the orbit.

Space Module

The Dragon capsule is developed by SpaceX. An uncrewed version of the capsule has been launched already. It still needs a qualification test for human mission. To enhance the reliability of the mission, a radiation and Micrometeorite and Orbital Debris (MMOD) shielding is added. It protect the crew and the spacebus during the mission. Thus, the possibly catastrophic effects of the solar flare activity on man and its effects on electronics systems, thermal control systems and other subsystems will be decreased.

Communication and Data Handling

The communication and data handling subsystem is an important equipment. It includes Telemetry, Tracking and Communications (TT&C), and Command and Data Handling (C&DH).Communication and data handling have been in use and development for last decades. They are thereby highly predictable and reliable. Also, the TT&C and C&DH of the Dragon capsule are already tested and are sufficiently reliable.

Environmental Control and Life Support System

Environmental Control and Life Support System (ECLSS) should be available constantly during the mission. For a manned mission to Mars, any kind of failures are unacceptable, so the reliability of this system needs to be high.

Electrical Power Subsystem

Spacecraft electrical power (SEP)consists of two fuel cells, four solar arrays and five secondary batteries as well as power management systems. SEP management and distribution systems are highly reliable, since they have been investigated and developed thoroughly during past years.

Software

Spacecraft operations are becoming increasingly dependent on the software, especially in deep space missions. Reliability assessment of software is not a precise science and requires a sufficient number of tests. To increase the reliability of the software, an extant, simple and well structured one is chosen.

9.2 Availability

Availability of the design includes two aspects. First, it concerns the equipment's or application's capability of being used over a period of time. It measures the capability of being in an usable state. For this mission, most systems are off-the-shelf technologies and therefore they will be available on time. However, some components have to be qualified for manned space flight. This may compromise the availability of the product, since this testing and qualification has to be performed quite some time before the launch of the system. [132]
The Falcon Heavy launcher is the greatest risk concerning the availability. Its first launch is planned in 2014 [22] and therefore it is not operational yet. If problems arise and this date is postponed, problems will arise for the mission. Refueling in orbit is the next point of attention. It had been done before for less amounts of fuel and without cryogenic fluids. The aim is to test the refueling of cryogenic fluids in space before the launch.
The next concern is related to availability over a period of time. This measures the time that the subsystem is applicable before
Since extant technology is used, experimentally the available period can be measured. Each subsystem is designed in a way to be operational during the 500 days.

9.3 Maintainability

Maintainability at the system level requires an evaluation of the visibility, accessibility and repairability of the systems and the sub-systems. In this section, an overview of potential maintenance activities for the systems is explained. In addition, the failures are evaluated and divided to scheduled and unscheduled maintenances.
The mission has two crew members that are able to perform repairs. Since the crew has EVA suits; the outside of the spacecraft is accessible for maintainability. Furthermore, the maintenance equipment includes a 3-D printer, which is expected to reduce the maintenance equipment weight.

Communication and Data Handling

TT&C which is located outside the module is sensitive to debris and radiation. Therefore, the chance of failure for communication antennas is high. However, the spacecraft will rotate in such a way that antennas will be protected by the module. So the antenna will be assumed to be non-replaceable and only small fixes will be planned for movable parts.
C&DH which is the software part of the communication will be designed in such a way that the lack of specific knowledge of electronic of the crew is considered.

Propulsion

The propulsion system is used for a small part of the total mission time, for maneuvering and starting the trajectory. Therefore, the propulsion system and its subsystems are designed for no rate of failure and are required to achieve a probability of success for the total 501 days of mission.

Environmental Control and Life Support System

This subsystem consists of air system, food system, thermal system, waste system and water system. Thermal system and air system are located in the pressurize module such that replacement is possible.[133]
There are a number of items which realistically should not need to be repaired during the mission. Therefore, the design of these items has to be with no rate of failure. These items are: food system, water system and waste system.

Guidance, Navigation and Attitude Control

The sensors sets of this system are assumed to be non-repairable or non-replaceable and should have a high reliability. However, the subsystem packages like regulation and distribution components are identified to be replaceable depending on the crew skills.

Electrical Power Subsystem

The fuel cells and solar arrays are assumed to be non-repairable. However, the batteries have the possibility of a random failure and it will be possible to replace them individually. The power management of the EPS consists of power distribution, regulation and control.It composed of cabling, fault protection and switches to turn power on or off. These are planned to be replaced depending on the crew skills and knowledge of electrical systems. Since they are inside the pressurized module, it can easily be fixed.

Scheduled Maintenance

The scheduled maintenance occurs at preplanned time intervals. The requirements will be identified in a task analysis list. These tasks will be divided properly over all days; so the workload will be distributed over each day.

Unscheduled Maintenance

The unscheduled maintenance occurs randomly. The mission duration will be divided by three uneven periods of time. The expected failure of the first period is neglected. On the second period, unscheduled maintenance will be required with a low impact. In the last period a high unscheduled maintenance is expected.
Each time an unplanned failure will occur and the failure rate of that component will be calculated. However, the ECLSS and electronic subsystems have the highest expected percentage of failures and a much greater proportion of the repair time. The reason is that it includes lots of subsystems with frequent failures. It is of interest to note that this can be replaced easily, since it is located in pressurized module.

Conclusion

The scheduled maintenance are considerably more than the unscheduled maintenance. However, no unscheduled maintenance is expected in the first period. Furthermore, all internal parts of the spacecraft are pressurized, so the crew can access the internal parts.

9.4 Safety

One of the main mission aspects is to return the crew safely to the Earth. Safety can be classified into two categories; first related to personal protection, and second relating to spacecraft protection. [132]

Refueling

Refueling has a low reliability; however, it is only related to the mission. If the refueling fails, the mission has to be aborted. The crew is safe and will not launch to the orbit.

Space Module

The structure of the space module can support more than two times of the expected loads, this means the chance of failure could be neglected. The living module is shielded against MMOD and its risk of critical impact by meteorite is less than 1%. However, the chance that the spacebus get hit by the meteorites is high. If the crack is small, it can be fixed by the crew. If the damage is severe, as the worth case scenario, the depressurization will occur so fast and the crew will not make it.
Radiation protection must be designed for the crew to get a minimum amount of radiation during the entire mission. Therefore, an extra radiation shielding around the sleeping cabins is designed to increase the crew safety. This shelter gives the crew the opportunity to be protected against high solar array. If shield fails, the crew will be exposed to radiation and the mission will fails.

Re-entry

In order to succeed the mission and get the crew safe on the Earth, a safe re-entry into the Earth's atmosphere and a safe landing is required. There is the possibility of mission failure if the capsule disintegrates or does not get caught by the atmosphere. No feasible solutions are available to handle these problems; just for the case of parachute failure, redundant parachute is installed.

Communication and Data Handling

Failing of this subsystem will result in having no connection with the ground station; therefore, the crew will not be able to contact with ground station. It will have mental effects on the crew. Also the ground station cannot measure the status of the spacecraft and in case of meteoroids danger, the crew cannot be informed . If TT&C fails during the mission, the system can be repaired by the crew if the damage is minor. However, every component of the C&DH has a backup and could be replaced in the case of failure.

Propulsion

All current spacecraft use chemical rocket engines (bipropellant or solid-fuel) for launch. Therefore, a bipropellant engine using liquid oxygen and RP-1 is chosen which is sufficiently reliable and safe. Compared to the nuclear fission, bipropellant is fairly safe. However in case of any leak, the propulsion should be shut down. In case thruster fails during the mission, it could be replaced by the other thrusters.

Environmental Control and Life Support System

The ECLSS is directly related to crew safety; therefore in case of any failure which cannot be repaired, the crew is in danger. Taking that into account, the systems are located in pressurized part and are easy to access.

Guidance, Navigation and Attitude Control

GN&C is a critical subsystem. The GN&C actively controls the actuators at all times to maintain the desired attitude. Potential failures of sensors, actuators, and software must all be detected and tolerated to keep the spacecraft safe. The spacecraft would not be able to follow its trajectory and could get lost in space, in case of any permanent failure. Therefore, GN&AC provides a functional backup to each component.

Thermal control

The thermal protection is very important to ensure the health of the crew and keep the spacecraft functional. Depends on how critical the failure is, the problem could be fixed. In less extreme cases, some non-critical components can be shut down, as to minimize the heat generated on board. In case the damage could not be fixed, the crew and the mission will not be able to survive.

Conclusion

The goal of the safety is to detect health-threatening faults, and to keep the spacecraft safe until landing on the Earth. The most critical systems of the mission are the LSS and thermal protection. They are directly related to the safety of the crew, since they are basic need of human. If they fails, the crew will not make it and the mission will fails instantly. The next category of critical aspects of spacecraft safety are the remaining systems like power, communications and navigation and other subsystems. They are indirectly connected to the safety of the crew. If these systems fail, the crew will for a while.

Chapter 10

Operations and Logistics

10.1 Project Development

The total lifetime of a project can be divided into seven stages [134], defined by the European Space Agency (ESA) as:

- Phase 0: Mission analysis, needs identification
- Phase A: Feasibility
- Phase B: Preliminary Definition
- Phase C: Detailed Definition
- Phase D: Qualification and Production
- Phase E: Utilization
- Phase F: Disposal

The current phase is phase A, a (pre-)feasibility study. The next steps in the project with their timeline is outlined in the Gantt Chart, see figure 10.2. The launch will take place in January 2018. Since mostly off-the-shelve components are used, the Qualification and Production phase needs less time when compared to projects that need to be fully developed.

10.2 Operations and Logistics

This section gives an overview of all operations needed to support the mission, as well as the logistics needed for the mission. This varies from the production of all components, to the on-board computer needed to control all subsystems, to the retrieval of the crew after they have landed back on Earth.

Production and Testing

Since the launch for this mission is planned for 2018, mostly off-the-shelf technologies are used. By doing this, the production time of the components can be reduced. Once the components are produced and quality is assured, they have to be integrated and the integration has to be tested, before the spacecraft can be mounted to the launch vehicle. In section 10.3 a more elaborate production plan can be found.

Transportation

Due to the fact that the individual components most probably come from different locations, transportation will be needed to collect all components safely without damaging components due to travel. This must happen in accordance with applicable laws, rules, and regulations of transportation within the space industry. The largest transportation operation will be the transportation of the two launch vehicles to the launch platform. For most units can be transported by commercial transport services, e.g. by road, ship or aircraft. For larger vehicles, dedicated transport vehicles may have to be used, or even specially developed [36].

Space Operations

Once the spacecraft is launched, a number of operations need to be performed to fulfill the mission. These space operations are listed below:

- Rendezvous and docking
- Refueling
- Guidance, Navigation and Control (GNC)

A rendezvous and docking maneuver has to be performed to connect the spacecraft with the fuel depot. Once this is done, the refueling phase can start. More details about this phase can be found in section 5.5. The position and orientation of the spacecraft are determined with the GNC subsystem. This supports the spacecraft to perform its maneuvers to get to Mars and back to Earth. It also maintains a constant knowledge of where the spacecraft is in its orbit. Since the GNC controls the orientation of the spacecraft w.r.t. the Earth, it also ensures that the antennas remain pointed at the Earth in order to maintain communications.

Crew Selection and Training

The crew needs extensive training before they can be send on the mission. They need to be trained to withstand high g-load during launch and re-entry, they need to be able to operate all systems in the spacecraft and they need to be trained for extra-vehicular activities (EVA). In section 6.1 more on this subject can be found.

Ground Operations and Communications

From the pre-launch phase till the landing, a team on Earth controls and observes the spaceflight. This team of operators will oversee and supervise the mission in all ways possible. For this purpose, a mission control center is needed to provide communications with the spacecraft and the crew. The crew must be able to contact the ground stations 24/7 and asks for assistance on their operations. The ground team must consist of engineers and experts on the spaceflight, but also doctors are needed to monitor the crew's health and assist them for medical procedures if and when needed. Another aspect of the ground operations is the Deep Space Network (DSN) and the way this is used for communication with the spacecraft. The facilities of the DSN are in California (U.S.A.), Madrid (Spain) and Canberra (Australia), about 120 degrees apart around the world. The DNS is part of the National Aeronautics and Space Administration (NASA), but there are several other deep-space networks that may be used for this mission, among others one by the European Space Agency (ESA) and the Soviet Deep Space Network. The mission aims to send the living module into space after the finalization of the mission, to continue its measurements. During the detailed planning of the mission, this has to be kept in mind, since this will require the use of the DSP and some form of mission control to receive the data. The pre-launch Operations consist of (amongst others) the preparation of the ground facilities, payload encapsulation, transportation to the launch pad, propellant loading etc.

Crew Retrieval

Once the re-entry capsule has landed, its location will be determined and the capsule will be retrieved. The crew needs to be brought to a medical centre to check their health and to retrieve other needed data. In section 6.3 more on this subject can be found.

10.3 Production Plan

In this section, the manufacturing, assembly and integration (MAI) plan will be discussed. An overview of the production phase can be found in the project development logic, figure 10.1.

10.3.1 Manufacturing

The first phase of the production is the manufacturing of all components. Since the time is very constrained for this mission, this phase has to start as soon as possible. To shorten the manufacturing, multiple contractors can produce parts at the same time. Since most components that are used are off-the-shelf, these components are already qualified. Therefore, no testing and qualification is needed these components, but there are tests needed to assure the quality of the components. For parts that have to be developed, extensive testing and qualification is needed.

10.3.2 Assembly

Once the components are produced, they have to be assembled to form the subsystems. This can be done in parallel with the manufacturing phase. If all components of one subsystem are ready, the assembly phase can start for that specific subsystem. This phase will also be finalized by tests to assure the quality and correct assembly of the subsystems.

10.3.3 Integration

The final step of the production plan is the integration of all subsystems to form the final spacecraft. This phase can be started once the assembly phase is done. All subsystems have to be transported to the same place, a place similar to the Vehicle Assembly Building (VAB) at Kennedy Space Center. The final phase of the integration is the integration of the system with the launch vehicle. This phase will start a few weeks before launch, and will be listed under the pre-launch ground operations. The vehicle will be assembled vertically in an assembly building, so the launch pad will not be occupied during the assembly (which may be up to a month if the launcher is assembled on the launch pad) and to allow the preparation of two launchers at the same time[36].

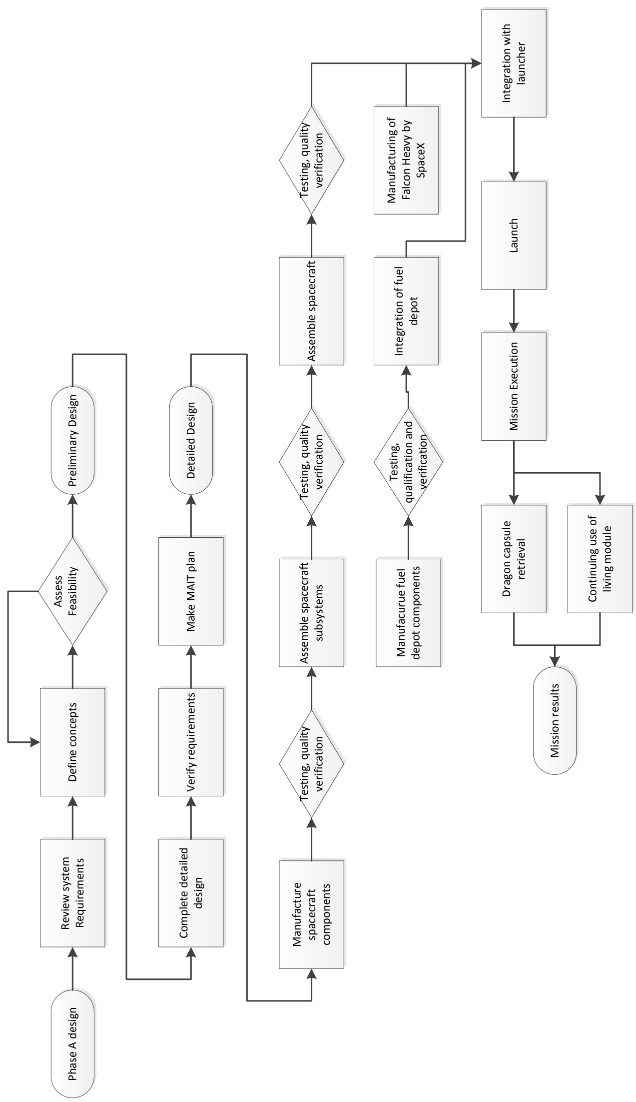

Figure 10.1: Project Development Logic

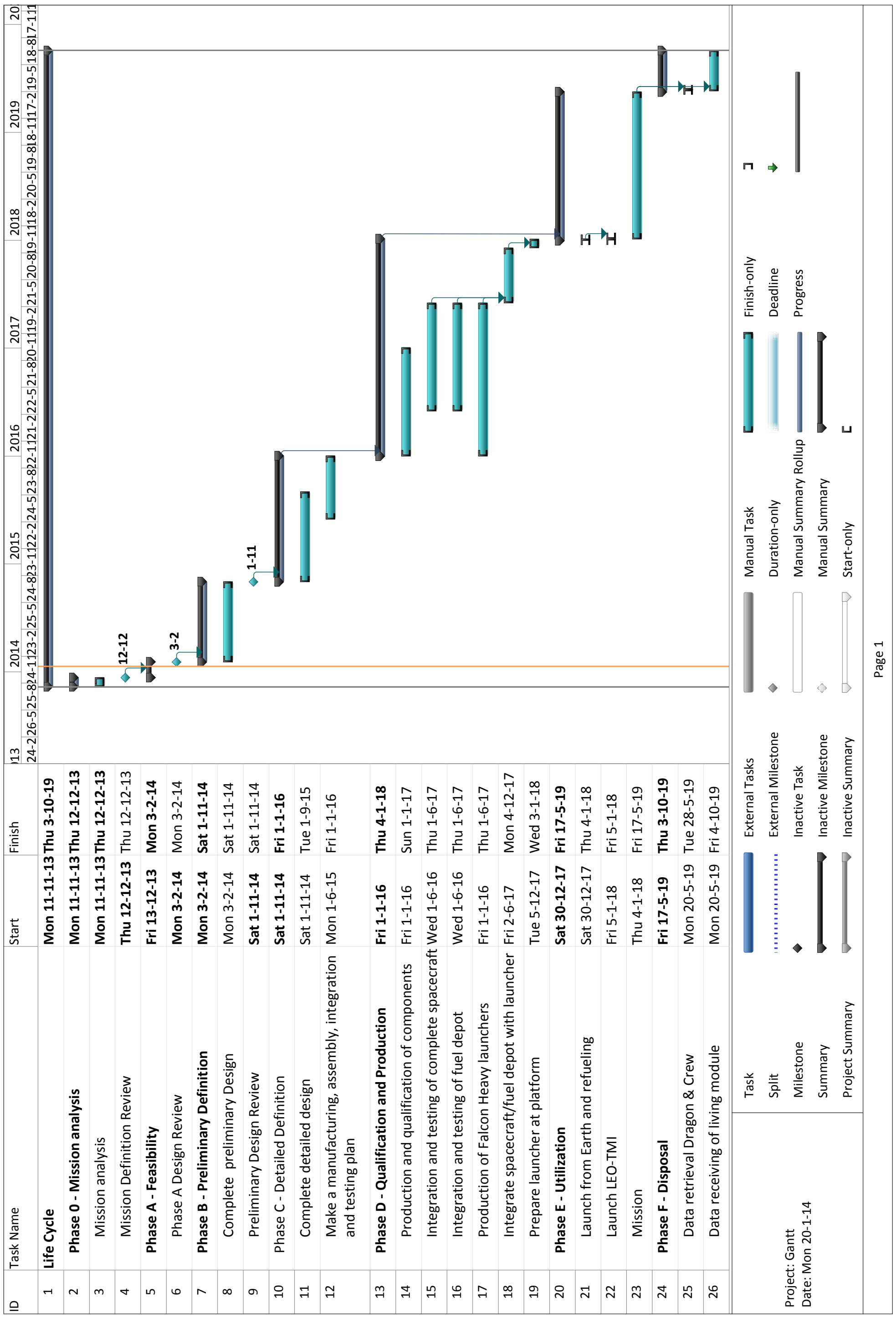

Figure 10.2: Project Gantt Chart

Chapter 11

Final Mission Design Overview

This chapter starts with a performance analysis of the presented design in 11.1. Section 11.2 describes the mission timeline, which presents the main mission events. Section 11.3 gives a final internal and external design of the spacecraft.

11.1 Performance Analysis

The spacecraft is launched in a Falcon Heavy launcher which provides an initial ΔV of 8.4 km/s. During this launch the spacecraft can carry a load factor of 6 g in the x-direction and 0.5 g in the y and z-directions. It is also able to withstand lateral vibrations greater than 10 Hz and axial vibrations greater than 25 Hz. When in parking orbit, the second stage of the Falcon Heavy engine is refuelled with 30,800 kg LOX and 13,689 kg RP-1 in less than 6 hours. The spacecraft is injected into its trajectory on 4 January 2018 with an ΔV of 5.0 km/s.

During the cruise phase of the mission the ECLSS system provides an environment which can sustain human life. The ECLSS also provides the food, water, waste and air management within the living module. The spacecraft is protected by a MMOD-shield capable of surviving an impact of a particle with a mass of maximum 1.5 grams. The radiation protection reduces the GCR dose to 6.4% and the SPE dose to 86%. The temperature inside the spacecraft is kept around 20 degC. The thermal control system is also capable of rejecting all 13 kW of peak power. The power is provided by fuel cells capable of providing an average power of 6.7 kW. The power system also includes 57.2 m^2 of solar arrays with an efficiency of 30% delivering a total power of 7.6 kW. The pointing of the solar arrays is performed by the autonomous GNC system. The GNC system is able to control its position within 250 km during cruise phase and determine its velocity within 0.25 m/s. The spacecraft has a pointing stability of 0.1 deg. The communications has a downlink frequency of 32.3 GHz and a maximum downlink data rate of 1 Mbps. The uplink frequency will be 34.7 GHz and the maximum uplink data rate 300 kbps. The computer throughput is 2.5 Millions of Instructions Per Second (MIPS) and have a processor speed of 10709 Source Lines Of Code (SLOC).

The spacecraft performs its fly-by on 20-08-2018. During the fly-by the GNC system will control its position within 1 km and determine its velocity within 0.1 m/s. After a trajectory back to Earth the spacecraft will approach Earth with a velocity of 14.2 km/s. During the direct re-entry the g-loads will remain below 8 g. The heat shield can withstand an peak heat flux of 3,100 kW/m^2 and can deteriorate 3.2 cm. For the parachute deployment the maximum g-load is below 4 g. On 20-05-2019 the dragon capsule will splashdown with a velocity below 10 m/s after 501 days of flight.

11.2 Mission Timeline

The mission consists of several phases in which different maneuvers need to be performed. Table 11.1 provides a timeline in which the main mission events are shown. The events are given for the launch, parking orbit, cruise and re-entry phase. The launch dates are an estimation, the on-orbit rendezvous maneuver has to be specified more to get the definite launch dates.

Table 11.1: Mission timeline

Event name	Start Date	Start Time	End Date	End Time	Phase
Launch Refueling Tanks	31 dec 2017	07:00:00	31 dec 2017	07:07:00	Launch
Burn 1st Stage	31 dec 2017	07:00:01	31 dec 2017	07:03:00	Launch
Burn 2nd Stage	31 dec 2017	07:03:01	31 dec 2017	07:07:00	Launch
Parking Orbit Refueling Tanks	31 dec 2017	07:07:00			Parking Orbit
Launch Spacecraft	02 jan 2018	07:00:00	02 jan 2018	07:09:15	Launch
Burn 1st Stage	02 jan 2018	07:00:01	02 jan 2018	07:03:00	Launch
Burn 2nd Stage	02 jan 2018	07:03:01	02 jan 2018	07:09:15	Launch
Parking Orbit Spacecraft	02 jan 2018	07:09:15			Parking Orbit
Rendezvous maneuver	02 jan 2018	07:09:20			Parking Orbit
Docking LOX Tank	03 jan 2018	11:00:00			Parking Orbit
EVA	03 jan 2018	12:00:00	03 jan 2018	15:00:00	Parking Orbit
Connect RP-1 Tank	03 jan 2018	14:30:00			Parking Orbit
Refuel	03 jan 2018	15:00:00			Parking Orbit
Disconnect	03 jan 2018	20:00:00			Parking Orbit
Orbit Insertion	04 jan 2018	07:00:00			Parking Orbit
Trajectory Keeping	04 jan 2018	07:00:00	20 may 2019	07:00:00	Cruise
Jetonize 2nd Stage	05 jan 2018				Cruise
Fly-by Mars	20 aug 2018				Cruise
EVA	17 may 2019				Cruise
Jetonize Living Module	18 may 2019				Cruise
Decelerating in the Atmosphere	20 may 2019	07:00:00			Re-entry
Jetonize Heat Shield	20 may 2019	07:10:00			Re-entry
Deploy Drogue Chutes	20 may 2019	07:10:10			Re-entry
Release Drogue Chutes	20 may 2019	07:11:23			Re-entry
Deploy Pilot Chutes	20 may 2019	07:11:24			Re-entry
Deploy Main Chutes	20 may 2019	07:11:44			Re-entry
Splashdown	20 may 2019	07:18:06			Re-entry
Inflation of Flotation Devices	20 may 2019	07:18:08			Re-entry
Retrieval	20 may 2019	09:00:00			Re-entry

11.3 Spacecraft Layout

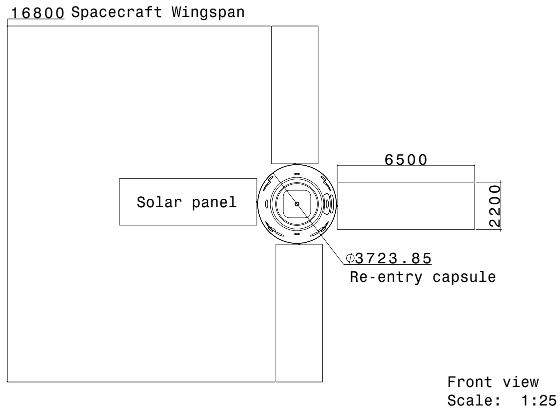

Figure 11.1: Front view of Adrestia

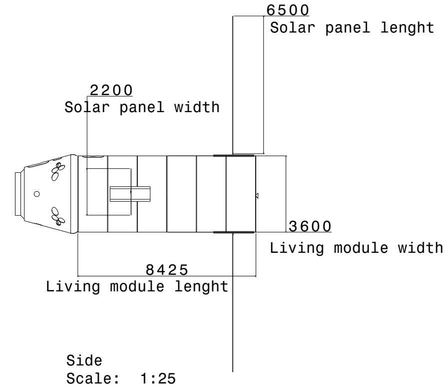

Figure 11.2: Side view of Adrestia

After all subsystems have been designed and integrated, the final external and internal layout of the spacecraft shall be demonstrated and briefly explained in this section.

Sectional views

The front, side and isometric view of the spacecraft, with fully deployed solar arrays, are shown with the most important dimensions in figures 11.1, 11.2, 11.3. The top view is almost identical as the side view but is missing the door dimensions, and is therefore not contributing further. All dimensions are in mm.

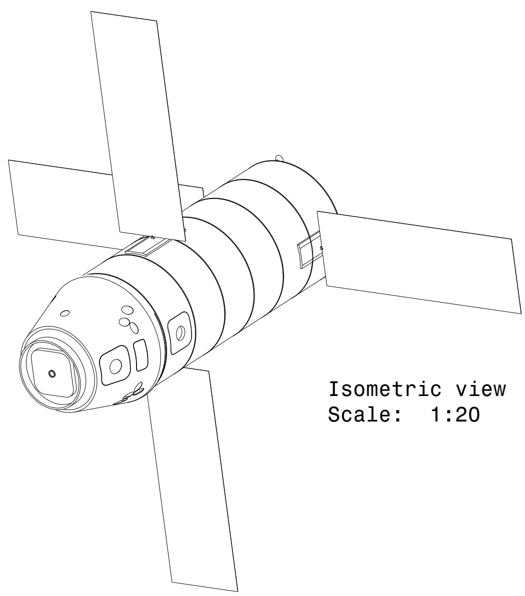

Figure 11.3: Isometric view of Adrestia

Internal layout

The internal layout of the spacecraft, is illustrated by a sectional cut in figure 11.4. The following enumerated items, have been placed inside Adrestia. The outer layer of the spacecraft is a 30 cm think MMOD protection.

The water tank (15), which is part of the ECLSS, has been placed behind the Sun pointing surface of the spacecraft, as means of an additional radiation protection. The crew compartment is surrounded by a wall of food storage. As the food is consumed during the mission, the emptied space is being filled in with the produced waste. Food and waste (10), as part of the ECLSS subsystem, both contribute as an extra radiation protection. With the same line of reasoning, the hydrogen (12) and oxygen (13) tanks, which are part of the power subsystem, for the fuel cells (which ratio is 1:8) are placed behind the water tank. The power, telecommunication, command and data handling, GNC and ECLSS subsystems have been placed in such a way, as to be accessible by the crew for maintenance and in case of malfunction. The thruster location(11) has been illustrated from the inside, however, they are located on the outer surface of Adrestia. The crew, to scale, has also been included in the figure, so as to realistically produce the layout. Lastly, compartments where the EVA units (3) and other items (2) shall be stored are placed on the walls as shown. The window (4) is located in the middle of the living module door.

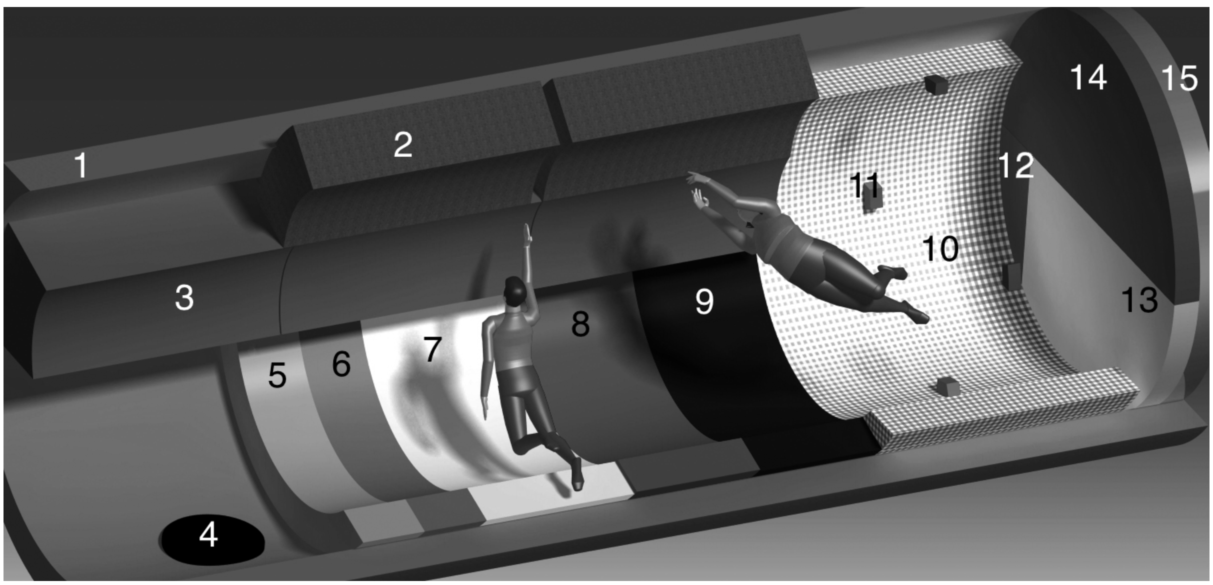

Figure 11.4: Internal view of Adrestia

1. MMOD protection
2. Storage compartments
3. EVA unit compartments
4. Window
5. Command and Data Handling Subsystem
6. GNC subsyster
7. ELSS (other)
8. Telecommunication subsystem
9. Thermal control subsystem
10. Food & Waste compartments
11. Thruster location
12. Hydrogen tank
13. Oxygen tank
14. Power subsystem
15. Water tank

Location, Mass, Volume and Power Budget

The total mass budget of the spacecraft changed throughout the whole design process with each iteration in the sub-system design. Table 11.2 presents the location, mass, volume and power budget for Adrestia. First, the total re-entry capsule mass is shown, together with the propellant needed for the re-entry maneuver. Afterwards the living module and each of its sub-systems characteristics are shown. The propulsion subsystem includes the propellant required for the interplanetary trajectory. Next, the Falcon Heavy second stage and required propellant for the Trans Mars Injection (TMI) are included. Finally, the center of gravity, mass, outside volume and power are displayed with and without margins. A 10% margin of the dry mass is added to the total mass as well as a 10% extra peak and average power. With a total volume of the subsystems in the living module of 63.21 m^3 and a outside volume of 87.53 m^3 there is a remaining 24.32 m^3. This allows to have a subsystem volume margin of 20% and still have extra 11.68 m^3 of additional free space for the crew.

Table 11.2: Adrestia mass budget

Sub-system	**Location (x,y,z)**	**Mass [kg]**	**Volume [m^3]**	**Power Peak/Avg [W]**
Re-entry Capsule				
Re-entry Capsule	0,0.5,0.9	4030	20.77	-
Crew	-	150	-	-
Living Module				
Structure	0,0,4.3	1131	32.23	-
ECLSS	0,0,7.4	4722	25.26	10914/5030
Scientific Payload	0,0,5.4	290	0.5	-
Propulsion	0,0,5.4	3627	2.35	-
GNC	0,0,8	41.22	0.95	68.9/68.9
C&DH	1,1,6	21	0.07	125/25
Comunications	0,1.8,5	32	0.035	239/129
Power	0,0,3.2	1281	1.15	-
Thermal Control	0,0,4.3	517	0.25	1710/843
Total	0,0,5.78	10447.75	63.21	12781/6844
TMI propulsion system				
Falcon Heavy 2^{nd} Stage	-	4976	-	-
Propellant TMI	-	74329	-	-
Total	-	79305	-	-
Adrestia Total without TMI propulsion system				
Total	0,0.1,6.37	14628	108.3	12781/6222
Dry Mass (DM)	-	9530.75	-	-
Total +10% Margin	0,0.1,6.37	15580.82	108.3	14158/6844

Chapter 12

Conclusion and Recommendations

Conclusion

The Inspiration Mars mission is the next step towards setting a footprint on Mars. The mission uses a combination of existing technologies to lower the cost, while maintaining compliance to the requirements. Each sub-system is designed towards the mission's requirements. These sub-systems are the life support system, thermal control, structures, propulsion, guidance navigation and control, command and data handling, telecommunications, and power. Additionally, the correct trajectory is determined along with the docking, re-fueling and re-entry procedure. To increase the sustainability of the mission along with providing activities for the crew, scientific payload is taken with on the mission. These aspects will all contribute to completing the mission statement by preforming an end-to-end fly-by mission to Mars.

A feasible trajectory was designed and optimized for departure. This resulted in a launch date on the 4th of January 2018. The mission will take a total of 501 days to preform a fly-by at Mars on the 20th August 2018 and return to Earth on the 20th May 2019 (section3). The mission consists of two launches, one launch will bring a fuel depot into parking orbit, the second brings the spacecraft (Adrestia) with the crew to that same orbit. The second stage of the Falcon Heavy launcher attached to Adrestia will then be re-fueled and re-ignite to execute a Trans-Mars Injection (TMI)(section 5.5). During this process Extra Vehicular Activity (EVA) will be required. Adrestia consists of a Dragon re-entry capsule and two extended trunks. The main structural component is a Kevlar rear wall which protects the spacecraft from micro meteorite collisions and radiation (section 5.2).The Environmental Control and Life Support System (ECLSS) of Adrestia consists of an advanced water recycling system which is high in efficiency (section 5.1) reducing the mass of the payload. The water tank will be direct towards the sun at all times to further shield the crew from Solar Particle Events (SPE). To achieve this pointing accuracy the autonomous GNC system will use a combination of thrusters and reaction wheels (section 5.4). The propulsion system designed for the spacecraft consists of 30 thrusters divided into eight clusters (section 5.3). The Telecommunication system will use the S-Band close to Earth and the K-band in deep space (section 5.6). These systems will be operated by the command and data handling system (C& DH) which is duplicated to prevent single point failures (section 5.7). To provide enough power the Electrical Power Subsystem (EPS) consists of two fuel cells (mainly used during Low Earth Orbit (LEO)), four solar arrays and five secondary batteries (used during Interplanetary Trajectory)(section 5.9. The Thermal Control System (TCS) consists of passive systems (multi-layer insulation and radiators) and active systems (pumped-fluid loops and heaters) to keep the temperature of Adrestia within the required values (section 5.10). During the mission, scientific payload will be used to increase Adrestia's sustainability and will give activities for the crew to do (section 5.8). A critical sustainability factor is that the spacecraft can be reused as a deep space measuring satellite (section 2.4). Finally, it has been concluded that it is possible to re-enter the earth atmosphere within the requirements by using the Dragon capsule (chapter 4).

Additional analyses were made in order to determine the credibility of the mission. A risk analysis identified all the major points of concern and a mitigation process was determined. The RAMS analysis was conducted and it can be concluded that of Adrestia complied with all requirements. The cost and market analysis then determined the budget of the mission, which will remain below five billion euros. A schedule was then made to determine to correct order to achieve the mission statement. Overall, Adrestia will revolutionize space travel while remaining in a budget that has never been accomplished for a similar manned mission.

Recommendations

In order to further improve the design some recommendations are given. These recommendations are specific per subsystem. Additionally, the recommendations for the trajectory and re-entry procedure will be explained.

The trajectory given, can be further optimized by doing a more detailed analysis on the trajectory perturbations. This would lower the margins needed therefore decrease the total amount of extra fuel needed on the spacecraft. The ECLSS can be further optimized by the reduction of power use. This can be done with the assistance of the crew, by using even more power generating equipment. The resistance training equipment can be transformed into a power generating unit. The thermal protection system analysis can be further optimized if all the different spacecraft parts are implemented in a model as thermal coupling nodes. That will result in a even more specific heat distribution around the spacecraft. Additionally, ESAs software ESTABAN can be made. Looking at the structure of Adrestia a more optimal spacecraft could be obtained for this mission if a completely new spacecraft could be designed. It is a specific mission therefore components from existing spacecraft will not yield the most optimal design. Radiation protection techniques through the use of advanced materials with hydrogen trapped inside (for example graphite nanofiber), should be studied. To optimize the launch the order needs to be investigated more thoroughly. The fuel depot is able to stay in parking orbit for several weeks, therefore it is preferred to launch the fuel depot first. This way, the crew can stay in parking orbit as short as possible. The refueling system is a new technology, therefore further testing and qualification is required before it can be used for a manned mission. There are multiple recommendations for improving the GNC system. The first is by having multiple tests of the autonomous GNC system. Although AutoNav has already proven its capability on the Deep Space 1 mission, it still needs to be tested further to ensure its safety and reliability for human space flight. Secondly, a more detailed analysis can be done on the recovery time of the system once a disturbance is present. To further improve the GNC system design, the noises need to be taken into account. This will give accurate component performances which could influence the mass and power budget of the GNC system. To improve the C&DH an investigation on state of the art on-board computers and their capacities should be conducted.

The recommendations for the power system is now determined. Regenerative fuel cells should be considered instead of secondary batteries to save overall weight of the spacecraft since fuel cells have a higher specific power and can be combined with radiation protection for this mission. Regenerative fuel cells use electrolysis to produce hydrogen and oxygen from water when extra power is available from the solar arrays working then as secondary batteries. The reason why they can be combined with radiation protection is that water is very good to shield against radiation. Recommendations for the communications subsystem are to make a more thorough estimation of the complete data rates. Also, an analysis according to the distance to earth can be made. The closer to earth, the less space loss. The complete mission is based on the maximum space loss, therefore taking this into consideration the communication system can be optimized. Lastly, the exact location and the mounting device of the antennas can be determined. The re-entry procedure can be improved by further optimizing the flight path trajectory and determining the exact corridor width. This would minimize the footprint to reduce recovery time. Additionally, the lift and drag ratios could be determined using a 3D simulation with the desired capsule shape. Currently a 2D model is used, to increase accuracy, a full 3D model to simulate the movement though the atmosphere would be the next step. For the Descent and landing System (DLS) the interaction of separate parachutes be should modeled. The final point of improvement is to investigate the radiated and absorbed heat as well the ablative properties of the heat shield. These recommendation points will improve the design of Adrestia.

Appendices

Appendix A

Requirement Compliance Matrix

Number	Description	Value	Unit	Check
A	**Crew**			
A1	The living environment reliability	0.9	%	✓
A2	**The maximum average radiation exposure level**	**0.16**	**cSv/day**	✓
A3	**The maximum acute radiation exposure level**	**0.5**	**Sv**	✓
A4	**The amount of food and water required for the mission**	**1140**	**kg**	✓
A5	The minimum hours of exercise per day	3	hrs	✓
A6	The minimum calorie intake per day	1500	kcal	✓
A7	**Amount of crew members**	**2**	**[-]**	✓
A8	The maximum height of a crew member	1.83	m	✓
A9	The minimum height of a crew member	1.57	m	✓
A10	Crew blood pressure measured in sitting position	140/90	[-]	✓
A11	Minimum distant visual acuity each eye	20/100	[-]	✓
A12	Distant visual acuity each eye (corrected)	20/20	[-]	✓
A13	The minimum spacecraft free living volume	10.2	m^3	✓
A14	Minimum Score on NASA's space physical	60	%	✓
A15	Minimum degree required	MSc.	[-]	✓
B	**Payload**			
B1	The maximum weight of the scientific payload	290	kg	✓
B2	The maximum weight of the crew	180	kg	✓
B3	The maximum spacebus weight	1500	kg	✓
B4	The maximum re-entry vehicle weight	5000	kg	✓
C	**Launchers**			
C1	The ΔV to LEO	8.4	km/s	✓
C2	Amount of times launcher is used for human flight	1	[-]	✓
C3	The launcher success rate	95	%	✓
D	**Spacebus**			
D1	Guidance Navigation and Control			
D1.1	**Accuracy of GNC during fly-by**	**1**	**km**	✓
D1.2	Attitude determination accuracy	0.012	deg	✓
D1.3	Slew rate	0.5	deg/s	✓
D1.4	Pointing stability	0.1	deg	✓
D1.5	Determining spacecraft velocity within	10	m/s	✓
D1.6	Knowing the position of the sun	100	%	✓
D1.7	Maximum angular velocity	30	deg/s	✓
D2	Materials & Structures			
D2.1	Structure reliability	99	%	✓
D2.2	Maximum load in x-axis	6	g	✓
D2.3	Maximum load in y-axis	6	g	✓
D2.4	Maximum load in z-axis	6	g	✓
D2.5	Minimum number of additional load path in case of failure	2	[-]	✓
D2.6	Reliability of the structure	90	%	✓
D2.7	Maximum axial vibration of the structure	30	Hz	✓
D2.8	Maximum lateral vibration of the structure	15	Hz	✓
D2.9	Outgassing limit	1	%	✓
D2.10	Exterior thermal requirement	-160 to 250	°C	✓

D2.11	Interior thermal requirement	-25 to 45	°C	✓
D3	Propulsion			
D3.1	**The ΔV from LEO to TMI**	**5.30**	**km/s**	✓
D3.2	Minimum thrust generated	100	N	✓
D3.3	The number of thrusters needed for attitude control	8	[-]	✓
D4	Power			
D4.1	Average EPS power provided	6844	W	✓
D4.2	Amount of power provided during and 8.5 hour interval	14158	W	✓
D4.3	The amount of time Power needs to be generated	550	days	✓
D5	Communication/Data Handling			
D5.1	Effective isotropic radiated power	58.9	W	✓
D5.2	LEO Downlink Frequency	2.3	Ghz	✓
D5.3	LEO Uplink Frequency	2.12	Ghz	✓
D5.4	TMI Downlink Frequency	32.3	Ghz	✓
D5.5	TMI Uplink Frequency	34.7	Ghz	✓
D5.6	Maximum data rate of communication systems	1	Mbps	✓
D5.7	Number of channels for commands	500	[-]	✓
D5.8	Number of channels for telemetry	500	[-]	✓
D5.9	**Lifetime**	**615**	**days**	✓
D6	Life support			✓
D6.1	The pressure within the living module	0.0337	MPa	✓
D6.2	The oxygen level within the living module	16	%	✓
D6.3	The density within the living module	1.21	kg/m^3	✓
D6.4	The volume within the living module	54.4	m^3	✓
D7	Thermal Control			
D7.1	**Crew compartment temperature range**	**-20 to 27**	**°C**	✓
D7.2	Power temperature range	-105 to 110	°C	✓
D7.3	Attitude control temperature range	-80 to 80	°C	✓
D7.4	Propulsion temperature range	-52 to 87	°C	✓
D7.5	Structure temperature range	-45 to 65	°C	✓
D7.6	Mechanisms temperature range	-45 to 80	°C	✓
D8	Compatibility			
D8.1	Crew members needed to operate the spacecraft	1	[-]	✓
D8.2	Language for the system	English	[-]	✓
D8.3	Unit system used	metric	[-]	✓
E	**Re-entry**			
E1	Guidance Navigation and Control			
E1.1	**The maximum Re-entry velocity**	**14.2**	**km/s**	✓
E1.2	The maximum Re-entry flight path angle	20	deg	✓
E1.3	The Re-entry attitude control accuracy	0.04	deg	✓
E1.4	Re-entry duration	60	min	✓
E2	Structure			
E2.1	**The maximum re-entry internal temperature**	**30**	**°C**	✓
E2.2	**Peak load during re-entry**	**8**	**g**	✓
E2.3	Average load during re-entry	4	g	✓
E2.4	Minimum re-entry living module volume	2	m^3	✓
E3	Descent & Landing			
E3.1	**Load during parachute deployment**	**6**	**g**	✓
E3.2	**The maximum impact velocity**	**10**	**m/s**	✓
E3.3	The Re-entry footprint	500	km	✓
E3.4	Number of redundent parachutes	1	[-]	✓
E3.5	Parachute deployment time	20	sec.	✓
F	**Operations**			

F1	The monitoring time from the ground station	9	hrs/day	✓
G	**Sustainability**			
G1	Spacecraft components should be recyclable	[-]	[-]	✓
G2	The crew should purify their waste water	[-]	[-]	✓
G3	Propulsive systems should use methods with a low carbon footprint	[-]	[-]	✓
H	**Costs**			
H1	The budget dedicated to the launcher	150M	$	✓
H2	**Complete budget below**	**9.0B**	**$**	✓
H3	In-mission below budget	2.0B	$	✓
H4	Development below budget	6,9B	$	✓
H5	Scientific experiment budget below	100K	$	✓
I	**Schedule**			
I1	**The launch date**	**30-12-2017**	**[-]**	✓
I2	The end of final testing	04-12-2017	[-]	✓
I3	Completion of spacecraft	01-06-2017	[-]	✓
I4	The end of the detailed design	01-01-2016	[-]	✓
J	**Trajectory**			
J1	Minimum parking orbit earth altitude	185	km	✓
J2	Inclination parking orbit	28.5	deg.	✓
J3	**The mars transfer Orbit**	**Heliocentric**	**[-]**	✓
J4	The travel duration	501	days	✓
J5	**The mars fly-by altitude**	**180**	**km**	✓

Appendix B

Index PM/SE Deliverables

Table B.1: Index PM/SE Deliverables

Task No.	Product	Project Plan	Baseline Report	Mid-term Report	Final Report
5	Functional Flow Diagram(s)		X		Chapter 2
6	Functional Breakdown		X		Chapter 2
8	Resource Allocation/ Budget Breakdown		X		Chapter 7
9	Technical Risk Assessment		X	X	Chapter 8
12	Market Analysis		X		Chapter 7
18	Operations and Logistics Description		X		Chapter 10
19	Project Design and Development Logic				Section 2.2
20	Project Gantt Chart				Chapter 10
21	Cost Breakdown Structure				Section 7.2
22	H/W, S/W block diagrams				Section 5.1
23	Electrical Block Diagram				Section 5.9
24	Data Handling Block Diagram				Section 5.7
25	Sustainable Development Strategy		X	X	Section 2.4
26	Compliance Matrix				Appendix A
27	Sensitivity Analysis			X	Chapter 3,4,5
28	Communication Flow Diagram			X	Section 5.6
29	Verification and Validation Procedures			X	Section 2.3
30	Manufacturing, Assembly, Integration Plan			X	Section 10.1
31	Return on Investment, Operational Profit			X	Section 7.1
32	RAMS Characteristics			X	Chapter 9
33	Performance Analysis			X	Section 11.1
34	Configuration/ Layout				Section 11.2
35	Spacecraft System Characteristics			X	Chapter 5
37	Aerodynamic Characteristics				Chapter 4
38	Structural Characteristics				Section 5.2
39	Stability and Control Characteristics				Section 5.5
40	Material Characteristics				Section 5.2
41	Astrodynamic Characteristics		X	X	Chapter 3

Appendix C

Individual Project Contribution

Table C.1: Individual Project Contribution

Name	Contribution to the Project
S. Ahmad	Sec 5.6, Sec 5.7
R.M.J. Caenen	Sec 5.4, Sec 5.5, Sec 5.10, Ch 11
R. Blanco Maceiras	Sec 5.2, Sec 5.9, Ch 11
P. Fatemi Ghomi	Sec 5.2, Ch 9
M.C. Georgiev	Cover Page, Sec 5.10, Ch 11, CATIA
G. Gezels	Preface, Report Assembly, Ch 1, Ch 3, Ch 7, App B and C
S. Hosseini	Abstract, Jury Summary, Sec 5.1, Sec 5.8, Ch 6
L.M. Kranendonk	Ch 4, Ch 8, Bibliography
C.D.J. Stevens	List of Abbreviations, Sec 5.3, Sec 5.5, Ch 10
T.J. Verschoor	Ch 2, Ch 4, Ch 12, App A, List of Symbols

Bibliography

[1] Rules for Mars Society International Student Design Competition, Accesed 21-01-2014. http://www.marssociety.org/home/inspiration-mars/rules

[2] Boyle G., "Renewable Energy: Power for a Sustainable Future", Oxford, 2004

[3] European Space Agency, Margins and reference frames, Engineering design model data exchange (2010)"

[4] Dr. ir. E. Mooij, "Project Guide Design Synthesis Exercise - Inspiration Mars", 2013

[5] Dennis Tito, et al, "Feasibility Analysis for a Manned Mars Free-Return Mission in 2018." Available at http://www.inspirationmars.com/Inspiration20Mars_Feasibility20Analysis_IEEE.pdf Retrieved on 21/11/2013

[6] NASA, "Mariner 10", http://solarsystem.nasa.gov/missions/profile.cfm?MCode=Mariner_10&Display=ReadMore, Viewed on 16/1/2018.

[7] William M. Folkner, James G. Williams, Dale H. Boggs, NASA, "The Planetary and Lunar Ephemeris DE 421", 15/08/2009

[8] Wertz, James R., Larson, Wiley J. "Space Mission Analysis and Design", Microprism Press and Springer, 1999, third edition, ISBN 978-1881883-10-4

[9] Verschoor, T., Hosseini, S., Gezels, G., Blanco Maceiras, R., Kranendonk, L.M., Caenen, R., Georgiev, M., Stevens, C.D.J., Ahmad, S., Fatemi Ghomi, P. "Mid-Term Report".

[10] K. Kumar et al. "Tudat Course: Interplanetary Orbit Transfers, Assignment 1." Astrodynamics & Space missions Faculty of Aerospace Engineering, Delft University of Technology, March 14, 2013.

[11] "The TU Delft Astrodynamics Toolbox WIKI" Tudat WIKI Repository, accessed December 12, 2013, http://tudat.tudelft.nl/projects/tudat/wiki.

[12] NASA, "General Mission Analysis Tool",http://gmat.gsfc.nasa.gov/

[13] The GMAT Development Team, "General Mission Analysis Tool (GMAT) User Guide", 18 May 2012

[14] D. Eagle, "A MATLAB Script for Interplanetary Gravity-Assist Trajectory Design and Optimization", available at: http://www.mathworks.com/matlabcentral/fileexchange/39462-gravity-assist-trajectory-design-and-analysis, 14 Dec 2012

[15] P.E. Gill, "Users Guide for SNOPT Version 7: Software for Large-Scale Nonlinear Programming", Department of Mathematics University of California, San Diego, La Jolla, CA 92093-0112, USA, 16 Jun 2008

[16] NASA/JPL (2005b), "Planetary Data System", http://pds.jpl.nasa.gov/ planets/choices/Mars.htm, Last accessed: December, 2013

[17] NASA/JPL (2005b), "Planetary Data System", http://pds.jpl.nasa.gov/ planets/choices/Earth.htm, Last accessed: December, 2013

[18] NASA/JPL (2005b), "Planetary Data System", http://pds.jpl.nasa.gov/ planets/choices/Venus.htm, Last accessed: December, 2013

[19] NASA/JPL (2005b), "Planetary Data System", http://pds.jpl.nasa.gov/ planets/choices/Sun.htm, Last accessed: December, 2013

[20] Wakker, K.F., "Astrodynamics I", Delft University of Technology, Faculty of Aerospace Engineering, Lecture notes ae4-873, 2007

[21] Wakker, K.F. , "Astrodynamics II", Delft University of Technology, Faculty of Aerospace Engineering, Lecture notes ae4-873, 2007b

[22] SpaceX, "Falcon Heavy". http://www.spacex.com/falcon-heavy, retrieved 17-1-2014.

[23] M.R. Patel, J.M. Longuski, and J.A. Sims, "Mars Free Return Trajectories," Journal of Spacecraft and Rockets, vol. 35, no. 3, pp. 350-354, MayJune 1998

[24] J.L. Horsewood, "Mission Analysis Environment (MAnE) for Heliocentric High-Thrust Missions, Version 3.1 for Windows 3.1 Users Guide," Adasoft, Inc., 1995.

[25] Larson, W. J., and Pranke, L.K. "Human Spaceflight, Mission Analysis and Design", The McGraw-Hill Companies, Inc. ISBN 0-07-236811-X.

[26] Dr. ig. Walpot, private communication, 13.01.2013

[27] Graves, C.A. and Harpold, J.C., "Apollo Experience Report - Mission Planning for Apollo Entry", NASA TN D-6725, Washington, D.C., March 1972

[28] Mooij, E., "Re-entry Systems Lecture Notes", 2013

[29] Mooij, E., Kremer, F.G.J. and Sudmeijer, K.J. "Conceptual Design of a Small Re-entry Test Vehicle" AIAA-99-1631, Fokker Space B.V., The Netherlands 1998

[30] Putnam, Z.R., Braun, R.D. and Rohrschneider, R.R."Entry System Options for Human Return from the Moon and Mars", *Journal of Spacecraft and Rockets*: Vol. 44, No. 1, 2007

[31] Chapman, D.R., "An approximate analytical method for studying entry into planetary atmospheres", *Technical Report*, NASA TR R-11, 1959

[32] Tran H. K., Johnson C. E., Rasky D. J., Hui F. C. L., Hsu M., Chen Y. K. "Phenolic Impregnated Carbon Ablators (PICA) for Discovery class missions", AIAA 96-1911, *Thermophysics Conference*, New Orleans 1996

[33] Ording, B." Design and analysis of parachute triggering algorithms for re-entry vehicles" Master Thesis, Delft University of Technology, 2010

[34] Hillje, E.R., " Entry Flight Aerodynamics from Apollo Mission", *NASA Technical Note*, 1967

[35] NASA, "Apollo Recovery Operations", *NASA Technical Note*, 2014

[36] Koelle, D. E., "Handbook of cost engineering for space transportation systems with TRANSCOST 7.0 - Statistical-Analytical model for Cost Estimation and Economical Optimization of Launch Vehicles", TCSTransCostSystems, 2000.

[37] Hanford, "Advanced Life Support Research and Technology Development Metric", The Mars Journal (2005): accessed January 7, 2014.

[38] Peterson, "Environmental Control and Life Support System" (presentation, NASA Johnson Space Center, 2009), `http://ntrs.nasa.gov/archive/nasa/casi.ntrs.nasa.gov/20090029327_2009028591.pdf`

[39] Cervone, private communication, email: January 10, 2014 1:02 PM

[40] MacCullum, "Inspiration Mars - Dennis Tito & Taber MacCallum - 16th Mars Society Convention" (presentation, August 16, 2013).

[41] Zandbergen, private communication, January 16, 2014

[42] Cervone, private communication, January 16, 2014

[43] Agarwal et al, "Conceptual Design and Architecture for a Deep Space Habitation Module", (prepared for the AIAA) June 10, 2012

[44] NASA, "Keeping Astronauts Healthy", June 2003 `http://www.nasa.gov/vision/space/travelinginspace/keeping_astronauts_healthy_prt.htm`

[45] Rask et al, "Space Faring: The Radiation Challenge", NASA, August 2008

[46] Messeguer, J., Perez-Grande, I. "Spacecraft Thermal Control", Woodhead Publishing, 2012

[47] Fortesque, P., Stark, J., Swinerd, G. "Spacecraft Systems Engineering", Wiley, 2003

[48] Bhhandari, P., Birur, G. et al. "Mars Science Laboratory thermal control architecture", *35th International Conference on Environmental Systems*, Rome, Italy, 11-14 July 2005.

[49] Tsuyuki, G.T., Avila, A., et al, "Mars Exploration Rover: Thermal design is a system engineering activity" *34th International Conference on Environmental Systems* Paper 2004-01-2411, Colorado Springs, Colorado, USA, 19-22 July 2004

[50] Finckenor, M., "Multilayer Insulation Material Guidelines",Marshall Space Flight Center, Marshall Space Flight Center, Alabama

[51] Thermal Optical Properties, NASA Nonmetallic Material Testing, performed using procedures specified in NHB 8060.1B and SP-R-0022A

[52] M. Lemmen, private conversation, 17.01.2014

[53] M. Lemmen, private e-mail correspondence, 27.01.2014

[54] Wertz, James R., Larson, Wiley J. "Space Mission Analysis and Design", Microprism Press and Springer, 1999, second edition, ISBN 978-1881883-10-4

[55] Christiansen, Eric L., Shannon Ryan, "Handbook for Designing MMOD Protection", Johnson Space Center, Texas, 2009.

[56] Norcross, Jason "Effect of the 8 psi 32% Oxygen atmosphere on the Human in the Spaceflight Enviroment" , PHD diss., Hanover, 2013

[57] Kassapoglou, Christos, "Week 2.6 Lecture 12",from Delft University of Technology, 2013

[58] Kassapoglou, Christos, "Week 2.4 Lecture 7 and 8",from Delft University of Technology, 2013

[59] Mr. Julius Smith, 'Technical Guide Kevlar Aramid Fiber',1992

[60] Callister, W. and Rethwisch, D., "Materials science and engineering: an introduction", John Wiley & Sons New York:, 2007.

[61] Rapp, Donald, Radiation Effects and Shielding Requirements in Human Missions to the Moon and Mars, South Pasadena, California, *The International Journal of Mars Science and Exploration*, No. 2, pp. 46-71, 2006.

[62] Cucinotta, Francis A., "Radiation Risk Acceptability and Limitations".

[63] Hellweg, C. E. and C. Baumstark-Khan, "Getting Ready for the Manned Mission to Mars: The Astronauts' Risk from Space Radiation," *Naturwiss. 94, 517* 2007

[64] Destefanis, R. et al. "Space Environment Characterisation of Kevlar: Good for Bullets, Debris and Radiation Too". TAS-1-Thales Alenia Space.

[65] Townsend, L.W., "Implications of the Space Radiation Environment for Human Exploration in Deep Space" *Radiat. Prot. Dosimetry 115,44* 2005

[66] Cucinotta, F. A., Space Radiation Organ Doses for Astronauts on Past and Future Missions

[67] Rapp, Donald, Radiation Effects and Shielding Requirements in Human Missions to the Moon and Mars, South Pasadena, California, The International Journal of Mars Science and Exploration, No. 2, pp. 46-71, 2006

[68] SpaceX, Dragon Lab Fact Sheet version v.2.1

[69] Noomen, R., AE2104-11, "Flight and Orbital Mechanics" lecture slides.

[70] Space Exploration Technologies, "SpaceX's Merlin 1D Engine Achieves Flight Qualification",*press release*, March 20, 2013.

[71] Space Exploration Technologies, "Falcon 9". `http://www.spacex.com/falcon9`, retrieved 17-1-2014.

[72] Humble, R.W., Henry, G.N., and Larson, W.J. "Space Propulsion Analysis and Design", The McGraw-Hill Companies, Inc. ISBN 0-07-031320-2.

[73] Space Exploration Technologies, "Falcon 9 Launch Vehicle, Payload User's Guide", review 1, 2009.

[74] Vozoff, M., and Couluris, J. "SpaceX Products - Advancing the Use of Space" *paper presented at the AIAA SPACE 2008 Conference and Exposition*, September 9-11, 2008, San Diego, California.

[75] Cervone, A. "Lecture notes AE2203, Propulsion and Power", 2012.

[76] Spaceflight 101, "Atlas V 551 specifications".

[77] Bhaskaran, S. "'Autonomous Navigation for Deep Space Missions", *Jet Propulsion Laboratory*, Pasadena

[78] Sheikh, I. et al., "Deep Space Navigation Augmentation Using Variable Celestial X-ray Sources"

[79] Wertz, J. "Autonomous Navigation and Autonomous Orbit Control in Planetary Orbits as a Means of Reducing Operations Cost" Pasadena, 2003

[80] Riedel J.E. "Autonomous Optical Navigation (AutoNav) DS1 Technology Validation Report", *Jet Propulsion Laboratory* Pasadena.

[81] Riedel J.E. "Configuring the Deep Space Impact AutoNav System for Lunar, Comet and Mars Landing", 2014

[82] Rodgers D.H. "Advanced Technologies Demonstrated by the Miniature Integrated Camera and Spectrometer (MICAS) Aboard Deep Space 1", 2007

[83] Riedel J.E. et all., "Navigation for the New Millennium Navigation for Deep Space 1" *Jet Propulsion Laboratory* Pasadena

[84] Blackburn, E.P. "Spacecraft Magnetic Torquers" 1969.

[85] Muirden, J. "Stars and Planets" 1996.

[86] "Nine Planet", accessed January 17, 2014, `http://nineplanets.org/data.html`

[87] "Earth Matrix", accessed January 17, 2014, `http://earthmatrix.com/sciencetoday/solar_constants_planets.html`

[88] Heimler, N. "Principles of Science" Merill, 1979.

[89] Goff, J.A. et al, "Realistic Near-Term Propellant Depots: Implementation of a Critical Spacefaring Capability" *American Institute of Aeronautics and Astronautics* 2009.

[90] Hamilton, W., "Automatic Refueling Coupling for On-Orbit Spacecraft Servicing *paper presented at the 25th Joint Propulsion Conference, Monterey, California* July 10-12, 1989

[91] Chato, Dr. D.J., "Techonologies for Refueling Spacecraft ON-Orbit" *paper presented at the AIAA Space 2000 Conference and exposition* September 19-21, 2000, Long Beach, California

[92] Chato, Dr. D.J. "Low Gravity Issues of Deep Space Refueling". *43rd AIAA Aerospace Sciences Meeting and Exhibit* 2005.

[93] de Kruif, J.S. and Kutter, B.F. "Centaur Upperstage Applicability for Several-Day Mission Durations with minor Insulation Modification" *paper presented at the annual AIAA Joint Propulsion Conference and Exhibit*, Cincinnati, Ohio, July 8-11, 2007

[94] Chato, Dr. D.J., "Cryogenic Fluid Transfer for Exploration". NASA Glenn Research Center.

[95] Zandbergen, B.T.C. "Thermal Rocket Propulsion (v2.04)", Jan 29, 2010.

[96] Rauschenbakh, B.V.,Ovchinnikov, M.Y. and McKenna-Lawlor, S. "Essential Spaceflight Dynamics and Megnetospherics", Kluwer Academic Publishers, 2003

[97] G. Szatkowski et al, "Centaur Extensibility for Long Duration" (paper presented at the 2006 AIAA Space Conference, 19-21 September 2006, San Jose, California).

[98] Taylor, J., Lee, D.K. et al. "Article 12 Mars Reconnaissance Orbiter Telecommunications", *DESCANSO Design and Performance Summary Series* Jet Propulsion Laboratory California Institute of Technology, 2006

[99] "Nasa's Deep Space Network", Jet Propulsion Laboratory, California Institute of Technology, accessed January 08, 2014, http://deepspace.jpl.nasa.gov/dsn/

[100] Prem Sundaramoorthy,personal consultation, multiple occasions

[101] Reid, M.S., "Low-Noise Systems in the Deep Space Network", *Deep Space Communications and Navigation Series*, Jet Propulsion Laboratory, California Institute of Technology, 2008

[102] Hammond, W.E., "Design methodologies for space transportation systems" *American Institute of Aeronautics and Astronautics, Inc.*, Reston, Virginia, 2001

[103] ISS Utilisation Department, "Information Kit, Mars500 Isolation Study", ESA, February 2011

[104] Human Dynamo, "Technical Information", accessed on January 14, 2013 `http://www.humandynamo.com/technical_info.html`

[105] Lu, "Expedition 7", NASA, August 15, 2003

[106] Harris et al, "International Space Station Utilization and Advancing Research in Space", *AIAA SPACE 2013 Conference and Exposition*, 2013

[107] "Mars500 Study Overview", ESA,

[108] Burke, K.A. "Fuel Cells for Space Science Applications" *American Institute for Aeronautics and Astronautics* November 2003

[109] Zandbergen, B.T.C. Aerospace Vehicle Electrical power systems AE2203: Propulsion & Power.

[110] Space Shuttle Fuel Cell Power Plants (January 2013) `http://spaceflight.nasa.gov/shuttle/reference/shutref/orbiter/eps/pwrplants.html`

[111] Jacobs, private communication, January 6, 2014

[112] ESA, "European Astronaut Selection", March 2008, accessed on January 13 2014 `http://www.esa.int/Our_Activities/Human_Spaceflight/European_Astronaut_Selection/FAQs_Qualifications_and_skills_required`

[113] Lyndon, "ISS Exercise Countermeasures", Johnson Space Center, (presentation, April, 2001) `http://snebulos.mit.edu/projects/announcements/ILSRA-2001/01-OBPR-03-ESlides.pdf`

[114] NASA, "International Space Station Timelines (January 2013)", January 2014 `http://www.nasa.gov/mission_pages/station/timelines/1_2013_tl.html`

[115] Herridge, "Astronaut Health Top Priority", NASA's John F. Kennedy Space Center, August 2009.`http://www.nasa.gov/mission_pages/shuttle/behindscenes/medteam.html`

CNN. Google Privacy Policy. Last modified March 11, 2009. http://www.google.com/intl/en/privacypolicy.html.

[116] Mars One - The Technology, `http://mars-one.com/en/mission/technology`, June 2012, viewed on 21/01/2014.

[117] CNN. "More than 100,000 want to go to Mars and not return, project says", `http://edition.cnn.com/2013/08/09/tech/innovation/mars-one-applications/`, August 2013, viewed on 21/01/2014

[118] Reuters, "India's Mars mission enters second stage; outpaces space rival China',`http://www.reuters.com/article/2013/12/01/us-india-mars-idUSBRE9B000S20131201`, December 2013, viewed on 21/01/2014

[119] NASA, "NASA Announces Robust Multi-Year Mars Program; New Rover to Close Out Decade of New Missions", `http://www.nasa.gov/home/hqnews/2012/dec/HQ_12-420_Mars_2020.html`, December 2012, viewed on 21/01/2014

[120] BBC, "China to launch space station by 2023",`http://www.bbc.co.uk/news/science-environment-24282060`, September 2013, viewed on 21/01/2014

[121] NBC, "Millionaire revises plan for Mars flyby in 2018: Now it's up to NASA", `http://www.nbcnews.com/science/millionaire-calls-partnership-nasa-mars-flyby-mission-2D11624563`, November 2013, viewed on 21/01/2014

[122] RedBull, "Red Bull Stratos release final mission data", `http://www.redbullstratos.com/`, February 2013, viewed on 21/01/2014

[123] NBC, "Millionaire seeks an assist for Inspiration Mars mission" `http://www.nbcnews.com/science/millionaire-seeks-assist-inspiration-mars-mission-6C10932930`, August 2013, viewed on 21/01/2014

[124] NBC, "Kickstarter pledges topped $480 million in 2013", `http://www.nbcnews.com/technology/kickstarter-pledges-topped-480-million-2013-2D11890658`, January 2014, viewed on 21/01/2014

[125] Shiller, Robert J., *Irrational Exuberance.*

[126] NASA, "DSN Aperature Fee Tool", 2000, `http://deepspace.jpl.nasa.gov/advmiss/`

[127] Van Pelt and Hunt, "Comparing NASA and ESA Cost Estimating Methods for Human Missions to Mars", 2004.

[128] Brown et al, "System study of a surface habitat and a tranfer vehicle from manned mission to and from Mars"

[129] "Mars Science Laboratory/Curiosity", NASA, accessed on December 19, 2013, `http://solarsystem.nasa.gov/missions/profile.cfm?InFlight=1&MCode=MarsSciLab&Display=ReadMore`

[130] "Mars Direct FAQ", The Mars Society, accessed on December 19, 2013, `http://www.marssociety.org/home/about/faq#TOC-Q:-Why-are-cost-estimates-for-a-Mars-mission-so-different-`

[131] J.M. Salotti, "Simplified scenario for manned Mars missions", Acta Astronautica, 2011

[132] Stapelberg, Rudolph Frederick *Handbook of Reliability, Availability, maintainability and Safety in Engineering Design* Springer, London, 2009

[133] Larsen, M. et al.,*Safety Design for Space Systems* Elsevier, UK, 2009

[134] European Cooperation for Space Standardization, *Space project management: Project planning and implementation* 2007